TOWARDS MODELLING OF REINFORCED CONCRETE MEMBERS WITH EXTERNALLY-BONDED FIBRE REINFORCED POLYMER (FRP) COMPOSITES

by

Rita Sheung Ying Wong

A thesis submitted in conformity with the requirements

for the degree of Master of Applied Science

Graduate Department of Civil Engineering

University of Toronto

© Copyright by Rita Sheung Ying Wong 2001

National Library of Canada
Acquisitions and Bibliographic Services
395 Wellington Street
Ottawa ON K1A 0N4
Canada

Bibliothèque nationale du Canada
Acquisitions et services bibliographiques
395, rue Wellington
Ottawa ON K1A 0N4
Canada

Your file Votre référence

Our file Notre référence

The author has granted a non-exclusive licence allowing the National Library of Canada to reproduce, loan, distribute or sell copies of this thesis in microform, paper or electronic formats.

The author retains ownership of the copyright in this thesis. Neither the thesis nor substantial extracts from it may be printed or otherwise reproduced without the author's permission.

L'auteur a accordé une licence non exclusive permettant à la Bibliothèque nationale du Canada de reproduire, prêter, distribuer ou vendre des copies de cette thèse sous la forme de microfiche/film, de reproduction sur papier ou sur format électronique.

L'auteur conserve la propriété du droit d'auteur qui protège cette thèse. Ni la thèse ni des extraits substantiels de celle-ci ne doivent être imprimés ou autrement reproduits sans son autorisation.

0-612-62958-9

Canada

Thesis Title: Towards Modelling of Reinforced Concrete Members with Externally-Bonded Fibre Reinforced Polymer (FRP) Composites
Degree: Master of Applied Science
Year of Convocation: 2001
Student Name: Rita Sheung Ying Wong
Graduate Department of Civil Engineering
University of Toronto

ABSTRACT

Fibre reinforced polymer (FRP) composites have been increasingly studied for their application in the flexural or shear strengthening of reinforced concrete members. Although substantial increases in strength have been achieved, reductions in ductility have also been reported, as a result of debonding failures near the concrete-FRP interface. The debonding phenomenon has been the subject of numerous investigations, including the experimental program described herein, which involved the strengthening of shear-critical beams using carbon FRP strips. It has been determined that the bond-slip behaviour at the bond interface must be considered in the numerical modelling of externally-reinforced members. Essential to analyses utilizing a finite element program are the formulation of bond elements and their constitutive relations. The implementation of link and contact elements, along with linear elastic and elastic-plastic bond laws, has produced accurate predictions of member response.

ACKNOWLEDGEMENTS

My most grateful appreciation goes to Professor Frank J. Vecchio for his knowledgeable insight, expert guidance and continuing patience, without which this thesis would not have been possible. The advice from Professor Shamim A. Sheikh and his assistance in obtaining the repair materials for my experiment are also greatly appreciated. In addition, Professor Evan Bentz's assistance with computer programming must be recognized.

The National Science and Engineering Research Council (NSERC) is acknowledged for its financial contribution towards my research, and the repair materials for my beam tests were contributed by R. J. Watson Inc. and Fyfe Company.

Sincere thanks are extended to the staff of the Structural Laboratories, in particular, Renzo Basset, Mehmet Citak, Peter Heliopoulos, John McDonald, Joel Babbin, and Giovanni Buzzeo, for their kind assistance with the experimental program of my thesis. Roman Yaworsky is thanked for his assistance with photography.

The advice and friendship of numerous students formed an integral part of my academic experience at the University of Toronto. Mukhtar Homam, Simon Pong, Youai Gan, and Cao Shen are thanked for their valuable input regarding my research, and the assistance from William Shim, Yuichi Sato, Corey Fan, Karen Liu, Esneyder Montoya, Almila Uzel, Dan Palermo, and Neil Hoult is also acknowledged.

Last, but not least, I wish to thank my mother for her love, constant support and encouragement throughout the duration of my graduate studies.

TABLE OF CONTENTS

ABSTRACT	ii
ACKNOWLEDGEMENTS	iii
LIST OF TABLES	viii
LIST OF FIGURES	x
NOTATION	xvi

CHAPTER 1 INTRODUCTION

1.1 Background	1
1.1.1 Field Applications of FRP Composites	2
1.1.2 Research Work Involving FRP Composites	2
1.2 Objective of Current Research	3
1.3 Layout of Chapters	4

CHAPTER 2 LITERATURE REVIEW

2.1 Introduction	5
2.2 Flexural Strengthening with FRP Composites	6
2.2.1 Global Behaviour	6
2.2.1.1 Analyses Not Including Characteristics of Adhesive Layer	6
2.2.1.2 Analyses Including Characteristics of Adhesive Layer	10
2.2.2 Local Behaviour	18
2.2.2.1 Failure of Concrete Cover	20
2.2.2.2 Peeling-off of FRP	22
2.2.2.3 Consideration of Both Failure Modes	27
2.3 Shear Strengthening with FRP Composites	36
2.3.1 Experimental Work	37
2.3.2 Design Equations	53

2.4 Bond Characterization 67
2.4.1 Measures of Bond Strength 68
2.4.2 Factors Influencing Bond Strength 75
2.4.3 Debonding Mechanism 78
2.4.4 Bond Stress-Slip Relationships 83

CHAPTER 3 FINITE ELEMENT FORMULATIONS

3.1 Introduction 92
3.2 The Modified Compression Field Theory (MCFT) 92
3.3 Finite Element Procedure 98
3.4 Modelling of Repaired Structures 101
3.5 Modelling Externally-Bonded FRP Composites 103
3.5.1 Constitutive Relation for FRP Composites 103
3.5.2 Constitutive Relations for Bond Interface 104
3.6 Modelling Bond-Slip Behaviour with Bond Elements 105
3.6.1 Link Element 106
3.6.1.1 General 106
3.6.1.2 Element Stiffness Matrix 107
3.6.2 Contact Element 108
3.6.2.1 General 108
3.6.2.2 Element Stiffness Matrix 109

CHAPTER 4 EXPERIMENTAL PROGRAM

4.1 Introduction 111
4.2 Preparation of Specimens 111
4.2.1 Fabrication 111
4.2.2 Application of CFRP Strips 114
4.3 Material Properties 116

4.4 Testing Procedure 122
4.5 Experimental Observations 124
4.5.1 Beam RWOA-1 124
4.5.2 Beam RWOA-2 126
4.5.3 Beam RWOA-3 128
4.6 Test Results 129
4.7 Analytical Results 132
4.8 Discussion 133

CHAPTER 5 NUMERICAL ANALYSIS WITH FEM

5.1 Introduction 138
5.2 Specimens Strengthened in Flexure with FRP Composites 138
5.2.1 Žarnić Specimens 139
5.2.1.1 Experimental Details 139
5.2.1.2 Numerical Modelling 141
5.2.1.2.1 Finite Element Mesh and Special Considerations in Analysis 141
5.2.1.2.2 Analysis Results and Discussion 144
5.2.2 El-Refaie Specimens 149
5.2.2.1 Experimental Details 149
5.2.2.2 Numerical Modelling 153
5.2.2.2.1 Finite Element Mesh and Special Considerations in Analysis 153
5.2.2.2.2 Analysis Results and Discussion 155
5.2.3 De Rose Slab Specimens 158
5.2.3.1 Experimental Details 159
5.2.3.2 Numerical Modelling 162
5.2.3.2.1 Finite Element Mesh and Special Considerations in Analysis 162
5.2.3.2.2 Analysis Results and Discussion 166
5.3 Specimens Strengthened in Shear with FRP Composites 171
5.3.1 De Rose Beam Specimen 171

5.3.1.1 Experimental Details 172
5.3.1.2 Numerical Modelling 176
5.3.1.2.1 Finite Element Mesh and Special Considerations in Analysis 176
5.3.1.2.2 Analysis Results and Discussion 177
5.3.2 RWOA Beam Specimens 179
5.3.2.1 Finite Element Mesh and Special Considerations in Analysis 180
5.3.2.2 Analysis Results and Discussion 183
5.3.2.1.1 Beam RWOA-1 183
5.3.2.1.2 Beam RWOA-2 185
5.3.2.1.3 Beam RWOA-3 187

CHAPTER 6 DISCUSSION

6.1 Trends in Experimental Behaviour 192
6.1.1 Flexural Strengthening with FRP Composites 192
6.1.2 Shear Strengthening with FRP Composites 193
6.2 Need for Future Experimental Work 194
6.2.1 Global Response 194
6.2.2 Local Behaviour 195
6.3 Strengths/Weaknesses in Analytical Methods 196
6.4 Need for Future Analytical Work 198

CHAPTER 7 CONCLUSIONS 200

REFERENCES 202
APPENDIX A 211
APPENDIX B 221
APPENDIX C 231
APPENDIX D 235
APPENDIX E 295

LIST OF TABLES

CHAPTER 2

Table 2.1: Type and Quantity of FRP Reinforcement Used by Funakawa *et al.* 40

Table 2.2: Values of Parameters in Equivalent Bond Constitutive Model 66

Table 2.3: Failure Modes Observed in Bond Tests 71

Table 2.4: Values Defining Bond Stress-Slip Relationship in Homam's Study 83

CHAPTER 4

Table 4.1: Measured Material Properties for RWOA Beam Specimens 117

Table 4.2: Mechanical Properties of CFRP and Epoxy for RWOA Beams 119

Table 4.3: Failure Mode of CFRP Coupons 122

Table 4.4: Actual and Predicted Values of FRP Shear Contribution 132

Table 4.5: Reinforcement Properties for the TOA, TA and RWOA Beam Series 133

Table 4.6: Maximum Load and Deflection for Beam Series TOA, TA and RWOA 134

CHAPTER 5

Table 5.1: Material Properties for Žarnić Slab Strips and Beams 139

Table 5.2: Predicted Results for Žarnić Slab Strip Bonded with CFRP Plate 145

Table 5.3: Predicted Results for Žarnić Beam Bonded with CFRP Plate 148

Table 5.4: Strengthening Scheme and Properties of CFRP for El-Refaie Specimens 151

Table 5.5: Properties of Concrete and Steel Reinforcement for El-Refaie Specimens 151

Table 5.6: Load and Moment Enhancement Ratios for El-Refaie Specimens 152

Table 5.7: Bond Stress-Slip Values for El-Refaie Specimens 154
Table 5.8: Comparison of Results from Experiments and Analyses of El-Refaie Specimens 157
Table 5.9: Material Properties for De Rose Slab Specimens 160
Table 5.10: Elastic-Plastic Bond Law Values for De Rose Slab Analyses 165
Table 5.11: Experimental and Predicted Results for De Rose Slab Specimens 169
Table 5.12: Material Properties for De Rose Beam Specimens 172
Table 5.13: Bond Stress-Slip Values for RWOA Beams 180
Table 5.14: Experimental and Analytical Results for RWOA Beams 183
Table 5.15: Predicted and Calculated Effective FRP Strains 190

LIST OF FIGURES

CHAPTER 2

Figure 2.1: Experimental and FEA results for beams bonded with CFRP plates 7

Figure 2.2: Load-deflection response assumptions in beam section analysis 8

Figure 2.3: Comparison between analytical, FEM and experimental results by Ross *et al.* 9

Figure 2.4: Comparison between analytical and experimental results for beams tested by M'Bazaa and Chicoine 10

Figure 2.5: Concrete-adhesive specimens: (a) tension and shear, (b) compression and shear 11

Figure 2.6: Comparison between analytical and experimental results by Arduini and Nanni 12

Figure 2.7: Comparison between analytical and experimental results by Bokan-Bosiljkov 13

Figure 2.8: Typical FE mesh for RC beam with externally-bonded FRP reinforcement 15

Figure 2.9: (a) Predicted and (b) actual shear stress distribution at concrete-FRP interface 16

Figure 2.10: Finite element mesh employed by Limam and Hamelin 17

Figure 2.11: Characterization of bond interface behaviour 17

Figure 2.12: Comparison between analytical and experimental results by Limam *et al.* 18

Figure 2.13: (a) Failure modes in FRP-bonded beams 18

Figure 2.13 (continued): (b) Sample load-deflection curves 19

Figure 2.14: Potential crack paths in FRP debonding failures 20

Figure 2.15: Composite model of concrete beam bonded with FRP plate 21

Figure 2.16: Crack openings leading to FRP peeling-off 23

Figure 2.17: Locations of bond failure due to FRP peeling-off 24

Figure 2.18: Mesh definition at the FRP plate cut-off point 25

Figure 2.19: Comparison of shear and normal stresses near FRP plate end 26

Figure 2.20: Flow-chart of calculations for theoretical model 28

Figure 2.21: Cracked beam and concrete tooth acting as cantilever beam 29

Figure 2.22: Comparison of predicted beam responses and test data 31

Figure 2.23: Variations of internal forces before and after yielding moment 32
Figure 2.24: Displacements in FRP-bonded beam due to shear 34
Figure 2.25: Free-body diagram for truss model 35
Figure 2.26: FRP shear reinforcement configurations 36
Figure 2.27: Failure modes of shear-strengthened beams tested by Taerwe *et al.* 38
Figure 2.28: (a) Cracking patterns and (b) load-deflection curves from Li *et al.* 39
Figure 2.29: Load-deflection curves for beams tested by Funakawa *et al.* 40
Figure 2.30: Delamination of CFRP based on bonding configuration 41
Figure 2.31: Load-deflection curves for beams tested by Chaallal *et al.* 43
Figure 2.32: Load-deflection curves: effects of CFRP (a) quantity and (b) orientation 44
Figure 2.33: Experimental, analytical (A) and numerical (FE) results for beams studied by Arduini *et al.* 46
Figure 2.34: Delamination of CFRP in beam (a) without and (b) with anchorage, (c) corresponding load-deflection curves 48
Figure 2.35: Systems of CFRP anchorage 48
Figure 2.36: Behaviour of beams with various CFRP anchorage systems: (a) S and (b) M series 49
Figure 2.37: Stress field for Type 3 anchorage system: (a) truss and (b) arch actions 49
Figure 2.38: (a) Strengthening schemes and (b) test results for T-beams studied by Khalifa and Nanni 50
Figure 2.39: Failure modes of beams (a) BT4 and (b) BT5 51
Figure 2.40: Vertical strains in FRP strips bonded onto T-beam 52
Figure 2.41: (a) Schematic of FRP stress bearing mechanism, (b) simplified FRP tensile stress along shear crack 57
Figure 2.42: Effective width of FRP: (a) in U-wrap, (b) bonded to beam sides only 60
Figure 2.43: Schematic illustration of shear and FRP failures 61
Figure 2.44: FRP contribution to shear capacity in terms of $\rho_f E_f$ 64
Figure 2.45: Shear stress-displacement relationships: (a) from experiments, (b) equivalent 66
Figure 2.46: Models used for calculating peeling-off length: (a) global, (b) local 67

Figure 2.47: Common locations for FRP strips on beam webs to debond 68
Figure 2.48: Typical bond test specimens 69
Figure 2.49: Relationship between bond strength, test type and concrete strength 71
Figure 2.50: Schematic of strain distribution in CFRP sheet during shear bond test 73
Figure 2.51: Finite element mesh for analysis of CFRP-bonded concrete prism 73
Figure 2.52: Strain distribution along GFRP-concrete joint 76
Figure 2.53: Crack propagation and formation of debonding 79
Figure 2.54: Constitutive relationship for bond interface: (a) prior to debonding, (b) after debonding 79
Figure 2.55: RC member bonded with CFRP sheet: general representation and connection of delamination between FRP and concrete 80
Figure 2.56: Computational flow for determining tensile properties of FRP-bonded RC member 82
Figure 2.57: Example of effective bond length 86
Figure 2.58: Measured bond stress-slip curves for specimens tested by Nakaba *et al.* 87
Figure 2.59: Bond stress-slip models for FRP bonded to concrete 88

CHAPTER 3

Figure 3.1: Average strains and stresses in a reinforced concrete element 93
Figure 3.2: Constitutive relation for cracked concrete in compression 95
Figure 3.3: Constitutive relation for concrete in tension 96
Figure 3.4: Constitutive relation for reinforcing steel 96
Figure 3.5: Flowchart for finite element procedure 99
Figure 3.6: Analysis of beam bonded with FRP plate: (a) finite element mesh, (b) load history, (c) strains in FRP element, (d) determination of secant modulus 102
Figure 3.7: Constitutive relation for FRP reinforcement 104
Figure 3.8: Constitutive relationship for bond interface: (a) elastic-plastic, (b) linear elastic 105

Figure 3.9: Representation of link element 106
Figure 3.10: Representation of 1-D contact element 109

CHAPTER 4

Figure 4.1: Cross-section details of RWOA beams 112
Figure 4.2: Elevation views of RWOA beams 112
Figure 4.3: Formwork for casting of RWOA beam (along with other test beams) 113
Figure 4.4: Beams cast in formwork 114
Figure 4.5: Application of CFRP strips to the sides of RWOA beams 115
Figure 4.6: Geometry of CFRP coupons tested for RWOA beams 118
Figure 4.7: TYFO S® High Strength Graphite Fibrwrap® SCH41 CFRP fabric 119
Figure 4.8: Fabrication of panel for CFRP coupons 120
Figure 4.9: Completed CFRP coupons 120
Figure 4.10: Stress-strain curves from CFRP coupon tests 121
Figure 4.11: Typical test set-up for RWOA beams 123
Figure 4.12: Beam RWOA-3 set up in the MTS testing machine frame 123
Figure 4.13: Beam RWOA-1 at failure: (a) debonding of CFRP strips, (b) concrete failure viewed from below 125
Figure 4.13 (continued): Beam RWOA-1 at failure: (c) overall crack pattern 126
Figure 4.14: Beam RWOA-2 at failure: (a) debonding of CFRP strips, (b) concrete failure viewed from below, (c) overall crack pattern 127
Figure 4.15: Beam RWOA-3 at failure: (a) debonding of CFRP strips, (b) overall crack pattern 129
Figure 4.16: Experimental load-deflection response for RWOA beams 130
Figure 4.17: Mid-span surface strains at the level of longitudinal reinforcement: beam (a) RWOA-1, (b) RWOA-2, (c) RWOA-3 131
Figure 4.18: Load-deflection curves for beam series: (a) 1, (b) 2 and (c) 3

(comparison between TOA, TA and RWOA beams) 135

CHAPTER 5

Figure 5.1: Geometry of Žarnić specimens: (a) slab strip and (b) beam 140
Figure 5.2: Finite element mesh for (a) Žarnić slab strip and (b) Žarnić beam 142
Figure 5.3: Load-deflection curves for Žarnić slab strip bonded with CFRP plate 144
Figure 5.4: Effects of varying maximum bond stresses for Žarnić slab strip 145
Figure 5.5: Bond stress distribution for Žarnić slab strip with bonded CFRP plate 147
Figure 5.6: Load-deflection curves for Žarnić beam bonded with CFRP plate 147
Figure 5.7: Bond stress distribution for Žarnić beam with bonded CFRP plate 149
Figure 5.8: Details of El-Refaie specimens 150
Figure 5.9: Experimental load-deflection curves for El-Refaie specimens 152
Figure 5.10: Finite element mesh for El-Refaie specimens 153
Figure 5.11: Load-displacement curves from numerical analyses of El-Refaie specimens 156
Figure 5.12: Bond-stress distribution for El-Refaie specimens: (a) FRP on top surface (near 170 kN), (b) FRP on bottom surface (near 200 kN) 158
Figure 5.13: De Rose slab dimensions and reinforcement details 160
Figure 5.14: Loading and support conditions for De Rose slab 161
Figure 5.15: Application of FRP fabric to De Rose slab 161
Figure 5.16: Experimental load-deflection curves for De Rose slab specimens 162
Figure 5.17: Finite element mesh for the De Rose slab specimen 163
Figure 5.18: Schematic diagram of the connection between concrete and FRP truss elements 164
Figure 5.19: Predicted load-deflection curves for CFRP-repaired De Rose slab 166
Figure 5.20: Predicted FRP strains and bond stresses for CFRP-repaired De Rose slab 168
Figure 5.21: Predicted load-deflection curves for GFRP-repaired De Rose slab 168
Figure 5.22: Predicted FRP strains and bond stresses for GFRP-repaired De Rose slab 170

Figure 5.23: Analytical results for De Rose slab specimens (not accounting for bond-slip): (a) CFRP-repaired 170
Figure 5.23 (continued): Analytical results for De Rose slab specimens (not accounting for bond-slip): (b) GFRP-repaired 171
Figure 5.24: De Rose beam details 173
Figure 5.25: Loading and support locations for De Rose beam 173
Figure 5.26: Layout for De Rose beam repaired with CFRP 175
Figure 5.27: Experimental load-deflection behaviour of De Rose beam specimens 175
Figure 5.28: Finite element mesh for the De Rose beam specimen 176
Figure 5.29: Predicted load-deflection response of CFRP-repaired De Rose beam 177
Figure 5.30: Analytical results for De Rose beam specimen (not accounting for bond-slip) 178
Figure 5.31: Predicted FRP strains and bond stresses for CFRP-repaired De Rose beam 179
Figure 5.32: Finite element mesh for beams: (a) RWOA-1, (b) RWOA-2, (c) RWOA-3 181
Figure 5.33: Analytical and experimental load-deflection curves for beam RWOA-1 184
Figure 5.34: Predicted FRP strains and bond-slip distribution for beam RWOA-1 at peak load 185
Figure 5.35: Analytical and experimental load-deflection curves for beam RWOA-2 186
Figure 5.36: Predicted FRP strains and bond-slip distribution for beam RWOA-2 at peak load 187
Figure 5.37: Analytical and experimental load-deflection curves for beam RWOA-3 188
Figure 5.38: Predicted FRP strains and bond-slip distribution for beam RWOA-3 at peak load 189
Figure 5.39: Bond test specimen utilized by Sato 191
Figure 5.40: (a) Bond stress-slip curves and (b) equivalent bilinear relationship 191

NOTATION

a	shear span, half of distance between two cracks, maximum aggregate size
A_f	cross-sectional area of FRP per unit length of the beam
A_i	cross-sectional area of i^{th} FRP strip
A_m	area of a pair of FRP plates
b	beam width
b_c	width of concrete member
b_f	width of FRP laminate (in flexural strengthening)
b_p	width of FRP plate (in flexural strengthening)
b_w	width of beam web
c_m	thickness of concrete cover
$[D]$	material stiffness matrix
d	effective depth
d', d''	concrete cover thickness
d_{cf}	initial debonding length
d_f	height of FRP sheets bonded to beam web, effective depth of FRP laminate
d_m	shear depth of the beam section
d_p	distance between the top of the beam to the center of the FRP plate (in flexural strengthening)
$(d\varepsilon/dx)_{avg}$	average strain gradient for the effective bond length
$(d\varepsilon/dx)_0$	strain gradient for the effective bond length
E_a	elastic modulus of adhesive
E_b	slip modulus of FRP-concrete bond interface
E_c	elastic modulus of concrete (initial tangent modulus)
$\overline{E}_{c1}$	secant modulus of concrete in principal tensile direction
$\overline{E}_{c2}$	secant modulus of concrete in principal compressive direction
E_f	elastic modulus of FRP laminate
E_p	elastic modulus of FRP plate
E_s	elastic modulus of steel reinforcement
$\overline{E}_{sx}$	secant modulus of steel reinforcement in x direction
$\overline{E}_{sy}$	secant modulus of steel reinforcement in y direction
F	axial force

f_a	tensile strength of adhesive
f_{bond}	bond strength
f'_c	concrete cylinder compressive strength
f'_t	tensile strength of concrete, FRP or epoxy resin
f_{c1}	principal tensile stress
f_{c2}	concrete stress in principal compressive stress direction
f_{ci}	compressive stress on the crack
f_{ct}	pull-off strength of concrete surface
f_{cu}	concrete cube compressive strength
f_{cx}	concrete stress in x direction
f_{cy}	concrete stress in y direction
F_f, F_{fu}, f_f, $f_{f,u}$	tensile strength of FRP material
$f_{f,e}$	effective FRP stress
$f_{f,u}$	ultimate FRP stress
f_m	stress in FRP plates
F_{max}	ultimate load
f_p	maximum compressive stress for cracked concrete in compression
f_r	modulus of rupture of concrete
f_{si}	average stress of steel reinforcement in i^{th} direction
f_{sp}	concrete tensile splitting strength
f_{sx}	average stress in x-direction steel reinforcement
f_{sy}	average stress in y-direction steel reinforcement
f_u	ultimate strength of steel reinforcement
f_{ui}	stress at failure in i^{th} FRP strip at intersection with shear crack
f_x	uniform axial stress applied in x-direction
f_y	uniform axial stress applied in y-direction, yield strength of steel reinforcement
f_{yi}	yield stress of steel reinforcement in i^{th} direction
f_{yx}	yield strength of x-direction steel reinforcement
f_{yy}	yield strength of y-direction steel reinforcement
G_a	shear modulus of adhesive
G_c	shear modulus of concrete
G_f	fracture energy
G_{IIC}	critical strain energy release rate for the bond interface

G_r	bond modulus in tangential direction (in contact element)
G_t	bond modulus in normal direction (in contact element)
h	height of beam section, height of FRP plate
I	equivalent moment of inertia
I_c	cracked equivalent moment of inertia of composite beam section
I_t	transformed second moment of area in terms of concrete
[k]	element stiffness matrix
k_E	number of FRP free edges on one side of the beam
k_L	factor accounting for FRP laminate directions
[K]	structure stiffness matrix
K_h	spring stiffness in the *h* direction (in link element)
K_v	spring stiffness in the *v* direction (in link element)
l , L , L_b , L_j	bonded joint length
L_0	initial transfer length
l_c	flexural crack spacing
l_{dev} , L_{jd}	bond development length
L_e	effective bond length
L_f	development length of FRP laminate
L_s	shear span
L_t	transfer length
M_c	applied bending moment at the transition point between bond-development and composite zones
N	number of cracks, north side of beam
n_s	total number of stirrups crossing a shear crack
P	applied load
P_{sep}	FRP plate separation load
R_{Icf}	fracture resistance of plain concrete
R_r^{ik}	force between nodes *i* and *k* in the r direction (in contact element)
s	slip at concrete-FRP bond interface
S	average crack spacing, south side of beam
s_f , s_m	spacing of FRP strips (in shear strengthening)
$s_{f,max}$	maximum spacing of FRP strips (in shear strengthening)
s_{max} , S_m , S_{max}	slip at bond interface when maximum bond stress is reached
S_u , S_{ult}	ultimate slip at bond interface

[T]	transformation matrix
t_a	thickness of adhesive layer
t_f	thickness of FRP laminate
T_{FRP}	shear contribution of FRP laminate
t_p	thickness of FRP plate
T_u	ultimate capacity of bonded FRP-concrete joint
u	displacement
u_b	horizontal displacement of beam
u_f	horizontal displacement of FRP laminate
U_f , U_{max} , U_y	bond strength of adhesive or FRP-concrete interface
v	vertical crack opening
V	shear force
v_{ci}	shear stress across the crack
v_{cimax}	maximum transmissible shear stress across the crack
v_{cxy}	concrete normal shear stress
V_f	shear contribution of FRP laminate
V_{strips}	shear contribution of FRP strips
v_{xy}	applied shear stress
w	horizontal crack opening, average crack width, width of FRP laminate
w_f	width of FRP strips (in shear strengthening)
w_{fe}	effective width of FRP laminate
y_p	distance from neutral axis to FRP plate (in flexural strengthening)
α	reduction factor, or direction of principal FRP fibres measured from longitudinal axis of beam
β	direction of principal FRP fibres measured from longitudinal axis of beam
β_d	damage factor for cracked concrete
Δ_r^{ik}	relative displacement between nodes *i* and *k* in the r direction (in contact element)
δ	shear displacement
δ_1	slip at bond interface when maximum bond stress is reached
δ_f	ultimate slip at bond interface
δ_z	maximum slip in equivalent (linear) bond relationship
ε_1	principal tensile strain
ε_2	principal compressive strain

ε_{cr}	cracking strain of concrete
ε^{e}	elastic strains
$\varepsilon_{f,e}$	effective FRP strain
$\varepsilon_{f,e,A}$	effective FRP strain (ACI format)
$\varepsilon_{fk,e}$	characteristic value of effective FRP strain
$\varepsilon_{f,u}$	ultimate FRP strain
ε_h	strain in the *h* direction (in link element)
ε_o	strain in concrete cylinder at f'_c
ε_p	strain corresponding to f_p
ε^{p}	plastic offset strains
ε_{ui}	strain at failure in i^{th} FRP strip at intersection with shear crack
ε_{ult}	ultimate strain of steel or FRP reinforcement
ε_v	strain in the *v* direction (in link element)
ε_{vcu}	ultimate vertical tensile strain of concrete
ε_x	normal strain in x-direction
ε_y	normal strain in y-direction
γ , γ_{xy}	shear strain
γ_{cf}	debonding fracture energy per unit area of FRP-concrete crack surface
γ_f	partial safety factor for FRP in tension
η_i	modular ratio
φ_c	strain energy of concrete containing N cracks, without debonding and sliding of rebars and the debonding of FRP sheet
φ_{dcf}	total debonding energies on all debonded interfaces between FRP and concrete
φ_{ds}	total debonding energies on all debonded interfaces between rebars and concrete
φ_f	strength reduction factor
φ_s	total sliding energies on all debonded interfaces between rebars and concrete
θ_c , θ_{st}	shear crack inclination
θ_i	angle between the centreline of rebars and the crack normal
θ_w	shear plane angle in the web
ρ_f , ρ_{wf}	shear reinforcement ratio of FRP laminates
ρ_s , ρ_{ws}	shear reinforcement ratio of stirrups
ρ_x	steel reinforcement ratio in x direction

ρ_y	steel reinforcement ratio in y direction
σ_f	tensile stress in FRP laminate
σ_{fu}	tensile strength of FRP material
σ_h	stress in the *h* direction (in link element)
σ_{sy}	yield strength of stirrups
σ_v	stress in the *v* direction (in link element)
$\Sigma\rho_w$	effective shear reinforcement ratio
$\tau(x)$	shear stress distribution along concrete-FRP interface
τ_{adm}	admissible shear stress at the bond interface
τ_z	maximum bond stress in equivalent (linear) bond relationship
$\tau_{b,max}$, τ_f, τ_m, τ_{max}	maximum bond stress
τ, τ_b, τ_{mean}, τ_s	average shear stress at the bond interface
ξ	relative load level
ξ_0	relative load level at which cracking initiates
ν	Poisson's ratio
ν_a	Poisson's ratio of adhesive

CHAPTER 1 INTRODUCTION

1.1 BACKGROUND

In recent years, there has been an increased need for the strengthening or rehabilitation of reinforced concrete (RC) structures, due to the aging of infrastructure, the demand for higher vehicle loads, updates in design codes or inadequate original designs. An effective method for increasing the capacity of reinforced concrete beams is through the use of externally-bonded reinforcement. Traditionally, steel plates have been bonded to the soffits of beams to raise their flexural strengths. However, within the past 10 years, the application of fibre reinforced polymers (FRP) as external reinforcement has received much attention from the structural engineering community. FRP plates or fabrics are preferred over steel plates mainly due to their high tensile strength, high strength-to-weight ratio and corrosion resistance. Increase in structural weight is negligible, while the durability of covered members is enhanced. Due to their light weight, field use of FRP plates or fabrics requires less labour and equipment, resulting in shorter periods of disruption to services. As FRP material is flexible, it can be utilized in any configuration to match the strength requirement of the RC member. Although the material costs may be high, they are offset by the low installation and maintenance costs.

1.1.1 *FIELD APPLICATIONS OF FRP COMPOSITES*

Field applications of FRP for flexural or shear strengthening of RC members can be found around the world today. FRP sheets are applied with the fibre direction oriented parallel to the longitudinal axis of the members to increase flexural strength, and are bonded to the webs of members to raise shear capacity. In Sherbrooke, Quebec, Canada, the rehabilitation of Webster Parkade, built in 1959, involved strengthening of the main beams with FRP sheets. An increase of 15% in flexural capacity and 20% in shear capacity was achieved [1]. Single-ply carbon fibre reinforced polymer (CFRP) strips were bonded to the deck soffit of Bridge J-857 in Phelps County, Missouri, USA to enhance its moment capacity. Although a 30% increase was desired, it was found after testing to failure (this bridge was scheduled for demolition) that the moment capacity increased by only 17%, with a combined failure mode of rupture and peeling of the CFRP sheets [2]. In Japan, not only has FRP composites been used for flexural and shear strengthening, but many structures have undergone seismic retrofitting using FRP since the 1995 Hansin Earthquake [3]. Many projects have been completed in Europe, with more than 1000 applications of CFRP plate bonding in Switzerland alone [4].

1.1.2 *RESEARCH WORK INVOLVING FRP COMPOSITES*

Rapidly advancing research in the area of FRP technology for the repair or strengthening of RC members have enabled practical applications to be undertaken. Numerous experimental studies have proved that externally-bonded FRP can significantly increase a member's strength and stiffness. However, there have also been reports of reductions in ductility associated with brittle behaviour due to bond failure [5-7]. Such premature failure leads to an inefficient use of the FRP material and prevents the strengthened members from reaching their full capacities.

To complement experimental tests, analytical methods must be established so that preliminary designs for specifying externally-bonded FRP can be verified. Detailed analyses of these designs can be performed with a nonlinear finite element program. Results from such a program have shown good agreement with experimental data, in terms of the increased stiffness of FRP-reinforced members. However, it was noted that the numerical program tended to overestimate the failure load of the member since debonding failure was not taken into account [8].

Debonding failures are governed by the local bond stress-slip relationship between the concrete and FRP. Thus, it is imperative to consider the relative displacement between them. The bond-slip at the interface between the two adherents must be modelled to accurately predict the ultimate capacity and failure mode of FRP-strengthened RC members. Since finite element programs are based on displacement compatibility at the element nodes, accounting for bond-slip can be accomplished through the use of interface bond elements.

1.2 OBJECTIVE OF CURRENT RESEARCH

The current research has been conducted to further the modelling capabilities of the nonlinear finite element program VecTor2 to include FRP-strengthened RC members while accounting for bond-slip. An experimental program was undertaken to study the debonding phenomenon in RC beams strengthened in shear with CFRP composites. Finally, the program VecTor2 was verified by corroborating with specimens studied by other researchers and with those tested in the current program. Trends noted in the experimental and analytical work will be summarized, along with suggestions for future research.

1.3 LAYOUT OF CHAPTERS

This report is divided into seven chapters, the remaining six of which are organized as follows:

Chapter 2 – a review of published literature regarding experimental and analytical work on RC members with externally-bonded FRP composites (for flexural or shear strengthening), and studies to characterize the bond behaviour between concrete and FRP

Chapter 3 – a description of the Modified Compression Field Theory and the nonlinear finite element program VecTor2, and formulations for bond elements (link and contact elements) used to model the concrete-FRP interface

Chapter 4 – details of an experimental program involving three shear-critical beams externally reinforced with FRP fabric, along with test observations, analysis and discussion of results

Chapter 5 – corroboration of program VecTor2 with test specimens strengthened in flexure or shear with FRP composites: experimental details, modelling considerations and results

Chapter 6 – discussion of trends in experimental and analytical work, and the need for future experimental and analytical work

Chapter 7 – conclusions drawn from the current research

CHAPTER 2 LITERATURE REVIEW

2.1 INTRODUCTION

Due to the many advantages of using FRP as external reinforcement for RC members, extensive research has been carried out regarding their performance. Much of the research has concentrated on flexural strengthening, where FRP laminates are bonded to the top or bottom surfaces of beams in the maximum moment regions. However, the number of experiments in which FRP is bonded on beam webs as shear reinforcement has also increased within the past few years. Besides studying the global response of beams strengthened with FRP, some researchers have focused their attention on the local behaviour at the bond interface. Attempts have been made to characterize the bond behaviour at the interface where premature failures initiate. To expedite the usage of FRP in field applications, design procedures must be developed. Numerous experiments were required to build up a database of results, leading to the large volumes of published literature regarding such tests. The amount of analytical work is also on the rise, pointing the way to comprehensive guidelines that can be used for the design of such members. As for numerical modelling employing the finite element method (FEM), successful attempts have been reported in the area of flexural strengthening, while simulations of shear-strengthened RC beams are limited in number.

2.2 FLEXURAL STRENGTHENING WITH FRP COMPOSITES

The main reason for the introduction of FRP laminates into structural engineering applications was to replace the heavy and corrosive-prone steel plates traditionally used for the flexural strengthening of RC beams. Thus, a large amount of research has ensued, in an effort to get a better understanding of the overall behaviour of strengthened beams and the local behaviour at the plate ends.

2.2.1 *GLOBAL BEHAVIOUR*

While earlier work was predominantly experimental, more recent tests have usually been followed by analytical or numerical modelling. The papers reviewed in this section will focus on analytical work that has been undertaken, both excluding and including the characteristics of the adhesive interface layer.

2.2.1.1 ANALYSES NOT INCLUDING CHARACTERISTICS OF ADHESIVE LAYER

RC beams strengthened with CFRP plates and sheets were tested by Arduini *et al.*[9], in which failure mechanisms included FRP rupture, concrete shear at the end of the FRP reinforcement, and FRP debonding. The beams were modelled with FE analysis, using a commercial package based on a smeared crack approach. Beams strengthened with CFRP plates were analyzed with a 2-D mesh, while those bonded with CFRP sheets were modelled in 3-D. FRP reinforcement was applied directly over the concrete elements, and perfect bond was assumed. Load-deflection curves for the beams bonded with FRP plates are given in Figure 2.1, with results obtained from experiments and numerical simulations. Although good accord was found between these curves, the numerical results were stiffer than the plots from the tests. This can be attributed to the perfect bond assumption, and the limited number

of nodes that could be used. The FE analysis showed that high shear stresses at the end of the FRP plate had caused the delamination failure of the beam.

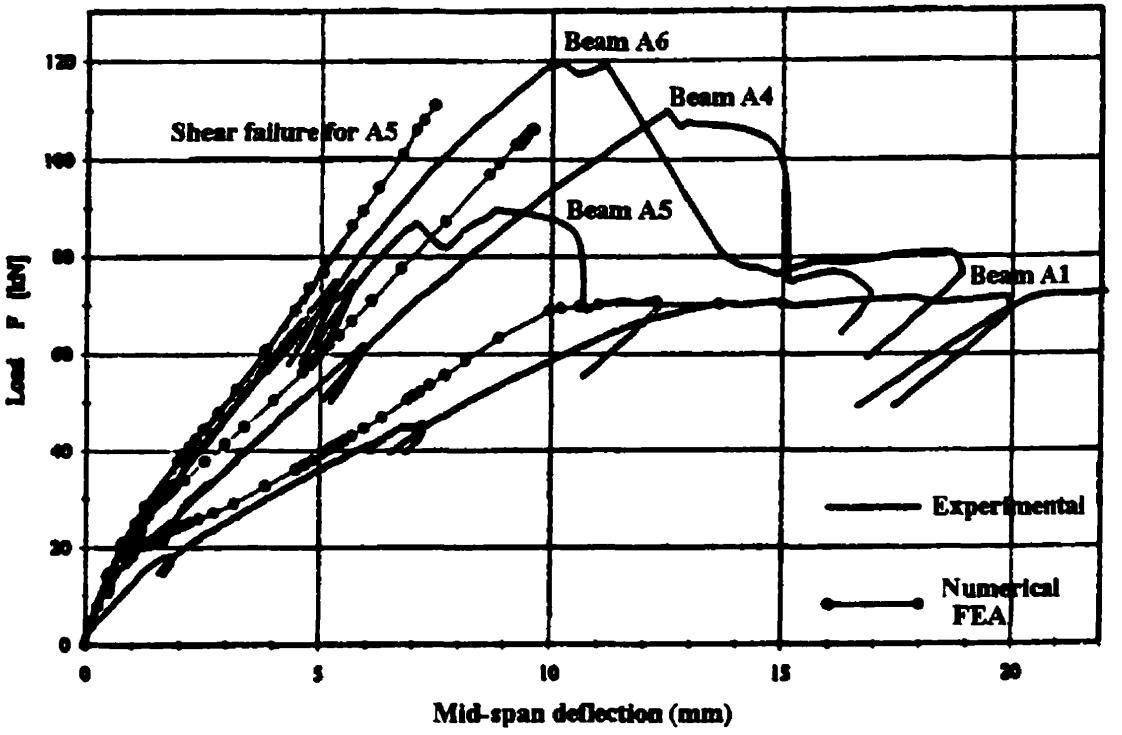

Figure 2.1: Experimental and FEA results for beams bonded with CFRP plates[adapted from 9]

Ross *et al.*[5] also tested large-scale RC beams strengthened in flexure with three-ply uniaxial CFRP laminates. For beams that were lightly to moderately reinforced with longitudinal steel (reinforcement ratio less than 1.5%), the failure was dominated by delamination between the CFRP plate and the adhesive. Despite the brittle failure, the peak load enhancement ratios (strengthened to control beams) for these beams ranged from 1.75 to 3.00. An elastic-plastic section analysis was used to produce the load-deflection curves for the beams tested. Each curve is divided into four regions, as shown in Figure 2.2, with a linear load-displacement relationship in each region. A trilinear curve is used to approximate the stress-strain behaviour of concrete, an elastic-plastic response is assumed for steel, and CFRP is linear elastic until failure. The points defining the load-displacement curve were determined using appropriate assumptions for the beam's behaviour within each region. In

region 4, concrete may crush before the FRP fails, but the FRP may debond at the FRP-adhesive interface (due to inadequate bond strength) or at the concrete-adhesive interface (due to low shear strength), so the calculated load P_4 is expected to be higher than the actual failure load.

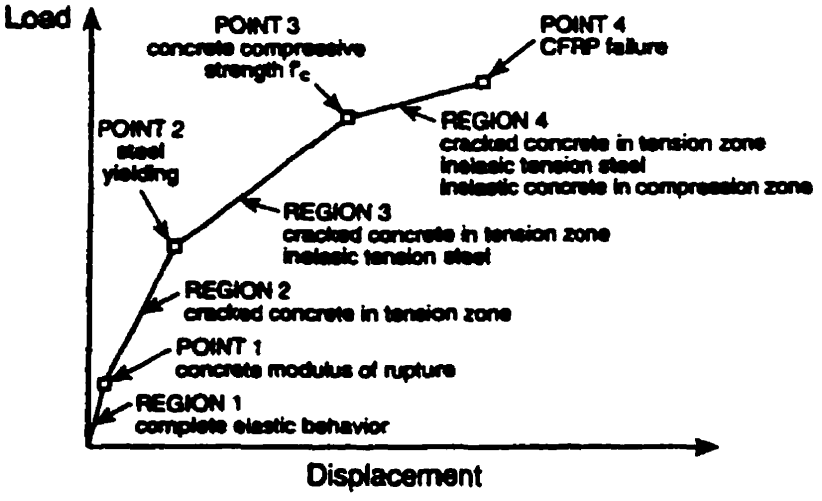

Figure 2.2: Load-deflection response assumptions in beam section analysis [5]

Nonlinear FEM analyses were performed for some of the beams tested using program ADINA. Two-dimensional, eight-noded plane stress elements were used to represent the concrete, while the reinforcing steel and FRP plates were modelled by three-noded truss elements. The constitutive relation for concrete was a hypo-elastic model based on a uniaxial stress-strain relationship that can account for biaxial and triaxial conditions. Material models for the steel and FRP were the same as those employed in the sectional analysis. The load-displacement curves from the sectional and FEM analyses are compared to the experimental results for two groups of beams in Figure 2.3. Although both predicted curves are close to the actual response, the expected behaviour in region 4 is not achieved due to the delamination of the FRP plate. Thus, it was concluded that the single most important factor affecting the beams' response is the bond strength between concrete and FRP. The use of an anchorage system is suggested to prevent debonding and to utilize the full capacity of the plate.

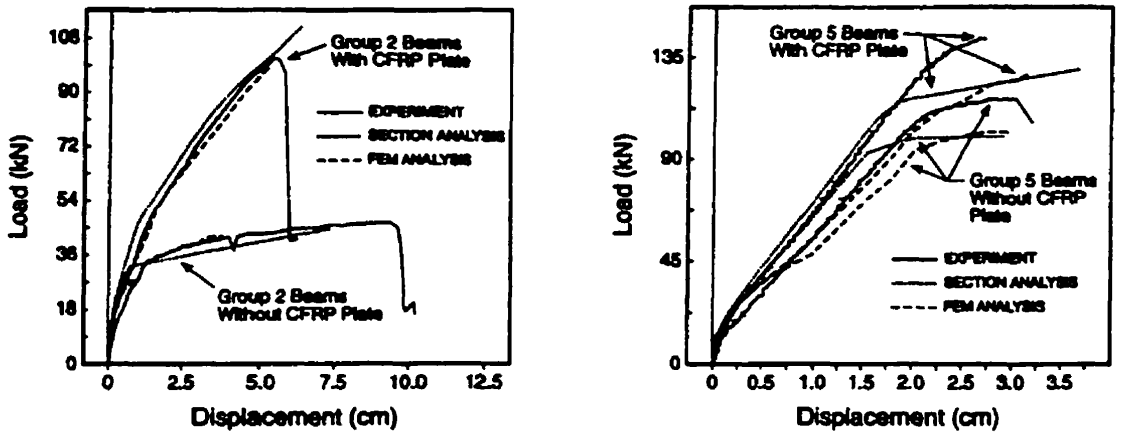

Figure 2.3: Comparison between analytical, FEM and experimental results by Ross *et al.*[5]

A nonlinear FE layered model was used by Nitereka and Neale [6] to simulate the behaviour of RC beams strengthened in flexure with FRP laminates. The beam is divided into several layers, in which the properties are assumed to be constant in each layer. Concrete is assumed to be nonlinear in compression, with post-cracking tension stiffening effects, and steel reinforcement is modelled as elastic-plastic. Individual FRP laminae are linear elastic, while an equivalent elastic modulus for the whole composite is obtained by the classical lamination theory for composite structures. Both types of reinforcement are smeared into the beam and are transformed into layers of equivalent area. Full bond between concrete and steel reinforcement is assumed, and bond-slip at the interface between concrete and FRP is neglected. Shear deformations are disregarded, and equal displacements are imposed at the interfaces of adjacent layers to ensure interlayer compatibility.

The iterative displacement-controlled numerical analysis program was validated using published test results for RC beams bonded with FRP plates. In Figure 2.4, the experimental load-deflection curve for the beam tested by M'Bazaa (1995) [6], which experienced a delamination failure, is shown. The failure load of this beam was 60% of the predicted ultimate load. In a subsequent test by Chicoine (1997) [6], in which U-shaped composite anchors were added at the ends of the beam, the load capacity was raised to 95% of the theoretical value. From the numerical analysis, it was concluded that tension stiffening

effects gave a more continuous load-deflection response, and that the concrete cover should be divided into several layers such that the load transfer from the concrete to the FRP can be represented realistically. Also, it was noted that the FRP strains predicted by the analysis did not match those measured in the experiment. This implies that slippage at the concrete-FRP interface had led to the delamination of the composites. Hence, the perfect bond assumption used in the numerical analysis was not justified.

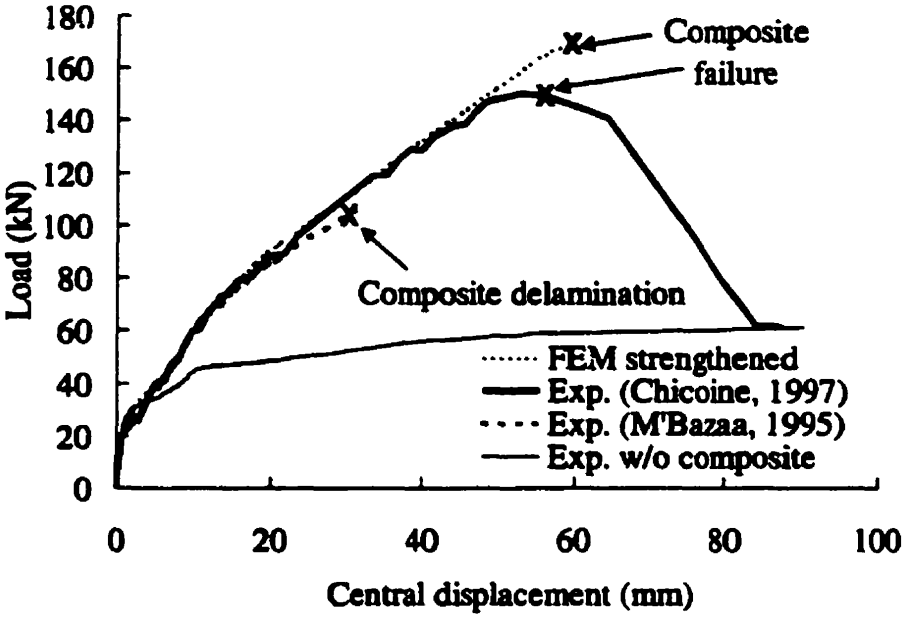

Figure 2.4: Comparison between analytical and experimental results for beams tested by M'Bazaa and Chicoine [6]

2.2.1.2 Analyses Including Characteristics of Adhesive Layer

Arduini and Nanni [7] conducted experiments in which CFRP sheets were bonded to the soffits of precracked RC beams. They concluded that the CFRP significantly enhanced the ultimate load capacity of the beams, while the flexural stiffness was increased to a lesser extent. However, the ductile response of the control specimens was often changed to a brittle failure mode in the members bonded with FRP. The authors recommended further studies in

the area of concrete-FRP adhesion in order to limit the extent of FRP peeling so that the strengthening technique can be more effective. Two tests were performed to determine the bond interface characteristics: a tension + shear test (Figure 2.5(a)) and a compression + shear test (Figure 2.5(b)), where two saw-cut pieces of concrete were joined by a layer of adhesive and subjected to tension or compression. A Mohr-Coulomb failure envelope was constructed from the results, from which it was found that the shear strength at the concrete-adhesive interface was approximately 5 MPa for the adhesives tested. A similar test in which two FRP plates were first bonded to the concrete surfaces, and then glued together, was later conducted. It was concluded that the shear strength of the FRP-adhesive interface was about three times higher than that of the concrete-adhesive interface.

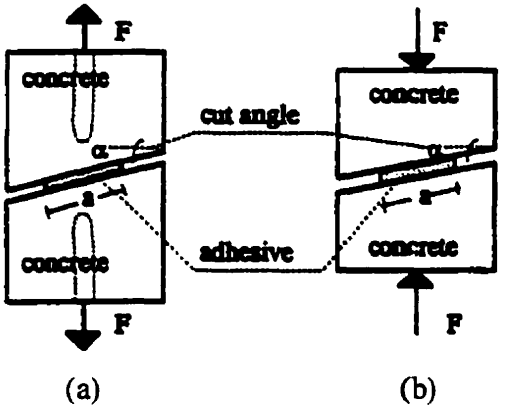

Figure 2.5: Concrete-adhesive specimens: (a) tension and shear, (b) compression and shear[7]

An analytical model (described by Arduini *et al.*[9]) was also used to predict the response of the beams, using nonlinear constitutive relations for concrete, bilinear elasto-hardening response for steel, and linear elastic behaviour for FRP and adhesive. The beam was discretized into a certain number of segments, and cracks were uniformly distributed along each segment. The equilibrium equations for flexural moments and normal forces must be satisfied for each segment. At the concrete-FRP interface, shear stresses arise from the difference in normal forces acting on the two ends of the FRP segment, and a triangular shear stress distribution was assumed. The distribution of the normal stresses caused by secondary effects at the interface was assumed to be linear with maximum values at the ends of the

segments. Four failure modes could be predicted by this model: shear failure and tensile fracture of concrete, FRP rupture, and local failure of the adhesive (when its ultimate tensile strain was reached). Once the maximum value of shear stress or normal stress was reached at the bond interface of one segment of the beam, the FRP reinforcement would be disconnected from the concrete in that segment.

Analytical and experimental load-deflection curves for a set of specimens are given in Figure 2.6. Near the ultimate load, the analytical curves were stiffer than the experimental results, and tended to overestimate the failure loads. This may be attributed to the "plane sections remain plane" assumption and the fact that the effects of local debonding were not included. In the tests, it was noted that the FRP sheet delaminated at a crack in the constant moment region, leading to the progressive debonding of the sheet. However, for the results presented, the analytical-to-experimental ratios of ultimate load and ultimate deflection were 1.06 and 0.96, respectively, and the predicted failure modes agreed with those observed.

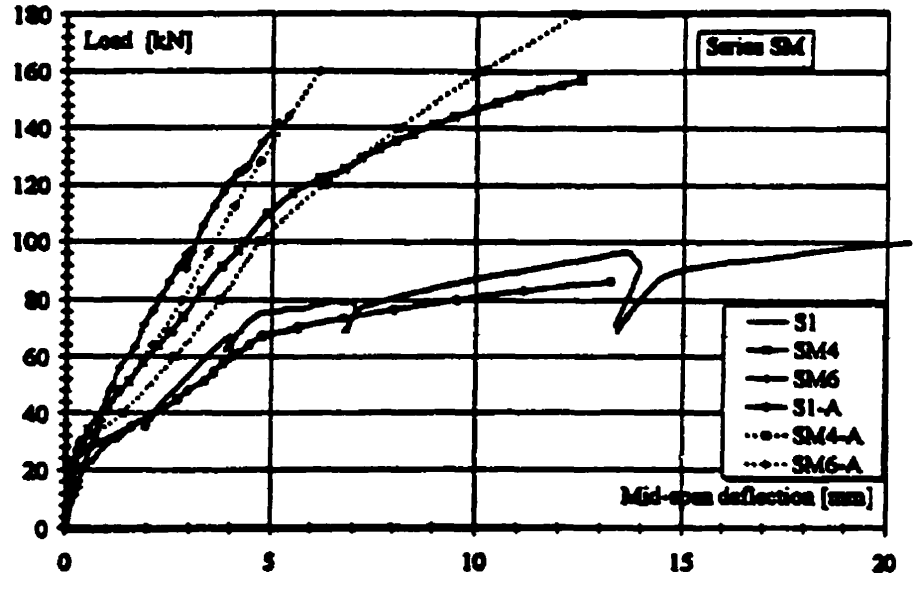

Figure 2.6: Comparison between analytical and experimental results by Arduini and Nanni[7]

Small-scale beams with CFRP plates bonded to the soffits were studied by Bokan-Bosiljkov *et al.*[10]. Numerous drops in flexural load were observed during the test. These were attributed to the progressive separation of the CFRP plate from the concrete just above the adhesive layer at local shear-peeling cracks, a process that had initiated from the plate end. The CFRP plates delayed crack development, and changed the failure mode from flexural-shear to a shear dominated failure. The authors also used analytical formulae derived by Täljsten (1997) [10] to estimate the shear and peeling stresses at the plate ends when plate separation started. The calculated peak shear stress of 4.2 MPa was much lower than the bond shear strength between epoxy and concrete of 15 MPa. However, the maximum peeling (normal) stress of 3.3 MPa was close to the bond tensile strength between concrete and adhesive of 4 MPa. Thus, it was deduced that the high peeling stresses at the plate end had caused the separation of the plate from the beam soffit. A nonlinear 3-D FEM program (described by Žarnić *et al.*[11]) was used to model the short-span beams. Each component of the beam (concrete, steel reinforcement, epoxy and CFRP plate) was represented separately. CFRP was assumed to be elastic, while all other materials were modelled with strain softening. Results of the numerical modelling are plotted in Figure 2.7. Although the initial stiffness matched the experimental results, the post-cracking stiffness was higher than the test data. Nonetheless, the predicted ultimate loads were close to the actual values.

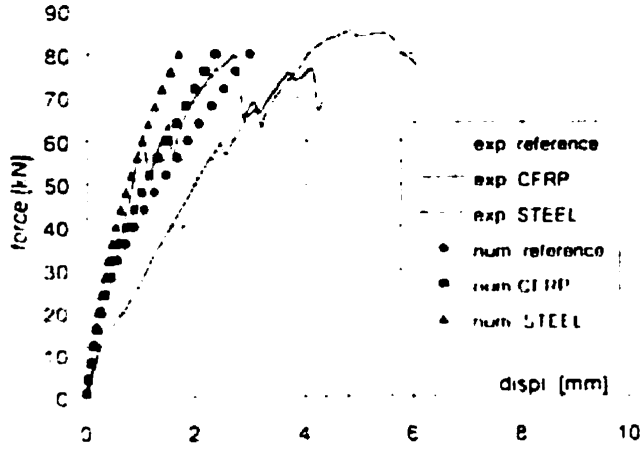

Figure 2.7: Comparison between analytical and experimental results by Bokan-Bosiljkov *et al.*[10]

Rahimi and Hutchinson [12] tested concrete beams with CFRP or glass FRP (GFRP) laminates bonded to the soffit in four-point bending. Similar to the experiments performed by other researchers, it was found that the CFRP plates enhanced both the stiffness and strength of the beams, with a maximum increase in ultimate load-carrying capacity of 230%. The authors also concluded that the amount of tensile steel and internal shear reinforcement affected the magnitude of the performance enhancement. It has been noted that the tensile force in FRP increases at a greater rate after the flexural steel yields. For highly reinforced beams, the compressive strain of concrete is close to the ultimate value when the flexural steel yields. Thus, the enhancement of the beam's load capacity by the FRP reinforcement is limited. As the quantity and modulus of the CFRP laminates increased, the strength and post-cracking stiffness of the beams rose accordingly. The characteristics of the concrete cover play a large role in determining the ultimate load of plated beams. In beams with thinner laminates, the failure was in the concrete cover close to the loading point within the shear span. A layer of adhesive and cement paste was found on the FRP surface where plate detachment occurred. For beams with thicker plates, the failure location shifted towards the plate ends where the shear and normal peeling stresses increased. At ultimate load levels, the interface shear stress averaged along the beam was higher for beams with thicker FRP plates. However, peeling at the plate ends was not a primary failure mechanism for the FRP-bonded beams, as is usually the case for steel-plated beams. For all of the FRP-strengthened beams tested, plate delamination was involved, preceded either by failure within the cover or by concrete shear failure resulting in cover separation.

The LUSAS FE program was then utilized to predict the response of the externally-reinforced beams. This program is based on a smeared crack concept, and incorporates an isotropic damage model to simulate the nonlinear behaviour of concrete. Four-noded or eight-noded quadrilateral isoparametric elements were used to model concrete, while steel rebars were smeared onto concrete as two- or three-noded bar elements. For strengthened beams, triangular elements were placed in the transition zone to reduce the element size toward the bond zone, as illustrated in Figure 2.8. The adhesive layer and FRP laminates

were each modelled with a row of four- or eight-noded elements and the adhesive was assumed to be elastic.

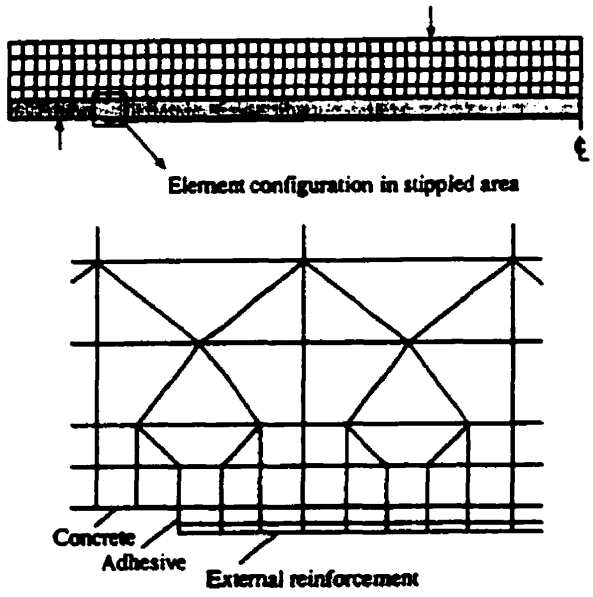

Figure 2.8: Typical FE mesh for RC beam with externally-bonded FRP reinforcement [12]

The FE predictions were sensitive to the concrete tensile strength, and a value of 1.5 MPa (for compressive strengths ranging from 54 to 69 MPa) was found to give the best agreement with the experimental load-deflection curves. The stiffness was slightly overestimated, but all predicted solutions for beam strengths were within 20% of the test results. Interface shear stress values were estimated; peak stresses occurred at the plate ends at low load levels, but the location of the peak stress shifted as loading increased, depending on the type and amount of external reinforcement (Figure 2.9). However, the magnitudes of the predicted peak stresses were up to three times lower than the maximum values measured from the experiments. In the FE analyses, principal stress was chosen as the failure criterion parameter since it combines the effects of normal and shear stresses. The limiting principal stress at the concrete-FRP interface was determined to be 1.7 MPa, and its exact location depended on the thickness of the FRP laminates. A higher principal stress would lead to failure just within the concrete, since the tensile strength of concrete is much lower than that of the adhesive.

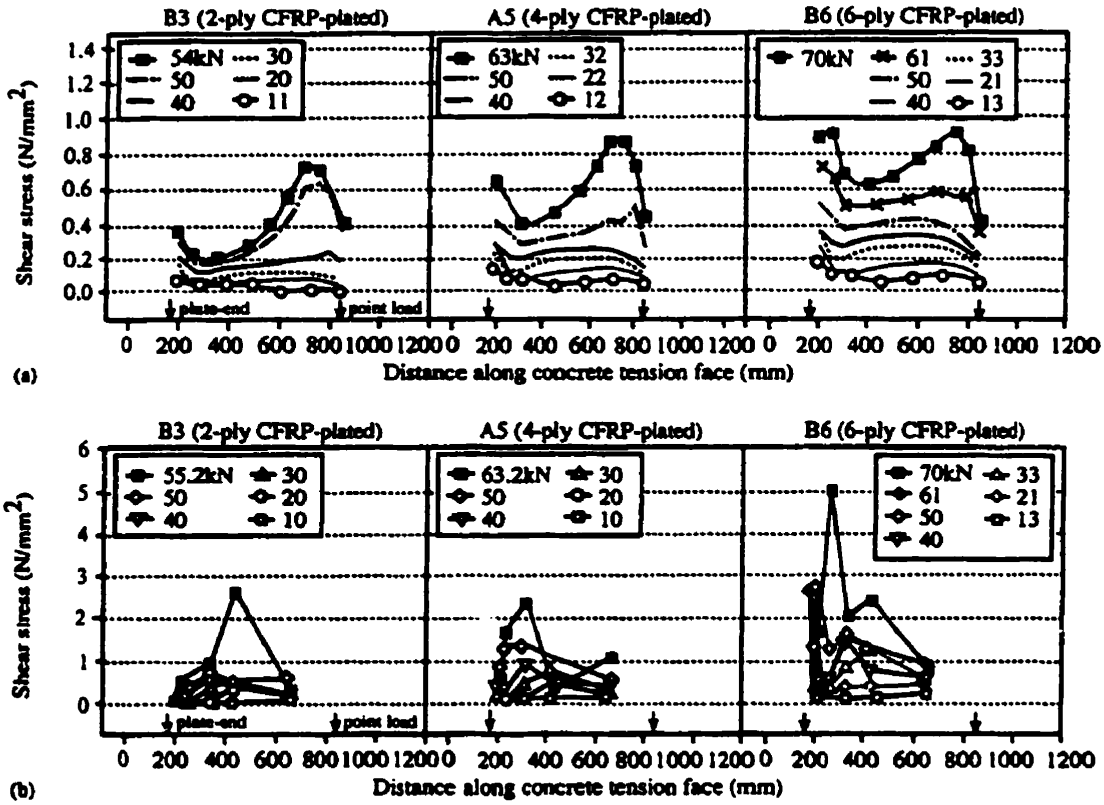

Figure 2.9: (a) Predicted and (b) actual shear stress distribution at concrete-FRP interface[12]

In a study by Limam and Hamelin [13], 2-D nonlinear FE simulation was used to predict the response of RC beams with CFRP sheets bonded to the tension face. In the FE model, eight-noded membrane elements were used to represent concrete, two-noded truss elements were adopted for steel and CFRP reinforcement (Figure 2.10). Whereas perfect bond was assumed between steel reinforcement and concrete, bond-slip was considered in the concrete-FRP interface through the use of two-noded continuous contact elements.

Experiments were performed to examine the behaviour of the bond interface, and it was found that the nonlinear behaviour varied according to different combinations of materials, as depicted in Figure 2.11. Factors affecting the stiffness of the interface behaviour included the mechanical properties of concrete, the characteristics of the adhesive, and the surface treatment.

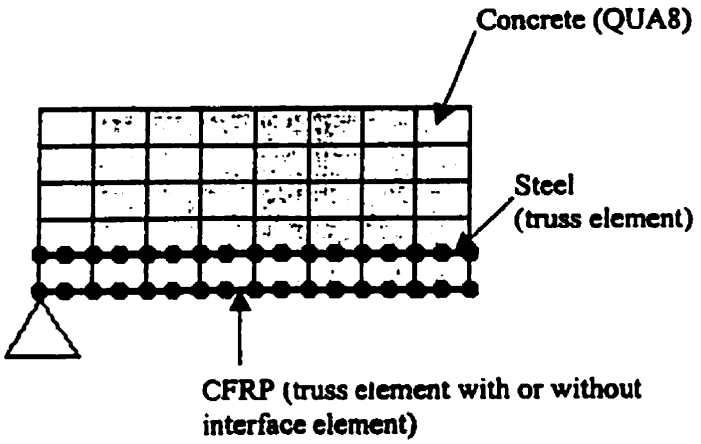

Figure 2.10: Finite element mesh employed by Limam and Hamelin [13]

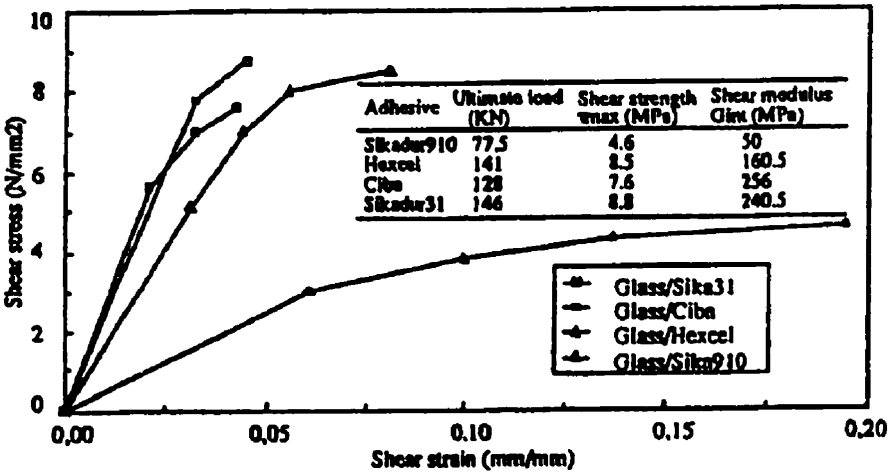

Figure 2.11: Characterization of bond interface behaviour [13]

The concrete model was based on different yield surfaces in the tensile and compressive regions, and a smeared crack approach was applied. Steel reinforcement was idealized by an elasto-plastic model with strain hardening. Results from experimental tests were used to define a constitutive law for the interface layer of Mohr-Coulomb junction elements. Figure 2.12 compares the numerical results with the experimental data. Accurate modelling of the interface (P_1 (num)) predicted an ultimate load and deflection that were within 10% of the actual values. On the other hand, a non-realistic model for the interface led to large discrepancies between the analytical curve (P_a) and the test results (P_1 (exp)).

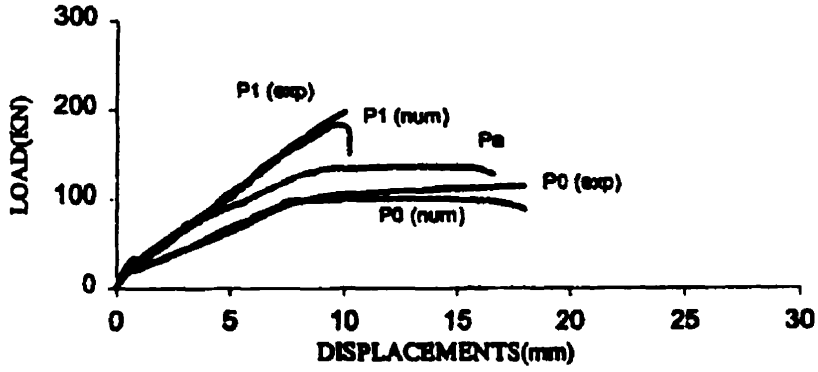

Figure 2.12: Comparison between analytical and experimental results by Limam and Hamelin [13]

2.2.2 *LOCAL BEHAVIOUR*

After extensive studies on the global behaviour of RC beams retrofitted with FRP in flexure, researchers have grouped the failure modes into the following categories: (i) steel yield and FRP rupture, (ii) crushing of concrete in compression, (iii) shear failure, (iv) debonding of concrete cover along the flexural steel, (v) delamination of the FRP plate, and (vi) peeling of FRP due to shear cracks. These failure modes, along with sample load-deflection curves, are illustrated in Figure 2.13 (a) and (b).

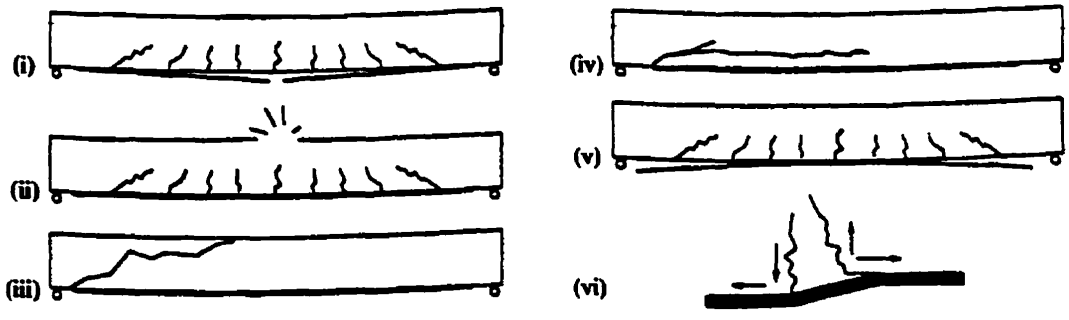

(a)

Figure 2.13: (a) Failure modes in FRP-bonded beams [14]

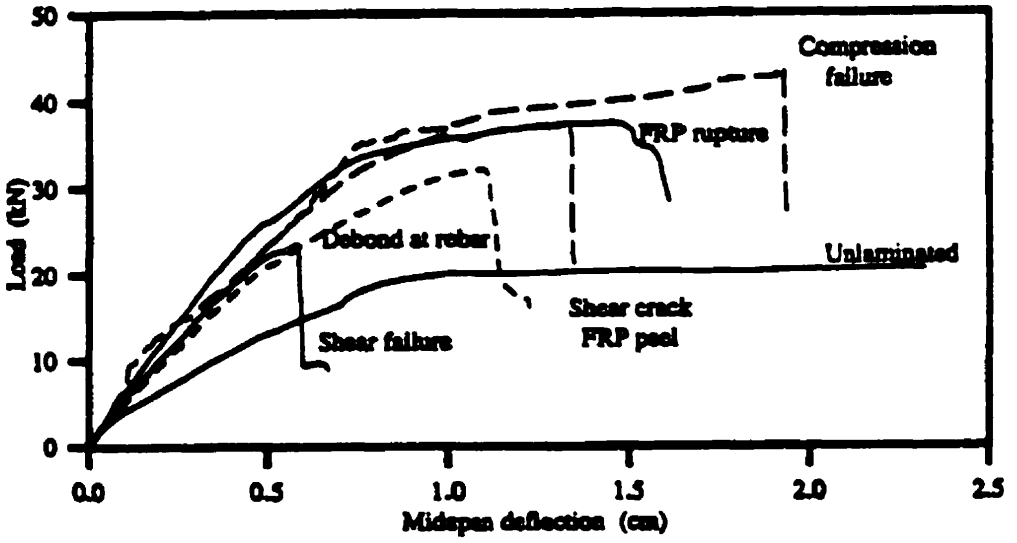

(b)

Figure 2.13 (continued): (b) Sample load-deflection curves [14]

While the conventional failure modes are affected by the ratios of the steel and FRP reinforcement, shear and debonding failures depend on factors such as the amount of shear reinforcement, existing cracks prior to retrofitting, the length of the FRP laminate, and the relative stiffnesses of the laminate, adhesive, and concrete. In the experimental program undertaken by Buyukozturk and Hearing [14], it was found that debonding failures occurred in beams with higher shear resistance. Debonding of the concrete cover along the flexural rebars took place in beams with shorter FRP laminates, in which interfacial stresses concentrated in the anchorage zone. On the other hand, peeling at shear cracks tended to occur in beams with longer FRP laminates, where significant shear cracks could be found. Some of the potential crack paths in debonding failures are illustrated in Figure 2.14.

It is widely recognized that debonding often leads to the premature failure of these beams. Numerous researchers have described these debonding mechanisms using various approaches. Local failure mechanisms can be generally categorized into two main groups: failure of the concrete cover (near the plate ends or along the beam) and peeling of the FRP (at the anchorage zone or at cracks along the beam).

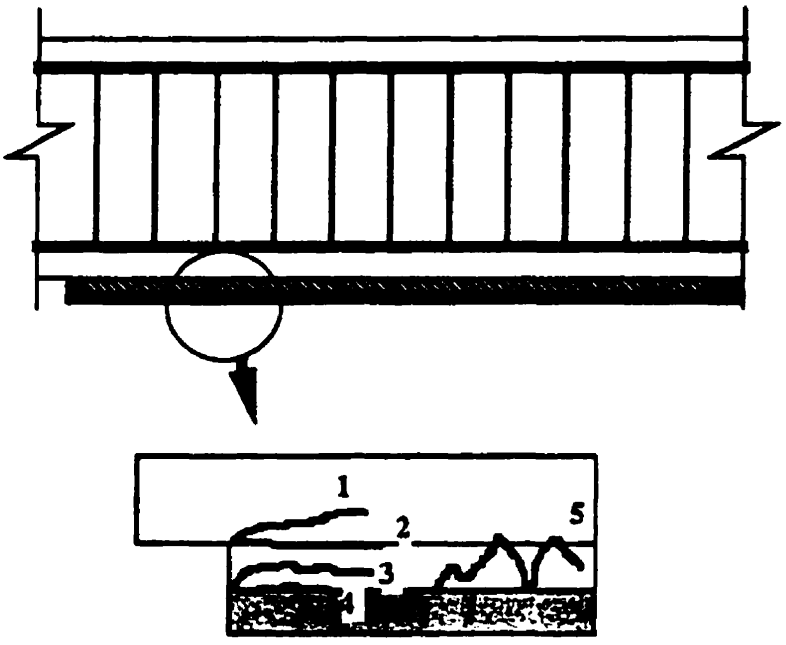

1: Peel failure into concrete
2: Interfacial failure between concrete and adhesive
3: Cohesive failure in the adhesive
4: Interfacial crack between the adhesive and the composite
5: Alternating crack path between the two interfaces

Figure 2.14: Potential crack paths in FRP debonding failures [15]

2.2.2.1 FAILURE OF CONCRETE COVER

Shear failure of the concrete cover between the steel reinforcement and FRP laminates can lead to the separation of the FRP plate. In this case, debonding usually starts from the end of the plate where high interface shear stresses arise. Delamination from the anchorage zone occurs when the interface shear stress reaches the limiting value (defined as a function of the concrete strength f'_c). This value has been found to be approximately 8 MPa for normal strength concrete [16].

An analytical formulation to predict the ultimate load of CFRP-plated beams due to concrete cover ripping was presented by Nguyen *et al.*[17]. This model is based on the

composite action of the RC beam and the FRP plate. Whereas plate debonding results from high local bond stresses and peeling forces near the FRP plate ends in the adhesive interface, the critical stresses for ripping of concrete are at the flexural steel level after shear cracks have developed at the plate ends. The shear crack causes an eccentricity between the tensile forces in the FRP plate and in the steel bars, leading to the ripping out of the concrete cover. From the experimental results, Nguyen *et al.* divided the composite behaviour of the FRP-plated beam (at ultimate) into three zones: (1) a "destressed" zone at the end of the plate where strains were approximately zero, (2) a "bond-development" zone in which the strains increased linearly, and (3) a "composite" zone where the plate acted compositely with the beam. The composite model, along with these three zones, is illustrated in Figure 2.15.

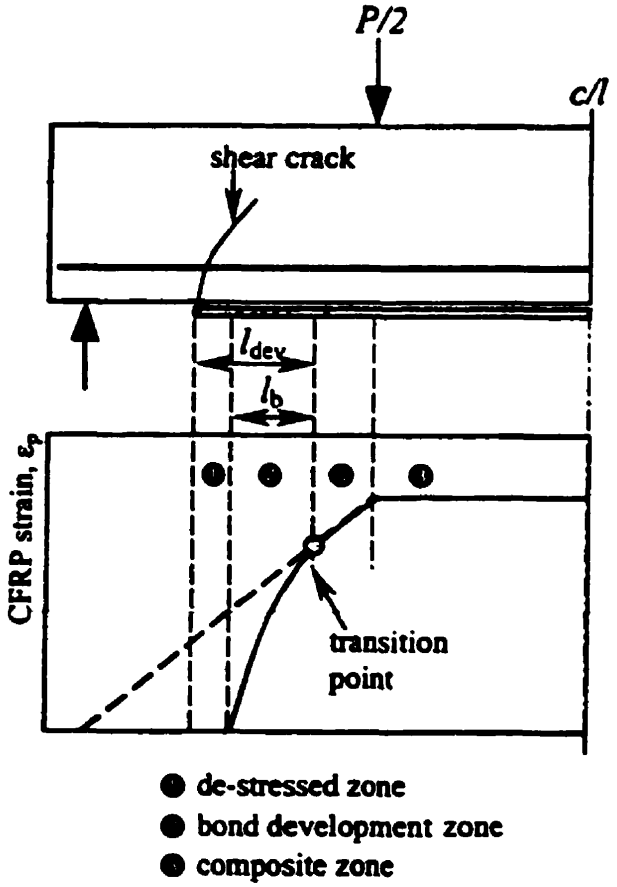

Figure 2.15: Composite model of concrete beam bonded with FRP plate [17]

It was concluded that if the plate strain at the transition point between the "bond-development" and "composite" zones was limited to a critical value (0.0017 in this case), ripping failures could be prevented. The axial strain in the plate at the transition point (ε_{pe}) is given as

$$\varepsilon_{pe} = \frac{1}{E_c}\frac{M_e}{I_c}(d_p - x) \tag{2-1}$$

where M_e is the applied bending moment at the transition point, E_c is the elastic modulus of concrete, I_c is the cracked equivalent moment of inertia of the composite beam section, d_p is the distance between the top of the beam to the center of the plate, and x is the distance from the top of the beam to the neutral axis. The location of the transition point from the plate end is determined by the bond development length (l_{dev}), which is determined by:

$$l_{dev} = c_m + \frac{d_p}{2} + \frac{4.61}{\lambda} \quad , \qquad \lambda^2 = \frac{1}{E_p t_p}\frac{G_a G_c}{G_c t_a + G_a c_m} \tag{2-2}$$

where c_m is the thickness of the concrete cover, E is the elastic modulus, G is the shear modulus, t is the thickness, and the subscripts p, a and c represent FRP plate, adhesive layer and concrete, respectively. The total bond development length was found to be independent of the applied load, the length of the plate and the shear span. Using a plate strain limit determined from simple bond tests and the two equations given above, the failure load of the beam due to concrete ripping can be predicted.

2.2.2.2 PEELING-OFF OF FRP

The propagation of a crack along the concrete-FRP interface can cause the bond to fracture in a brittle manner. Such a crack can form due to: non-uniform application of the adhesive, flexural cracks in the concrete, FRP peeling-off from an uneven concrete surface,

or fatigue loading. When the FRP composite on the beam soffit is subjected to tensile forces, the adhesive layer is loaded in shear to provide shear connection between concrete and FRP. Therefore, the crack propagation will be similar to fracture mode II. The critical strain energy release rate for the interface (G_{IIC}) is given by Triantafillou and Plevris [16] as

$$G_{IIC} = \frac{kP^2}{b}\frac{\partial C}{\partial a} \tag{2-3}$$

where k is a constant, P is the applied load, b is the member's width, C is the inverse of the gradient of the load-deflection curve, and a is the crack length. Fracture occurs when the value G_{IIC} is reached, and the load causing debonding can then be found.

Peeling-off of FRP laminates is associated with the formation of shear cracks in the concrete beam, which give a combination of horizontal (w) and vertical (v) openings, shown schematically in Figure 2.16. A relative vertical displacement between the two sides of a shear crack can initiate the peel-off.

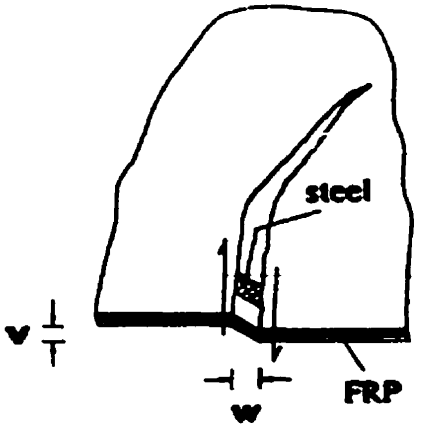

Figure 2.16: Crack openings leading to FRP peeling-off [16]

Assuming that the deformations in the longitudinal steel and FRP at the crack location are mainly due to shear, the load (P) at which FRP peels off can be written as:

$$P \propto \left(\frac{v}{w}\right)_{cr} \Sigma GA \tag{2-4}$$

where $(v/w)_{cr}$ is the critical ratio of vertical to horizontal crack opening (a property of the concrete-FRP bond) and ΣGA is the total shear stiffness of the steel rebar and FRP laminates. This type of failure is mostly found in beams with thicker laminates. Therefore, the thickness of the FRP laminate should be limited so that brittle peeling failure can be prevented.

Additionally, Blaschko *et al.* [18] listed four cases of FRP peel-off situations (besides peeling-off at shear cracks), as illustrated in Figure 2.17:

- FRP peeling-off beyond the outermost flexural crack in the uncracked anchorage zone
- FRP peeling-off at flexural cracks between the outermost crack and the maximum moment area
- FRP peeling-off at flexural cracks in the maximum moment region
- FRP peel-off due to uneven concrete surfaces

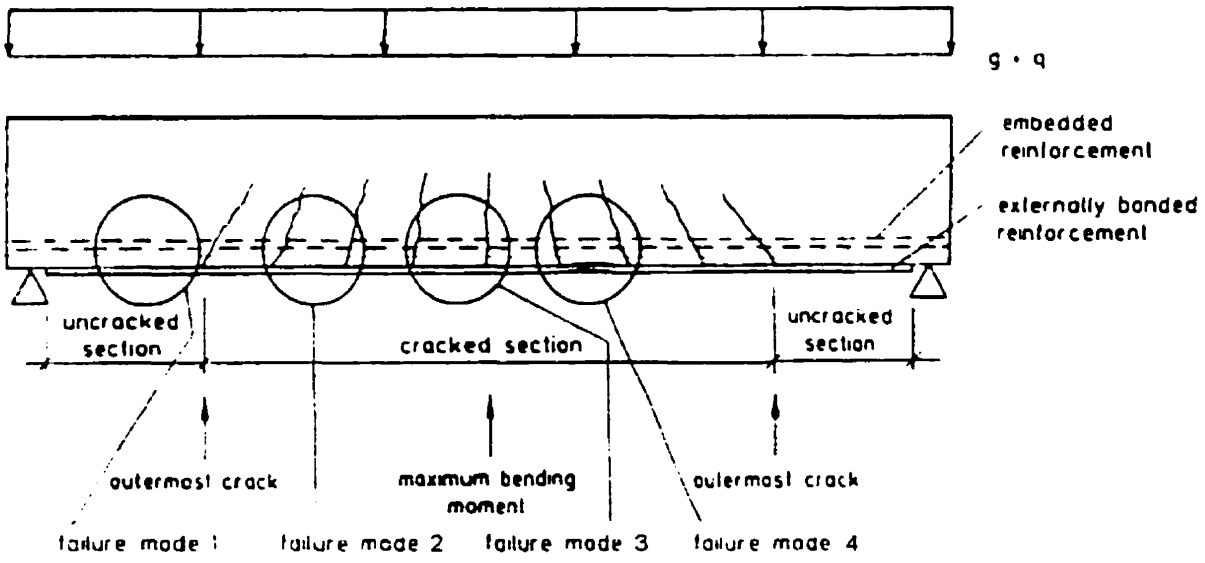

Figure 2.17: Locations of bond failure due to FRP peeling-off [adapted from 18]

For the case of FRP peeling-off beyond the outermost flexural crack in the uncracked anchorage zone, the authors suggested using an equation based on fracture mechanics to determine the maximum tensile force which can be sustained. It is recommended that the elongation of the FRP laminates be limited so that slippage and the occurrence of debonding can be reduced at flexural cracks. Within the maximum moment region, the bond behaviour is influenced by the amount of internal and external flexural reinforcement. FRP sheets bonded to an uneven beam soffit will be subjected to perpendicular diverting forces that can destroy the bond. Values for the permissible unevenness of the concrete surface were proposed (up to 5 mm over a length of 2 m for FRP thickness greater than 1 mm); thicker and stiffer laminates can tolerate higher deviations in surface roughness.

Malek *et al.* [18] presented closed-form solutions for calculating the maximum shear and normal stress concentrations in the interface at the plate cut-off point. Linear elastic behaviour was assumed for the materials, and a discrete crack model was applied. The proposed method was verified by comparing its results with those from a finite element analysis using program ABAQUS. An example of the finite element mesh around the plate cut-off point, with five layers of elements in the adhesive, is depicted in Figure 2.18. Good agreement was found between the results, both for the interfacial shear and normal stresses near the cut-off point, as shown in Figure 2.19.

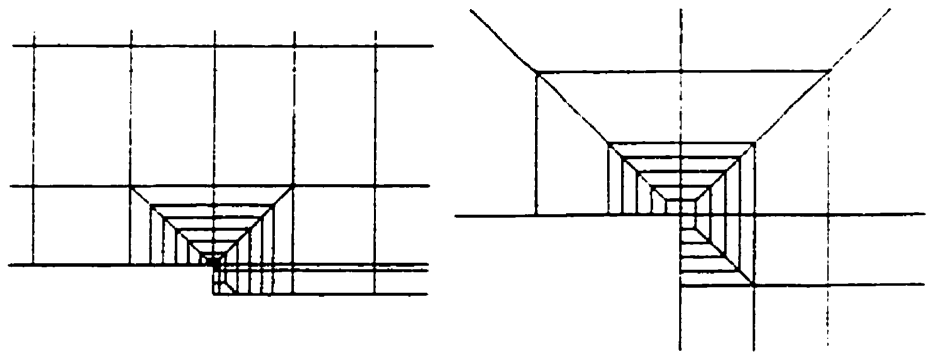

Figure 2.18: Mesh definition at the FRP plate cut-off point [19]

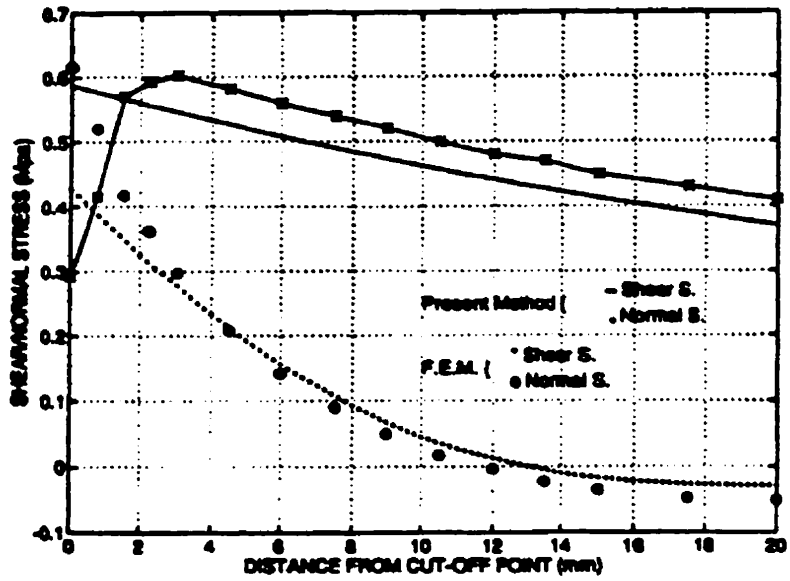

Figure 2.19: Comparison of shear and normal stresses near FRP plate end [19]

An approach for predicting the premature debonding phenomenon in RC beams bonded with FRP plates was presented by Mukhopadhyaya and Swamy [20]. Whereas the analytical models proposed by other researchers predicted shear and normal stress concentrations near the FRP plate ends, the model presented uses the interface shear stress to predict plate debonding failure. The concept of the interface shear stress is based on a limiting value of shear stress between the concrete and FRP plate which becomes critical near the plate cut-off end. From experiments in which FRP plates debonded at the cut-off point, it was found that the critical interface shear stress varied between 0.33 to 1.35 MPa for CFRP plates, and from 0.26 to 0.90 MPa for GFRP plates. As the stiffness and relative moment contribution of the FRP plate increased, the interface shear stress also increased. Plate debonding is more likely to take place in beams with a depth to width ratio of 2.0 or more, or in beams with a shear span to depth ratio greater than or equal to 6.0. A minimal increase in interface shear stress with an increase in concrete strength was noted.

2.2.2.3 CONSIDERATION OF BOTH FAILURE MODES

Varastehpour and Hamelin [21] developed an analytical model to predict the strength and stiffness of RC beams bonded with FRP plates, including failure modes such as concrete crushing, FRP fracture or FRP plate separation from the beam soffit. The model was based on the compatibility of deformations and equilibrium of forces, accounted for material nonlinearity, and simulated the bond-slip at the concrete-FRP interface. The general algorithm of calculation for this iterative analysis technique is depicted in Figure 2.20.

Since bond-slip lowers the stiffness and failure load of RC beams bonded with FRP, the mechanical properties of the interface must be determined. From the results of a direct shear test, it was concluded that the interface exhibits a bilinear stress-strain relationship, and is highly influenced by the surface treatment, as shown in Figure 2.11. Once the shear stress at the interface has been estimated, the corresponding slip can be determined from the stress-strain curve for the interface. This slip value is then subtracted from the FRP plate strain before calculating the FRP tensile stress for the equilibrium of forces in the section.

Based on the equilibrium of the internal forces, strain compatibility and the nonlinear behaviour of materials, the average shear stress at the interface (τ) is given by:

$$\tau = 0.5\beta^{0.5}(\lambda V)^{1.5} \tag{2-5}$$

$$\text{where} \quad \beta = \frac{1.26\times10^5 a}{0.7 h t_p E_p} \quad , \quad \lambda = \frac{y_p t_p \eta}{I_t} \quad , \quad \eta = \frac{E_p}{E_c}$$

in which V is the shear force, λ is the sectional rigidity, a is the shear span, h is the height of the beam section, and t_p and E_p are the thickness and elastic modulus of the FRP plate, respectively, y_p is the distance from the neutral axis to the FRP plate, I_t is the transformed second moment of area in terms of concrete, and η is the modular ratio.

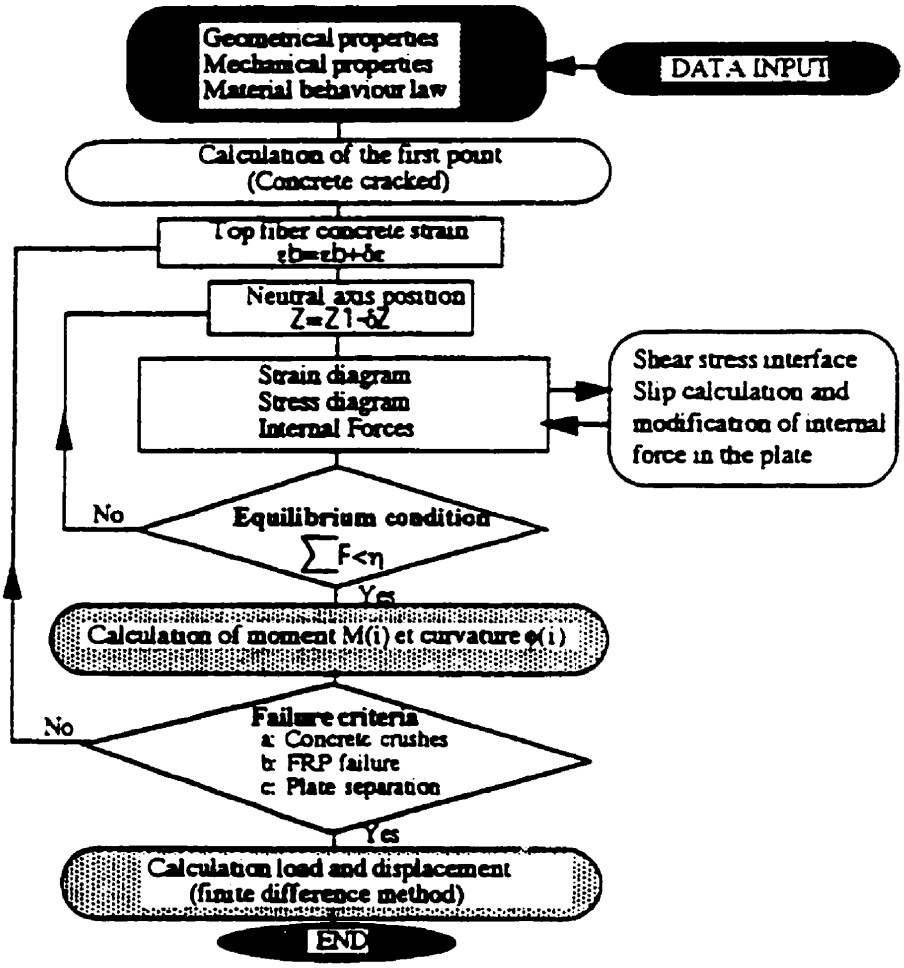

Figure 2.20: Flow-chart of calculations for theoretical model [22]

Equations defining the failure criteria for two types of premature beam failure were also presented. For failure of the concrete cover along the longitudinal steel reinforcement, the concrete between consecutive flexural cracks is assumed to behave as individual teeth, acting as cantilever beams under the influence of the lateral shear stresses at the FRP bond interface (Figure 2.21). Debonding occurs when the tensile stress near the longitudinal steel reaches the concrete tensile strength (f'_t). The admissible shear stress (τ_{adm}) at the interface is obtained as:

$$\tau_{adm} = \frac{(f'_t \, l_c / 6d')}{(b/b_p)} \tag{2-6}$$

where l_c is the flexural crack spacing (about equal to the stirrup spacing), d' is the concrete cover thickness (between steel and FRP), b is the beam width, and b_p is the width of the FRP plate.

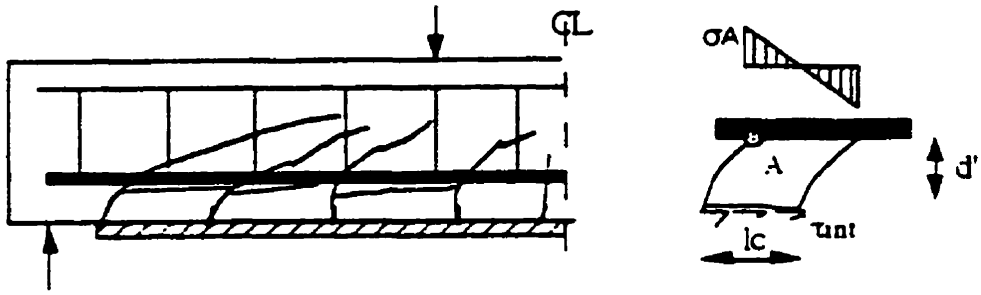

Figure 2.21: Cracked beam and concrete tooth acting as cantilever beam [21]

For the case of plate debonding, where the failure is governed by the Mohr-Coulomb law, the admissible shear stress (τ_{adm}) that can be sustained at the interface is determined to be:

$$\tau_{adm} = \frac{5.4}{1 + K \tan 33^\circ} \tag{2-7}$$

$$\text{where} \quad K = 1.31 \left(\frac{t_p E_a}{t_a E_p} \right)^{1/4}$$

T and E denote thickness and elastic modulus, while the subscripts p and a represent the FRP plate and adhesive, respectively. This model does not account for the concrete strength nor the effective bond length (the distance over which bond stress can be effectively transferred).

For a beam subjected to four-point bending, the plate separation load can be calculated as

$$P_{sep} = \frac{3.2\tau_{adm}^{2/3}}{\lambda\beta^{1/3}} \quad (2\text{-}8)$$

where τ_{adm} is the minimum of the values given by equations (2-6) and (2-7). For beams bonded with thick FRP plates, the separation load corresponds to the ultimate capacity of the beam. This theoretical model was validated against experimental results for four FRP-strengthened beams which had failed by plate separation due to failure of the concrete cover. The predicted moment-curvature relationships matched the test results almost perfectly.

Estimation models for three debonding failure mechanisms for RC beams bonded with FRP sheets on the tension face were also presented by Wang and Ling [22]. The tooth peeling failure model is similar to that proposed by Varastehpour and Hamelin [21], as described previously. When the interface shear stress reaches the allowable value, defined by Eqn. 2-6, debonding can occur at the steel-concrete interface or concrete-FRP interface. The anchorage shear failure model is based on comparing the uniform shear stress (τ_s) at the concrete-FRP interface against three shear strength values. The shear stress can be estimated by Eqn. 2-9, in which σ_f is the tensile stress in the FRP of thickness t_f and L_s is the shear span.

$$\tau_s = \frac{\sigma_f t_f}{L_s} \quad (2\text{-}9)$$

The values to be checked include the shear strength of the adhesive, the interfacial friction resistance between the concrete and adhesive, and the shear strength of the concrete. In general, the concrete's shear strength is the weakest, and will govern the anchorage shear debonding failure. The response of RC beams bonded with two plies of FRP sheet was predicted with an analysis neglecting debonding failure, and with the two models mentioned above. Results from the two debonding models were in close agreement with the test data, while the analysis disregarding debonding overestimated the ultimate load, as shown in Figure 2.22.

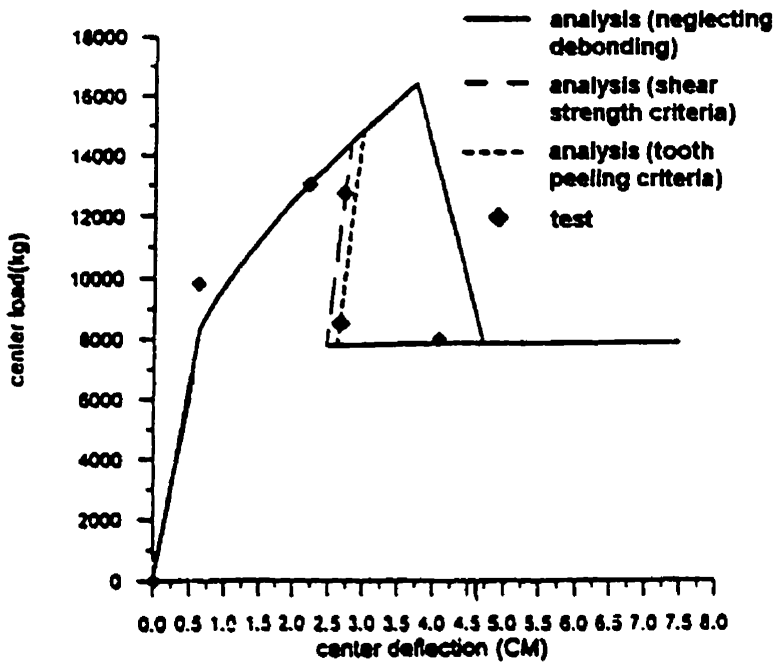

Figure 2.22: Comparison of predicted beam responses and test data [adapted from 22]

Wang and Ling also proposed a discontinuous interfacial shear stress model in which a jump in the interfacial shear stress occurs when the yield moment is reached. This is based on the observation that after the steel reinforcement yields, the internal force of the FRP greatly increases. The interfacial shear stress (τ_s) may be calculated by

$$\tau_s = \frac{S1 \times V}{b_f} \qquad (\text{for } M < M_y) \qquad (2\text{-}10a)$$

$$\tau_s = \frac{S2 \times V}{b_f} \qquad (\text{for } M > M_y) \qquad (2\text{-}10b)$$

where S1 and S2 are the slopes as defined in Figure 2.23 and are determined by the properties of the beam cross-section, V is the shear force, and b_f is the width of the FRP layer.

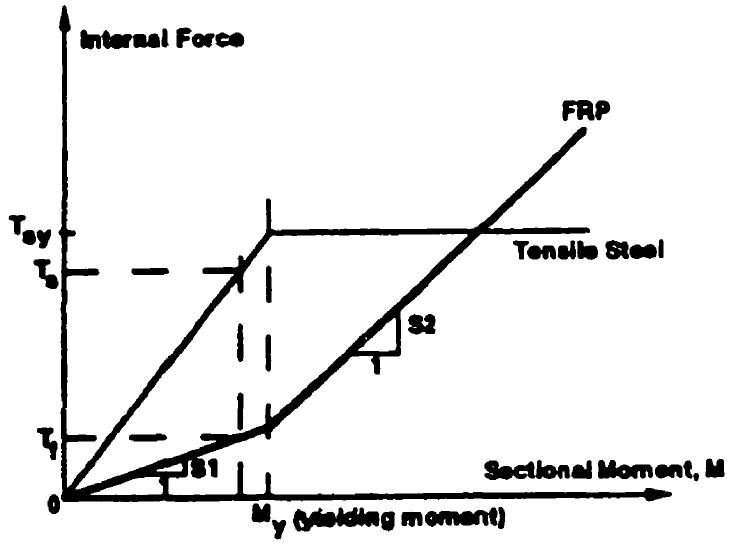

Figure 2.23: Variations of internal forces before and after yielding moment [22]

The uniformly distributed interfacial shear stress changes into a discontinuous distribution once the yield moment is exceeded in any section, and the location of the discontinuity shifts from the loading point towards the support as the load increases. This also justifies the commonly observed debonding propagation from the mid-span to the supports. Besides comparing the interfacial shear stress with the shear strength of the concrete, the development length of the FRP laminate (L_f), determined by Eqn. (2-11), should also be checked.

$$L_f = \frac{F_f t_f}{U_f} \tag{2-11}$$

where F_f is the tensile strength of the FRP material, t_f is the FRP thickness, and U_f is the bond strength of the adhesive or the FRP-concrete interface. Once the debonding front passes the boundary for the required development length, unstable crack growth can occur in the interface, leading to debonding failure of the FRP laminate.

An analysis of debonding failure modes, including shear-tension failure and peeling of FRP, was conducted by Buyukozturk and Hearing [14]. At the end of the FRP laminate, a change in stiffness and discontinuity of beam curvature leads to a stress concentration in the concrete. Thus, cracks are initiated at the anchorage zone, and can result in shear-tension failure leading to debonding at the rebar level, or peeling at the shear crack mouth leading to delamination along the concrete-FRP interface. The following two equations can be used iteratively to determine the shear stress transferred across the concrete-FRP interface.

$$E_f \frac{\delta^2 u_f}{\delta x^2} = -\frac{G_a(u_b - u_f)}{t_f t_a} \tag{2-12}$$

$$u_b = \int_0^x \frac{My}{E_c I} dx \tag{2-13}$$

where E and G are the elastic and shear moduli, u_b and u_f are displacements of the beam and FRP laminate (Figure 2.24), t is the layer thickness, I is the equivalent moment of inertia, and the subscripts f, a, and c represent FRP, adhesive, and concrete, respectively. Peeling of the FRP may initiate from the ends of the laminate or from existing cracks in regions subjected to pure moment or to mixed moment and shear. The authors also proposed using advanced interfacial fracture mechanics with finite element analysis to relate local FRP peeling processes to the global behaviour of the beam.

Colotti and Spadea [23] proposed a truss model to describe the ultimate behaviour of RC beams with externally-bonded plates. The truss model is based on the theory of plasticity, and includes load transfer by bond to account for failure due to plate separation. The global force flow of plane stress field at the interface is represented by the bond stress resultant U. A constant bond strength model with zero tension cutoff is used as a yield condition for the interface. Estimates of bond strength were suggested for the two modes of debonding. For the case of concrete cover failure, the bond strength is determined as

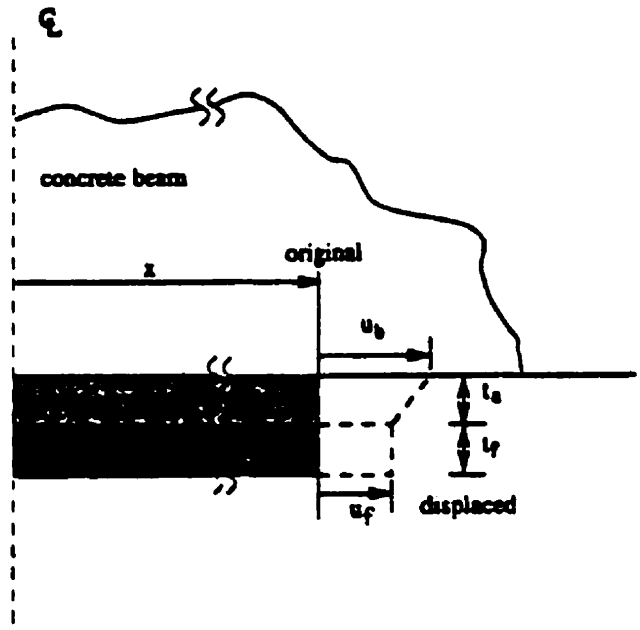

Figure 2.24: Displacements in FRP-bonded beam due to shear [14]

$$U_y = \frac{f'_t \, l_c b}{6d''} \tag{2-14}$$

where f'_t is the tensile strength of concrete, l_c is the crack spacing, and d'' is the concrete cover thickness. For debonding of the FRP plate from the concrete, the bond strength (U_y) is given by:

$$U_y = b_p (2.17 + 0.02 (f'_c - 20)) \qquad \text{for } 20 < f'_c \leq 50 \text{ MPa} \tag{2-15a}$$

$$U_y = b_p (2.77 + 0.06 (f'_c - 50)) \qquad \text{for } f'_c > 50 \text{ MPa} \tag{2-15b}$$

where b_p is the width of the FRP plate and f'_c is the cylinder compressive strength of the concrete. The effective bond strength is the minimum value calculated from the above two equations. The bond failure mechanism is characterized by the slipping of the plate within the shear span, coupled with a shear crack along path ON (refer to Figure 2.25) and the

yielding of stirrups crossing the crack. The load-carrying capacity for several failure modes were presented, including bond failure, and various combinations of concrete crushing, yielding of flexural and transverse reinforcement, and FRP rupture. The model was validated against the test results of more than 20 beam specimens tested by various researchers. The predicted shear strengths and failure modes were found to be reasonably accurate, with an average analytical-to-experimental strength ratio of 1.04.

The analytical models proposed by various researchers provide a simple tool for the preliminary design of RC members strengthened in flexure by FRP laminates, while accounting for both the global behaviour and the local failure modes.

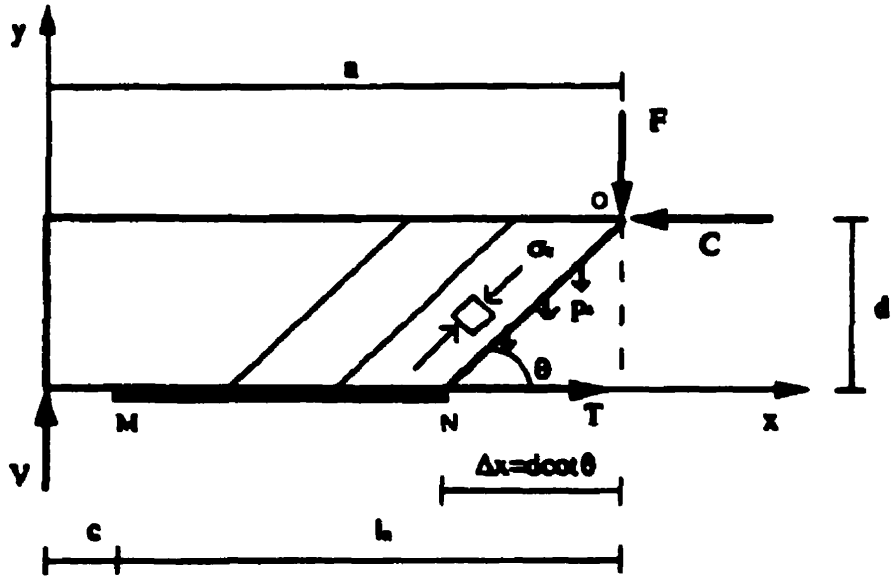

Figure 2.25: Free-body diagram for truss model [23]

2.3 SHEAR STRENGTHENING WITH FRP COMPOSITES

Although FRP research has focused predominantly on flexural applications, more attention has been given to the usage of FRP for shear strengthening since 1991 [24]. Bonding configurations can be in the form of bonding on the sides only, as a U-wrap around the underside of the beam, or completely wrapped around the beam. However, the latter option is not likely to be adopted in the field since most beams are cast monolithically with a slab. FRP laminates can be bonded to RC beams, either as strips or as a continuous sheet, to act as shear reinforcement. Advantages of strips include the ability to select their number based on the shear strength requirement, and the ease of achieving a uniform epoxy thickness. The FRP strips or sheets can be oriented vertically or at an angle (usually ±45°) to the beam axis to counteract the tensile forces generated by shear. Some common bonding configurations are depicted in Figure 2.26.

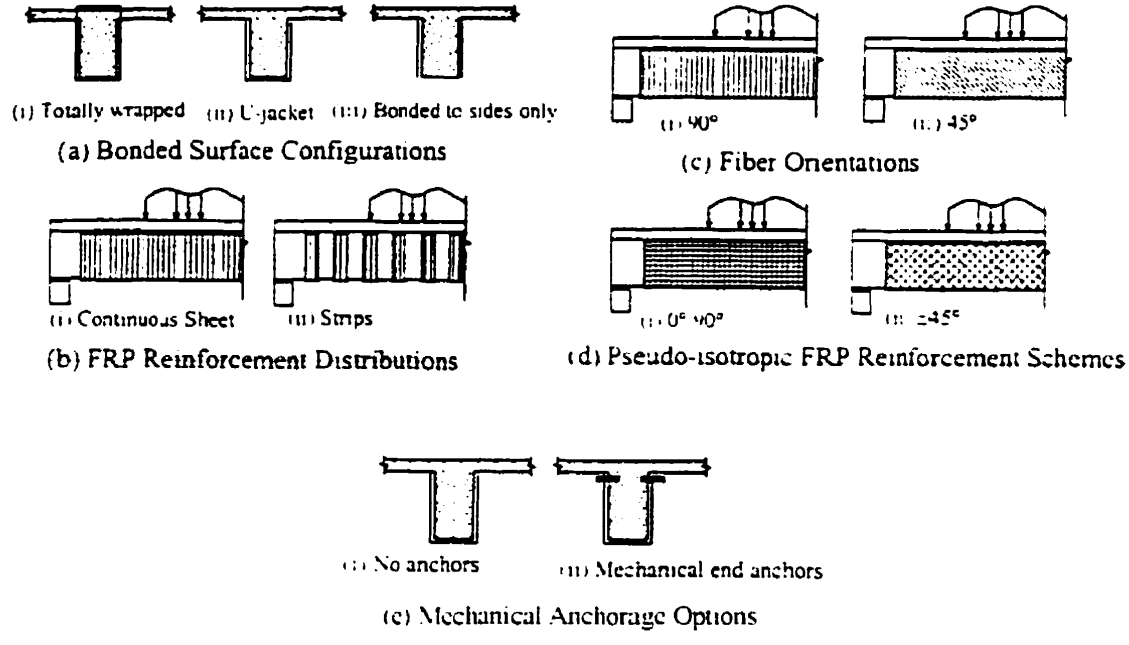

Figure 2.26: FRP shear reinforcement configurations [25]

Experimental work is slowly increasing to build up a database of results for RC members strengthened in shear with FRP, but the analytical models proposed in the literature are numerous and in most cases contradictory [26]. Very few accounts of FEM work relating to shear strengthening of RC members with FRP have been published.

2.3.1 *EXPERIMENTAL WORK*

Taerwe *et al.* [27] tested five full-scale RC beams strengthened in shear with CFRP sheets, both in the form of jackets (continuous sheet) and as vertical strips with various spacing. Gains in shear strength ranged from 20% to 85%, with the mode of failure switching from diagonal tension (in the control beams) to flexural failure or peeling-off of CFRP. In the beam bonded with a continuous CFRP jacket over its shear spans, flexural failure was obtained, although strains measured on the sheets indicated that a shear crack had formed underneath. The remaining beams that were bonded with various configurations of CFRP strips failed in shear with concrete crushing near the loading point. At the major diagonal shear crack, fracture and peeling-off of the CFRP strips were noted. The CFRP peeling-off, accompanied by a layer of concrete, was due to tension in the sheet arising from the shear crack near the edge of the strips. Typical failure modes and locations of shear cracks are illustrated in Figure 2.27, along with comparisons against unstrengthened control beams.

The authors also used Eqn. 2-16 to predict the contribution of the CFRP strips (V_{strips}) to the beams' shear capacity:

$$V_{strips} = \Sigma (f_{ui}A_i) = \Sigma (E\varepsilon_{ui}A_i) \qquad (2\text{-}16)$$

where f_{ui} and ε_{ui} are the stress and strain at failure in the i^{th} strip at its intersection with the shear crack, A_i is the cross-sectional area of i^{th} strip, and E is the elastic modulus of the CFRP sheet. It was concluded that using CFRP strips as external shear reinforcement is similar to internal steel stirrups, where the spacing and width of the strips have a large influence on the magnitude of shear contribution. In contrast to steel stirrups that are usually

assumed to have yielded at the shear crack, the shear contribution of CFRP strips is based on their tensile strains, which are usually less than the ultimate strain of the material. The strains of the strips depend on the distribution and location of each strip, as these parameters influence the location and inclination of the shear cracks. Once the ultimate strain of a strip crossing the midpoint of a shear crack has been attained, the contribution of the stirrups and strips near the ends of the crack may be reduced.

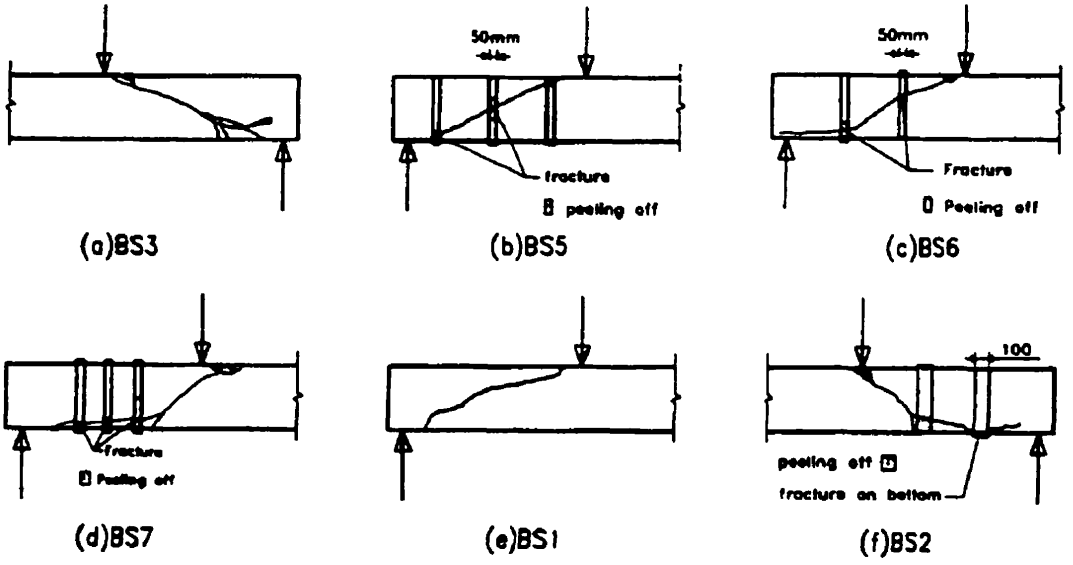

Figure 2.27: Failure modes of shear-strengthened beams tested by Taerwe *et al.* [27]

Li *et al.* [24] studied five beams in four-point bending: one of which was strengthened only in flexure, while the remaining four were strengthened in flexure and shear. Strengthening in shear was accomplished by bonding continuous CFRP sheets up to various heights on the sides of the beams. It was found that initial cracking in the concrete was delayed in the shear strengthened beams and that the location of the shear strengthening sheets affected the cracking mode of the beams, as shown in Figure 2.28(a). As the CFRP sheet area increased, the stiffness of the beam increased due to the sheets' restraining effect on crack development, although ductility was slightly reduced (Figure 2.28(b)).

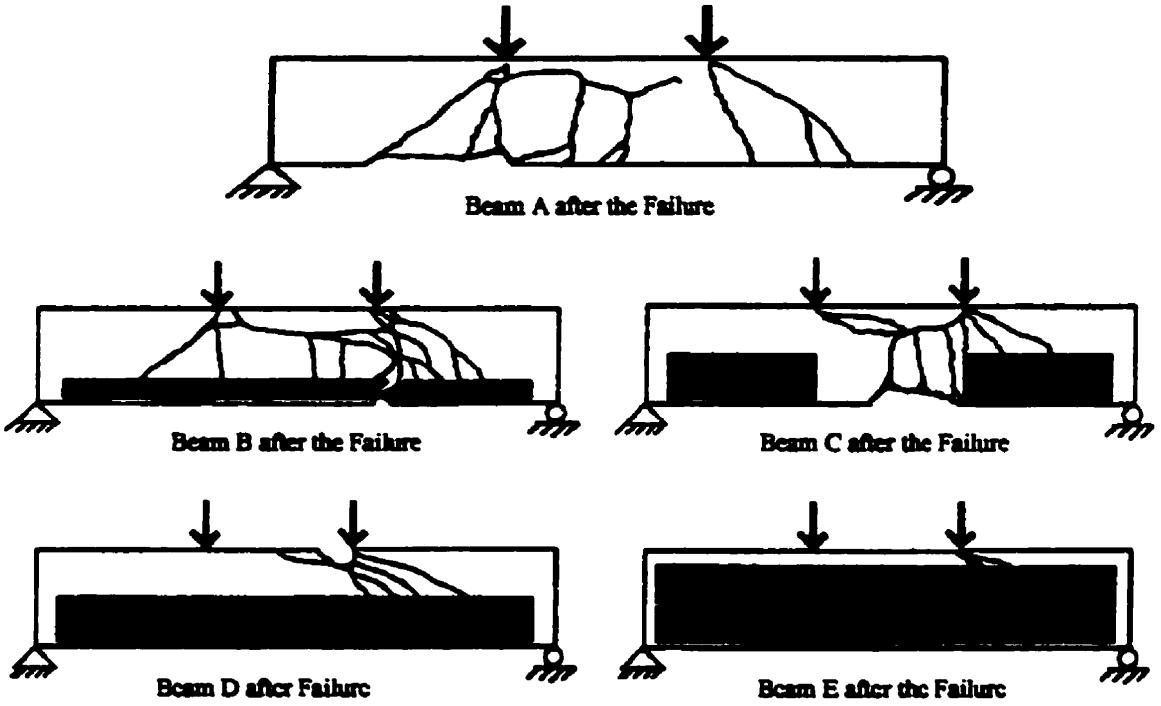

(a)

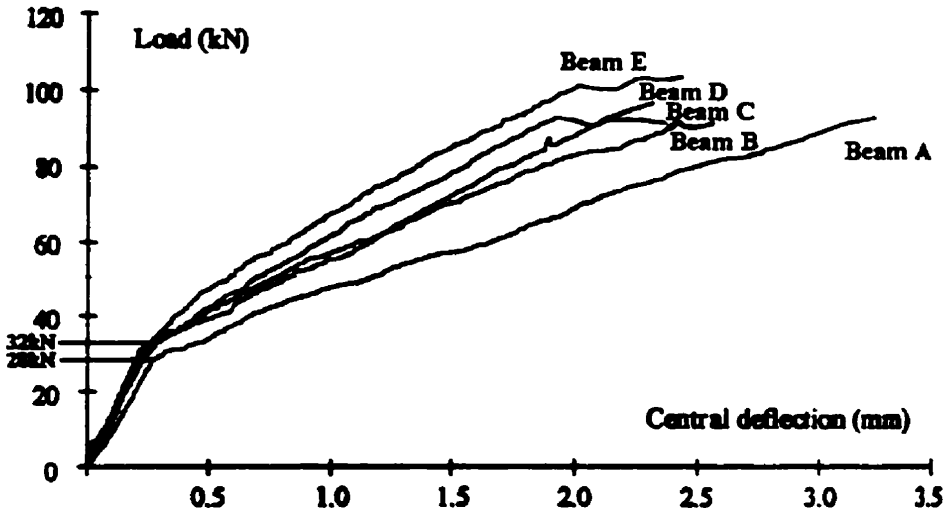

(b)

Figure 2.28: (a) Cracking patterns and (b) load-deflection curves from Li *et al.* [24]

As opposed to the epoxy resin commonly used for bonding of FRP, Funakawa *et al.* [28] tested FRP-strengthened beams bonded with methyl methacrylate (MMA) resin, which can cure quickly at low temperatures. The specimens differed in the number and type of FRP sheets used. As the number of FRP sheets was increased, a larger deflection was reached before the fibres fractured, and shear strength increases of 54 to 110% were measured. The FRP reinforcement used for the specimens and the corresponding load-deflection curves are given in Table 2.1 and Figure 2.29. It was noted that the addition of the aramid FRP (AFRP) sheet enhanced the deformation capacity more than the load capacity of the beam.

Table 2.1: Type and Quantity of FRP Reinforcement Used by Funakawa *et al.* [28]

Specimen Number	Number of CFRP Sheet(s)	Number of AFRP Sheet
S-1	0	0
S-2	1	0
S-3	2	0
S-4	3	0
S-5	1	1

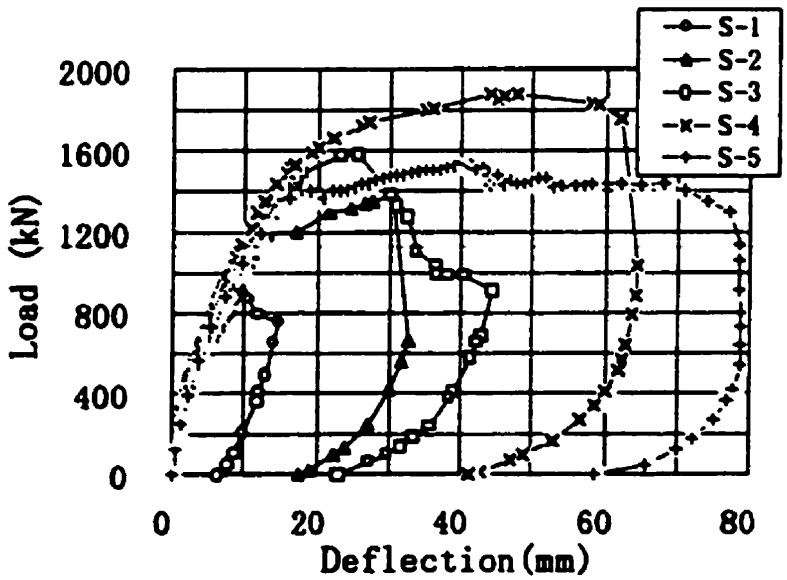

Figure 2.29: Load-deflection curves for beams tested by Funakawa *et al.* [28]

Sato *et al.* [29] studied the effect of CFRP bonded vertically onto the sides of concrete beams, both with and without steel stirrups. The parameters tested were the location and quantity of CFRP (strips versus continuous sheets, application on sides only or in a U-shape configuration), and the amount of stirrups. In terms of shear strength, the beams with CFRP bonded in a U-wrap were superior. Even after the CFRP on the sides had peeled off, the laminate on the soffit could still sustain tensile force. As for the failure mode (depicted in Figure 2.30), delamination took place below the shear crack in the region between the centre of the shear span and the support in the beam with CFRP bonded to the sides (specimen S2). On the other hand, the beam with CFRP bonded in a U-wrap (specimen S3) experienced complete laminate peeling in the same region of the beam. For both types of configuration, delamination of CFRP above the main shear crack occurred in the region between the loading point and the centre of the shear span.

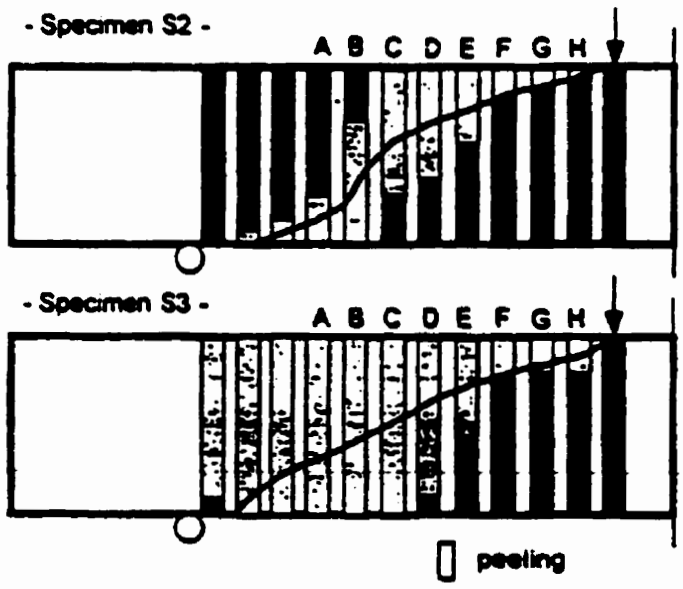

Figure 2.30: Delamination of CFRP based on bonding configuration [29]

The researchers noticed the similarity in the strain distribution of CFRP and steel stirrups along a major shear crack. Hence, they proposed a method of predicting the shear force carried by the CFRP based on the reduction factor for stirrups proposed by Ueda and

Okamura (1984) [29]. A shear crack pattern is assumed, and the shear capacity of a CFRP strip is determined from its strain in the shear cracking zone when the CFRP stress reaches the bond strength. The lowest value calculated along the shear span is taken as the actual shear capacity of the CFRP. Discrepancies between the predicted values and the test data were attributed to the estimations of bond strengths from uniaxial bond tests by Tanaka (1996) [29]. It was concluded that the shear force carried by CFRP was larger when the stirrup ratio was lower. Also, despite its lower stiffness (area times Young's modulus), CFRP carried more shear force than stirrups due to localized elongation at a shear crack and better bond characteristics.

Three series of 1.3 m long RC beams shear strengthened with CFRP strips were tested by Chaallal *et al.* [30]. The beams in one series were fully reinforced in shear (FS) with steel stirrups, while beams in the second series were under-reinforced in shear (US). In the third series, the beams were fabricated in the same manner as in the second series, and then bonded in the shear span with 50 mm wide CFRP side strips either perpendicularly (RS90) or diagonally (RS135) to the beam's axis (where the number following RS represents the angle of orientation of the strips). The RS series was designed to achieve the same shear capacity as the FS series. Whereas the beams in the US series failed in shear, the beams in the RS and FS series achieved the yielding load of the tension reinforcement. For the two RS series, the CFRP strips reduced the extent and severity of the shear cracks, thereby increasing the shear strength and stiffness of the beams, as can be seen in their load-deflection curves shown in Figure 2.31. The vertical strips in series RS90 forced the diagonal cracks to bend less than in conventional RC beams, while the diagonal strips in series RS135 limited the propagation of shear cracks. Most of the beams in the RS series failed due to concrete peeling from excessive longitudinal and transverse cracking at the bottom of the beams along the longitudinal steel reinforcement. These cracks were ascribed to the high peeling (normal tensile) stresses developed at the ends of the CFRP strips near the bottom of the beams, especially at high load levels. The authors concluded that although strips oriented at 135° to the beam axis outperformed the perpendicular strips, U-strips or U-jackets should be utilized to minimize the peeling stresses at the ends of the strips leading to premature beam failure.

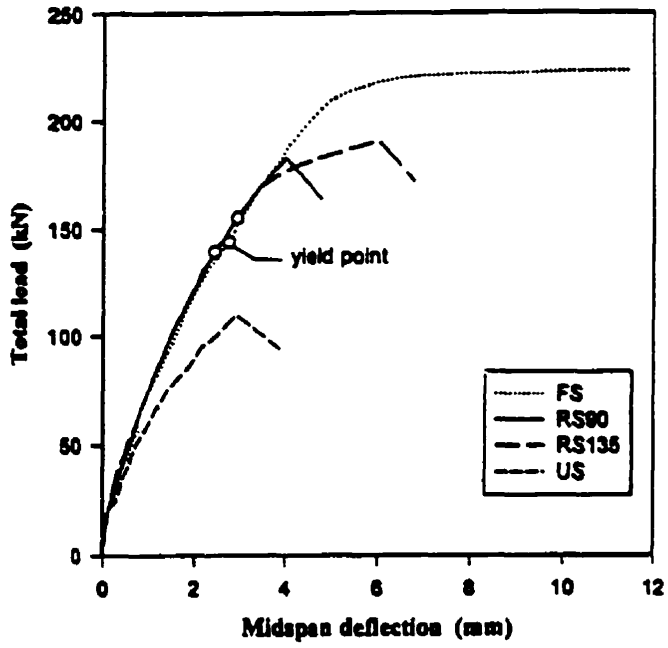

Figure 2.31: Load-deflection curves for beams tested by Chaallal *et al.* [30]

The effect of using CFRP sheets for the shear strengthening of RC beams with corroded stirrups was the subject of a study by Kage *et al.* [31]. It was found that as the quantity of sheets increased, the shear capacity increased but deformation at maximum load decreased. In Figure 2.32(a), specimen SB1110 had one sheet bonded horizontally, while specimen SB1130 was bonded with three sheets. CFRP sheets that were bonded horizontally experienced diagonal splitting in the direction of the fibre due to shear stress, lowering the shear capacity of the beam. The beam response was tougher when the sheets were bonded perpendicularly to the beam axis (specimen SB1210), and deflections were larger than when the sheets were bonded horizontally (specimen SB1110), as shown in Figure 2.32(b). The most effective configuration was obtained when two sheets were bonded at right angles to each other (specimen SB1310). Anchoring the CFRP sheet around the corner of the beam substantially increased its deformability.

Norris *et al.* [32] also concluded that the orientation of CFRP sheets influenced beam response and failure modes. When the CFRP fibres were bonded perpendicularly to cracks in

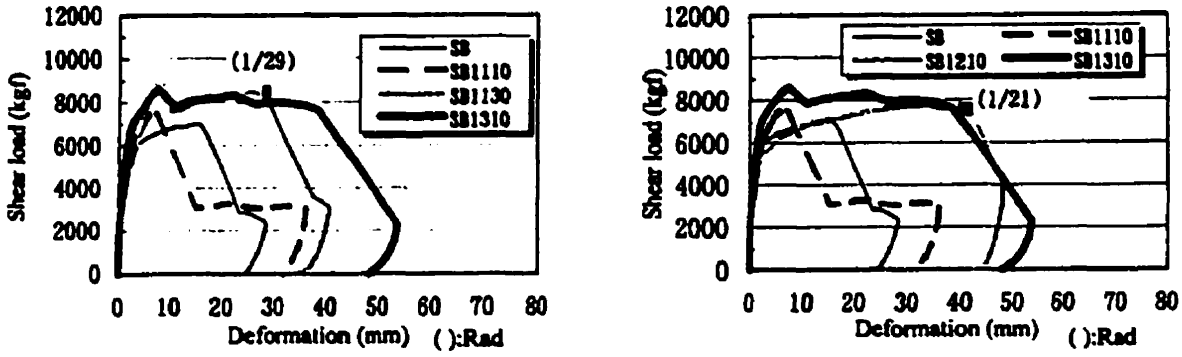

Figure 2.32: Load-deflection curves: effects of CFRP (a) quantity and (b) orientation [31]

the beam, large increases in stiffness and strength were obtained, accompanied by brittle failures in which concrete ruptured due to stress concentrations near the ends of the CFRP. Where CFRP fibres were placed obliquely to the cracks, a smaller increase in strength and stiffness was noted. However, the resulting failure mode was more ductile and was preceded by warnings such as snapping sounds or peeling of the CFRP.

Arduini *et al.* [33] tested two-span continuous RC beams bonded with CFRP sheets for flexural and shear strengthening. Two plies (at 0° and 90°) of CFRP were bonded onto the sides of one beam (beam L4), while the second beam was also strengthened for flexure in the maximum moment regions (beam L5). Beam L4 failed in a brittle manner, whereas the response of beam L5 was more ductile. The addition of CFRP sheets on the top and soffit of beam L5 raised the maximum load and controlled the propagation of cracks.

Analytical and numerical models were also used to predict the behaviour of these beams. In the analytical model based on the plane section assumption, each span of the beam was discretized into a finite number of segments, for which equilibrium equations of normal forces and flexural moments had to be satisfied. The CFRP sheets were considered to be linear elastic until rupture. Perfect bond was adopted until failure occurred in the adhesive, and the adhesive thickness was neglected. At the concrete-adhesive interface of each

segment, shear stresses were generated from the difference between the normal forces acting at the two ends of the FRP reinforcement, and the shear stress distribution was assumed to be constant throughout the segment. The mechanisms of failure which could be detected include: local adhesive failure when its ultimate tensile strain was reached, shear failure in concrete when the shear strength at the concrete-adhesive interface (taken to be 5 MPa) was attained, and FRP rupture when its ultimate strain was reached. Numerical analyses were also conducted using finite element analysis in which the smeared crack approach was adopted. A 3-D mesh of 8-noded brick elements was used to model the concrete beam, over which elements representing FRP reinforcement were directly applied to simulate the perfect bond assumption.

Figure 2.33 compares the analytical and numerical results against the experimental data. The analytical response was stiffer and less ductile than the test curves, but the numerical predictions were in good accord with the measured values. However, the peak loads and mid-span deflections were slightly overestimated by the FE analyses, which may be attributed to the assumption of perfect bond. As well, the assumption of plane sections was invalidated by premature debonding and shear failure of the concrete cover observed in the experiment. The analytical methods also did not account for the spreading of large cracks in a punching manner near the central support at high load levels.

The shear capacity of RC members retrofitted with continuous fibre sheets was studied by Araki *et al.* [34]. Thirteen beams, strengthened by various types and amounts of FRP sheets, were subjected to anti-symmetrical loading conditions. It was determined that the shear strength of the members increased in proportion to the amount of sheets used. The researchers found that the shear capacity of such beams can be evaluated by using the effective shear reinforcement ratio ($\Sigma\rho_w$). However, it was necessary to multiply the tensile strength of the FRP sheets by a reduction factor α, which was proposed to be 0.60 and 0.45 for carbon and aramid sheets, respectively. These values were based on the ratio of average stress in the sheets at peak load to the FRP's tensile strength. The effective shear reinforcement ratio is defined as:

$$\Sigma\rho_w = \rho_{ws} + \rho_{wf}\,\alpha\,\frac{\sigma_{fu}}{\sigma_{sy}} \tag{2-17}$$

where ρ_{ws} and ρ_{wf} are the shear reinforcement ratios of stirrups and FRP sheets, respectively, α is the reduction factor as described above, σ_{fu} is the tensile strength of the sheets and σ_{sy} is the yield strength of the stirrups. The effective shear reinforcement ratio can then be applied in equations for conventional RC members to calculate the capacity of the strengthened beams.

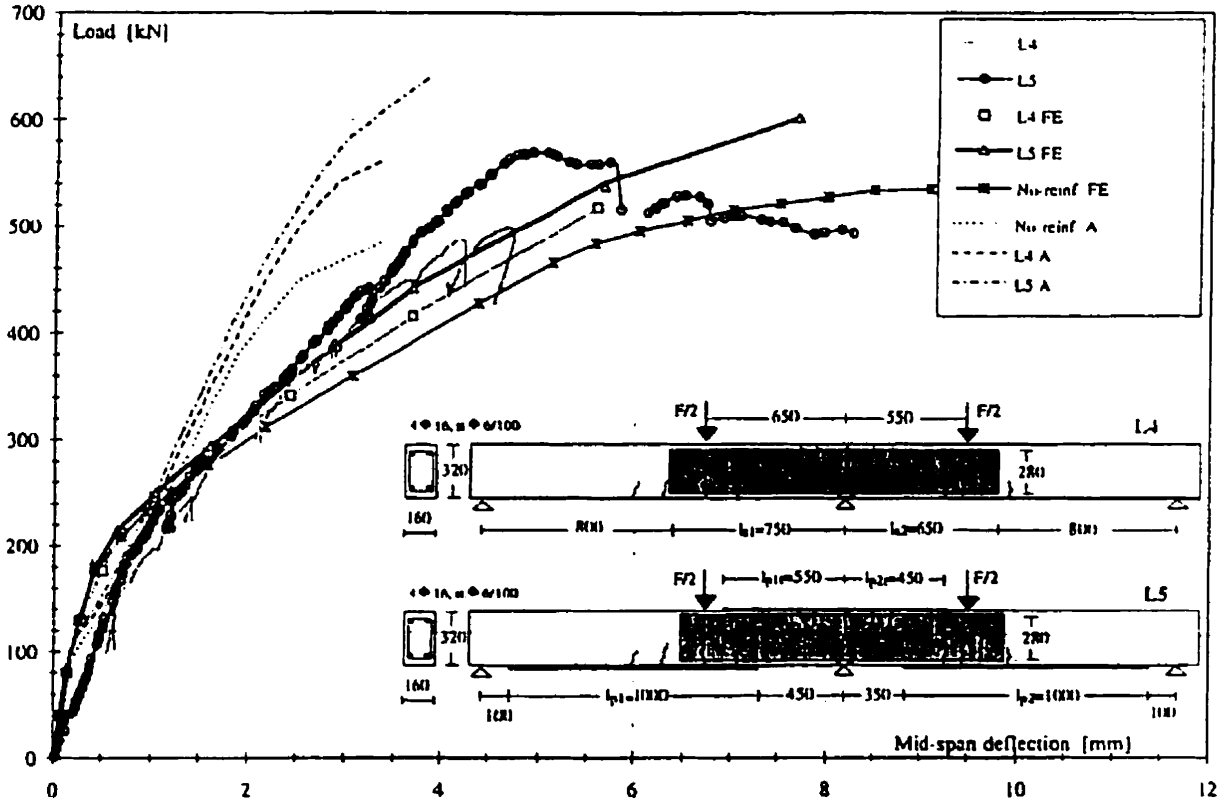

Figure 2.33: Experimental, analytical (A) and numerical (FE) results for beams studied by Arduini *et al.* [33]

Grace *et al.* [35] tested 14 RC beams strengthened with FRP laminates, both in flexure and in shear. From their experiments, it was found that the cracks in the shear-strengthened beams were smaller and more evenly distributed. The bonding of vertical fibres over the whole span of the beam reduced the number of diagonal cracks, thus allowing the longitudinal fibres to be fully utilized. All of the strengthened beams exhibited poor ductility, measured in terms of an energy ratio (ratio of absorbed energy at failure to total energy). Failures were sudden and were accompanied by the release of large amounts of energy. This brittle behaviour implies that a high factor of safety is required in the design of such members.

The common occurrence of FRP sheets peeling from RC beams strengthened in shear has prompted research into the effectiveness of anchorage systems. One such study has been carried out by Sato *et al.* [36]. They studied T-beams with CFRP sheets bonded to the sides of the web and wrapped around the bottom, one without end anchorage (specimen No.2) and one with mechanical anchorage in the form of anchor plates and bolts (specimen No.3). The resulting increases in shear strengths were 12% and 33% for the unanchored and anchored beams, respectively. The CFRP sheet changed the failure mode of the beam from shear compression to shear failure after the delamination of the sheet. In the specimens bonded with CFRP, the areas of debonding were similar, although the loads at which delamination occurred were higher for the beam with mechanical anchorage (Figure 2.34). Delamination of the CFRP sheet lowered the stiffness and ultimate shear strength of the beams.

In the beam with mechanical anchorage, the shear force at yielding of the stirrups and the ultimate shear strength were higher than the unanchored beam because the delamination of the CFRP sheet was delayed. As well, even after initial delamination, the tensile force carried by the CFRP in the anchored beam increased since the anchor bolt could sustain shear. Due to the presence of epoxy between concrete and CFRP and between CFRP and the anchor plate, the bond area was greater than that for the unanchored sheet. Therefore, for the same applied force, the bond stress was lower. Thus, the load at delamination of the anchored sheet was higher than that of the unanchored case.

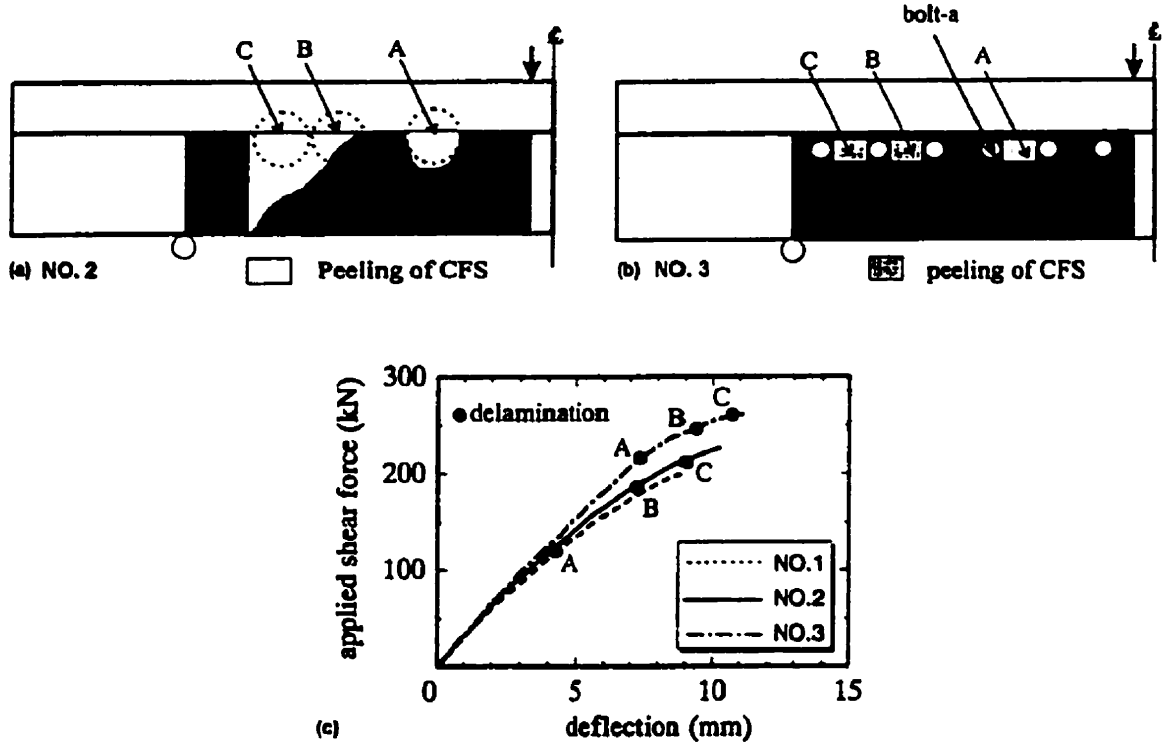

Figure 2.34: Delamination of CFRP in beam (a) without and (b) with anchorage, (c) corresponding load-deflection curves [36]

A more in-depth look at anchoring systems was conducted by Sato *et al.*[37], in which four anchorage schemes were tested (refer to Figure 2.35).

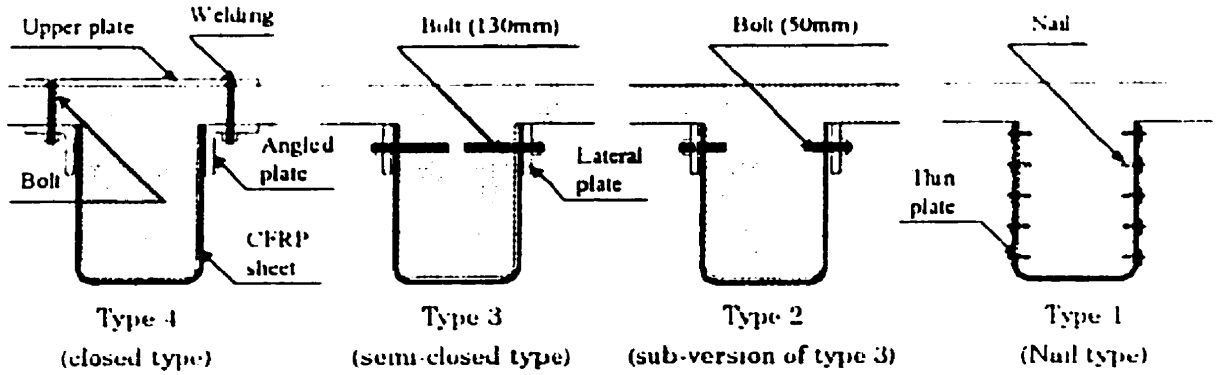

Figure 2.35: Systems of CFRP anchorage [37]

The effectiveness of the various anchorage methods is depicted in Figure 2.36(a) and (b), where the S series were T-beams and the M series were rectangular beams, with the anchorage system represented by the number following the series letter. The combination of lateral steel plates and bolts was found to be adequate, even under cyclic loading conditions. Therefore, anchorage system Type 3 was recommended, both in terms of performance and in terms of practicality in field applications.

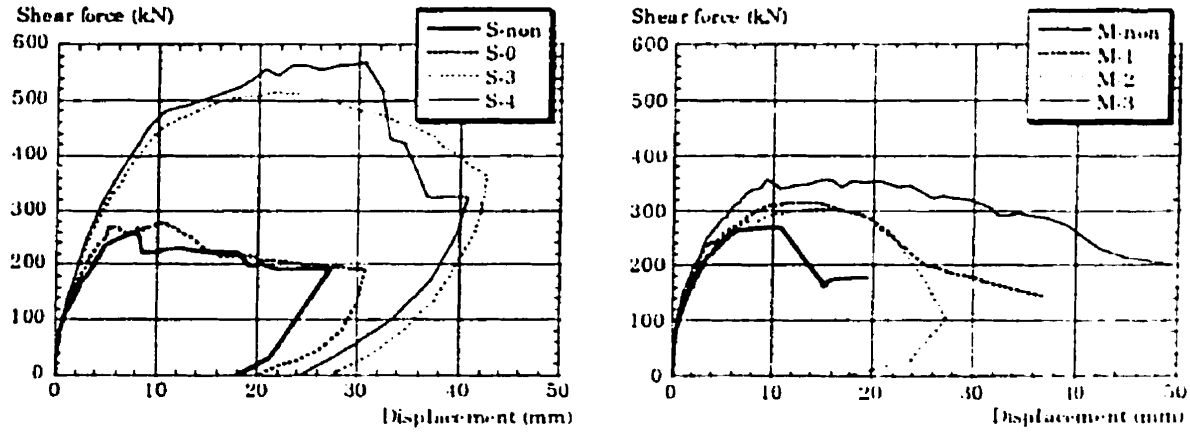

Figure 2.36: Behaviour of beams with various CFRP anchorage systems:
(a) S and (b) M series [37]

The researchers reported that the shear strength of CFRP-strengthened RC beams can be estimated using a model based on truss and arch actions, the stress fields of which are shown in Figure 2.37(a) and (b).

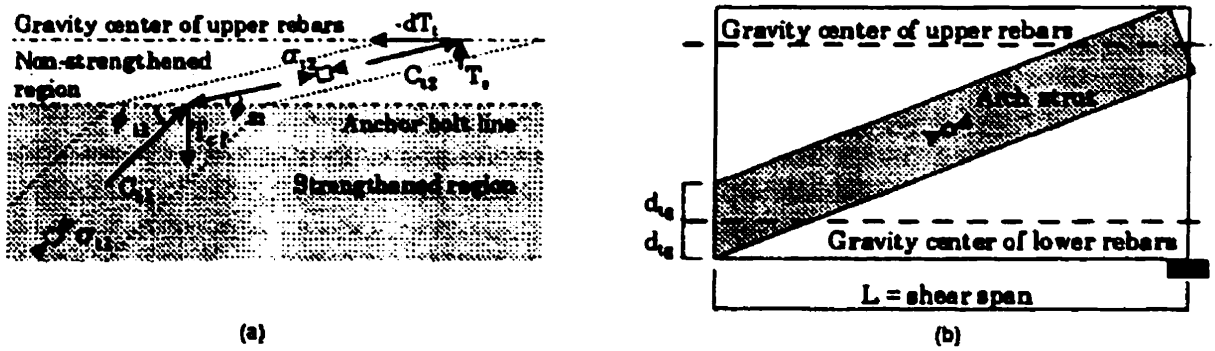

Figure 2.37: Stress field for Type 3 anchorage system: (a) truss and (b) arch actions [37]

Khalifa and Nanni [38] investigated the performance of T-beams strengthened in shear with CFRP composites. They found that by using various configurations of CFRP sheets, the shear capacity of the beams could be increased by 35 to 145%, as substantiated by Figure 2.38.

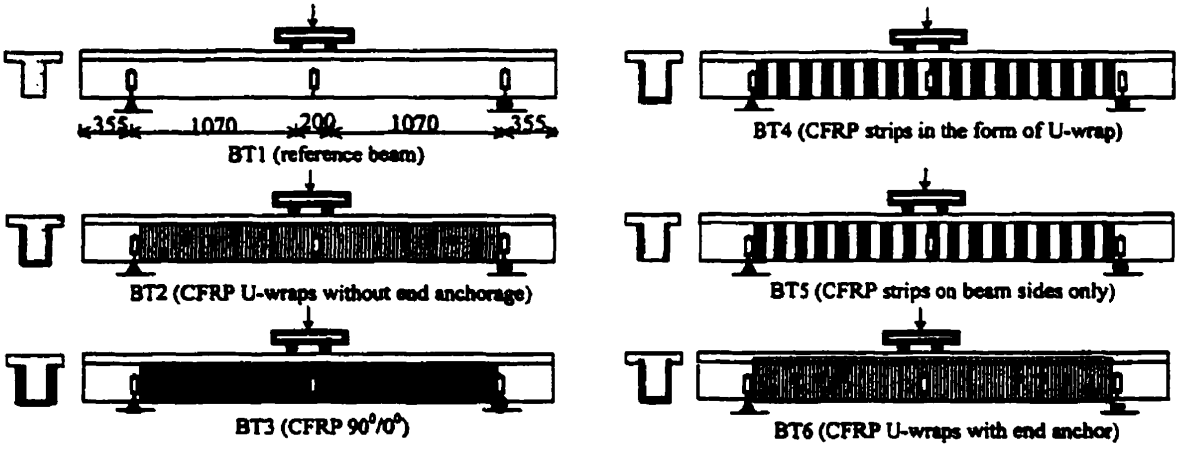

(a)

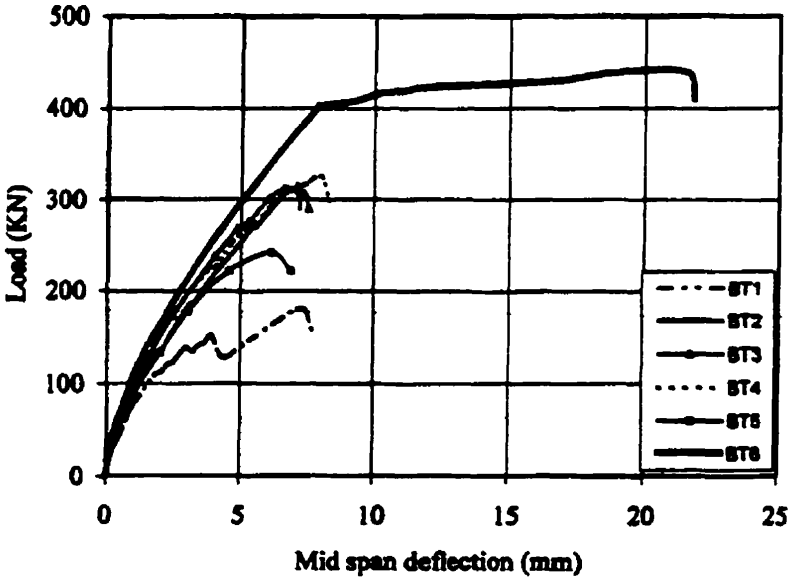

(b)

Figure 2.38: (a) Strengthening schemes and (b) test results for T-beams studied by Khalifa and Nanni [38]

It was also noted that an optimum quantity of FRP exists, beyond which the strengthening effectiveness is uncertain. Strips of FRP applied only to the beam sides (BT5) provided less strength enhancement than those bonded in a U-shaped configuration (BT4), and their failure modes are compared in Figure 2.39. Although strips proved to be as effective as continuous sheets, it was advised that sheets be utilized in field applications since damage to an individual strip is more detrimental to its behaviour.

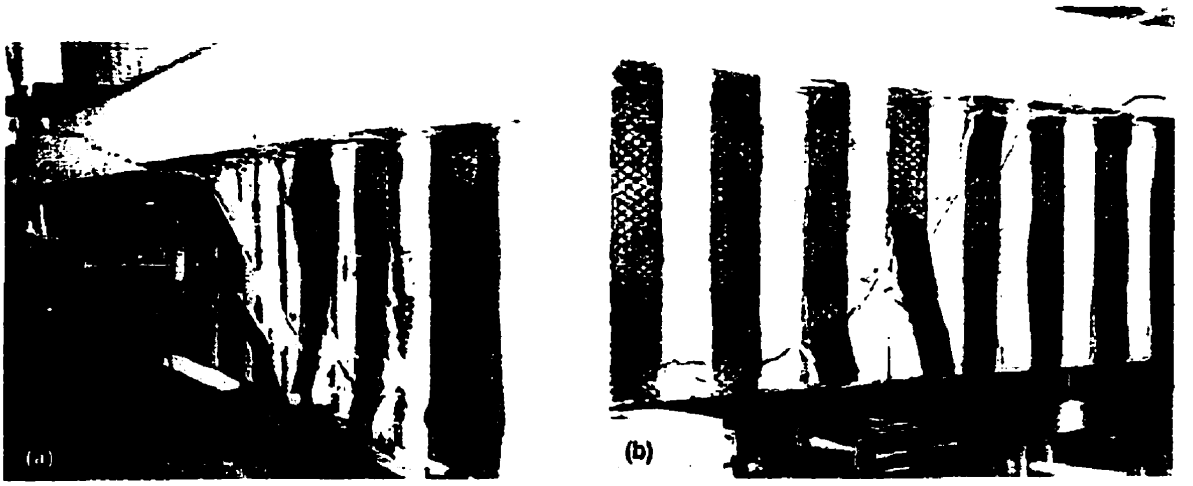

Figure 2.39: Failure modes of beams (a) BT4 and (b) BT5 [38]

The shear behaviour of RC T-beams bonded with FRP sheets or strips was also studied by Deniaud and Cheng [39]. Eight full-scale beams were tested to examine the interaction of concrete, steel stirrups and FRP sheets in carrying shear loads, and several important conclusions were drawn. The shear contribution of the FRP sheets was dependent on the amount of internal shear reinforcement. For beams that were more heavily reinforced with steel stirrups, the FRP sheets were less effective. The FRP sheets could eventually reduce the shear capacity of the beam by changing the critical shear path, resulting in an even more sudden shear failure. It was noted that the FRP strains were uniformly distributed among the FRP strips crossing the shear crack (Figure 2.40), contrary to the assumption of linear distribution previously proposed. The failure modes of the beams were characterized by the debonding and peeling of the sheets above the web shear crack. The FRP sheets were

found to have delayed the loss of plane section behaviour and the change from full beam action to partial arching action.

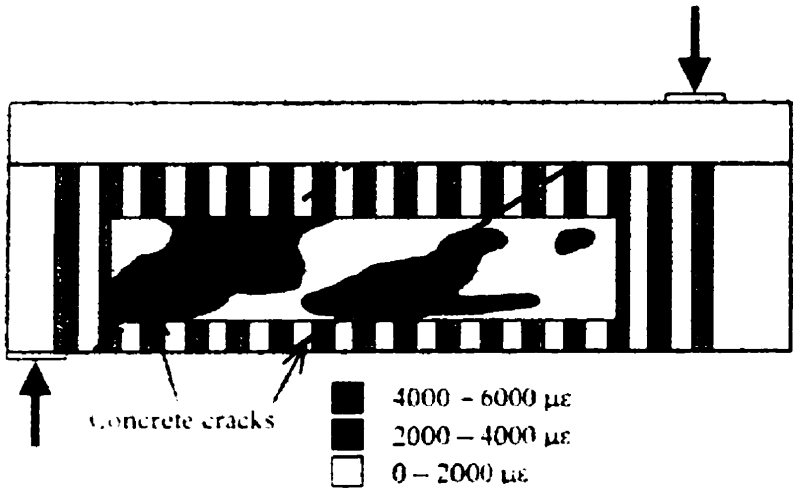

Figure 2.40: Vertical strains in FRP strips bonded onto T-beam [39]

The authors proposed a mechanical design model based on the combination of the strip method and the shear friction approach. In the strip method, the FRP sheets crossing the web crack are divided into a series of strips. Using geometrical parameters such as the anchorage conditions and the bonded length of strips above and below the crack, the maximum allowable strain for each strip is determined. A uniform strain distribution assumption is adopted, and the applied load is sequentially redistributed to strips with higher critical allowable strains until the load reaches a maximum value. Then, the maximum FRP strain value and the ratio R_L (remaining bond length over initial total length) are recorded. According to the shear friction approach, the governing shear strength is given by the lowest shear strength among all the potential failure planes along which slippage can occur. The contribution of the FRP strips (T_{FRP}) can be calculated as

$$T_{FRP} = d_f t_f E_f \varepsilon_{\max} R_L \left(\frac{w_f}{s_f}\right)^2 \left(\frac{\sin\alpha}{\tan\theta_w} + (n_s + 1)\cos\alpha\right)\sin\alpha \qquad (2\text{-}18)$$

where d_f is the height of FRP sheets bonded to the beam web, t_f is the thickness of the FRP sheets, E_f is the elastic modulus of FRP in the principal fibre direction, ε_{max} is the maximum FRP strain over the remaining bonded length, w_f and s_f are the width and spacing of the FRP strips, n_s is the total number of stirrups crossing the shear crack, α is the direction of the principal fibres measured from the longitudinal axis of the beam, and θ_w is the shear plane angle in the web. The proposed methods gave reasonably accurate strength predictions for the beams tested by the authors. The ratios of experimental to predicted shear strengths were close to 1.00, with unconservative estimates (within 10%) for the two beams which had failed by buckling of the FRP sheets.

2.3.2 *DESIGN EQUATIONS*

In preparation for the inclusion of design procedures for FRP-shear-strengthened RC beams in the various codes, numerous researchers have presented several design equations. Triantafillou [40] described some of the earlier proposed criteria for determining the FRP contribution to a RC beam's shear capacity. In Uji's (1992) [40] model, the FRP-concrete interface carries average shear (bond) stresses approximately equal to 1.3 MPa at the time of debonding, and the upper bound to the FRP contribution is given by its tensile strength. For GFRP, the average shear stresses at the time of peel-off were determined by Al-Sulaimani *et al.* (1994) [40] to be 0.8 MPa and 1.2 MPa for plates and strips, respectively. In the work of Ohuchi *et al.* (1994) [40], the limiting strain for CFRP wraps was equal to its ultimate tensile strain or 2/3 of this value, depending on the fabric thickness.

Another preliminary proposal was put forward by Chajes *et al.* [41], in which the FRP contribution to shear capacity was based on the expected strain at failure. For continuous FRP reinforcement with fibres oriented at 90°, the theoretical shear capacity (V_f) is given by

$$V_f = A_f \sigma_{fu} d = A_f E_f \varepsilon_{vcu} d \qquad (2\text{-}19)$$

where A_f is the cross-sectional area per unit length of the beam, σ_{fu} is the FRP stress at failure, and d is the effective depth. The equation was further rewritten by utilizing the linear stress-strain relationship of FRP in tension, by recognizing that failure of the beam is initiated by failure of the concrete, and by assuming that perfect bond exists between concrete and FRP prior to failure. E_f is the modulus of elasticity of the impregnated fabric, and ε_{vcu} is the ultimate vertical tensile strain of concrete (average value measured to be 0.005). Using the average value of strain at failure precludes the ability to account for different ultimate strains that may result from various FRP orientations. The proposed method led to theoretical values of shear contribution which were up to 13% higher than the measured data.

Gendron *et al.* [42] presented a theoretical model to determine the shear strength of a RC beam bonded with FRP plates. Among the assumptions used was that of no slipping between the plates and concrete so that the full strength of the plates can be developed. The analysis consists of three phases: evaluation of the member's nominal shear strength using the compression field theory or the modified compression field theory, selection of FRP plates such that the shear strength is increased up to a pre-determined value, and the verification of the shear-bending interaction. In the second phase, the shear strength attributed to the FRP plates (V_f) is calculated as

$$V_f = \frac{A_m f_m d_m}{s_m}\left(\frac{1}{\tan\theta_{st}} + \frac{1}{\tan\alpha}\right)\sin\alpha \qquad (2\text{-}20)$$

where A_m is the area of a pair of FRP plates, f_m is the stress in the plates, d_m is the shear depth of the section, s_m is the horizontal spacing of the FRP plates, θ_{st} is the shear crack inclination corresponding to the shear force in the beam (at any load higher than the level at which strengthening was carried out), and α is the inclination of the FRP plates with respect to the member axis. The iterative procedure for evaluating the values of f_m and θ_{st}, as well as the steps for predicting the response of the beam in order to estimate the quantity of A_m

needed, are given in detail by Gendron *et al.* [42]. In the third and final phase, the member response must be recalculated using the plane section assumption to verify the yielding of the longitudinal rebars and the crushing of concrete in compression.

Closed-form solutions were developed by Malek and Saadatmanesh [43] to estimate the shear force carried by FRP fabric or plates bonded onto the web of RC beams. The analytical model presented was based on the compatibility of strains in the plate and the beam, and the assumptions of composite action (no slip between concrete and FRP) and linear elastic FRP material behaviour were applied. The force carried by the FRP fabric was thought to be made up of two components: the first of which is caused by the orthotropic behaviour of the plate (even in pure bending), while the second component is caused by the moment gradient in the beam. The proposed method was verified using the finite element program ABAQUS, in which 4-noded elements and one-dimensional bar elements were used to represent concrete and rebars, respectively. FRP plates were modelled with 4-noded composite membrane elements that were imposed directly onto the concrete elements. Although the predicted FRP axial strains were reasonably close to the measured values, the slight overestimations were ascribed to the negligence of slip.

The work described above was further extended by the researchers [44] to determine the effect of web-bonded FRP plates on the inclination of shear cracks and the beam's shear capacity at ultimate. The necessary equilibrium and compatibility equations were derived using truss analogy and the compression field theory, while the assumptions were the same as those previously applied. The theoretical procedure was utilized in a parametric study to investigate various parameters that may affect the inclination angle of shear cracks. It was found that the crack inclination angle stays constant prior to yielding of the steel stirrups but drops thereafter. Prior to yielding, the inclination angle increases as the FRP plate thickness increases, up to 50° for a 4 mm thick plate. The crack inclination angle and shear force in the composite plate oscillate as a function of the FRP fibre direction, with the maximum shear force in the plate occurring when the fibres are perpendicular to the shear crack. As the stirrup spacing increased, the crack inclination angle decreased and the shear force in the

FRP laminate increased. Once the angle of shear crack inclination (θ_c) has been determined, the contribution of the FRP plate to the shear capacity of the beam (V_f) can be estimated as

$$V_f = \frac{h}{\tan\theta_c} F_{fu}\, t_p \tag{2-21}$$

where h is the height of the FRP plate, F_{fu} is the ultimate capacity of the FRP (and should be reduced accordingly to the usable strength at failure), and t_p is the plate thickness.

Triantafillou [26] has proposed an analytical model for the design of RC members shear strengthened with FRP laminates, following the Eurocode format which is based on ultimate limit states. The model is established using an analogy with steel stirrups, with an effective FRP strain that decreases with an increasing FRP axial rigidity. The load carried by the FRP laminates at ultimate depends on their failure mechanism. Typically observed failure modes include peeling-off (debonding) through the concrete near the bond interface, and/or tensile fracture at a stress lower than the ultimate strength of the FRP due to stress concentrations (at debonded areas or at beam corners). Whether debonding or fracture will occur first depends on numerous factors such as the bond conditions, the anchorage length or type of anchorage used, the laminate thickness and stiffness, and the concrete strength.

In developing the shear contribution of FRP, the load bearing mechanisms in the FRP laminate at the ultimate state must be considered, a qualitative representation of which is given in Figure 2.41(a). Regions of full debonding, limited shear transfer through the concrete, and full shear transfer are depicted. The associated tensile stresses in the FRP are shown in Figure 2.41(b), where only a section of the FRP reaches its design tensile strength $f_{frp,d}$.

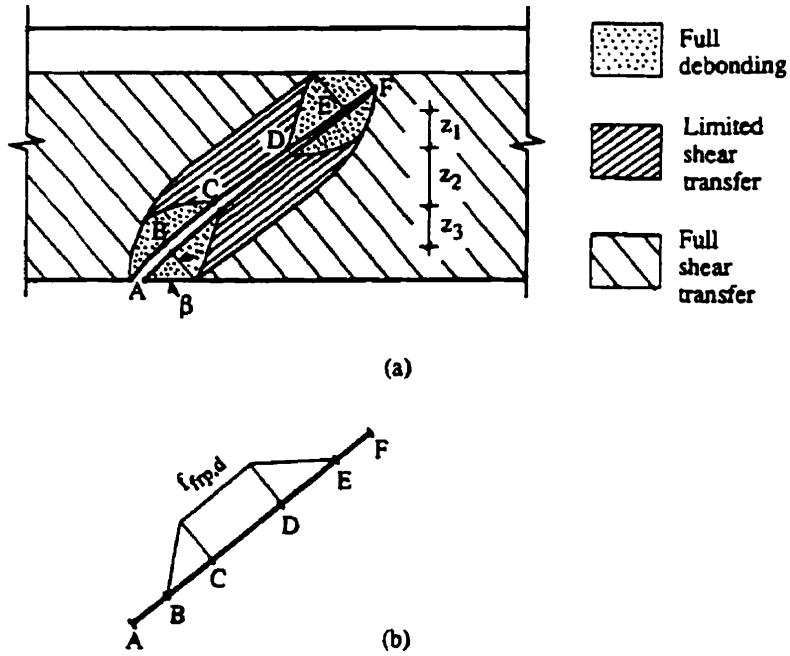

Figure 2.41: (a) Schematic of FRP stress bearing mechanism, (b) simplified FRP tensile stress along shear crack [40]

The FRP contribution to shear capacity (V_f) is expressed (in the Eurocode format) as

$$V_f = \frac{0.9}{\gamma_f} \rho_f E_f \varepsilon_{f,e} b_w d (1 + \cot\beta) \sin\beta \qquad (2\text{-}22)$$

where γ_f is a partial safety factor for FRP in tension (approximately equal to 1.15, 1.20 and 1.25 for CFRP, AFRP, and GFRP, respectively), ρ_f is the FRP shear reinforcement ratio (defined as $2t_f/b_w$ for continuous sheets, where t_f is the thickness of the FRP on each side of the beam and b_w is the width of the beam web, or as $(2\ t_f/b_w)/(w_f/s_f)$ for FRP strips of width w_f at a spacing s_f), E_f is the FRP's modulus of elasticity, d is the effective depth and β is the orientation angle of the FRP fibres to the longitudinal axis of the beam. The effective FRP strain is represented by $\varepsilon_{f,e}$, and depends on the FRP "development" length, defined as the

length needed to reach FRP tensile fracture before debonding. The development length is proportional to the FRP axial rigidity (area times elastic modulus, or $\rho_f \times E_f$). Hence, as the FRP laminates becomes stiffer or thicker, debonding dominates over tensile fracture and the effective strain decreases.

After a study of experimental results published in the literature, it was found that FRP fabrics wrapped completely around the cross-section tended to fail in tensile fracture, while those bonded to the sides only or in a U-shaped configuration failed by shear debonding. Based on best-fit trend lines, the relationship between $\varepsilon_{f,e}$ and $\rho_f E_f$ was suggested to be in the form of:

$$\varepsilon_{f,e} = 0.0119 - 0.0205(\rho_f E_f) + 0.0104(\rho_f E_f)^2 \text{ for } 0 \le \rho_f E_f \le 1 \text{ GPa}$$

$$\varepsilon_{f,e} = -0.00065(\rho_f E_f) + 0.00245 \text{ for } \rho_f E_f > 1 \text{ GPa} \qquad (2\text{-}23)$$

It was noted that a value of $\rho_f E_f = 0.4$ GPa presented a limit to the effectiveness of shear strengthening with FRP. Also, the actual value of $\varepsilon_{f,e}$ may be higher in reality since many of the experimental data used for the calibration of Eqn. 2-23 were obtained from small-scaled specimens.

Triantafillou's equation for describing shear failure combined with FRP fracture was slightly modified and calibrated with a few more test results by Khalifa *et al.* [25]. This method is termed the effective stress approach, in which the effective stress ($f_{f,e}$) is related to the level of strain at the time of FRP rupture. The equation presented by Triantafillou is written in the American Concrete Institute (ACI) code format as follows:

$$V_f = \frac{A_f f_{f,e} (\sin\beta + \cos\beta) d_f}{s_f} \qquad (2\text{-}24)$$

where A_f is the total thickness of the sheet ($2t_f$ for both sides of the beam) times the width of the CFRP strip w_f, d_f is the effective depth of the FRP shear reinforcement, and all other terms are defined as before. For continuous sheets, w_f and s_f should be equal. A strength reduction factor of 0.70 is suggested for the design value of V_f. To ensure that shear cracks will be intercepted by at least one FRP strip, the spacing of the strips (s_f) should be limited to $s_{f,max} = w_f + d/4$.

The effective stress is related to the ultimate FRP strength through the ratio of effective strain to ultimate strain ($f_{f,e} = R \times f_{f,u}$ and $\varepsilon_{f,e} = R \times \varepsilon_{f,u}$). For all the test data available at the time, $\rho_f E_f$ never exceeded 1.1 GPa, and R was calibrated to be

$$R = 0.5622 (\rho_f E_f)^2 - 1.2188 (\rho_f E_f) + 0.778 \leq 0.50 \qquad (2\text{-}25)$$

in which the upper limit of 0.50 has the effect of limiting the FRP strain to maintain the concrete's shear integrity, and applies only to low-modulus CFRP sheets with ultimate strain approximately equal to 1.5%. It was later suggested by Khalifa and Nanni [45] that the upper limit for R should be equal to $0.006/\varepsilon_{f,u}$. The effective stress approach is limited to CFRP reinforcement and to cases where debonding does not govern.

To describe shear failure combined with FRP debonding, Khalifa *et al.* [25] referred to the bond model proposed by Maeda *et al.* [46]. For FRP sheets that are bonded to the sides of the beam or in a U-shaped configuration, anchorage is only provided by the interfacial bond between the concrete and FRP. Delamination occurs when the interfacial bond fails as a result of the high tensile stresses developed in the FRP. These stresses are significantly increased when tension must be transferred by the FRP to the vertically-separated concrete on either side of the shear cracks. The concepts of effective bond length and average bond stress are applied to derive empirical equations for the ultimate capacity of CFRP sheets at

delamination. For debonding failure, the ratio R is calculated from Eqn. 2-26, taking into account the concrete strength and the bonding configuration.

$$R = \frac{0.0042(f'_c)^{2/3} w_{fe}}{(E_f t_f)^{0.58} \varepsilon_{f,u} d_f} \tag{2-26}$$

with w_{fe} representing the effective width of the FRP (evaluated as shown in Figure 2.42), $\varepsilon_{f,u}$ is the ultimate FRP strain, and d_f is the effective depth of the FRP shear reinforcement. The effective width concept is based on the reasoning that after a shear crack forms, only the portion of FRP extending past the crack by the effective bond length (L_e, found by Eqn.2-27) is capable of carrying shear.

$$L_e = e^{\left[6.134 - 0.58 \ln(t_f E_f)\right]} \tag{2-27}$$

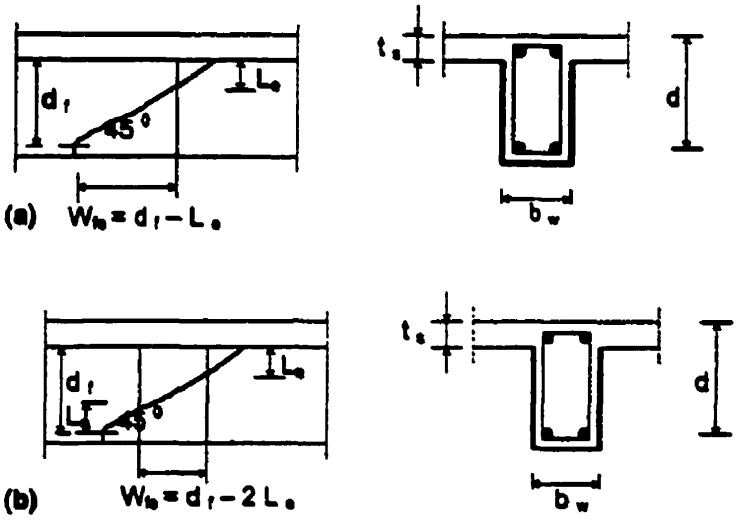

Figure 2.42: Effective width of FRP: (a) in U-wrap, (b) bonded to beam sides only [25]

Eqn.2-26 was later revised into the following form by Khalifa and Nanni [45]:

$$R = \frac{(f'_c)^{2/3} w_{fe}}{\varepsilon_{f,u} d_f}\left[738.93 - 4.06(E_f t_f)\right] \times 10^{-6} \quad (2\text{-}28)$$

The design equations previously presented by Triantafillou [26, 40] have been recently modified by Triantafillou and Antonopoulos [47]. The shortcomings of the former approach include: (1) FRP rupture was assumed to occur at the same time as shear failure (concrete diagonal tension), whereas it may occur after the peak shear capacity is reached, (2) one equation was proposed regardless of the mode of failure (FRP debonding or fracture) and the type of FRP material, and (3) the effect of the concrete strength on debonding failures was not considered. In the updated approach, the effective FRP strain is further multiplied by a reduction factor α of 0.8 to become the characteristic value of the effective strain ($\varepsilon_{fk,e}$). To obtain an estimate of the effective strain, the status of the FRP at shear failure of the beam must be identified. Although governed by the diagonal tension failure of concrete, this may occur prematurely due to FRP debonding, or the FRP may rupture exactly at or slightly past the peak load, as illustrated in Figure 2.43.

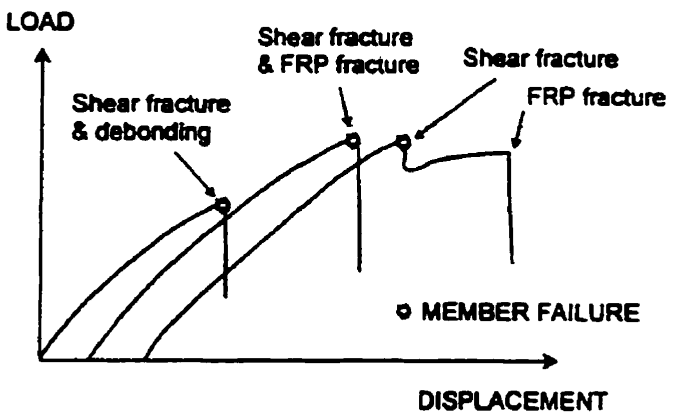

Figure 2.43: Schematic illustration of shear and FRP failures [47]

At the ultimate state, it can be expected that some debonding of the FRP will take place, as a result of the excessive straining in the FRP that leads to strain incompatibilities with the concrete and subsequent cracking. Such cracking will give rise to local debonding of the laminates. Therefore, the value of the effective strain is dependent on the bonded length of the FRP, its relation to the effective bond length through which interface shear stresses develop, and the relation of this length to the bond development length. Besides the FRP axial rigidity, the shear strength of the concrete also affects the development length, so the effective strain becomes a function of the quantity $(\rho_f E_f)/(f'_c{}^{2/3})$, where f'_c is the concrete compressive strength.

The newly proposed equation for the shear contribution of FRP is essentially the same as Eqn. 2-22, but the effective strain ($\varepsilon_{f,e}$) is replaced by the characteristic value ($\varepsilon_{fk,e} = 0.8\times\varepsilon_{f,e}$) and new values for γ_f and $\varepsilon_{f,e}$ are proposed. If shear failure is combined with or followed by FRP fracture, γ_f is equal to 1.20 for CFRP, 1.25 for AFRP, and 1.30 for GFRP. If failure is dominated by FRP debonding, then γ_f is equal to 1.30. These values may be adjusted as more experimental data become available. The expressions for the effective FRP strain are grouped according to the bonding configuration and the type of material used, as given in Eqn. 2-29.

Fully wrapped CFRP:

$$\varepsilon_{f,e} = 0.17\left(\frac{f'_c{}^{2/3}}{\rho_f E_f}\right)^{0.30} \varepsilon_{f,u} \qquad (2\text{-}29a)$$

Side-bonded or U-shaped CFRP:

$$\varepsilon_{f,e} = \min\left[0.65\left(\frac{f'_c{}^{2/3}}{\rho_f E_f}\right)^{0.56} \times 10^{-3},\ 0.17\left(\frac{f'_c{}^{2/3}}{\rho_f E_f}\right)^{0.30} \varepsilon_{f,u}\right] \qquad (2\text{-}29b)$$

Fully wrapped AFRP: $$\varepsilon_{f,e} = 0.048\left(\frac{f'^{2/3}_c}{\rho_f E_f}\right)^{0.47} \varepsilon_{f,u} \quad (2\text{-}29c)$$

Below a limiting value of $\rho_f E_f$, none of the FRP failure mechanisms were noted, giving a direct relationship between FRP shear contribution and $\rho_f E_f$. However, once this limiting value $(\rho_f E_f)_{lim}$ was exceeded, failure was governed either by debonding combined with shear failure if the FRP was not properly anchored, or by shear fracture combined with or followed by FRP rupture if anchored or fully wrapped. For both cases, the concrete strength affects the increase in shear strength, but in the second situation, the dependence on $\rho_f E_f$ is more prominent, as evidenced in Figure 2.44.

Therefore, the value of $\rho_f E_f$ should be limited unless debonding can be prevented with the use of anchorages. The limiting value is suggested to be

$$(\rho_f E_f)_{\text{lim}} = \left(\frac{0.65\times 10^{-3}\alpha}{\varepsilon_{\max}}\right)^{1/0.56} f'^{2/3}_c = 0.018 f'^{2/3}_c \quad (2\text{-}30)$$

where $\varepsilon_{max} = 0.005$, a limit imposed to ensure that the shear integrity of the concrete is maintained so that mechanisms such as aggregate interlock will remain effective. It was also recommended that if vertical FRP strips are employed, their spacing s_f should not exceed 0.8d.

The FRP shear contribution equation was also expressed in the ACI and Japan Concrete Institute (JCI) code formats. The ACI format is given as:

$$\varphi_f V_f = \varphi_f \varepsilon_{f,e,A} \rho_f E_f (\sin\beta + \cos\beta) bd \quad (2\text{-}31)$$

where φ_f is the strength reduction factor, equal to 0.75 for debonding failure and 0.80 for shear failure with FRP fracture, and $\varepsilon_{f,e,A} = 0.9\ \varepsilon_{f,e} \leq 0.006$. In the JCI code format, the only modification from the Eurocode format is that the value of $\varepsilon_{f,e}$ given by Eqn. 2-29 must be multiplied by 1.035. A comparison of experimental and theoretical values for the effective FRP strain showed that the proposed model gave better agreement than the models of Khalifa *et al.* [25] and the JCI approach, but the data analyzed had already been used in the calibration of the proposed equations.

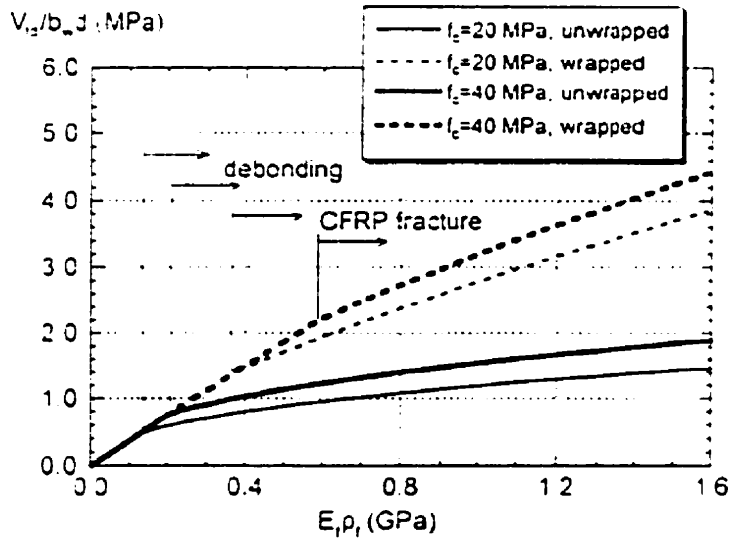

Figure 2.44: FRP contribution to shear capacity in terms of $\rho_f E_f$ [47]

A more recent empirical model for determining the effective FRP strain ($\varepsilon_{f,e}$) has been proposed by Schnerch [48]. The equation was based on experimental data published in the literature and concentrated on beam failures dominated by FRP debonding. FRP fracture was disregarded by the researcher as this mode of failure was noted to occur only in cases of complete wrapping with FRP (which is not practical in field applications) or when pseudo-isotropic laminates (with fibres oriented in more than one direction) are used. The model is in the form of:

$$\varepsilon_{f,e}=0.0012\frac{k_L}{\rho_s+0.0065}\left(\frac{f'_c}{\rho_f E_f}\right)^{3/4}\sqrt{\frac{\sin\beta}{k_E}\frac{d_f}{d}}\times10^{-3} \quad (2\text{-}32)$$

where k_L accounts for the laminate directions (1.0 for unidirectional and 1.4 for two or more orientations), ρ_s is the steel shear reinforcement ratio ($A_s/(b_w s)$), f'_c is the concrete strength, ρ_f is the FRP reinforcement ratio defined as $(2t_f/b_w)/(w_f/s_f)$ as before, E_f is the elastic modulus of FRP, β is the angle of the FRP fibres from the beam axis, k_E is the number of free edges on one side of the beam (1.0 for U-jackets and 2.0 for laminates bonded to the beam sides only), d_f is the height over which the FRP composites coincide with steel stirrups, and d is the effective depth. It was suggested that the effective strain does not have to be limited (except by the ultimate strain of the FRP material) to maintain the shear integrity of the concrete since the shear cracks formed are fine and closely spaced. Once the effective strain has been determined, it can be applied in Eqn. 2-24 to determine the shear contribution of FRP laminates. Of the 56 test results analyzed, the average value of experimental to predicted shear capacity for the proposed model was 1.34 (with a standard deviation of 0.22), while for the Khalifa model, the average was 2.13 (with a standard deviation of 0.93). However, since the test data were used to calibrate the equation, more independent experimental results are required to validate the model.

A system for evaluating the shear capacity of RC members bonded with CFRP sheets was presented by Kamiharako *et al.* [49], in which a constitutive model for the bond interface between concrete and FRP was included. The shear capacity of the beam is determined based on the ultimate deformation of the member and the bond behaviour of the CFRP sheet. To characterize the bond stress-strain relationship, uniaxial tests were performed on concrete prisms bonded with CFRP or AFRP composites. The shear stress-shear displacement curves obtained from the experiments are shown in Figure 2.45(a), and the general relationship is transformed from a bilinear curve to an equivalent linear elastic model as depicted in Figure 2.45(b). The values obtained for the parameters of τ_z and δ_z at which the bond fails are summarized in Table 2.2.

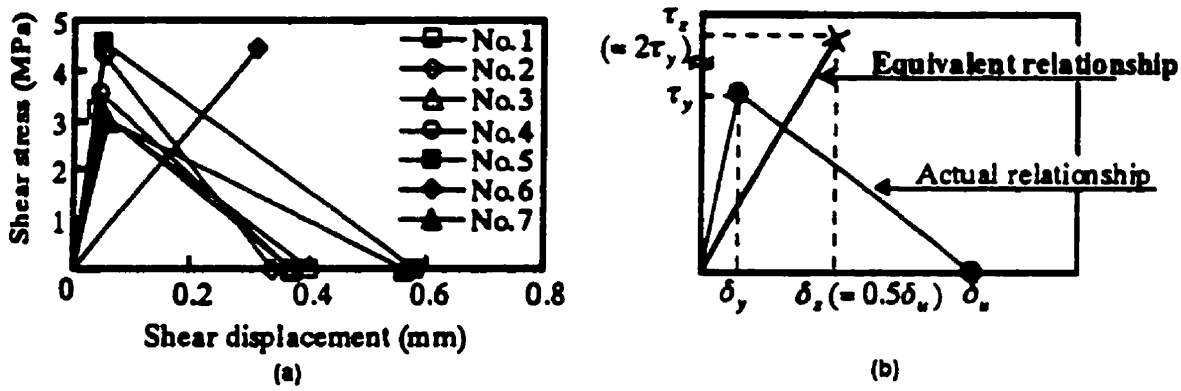

Figure 2.45: Shear stress-displacement relationships: (a) from experiments, (b) equivalent[50]

Table 2.2: Values of Parameters in Equivalent Bond Constitutive Model [50]

Type of FRP Sheet	Elastic Modulus of Epoxy (GPa)	τ_z (MPa)	δ_z (mm)
Carbon	0.7	4.47	0.31
	1.5	7.07	0.19
Aramid	0.7	5.92	0.28
	1.5	9.12	0.29

The proposed computational system is based on the fact that the tensile strain in the FRP depends on the shear crack width and the length of the peeling-off zone. The shear crack width is calculated from the rigid body rotation model, while the length of the peeling-off zone is determined by solving Eqn. 2-33 for δ:

$$t_f E_f \frac{d^2\delta}{dy^2} - k\delta = 0 \qquad (2\text{-}33)$$

where t_f and E_f are the thickness and elastic modulus of the FRP sheet, δ is the shear displacement at the border of the bonding and peeling-off zones (refer to Figure 2.46(a)), and $k = \tau_z/\delta_z$. Once δ exceeds δ_z, the FRP sheet will peel off from the concrete over the shear crack, schematically shown in Figure 2.46(b). The FRP strain is determined once equilibrium

equations for tensile force and compatibility of displacement are satisfied. Then, the shear force carried by the FRP element is found by multiplying the strain value by the FRP's elastic modulus and cross-sectional area. Although the values predicted by the proposed method agreed reasonably well with 32 sets of experimental data, the peeling-off zone was overestimated for large beams.

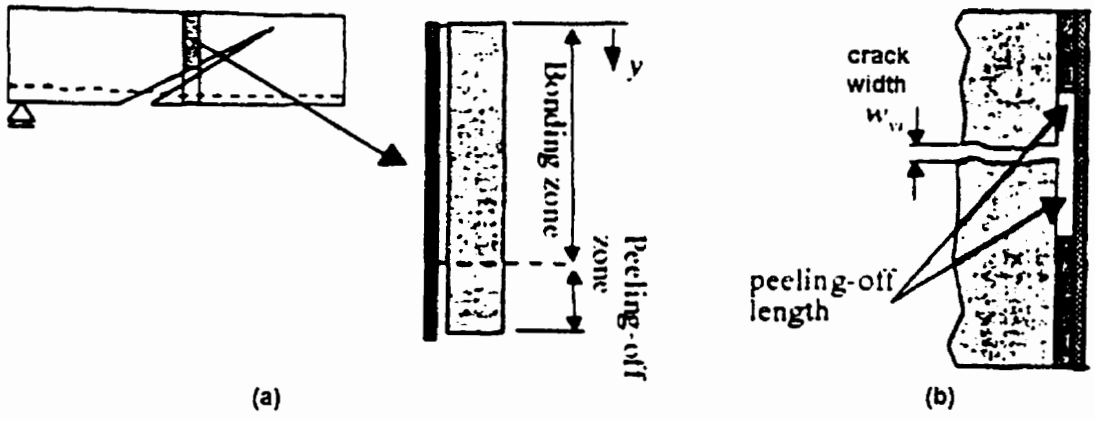

Figure 2.46: Models used for calculating peeling-off length: (a) global, (b) local [49]

2.4 BOND CHARACTERIZATION

Whether FRP composites are used for the flexural or shear strengthening of RC members, premature failure by debonding of the FRP laminates is prevalent. For beams strengthened in flexure, debonding may occur at the plate end due to high shear and normal stresses or near mid-span where high shear stresses exist around flexural cracks. For FRP sheets bonded to beam webs (refer to Figure 2.47), peeling may start from the intersection of a major shear crack and the boundary edge of the FRP sheet (case a), or debonding can take place near internal cracks once bond-slip exceeds the ultimate bond-slip value (case b).

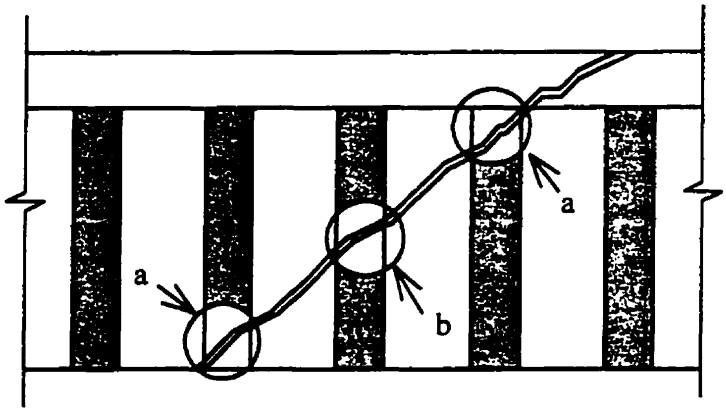

Figure 2.47: Common locations for FRP strips on beam webs to debond

Bond is of utmost importance in the strengthening system as it provides the shear transfer between concrete and FRP necessary for composite action. To attain a better understanding of the debonding phenomenon, researchers have performed bond tests in an attempt to characterize the bond behaviour. The major areas of study include the maximum shear stress and bond-slip that can be sustained by the bond interface, the relationship between bond stress and slip, the factors which influence this relationship, and the modes of failure. Experimental, analytical, and fracture mechanics approaches have been undertaken.

2.4.1 *MEASURES OF BOND STRENGTH*

Numerous experimental studies have been carried out to examine the bond behaviour between FRP composites and concrete. Several common specimen types employed in these tests are shown in Figure 2.48: specimen (a) is used to obtain the bond strength directly, types (b) and (c) are used to estimate the effects of shearing and bending, while specimen types (d) and (e) are designed to eliminate the load eccentricity that results when laminates are bonded on two faces.

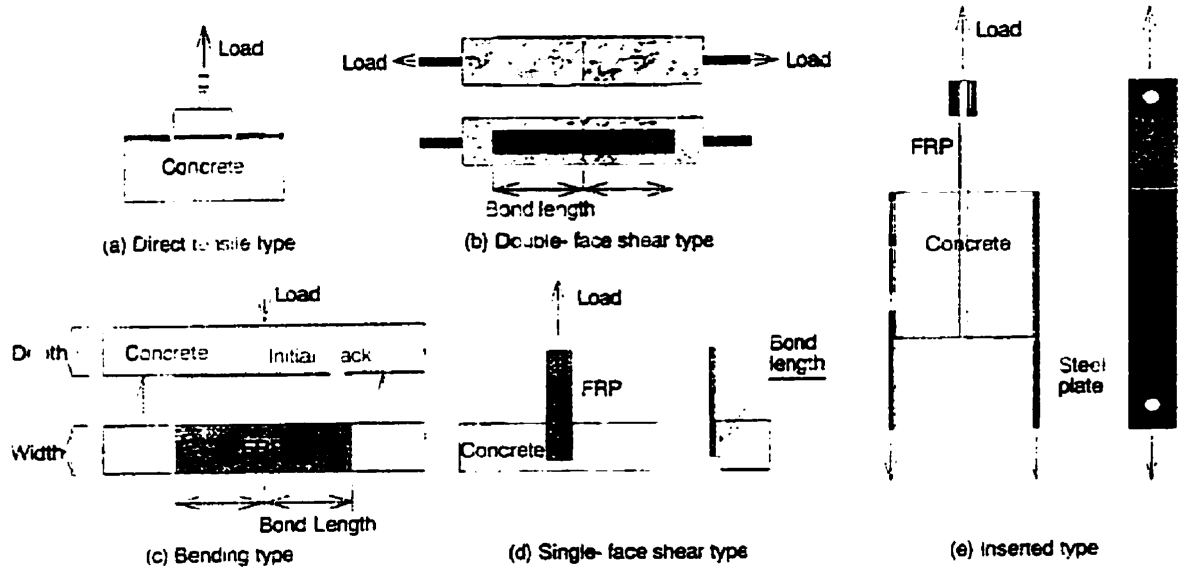

Figure 2.48: Typical bond test specimens [50]

One of the earlier studies was performed by Chajes *et al.* [51], in which single-lap shear test specimens and 25 mm wide CFRP plates were used. It was concluded that the concrete surface should be mechanically abraded or sandblasted and a primer should be applied, and the surface of the composite plate should be roughened. An "off-the-shelf" epoxy is sufficient but ductile adhesives (those with a low elastic modulus or a large strain to failure) are less effective. If the failure mode of the bond is governed by shearing of the concrete beneath the bond, the ultimate bond strength will be proportional to $f'_c{}^{0.5}$.

Tests with varying bond lengths were conducted to study the force transfer from the FRP plate to the concrete. The load transfer, indicated by the strain distribution measured on the FRP plate, is a shear flow that depends on the relative stiffnesses of the adherents and the adhesive. The strain distribution along the bonded length decreased at a linear rate, meaning that the force transfer was nearly uniform, giving a constant value of bond resistance R (equal to the shear stress multiplied by the width of the FRP plate). For a joint with a bond length L_b, the ultimate capacity (T_u) can be estimated by

$$T_u = RL_b \qquad \text{for } L_b < L_{jd}$$

$$T_u = RL_{jd} \qquad \text{for } L_b \geq L_{jd} \tag{2-34}$$

where L_{jd} is the bond development length beyond which no further increase in load can be achieved.

A series of shear bond tests was performed by Ueda *et al.* [52] to determine the maximum bond stress and factors that have an influence on its value. Conclusions reached include: bond strength does not increase with bond length once this length exceeds 100 mm; as the CFRP stiffness increased (up to 50 GPa-mm), the maximum local and average bond stresses at delamination increased and the CFRP strain gradient decreased; narrow strips of CFRP exhibited higher bond strength than wider strips; and steel plates anchored with tension bolts provided an enhancement to the bond strength. From the experimental data, Eqn.2-35 was proposed to calculate the value of the maximum bond stress (τ_{max}) using variables defined previously:

$$\tau_{max} = 0.19 t_f E_f \leq 7.3 \tag{2-35}$$

Two other empirical models relating the bond length (L) and the average bond shear stress at failure (τ_u) are those of Hiroyuki and Wu (1997) (Eqn.2-36) and Tanaka (1996) (Eqn.2-37) [53]:

$$\tau_u = 5.88 L^{-0.669} \tag{2-36}$$

$$\tau_u = 6.13 - \ln L \tag{2-37}$$

The maximum bond strength of the joint is obtained by multiplying τ_u by the width b_p and length L of the bonded area.

Horiguchi and Saeki [54] conducted three types of bond tests using concrete of three different strengths to determine the effect of test methods and quality of concrete on the bond strength of CFRP sheets. The tests involved subjecting CFRP sheets to shear, flexure and direct tension. The relationship between the bond strength, the test type and the concrete strength is depicted in Figure 2.49, while the observed failure modes are summarized in Table 2.3.

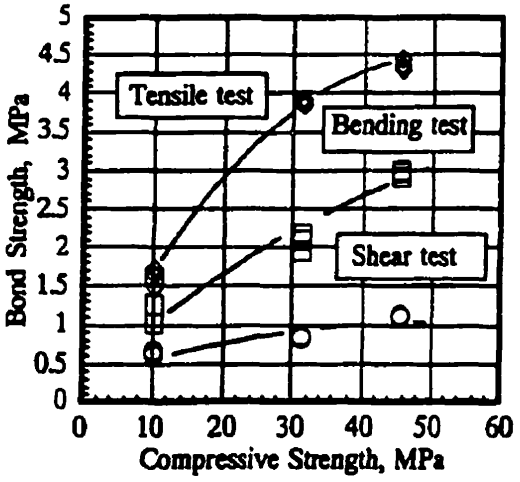

Figure 2.49: Relationship between bond strength, test type and concrete strength [54]

Table 2.3: Failure Modes Observed in Bond Tests [54]

Type of Bond Test	Concrete Compressive Strength (MPa)		
	11	31	46
Shear test	delamination	delamination	delamination
Bending test	concrete [1]	delamination	CFRP fracture
Tensile test	concrete [1]	delamination	concrete [2]

[1] mortar matrix fracture, [2] matrix/aggregate interfacial fracture

From the experimental results, the following estimations for bond strength (f_{bond}) were proposed:

$$f_{bond}\,(\text{shear}) = 0.09\,(f'_c)^{2/3}$$

$$f_{bond}\,(\text{bending}) = 0.22\,(f'_c)^{2/3}$$

$$f_{bond}\,(\text{tensile}) = 0.36\,(f'_c)^{2/3} \qquad (2\text{-}38)$$

In a study by Brosens and Van Gemert [55], double-shear prisms were used to examine the shear stress distribution and fracture behaviour of CFRP. The fracture loads were predicted with the models proposed by Täljsten and Van Gemert. A nonlinear fracture mechanics concept is adopted in Täljsten's (1994) [55] theory, in which the ultimate load is found from Eqn. 2-39 as

$$P_{max} = b_f \sqrt{\frac{2 t_f E_f G_f}{1+\alpha}} \tag{2-39}$$

$$\text{where} \quad \alpha = \frac{t_f E_f}{t_c E_c}$$

b_f is the width of the CFRP laminate, t is thickness, E is the modulus of elasticity, G_f is the fracture energy, and the subscripts f and c represent FRP and concrete, respectively. Difficulty arises in calculating the fracture energy from the measured values of load, deformation and shear stresses. A relationship between fracture energy and the concrete properties should be determined. The method proposed by Van Gemert (Eqn. 2-40), based on a triangular shear stress distribution over the full bond length, is simpler to apply, but the fracture load estimated is the one at first cracking while the remaining strength reserve is neglected:

$$P_{max} = \frac{b_f \, l \, f_{ct}}{2} \tag{2-40}$$

where l is the bond length and f_{ct} is the pull-off strength of the concrete surface.

Maeda *et al.* [46] carried out an experimental study on the bond mechanism of CFRP sheets using a double-face shear type specimen and attempted to simulate the strain distribution using FEM. It was found that the strain distribution curve of the FRP shifted from quadratic to linear as ultimate load was approached, and the active bonding area was shifted as delamination propagated, as seen in Figure 2.50. The effective bond length was noted to decrease as the CFRP stiffness increased.

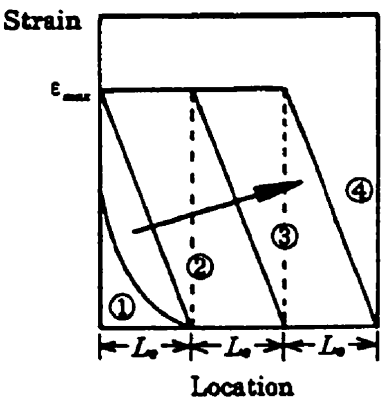

Figure 2.50: Schematic of strain distribution in CFRP sheet during shear bond test [46]

The CFRP strain distribution was simulated using the FEM program WCOMR, in which a smeared crack model and average stress-strain relationships were adopted. A typical mesh used for the analysis is drawn in Figure 2.51, while the elastic modulus, shear modulus and thickness of the bond elements representing the epoxy resin were 1.50 GPa, 0.58 GPa and 0.1 mm, respectively. The predicted distributions were found to be fairly accurate as long as the nonlinear behaviour caused by concrete cracking was considered.

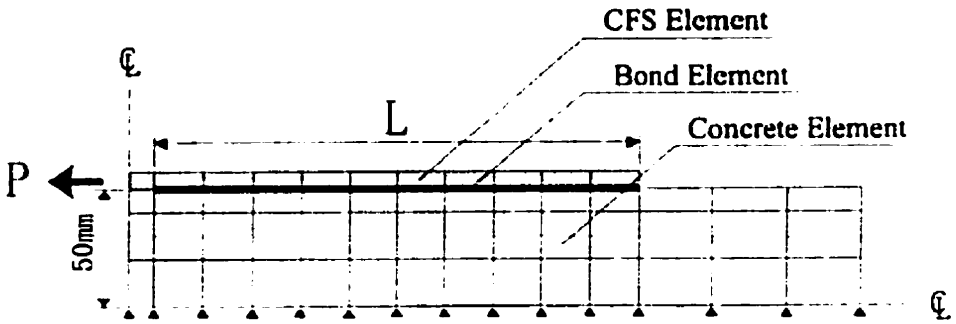

Figure 2.51: Finite element mesh for analysis of CFRP-bonded concrete prism [46]

The ultimate load that can be taken by the CFRP sheet (P_{max}) can be calculated from:

$$P_{max} = L_e b \tau_u \tag{2-41}$$

$$\text{where} \quad \tau_u = t_f E_f \left(\frac{d\varepsilon}{dx}\right)_0$$

L_e is the effective bond length calculated from Eqn. 2-27, t_f and E_f are the thickness and elastic modulus of the FRP, respectively, and $(d\varepsilon/dx)_0$ is the strain gradient for the effective bond length (measured to be 110.2 μ/mm in this test).

A flexural specimen was employed in Miller and Nanni's [56] investigation of the strain distribution between CFRP sheets and concrete. All of the specimens failed by peeling: the CFRP sheet assumed all of the load up to the level of localized peeling, then the effective bond length shifted until complete peeling had occurred. It was found that as the bond length increased, the bond strength decreased. Concrete strength did not have any effect on the bond strength as the specimens failed within the bond interface. Increasing the CFRP stiffness raised the bond strength, but the increase was not proportional to the number of plies used. The ultimate load (P_{max}) sustainable by the CFRP sheet can be determined by:

$$P_{\max} = L_e \, w \tau \tag{2-42}$$

$$\text{where} \quad L_e = -0.432\left(t_f E_f\right) + 94.3 \;, \qquad \tau = t_f E_f \left(\frac{d\varepsilon}{dx}\right)_{avg} \times 10^{-6}$$

in which L_e is the effective bond length, w is the width of the FRP sheet, τ is the average bond stress, t_f and E_f are the thickness and elastic modulus of the FRP, and $(d\varepsilon/dx)_{avg}$ is the average strain gradient for the effective bond length (found to be 88 μ/mm in this experiment).

2.4.2 *FACTORS INFLUENCING BOND STRENGTH*

The effect of various bonding conditions on the bond strength between CFRP sheets and concrete has been examined by Yoshizawa *et al.* [57]. Using double-face shear specimens, bonding conditions such as surface preparation (with water jet or sander), types of CFRP sheets (high tensile strength or high modulus), and debonding area rate (with varying amounts of film to simulate debonding) were assessed. It was reported that surface treatment by water jet was superior in enhancing the bond strength, and that the bond strength for high modulus CFRP was greater than that for low modulus, high tensile strength CFRP. The bond strength also increased as more layers of CFRP laminates were applied, but the artificially-induced debonding (from 6 to 13%) did not have any influence on the bond strength. Flexural tests involving full-scale beams were also conducted, from which it was found that fracture of the concrete cover occurred, rather than separation of the CFRP laminate from the concrete.

An experimental investigation performed by Tripi *et al.* [58] aimed to characterize the local and global deformations in tensile-loaded concrete prisms bonded with CFRP sheets. The main variables studied were the thickness of the adhesive layer and the modulus of the CFRP fibres. Among the observations was the indication that diagonal cracking affected load transfer near cracks. Thus, the concrete strength must be considered in the bond behaviour of external FRP reinforcement. It was concluded that the local deformations are dependent on the thickness of the adhesive layer; thicker layers created a gradual transfer of load between concrete and CFRP which was manifested in larger relative displacements and greater crack spacing. The modulus of the CFRP sheet had a large influence on the magnitude of peak longitudinal strains at cracks, but the relative displacements and crack spacing were only slightly affected. Hence, it was hypothesized that the FRP sheet extensional stiffness (modulus × thickness) controls the global behaviour while the epoxy shear stiffness (modulus ÷ thickness) controls the local behaviour. Since a stiff adhesive layer was found to promote cracking, the stiffness of a cracked RC member is best enhanced through the use of a high-modulus FRP laminate.

Bizindavyi and Neale [59] conducted an experimental and theoretical investigation into the shear conditions at the concrete-FRP interface. Single shear-lap specimens were tested, and three distinct profiles were noted in the FRP strain distribution curves, an example of which is shown in Figure 2.52. As the load was initially applied, the strain profile decreased exponentially starting from the loaded end. The distance required for the strain to reach zero is termed the initial transfer length. Once a crack was initiated in the concrete, the transfer region shifted towards the free end of the FRP laminate. The strain profile changed to a bilinear curve, with the transition point located at the limit of the initial transfer length. Near ultimate loads, the strain distribution became linearly decreasing. As for the shear stress distributions, the trend was also exponential at loads lower than the initial cracking load. After cracking occurred, the maximum shear stress location progressively transferred toward the unloaded end of the specimen until the joint failed completely.

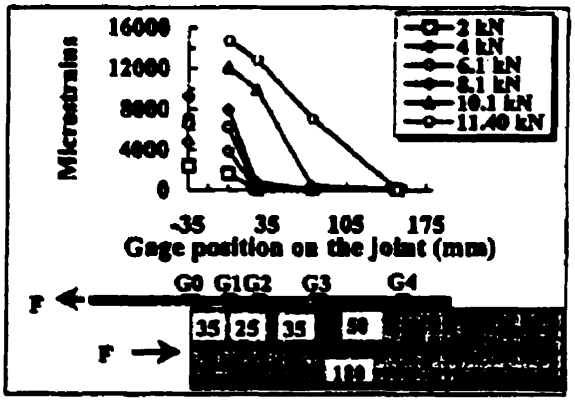

Figure 2.52: Strain distribution along GFRP-concrete joint [59]

The relationship between the transfer length and the relative load level is bilinear, with a constant value of transfer length for loads less than the cracking load and a linearly increasing portion up to failure. The transfer length (L_t) may be estimated using

$$L_t = L_0 \qquad \text{for} \quad \xi \leq \xi_0$$

$$L_t = L_0 + \left(\frac{\xi - \xi_0}{\xi_{max} - \xi_0}\right)(L_j - L_0) \quad \text{for} \quad \xi_0 \le \xi \le \xi_{max} \tag{2-43}$$

$$\text{where } L_0 = \frac{\xi_0 F_{max}}{b_f \tau_{mean}}$$

in which L_0 is the initial transfer length, ξ is the relative load level (F/F_{max}), ξ_0 is the relative load level at which cracking initiates, L_j is the joint length, F_{max} is the ultimate load, b_f is the FRP width and τ_{mean} is the average bond strength. Whether concrete shear failure or FRP rupture occurs depends on the transfer of forces exceeding the cracking load and the bond length available to carry additional loads.

A theoretical expression, based on the shear lag theory and valid only in the elastic range, was defined for the shear stress distribution ($\tau(x)$) on the FRP-concrete joint:

$$\tau(x) = B\cosh(\lambda x) + C\sinh(\lambda x) \tag{2-44}$$

$$B = \tau_m \frac{\lambda L_j}{\tanh(\lambda L_j)}, \quad C = -\lambda L_j \tau_m, \quad \tau_m = \frac{F}{b_f L_j}$$

$$\lambda = \left[\frac{G_a}{E_f t_f t_a}(1 + \eta\rho)\right]^{1/2}, \quad \eta = \frac{E_f}{E_c}, \quad \rho = \frac{A_f}{A_c}$$

where F is the applied load, G_a and t_a are the shear modulus and thickness of the adhesive, respectively, E is the elastic modulus and A is the cross-sectional area, while the subscripts f and c stand for FRP and concrete. The axial stress in the laminate ($f_p(x)$) is presented as

$$f_p(x) = \frac{\tau_m L_j}{t_f \sinh(\lambda L_j)}\left[\sinh\lambda(x - L_j)\right] \tag{2-45}$$

The proposed equations were applied to the test specimens from the study. Although the predicted strain distributions agreed well with the actual response at service load levels, the theoretical response was stiffer when thicker laminates were used since peeling failure was not considered in the analysis.

2.4.3 *DEBONDING MECHANISM*

Double-face shear type specimens were also the subject of study of Wu and Yoshizawa [60]. The test variables included two types of CFRP materials, two concrete strengths, two thicknesses of concrete cover, varying layers of CFRP sheets and different rebar ratios. The experimental results are given in detail by the researchers. The propagation behaviour of the crack front and the process of debonding, as observed from experiments, is illustrated in Figure 2.53. As the tensile crack propagates and joins with diagonal shear cracks near the FRP sheet, the shear stiffness of the interfacial layer is reduced. With the front of the diagonal crack along the bond interface, the possibility of debonding grows.

Since debonding is typically initiated by a tensile crack in the concrete, the constitutive relationship along the bond interface before the initiation of debonding can be expressed as in Figure 2.54(a). Bond fracture usually propagates along the bond interface between concrete and FRP or through the concrete adjacent to the interface. Therefore, the shear stress-displacement relationship after debonding can be related to the softening behaviour of concrete in shear (Figure 2.54(b)). The area G_f under the τ–δ curve including or excluding pre-peak shear displacement can be defined as the fracture energy based on a nonlinear fracture energy concept.

However, the bond between concrete and FRP may fail suddenly due to the catastrophic propagation of a crack along the bond interface. Thus, the debonding phenomenon becomes a problem involving fracture mechanics, in which fracture is considered to occur when the strain energy release rate equals the critical strain energy

release rate for the interface G_{IIC} (can be approximated by G_f). This arises from the assumption that debonding is a Mode II (forward shear) type failure mechanism.

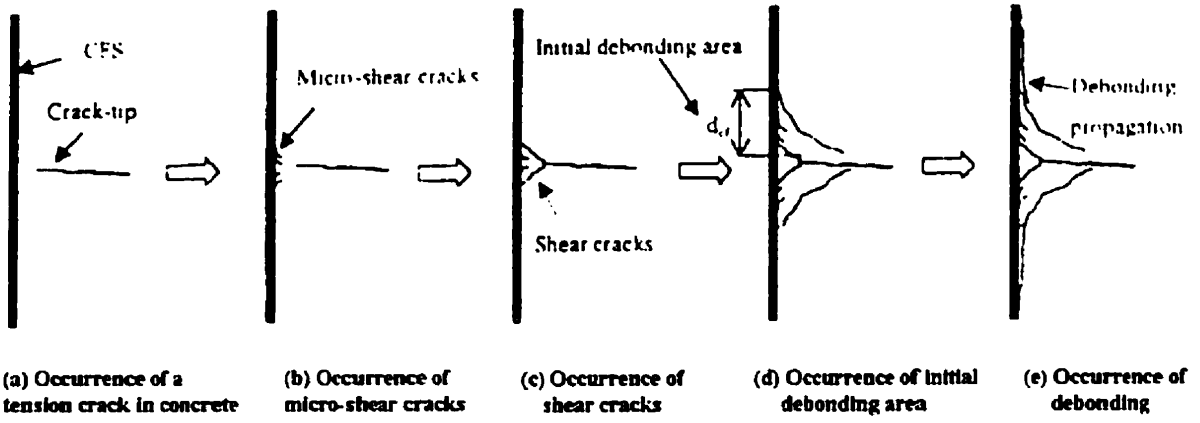

Figure 2.53: Crack propagation and formation of debonding [60]

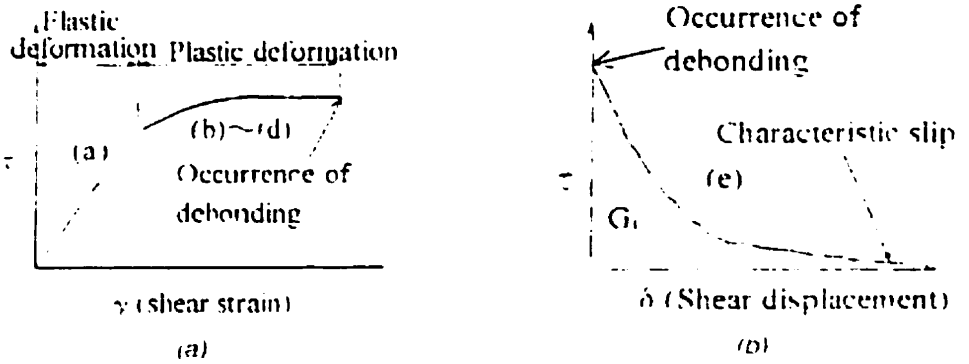

Figure 2.54: Constitutive relationship for bond interface: (a) prior to debonding, (b) after debonding [60]

The researchers proposed a model for analyzing the tensile properties of FRP-bonded RC members based on the fracture energy approach. Figure 2.55 shows a RC member subjected to a tensile stress σ resulting in N number of cracks. The symbols in the figure are defined as follows: L = length of member, b = width of member, E = elastic modulus, V =

volume ratio, d = debonding length, S = average crack spacing, t = thickness of RC member and the subscripts c, s and cf represent concrete, steel and CFRP, respectively. As the concrete member cracks, the FRP near the cracks starts to delaminate from the concrete. Once the FRP stress at the crack reaches the bond strength, the debonding areas connect together (Figure 2.55). Thus, the sheet becomes delaminated for the length of the concrete member except at the ends, and final debonding failure occurs when the sheet is completely separated from the concrete.

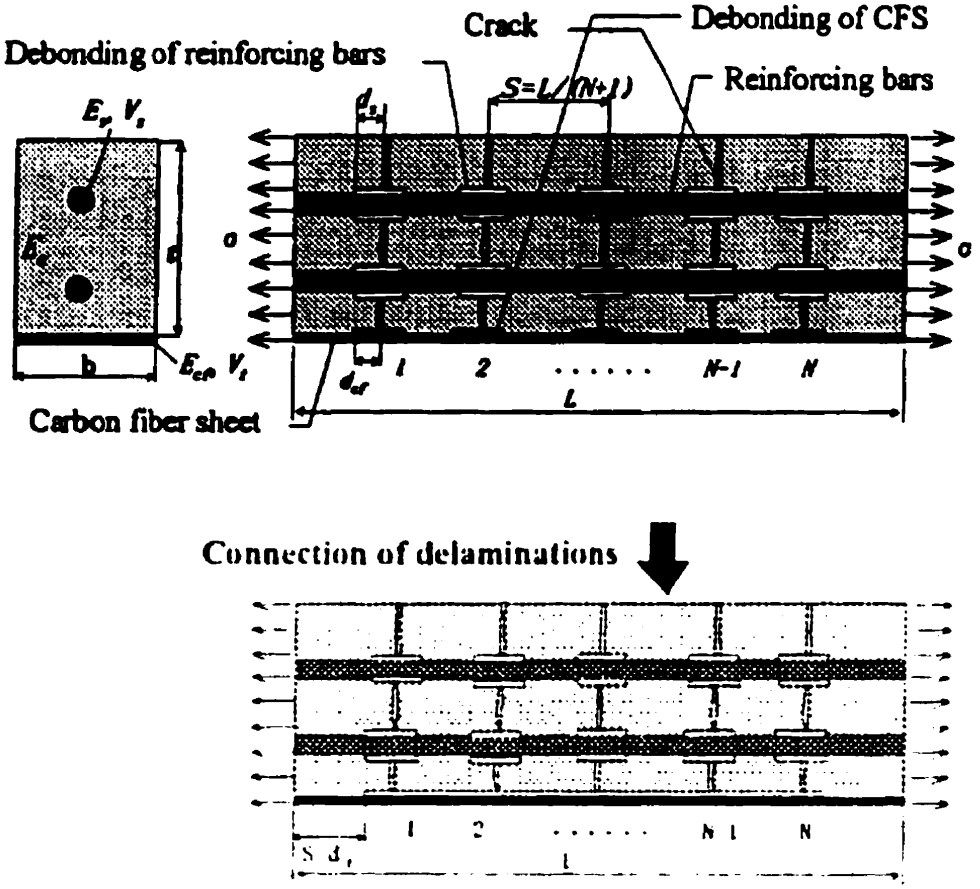

Figure 2.55: RC member bonded with CFRP sheet: general representation and connection of delamination between FRP and concrete [adapted from 61]

Essential to the development of the theoretical model is the energy equilibrium required during cracking. Thus, the strain energy release rate should be equal to the sum of the rate of the debonding energy and sliding energy at the rebar-concrete interface, the debonding energy along the FRP-concrete interface, and the fracture resistance of concrete, as stated by:

$$-\frac{1}{bt}\frac{\partial \varphi_c}{\partial N} = R_{lcf} + \frac{1}{bt}\frac{\partial(\varphi_s + \varphi_{ds} + \varphi_{dcf})}{\partial N} \tag{2-46}$$

where φ_c is the strain energy of concrete containing N cracks, without debonding and sliding of rebars and the debonding of FRP sheet, φ_s is the total sliding energies on all debonded interfaces between rebars and concrete, φ_{ds} is the total debonding energies on all debonded interfaces between rebars and concrete, φ_{dcf} is the total debonding energies on all debonded interfaces between FRP and concrete, and R_{lcf} is the fracture resistance of plain concrete. The debonding fracture energy φ_{dcf} can be calculated as follows:

$$\varphi_{dcf} = 2Nbd_{cf}\gamma_{cf} \tag{2-47}$$

where d_{cf} is the initial debonding length (measured to be 15 mm) and γ_{cf} is the debonding fracture energy per unit area of FRP-concrete crack surface ($\gamma_{cf} = G_{IIC} = G_f$). Using a double shear test, G_{IIC} was measured to be 6.0 N/m. The computational flow for the calculation of the tensile stresses and strains in the FRP-bonded RC member is given in Figure 2.56, while the equations used are detailed in the original paper. The load-deformation curves, crack widths and average crack constraining effect were well modelled using this analytical technique, but further research is needed regarding the FRP stress distribution and crack spacing, and the assumption of average strains must be modified.

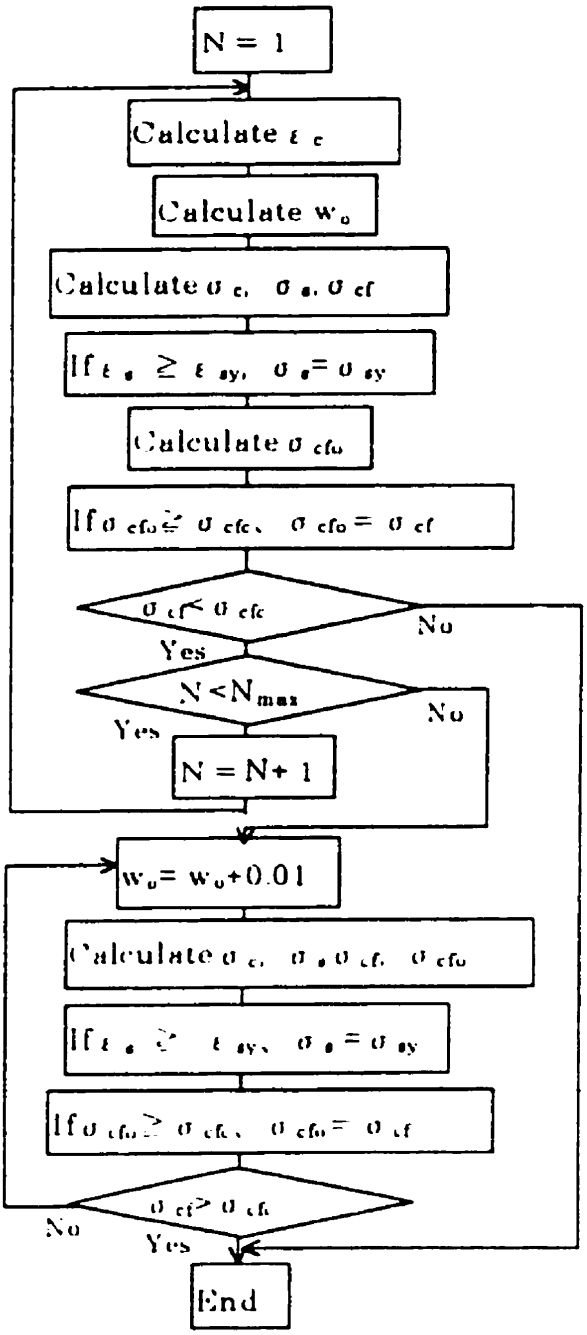

Figure 2.56: Computational flow for determining tensile properties of FRP-bonded RC member [61]

2.4.4 *BOND STRESS-SLIP RELATIONSHIPS*

In Homam's [62] study of the durability of CFRP and GFRP fabrics, double-face shear specimens were bonded with materials from the TYFO S® Fibrwrap® System. It was found that freeze-thaw cycles affected the mechanical behaviour of the FRP-concrete bond, but further investigations are required before more definite conclusions can be drawn. However, from the tests of the control specimens, it was concluded that the bond stress-slip curves resembled the stress-strain curves of ductile steel, with an initial linear elastic range followed by a plastic range. The shape of the relationship can be found in the next chapter (Figure 3.8(a)), while the average values defining the constitutive relationship are listed in Table 2.4.

Table 2.4: Values Defining Bond Stress-Slip Relationship in Homam's Study [62]

FRP Material	Maximum Bond Stress (MPa)	Slip at Maximum Bond Stress (mm)	Ultimate Slip (mm)
Carbon	3.42	0.01*	0.51
Glass	2.47	0.01*	0.67

* approximated from bond stress-slip curves

The bond stress-slip relationship adopted in Sato's [63] work is a bilinear elastic-plastic curve. The maximum bond stress (τ_m) is based on the equation given by Ueda *et al.* (Eqn. 2-35) for concrete strengths ranging from 24 to 46 MPa. Expressions for the slip when the maximum bond stress is reached (S_m) and for the ultimate slip (S_u) are given by

$$S_m = 1.96\times10^{-3}\,\frac{\tau_m}{4.56} + \frac{(b/2)\tau_m}{G_c/2} \qquad \text{(2-48a)}$$

$$S_u = 0.1 + \frac{S_m}{2} \qquad \text{(2-48b)}$$

where b is the width of the member, and G_c is the shear modulus of concrete ($G_c = 0.43\times E_c$).

Nanni *et al.* [64] and Lee *et al.* [65] presented a tension stiffening model for FRP sheets bonded to concrete, focusing on the bond-slip behaviour at the interface. Applying a linear bond stress-slip relationship, which is suitable for working loads, the slip of the FRP sheet (bonded to plain concrete) between primary cracks can be written as a second order differential equation:

$$\frac{d^2 s}{dx^2} - \frac{w_f E_b}{A_f E_f}(1+\eta\rho)s = 0 \tag{2-49}$$

With the appropriate boundary and equilibrium conditions, the above equation can be solved for expressions to calculate the axial force (F) and displacement (u) of the concrete and FRP, and the relative displacement, or slip (s), between the two materials. The resulting equations are given as Eqns. 2-50 to 2-53.

$$F_c(x) = \frac{w_f E_b C_1}{Z}(\cosh Za - \cosh Zx) \quad , \qquad F_f(x) = T - F_c \tag{2-50}$$

$$u_c = \left(\frac{\eta\rho C_1}{1+\eta\rho}\right)(Zx\cosh Za - \sinh Zx) \tag{2-51}$$

$$u_f = \frac{Tx}{A_f E_f} - \frac{C_1}{1+\eta\rho}(Zx\cosh Za - \sinh Zx) \tag{2-52}$$

$$s(x) = u_f(x) - u_c(x) \tag{2-53}$$

where $$Z^2 = \frac{w_f E_b (1+\eta\rho)}{A_f E_f} \quad , \qquad C_1 = \frac{T}{(Z\cosh Za)(A_f E_f)}$$

in which w_f is the width of the FRP sheet, E_b is the slip modulus, A_f is the cross-sectional area of FRP, E_f is the FRP's elastic modulus, η is the modular ratio between FRP and

concrete (E_f/E_c), ρ is the FRP reinforcement ratio (A_f/A_c), a is half of the distance between two cracks, T is the total uniform tensile force, and the subscripts c and f represent concrete and FRP, respectively. The slip modulus (E_b) can be estimated from a simple shear model as follows:

$$s = \gamma t, \quad \gamma = \frac{\tau}{G} \quad \Rightarrow \quad E_b = \frac{\tau}{s} = \frac{G}{t} \tag{2-54}$$

where τ is the shear stress and γ is the shear strain, and G and t are the shear modulus and thickness of the epoxy, respectively. No shear is assumed to exist in the FRP sheet or concrete in this model. After conducting an experimental study, it was found that this estimate of the slip modulus was higher than the test value, and that it was only applicable prior to secondary cracking.

The above approach was further extended by Lee *et al.* [66] to RC members bonded with FRP sheets. Using equilibrium conditions similar to those described above (with the inclusion of a reinforcing steel component), and assuming linear bond stress-slip behaviour, ordinary differential equations were developed. By imposing the necessary boundary conditions, the distribution of the force, displacement and slip were established and presented in Appendix I of the referenced paper. The researchers subjected several small-scale and large-scale double-face shear specimens to tension. Using the theoretical calculation, moiré interferometry and mechanical deformation measurements, trial values of the slip modulus at the concrete-FRP interface were found to be in the range of 137 to 5290 MPa/mm. Mechanical deformation data were affected by the shear deformation in the concrete, epoxy, and FRP sheet. Thus, the apparent slip modulus values were reduced. The slip modulus from the moiré interferometry (1690 MPa/mm) was considered to be the most reliable. It was lower than the shear stiffness of the epoxy but higher than the combined shear stiffness of the epoxy and concrete. The slip modulus was found to be independent of the type of FRP sheet used. It was also concluded that as the thickness of the epoxy layer decreased, the stiffness of the specimen increased. While the member with the highest slip modulus exhibited the

greatest tension-stiffening behaviour, the stiffness of the FRP and adhesive were not as influential as the number of tension cracks that had developed.

Nakaba *et al.* [50] examined the bond behaviour between FRP laminates and concrete to obtain the local bond stress-slip relationship. The parameters studied in the double-shear bond test were the mechanical properties of FRP fibres and concrete. The main conclusions drawn from the experiments include: the bond strength and maximum load increased as the FRP stiffness increased, the type of fibre affected the shape of the stress distribution but did not influence the local bond stress-slip relationship, the thickness of the adhesive layer did not affect the maximum load sustained, and the maximum local bond stress increased as the compressive strength of concrete increased. As for the effective bond length, in which the bond stress is distributed, previous studies have reported values ranging from 20 to 100 mm. The tests described here showed that the effective bond length increased as stiffer FRP laminates (with higher values of $t_f \times E_f$) were utilized. Also, the effective bond length was suggested to be the distance measured at 10% of the maximum bond stress, as shown in Figure 2.57.

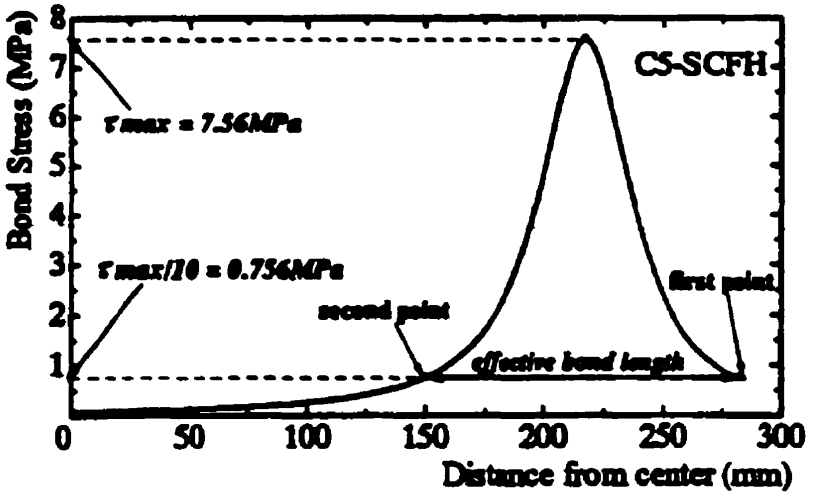

Figure 2.57: Example of effective bond length [50]

A typical plot of local bond stress-slip relationships obtained from the experiment is presented in Figure 2.58, in which it can be seen that the curves tended to be parabolic in form. Maximum local bond stress ($\tau_{b,max}$) varied from 5.6 to 9.1 MPa, while the slip at $\tau_{b,max}$ ranged from 0.052 to 0.087 mm.

The test data were fitted with Popovics' (1973) [50] equation, with the final bond stress-slip relation given as:

$$\frac{\tau_b}{\tau_{b,\max}} = \frac{s}{s_{\max}} \frac{n}{(n-1)+(s/s_{\max})^n} \tag{2-55}$$

where $\tau_{b,\max} = 3.5 f'^{0.19}_c$

τ_b is the local bond stress, s is slip, $\tau_{b,max}$ is the maximum local bond stress, s_{max} is the slip at $\tau_{b,max}$ (0.065 mm), n is a constant (3) and f'_c is the concrete compressive strength restricted to a range between 24 and 58 MPa.

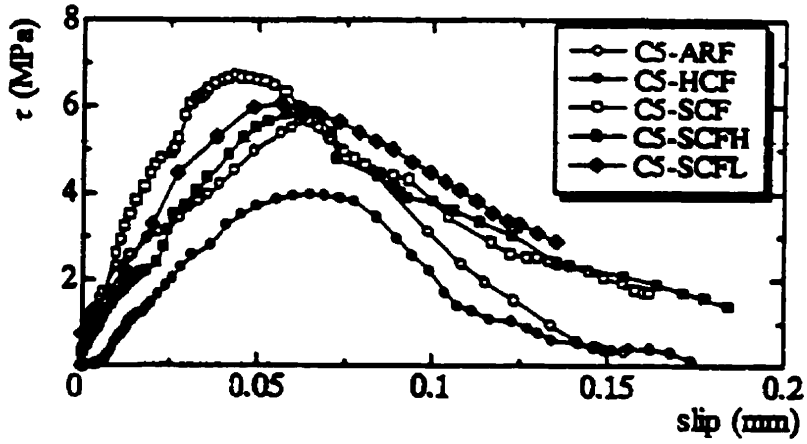

Figure 2.58: Measured bond stress-slip curves for specimens tested by Nakaba *et al.* [50]

Chen and Teng [53] reviewed the currently available anchorage strength models for concrete-FRP joints subjected to shear. The failure mode studied is shear anchorage or shear debonding failure, where cracks propagate parallel to the bonded laminate near or along the concrete-adhesive interface, starting from the most highly stressed region towards the anchored end. In single or double shear tests, there are six possible failure modes: concrete failure just beneath the concrete-adhesive interface, FRP tensile fracture, FRP delamination, adhesive failure, concrete-adhesive interfacial failure and FRP-adhesive interfacial failure. The first mode has been the most commonly reported, while the last three are rarely seen due to the high strength of adhesives used. Concrete surface failure is of primary concern since this type of failure is also noted in the first 20 to 50% of the bond length prior to FRP delamination.

In terms of fracture mechanics models, Yuan and Wu (1999) and Yuan *et al.* (2001) [53] employed linear elastic fracture mechanics (LEFM) and nonlinear fracture mechanics (NLFM) in their study of bond strength. The resulting equation from LEFM for bond strength was the same as that given by Täljsten (Eqn. 2-39), but α is replaced by α_γ (Eqn. 2-56), which accounts for the width of the FRP and concrete member.

$$\alpha_\gamma = \frac{b_f t_f E_f}{b_c t_c E_c} \tag{2-56}$$

The NLFM equations were solved for the five different bond stress-slip relationships depicted in Figure 2.59. The linearly ascending and then descending curve (Figure 2.59 (c)) may be closest to reality.

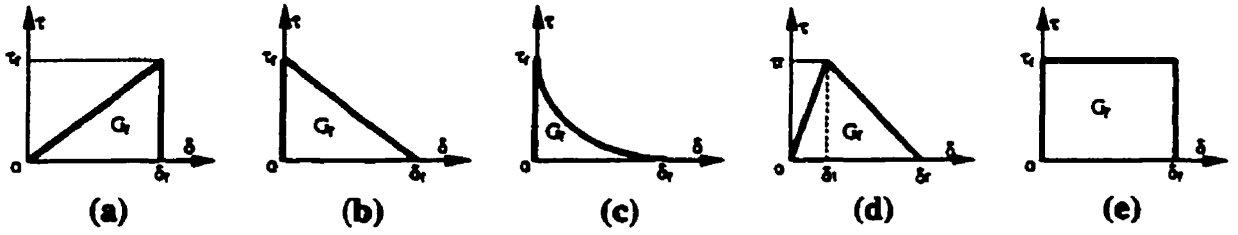

Figure 2.59: Bond stress-slip models for FRP bonded to concrete [50]

For this case, the maximum sustainable load (P_u) is given as

$$P_u = \frac{\tau_f b_f}{\lambda_2} \frac{\delta_f}{\delta_f - \delta_1} \sin(\lambda_2 a) \tag{2-57}$$

where $\tanh[\lambda_1 (L_e - a)] = \frac{\lambda_2}{\lambda_1} \tan(\lambda_2 a)$

$$L_e = a_0 + \frac{1}{2\lambda_1} \ln \frac{\lambda_1 + \lambda_2 \tan(\lambda_2 a_0)}{\lambda_1 - \lambda_2 \tan(\lambda_2 a_0)} \quad , \quad a_0 = \frac{1}{\lambda_2} \sin^{-1}\left(0.97 \sqrt{\frac{\delta_f - \delta_1}{\delta_f}}\right)$$

$$\lambda_1^2 = \frac{\tau_f}{\delta_1 t_f E_f}(1 + \alpha\gamma) \quad , \quad \lambda_2^2 = \frac{\tau_f}{(\delta_f - \delta_1) t_f E_f}(1 + \alpha\gamma)$$

in which τ_f is the maximum stress on the bond stress-slip curve, δ_1 is the corresponding slip and δ_f is the maximum slip.

Neubauer and Rostásy (1997) [50] preferred the shape of the bond stress-slip relationship as shown in Figure 2.59(d), and suggested that the fracture energy be calculated as $G_f = c_f \times f_{ct}$, where c_f was found to 0.204 mm from experiments, and f_{ct} is the tensile strength of concrete. The bond strength can be obtained from

$$P_u = \begin{cases} 0.64 k_p b_f \sqrt{t_f E_f f_{ct}} & \text{if } L \geq L_e \\ 0.64 k_p b_f \sqrt{t_f E_f f_{ct}} \frac{L}{L_e}\left(2 - \frac{L}{L_e}\right) & \text{if } L < L_e \end{cases} \tag{2-58}$$

where $k_p = \sqrt{1.125 \frac{2 - b_f / b_c}{1 + b_f / 400}}$, $L_e = \sqrt{\frac{t_f E_f}{2 f_{ct}}}$

Comparing the predictions of the published models with experimental results, it was found that when the effective bond length was not considered, the bond strength was greatly underestimated. The models proposed by Khalifa (1998) and Neubauer and Rostásy (1997) showed reasonable results, but these equations were calibrated using the experimental data.

Chen and Teng proposed a new model based on a linearly decreasing shear-slip model (Figure 2.59(b)) since typical slip values are $\delta_1 = 0.02$ mm and $\delta_f = 0.2$ mm (i.e., $\delta_1 << \delta_f$). The ultimate bond strength is given by

$$P_u = 0.427 \beta_p \beta_L \sqrt{f'_c} b_f L_e \tag{2-59}$$

where $\beta_p = \sqrt{\dfrac{2 - b_f / b_c}{1 + b_f / b_c}}$, $\beta_L = \begin{cases} 1 & \text{if } L \geq L_e \\ \sin\dfrac{\pi L}{2 L_e} & \text{if } L < L_e \end{cases}$

$$L_e = \sqrt{\frac{t_f E_f}{\sqrt{f'_c}}}$$

and the variables are the same as those previously defined. For ultimate strength design and serviceability state design, the coefficient in Eqn. 2-59 should be replaced by 0.315 and 0.2, respectively. If high stress needs to be attained in the FRP plate, a thin laminate with a high elastic modulus should be selected. However, to best utilize the full tensile strength of the FRP plate, a thin plate with a lower Young's modulus is recommended.

To summarize, most of the published literature are in agreement regarding the global behaviour and local failure modes observed in RC members flexurally strengthened with FRP composites. Good accord has been noted between numerically predicted responses and experimental data when the properties of the bond interface were considered. The breadth of

research and consequent understanding in the area of flexural strengthening with FRP can be ascribed to its similarity to bonding with steel plates, which has been studied in detail in the past. As for shear strengthening with FRP composites, comparable experimental results have been obtained in terms of the effects of the amount and orientation of the FRP, and the effectiveness of using U-wraps and anchorage systems. Several researchers have presented the concept of an effective FRP strain ($\varepsilon_{f,e}$) for estimating the shear contribution by FRP laminates. Whereas previous models focussed on the dependence of $\varepsilon_{f,e}$ on $\rho_f \times E_f$ and f'_c, more recent proposals have included the effects of the stirrup ratio and the configuration of the FRP laminates. More work is required with respect to the bond behaviour, both in determining the bond strength and the bond stress-slip relationship. Although researchers have identified numerous factors influencing the bond strength, not all of these parameters have been considered in the proposed bond strength models. Various relationships have been formulated between bond stress and slip, ranging from an elastic-plastic law to a triangular distribution to a parabolic shape, among others. Therefore, additional research is needed to pinpoint the form of the bond model, and to determine whether the type of bond law is dependent on the properties of the materials used.

CHAPTER 3 FINITE ELEMENT FORMULATIONS

3.1 INTRODUCTION

The two-dimensional nonlinear finite element program (VecTor2) used in the analytical portion of the current research has been developed at the University of Toronto. Concrete is represented by four-noded rectangular (8-degree-of-freedom (dof)) or three-noded triangular (6-dof) constant strain elements, while steel and FRP reinforcement are modelled by one-dimensional two-noded truss elements (4-dof). This program is based on an iterative, secant stiffness formulation and uses constitutive models from the Modified Compression Field Theory (MCFT) developed by Vecchio and Collins (1986) [67]. The details of the constitutive models and their implementation into the finite element program will be presented below.

3.2 THE MODIFIED COMPRESSION FIELD THEORY (MCFT)

The MCFT is a smeared, rotating crack model for analyzing reinforced concrete membranes, in which cracked concrete is represented as an orthotropic material with unique constitutive relations. Average stresses are related to average strains in a concrete element, while compatibility and equilibrium conditions must be satisfied. For an element subjected to

uniform axial (f_x and f_y) and shear (v_{xy}) stresses, the average strains and stresses can be represented by the Mohr's circle as shown in Figure 3.1.

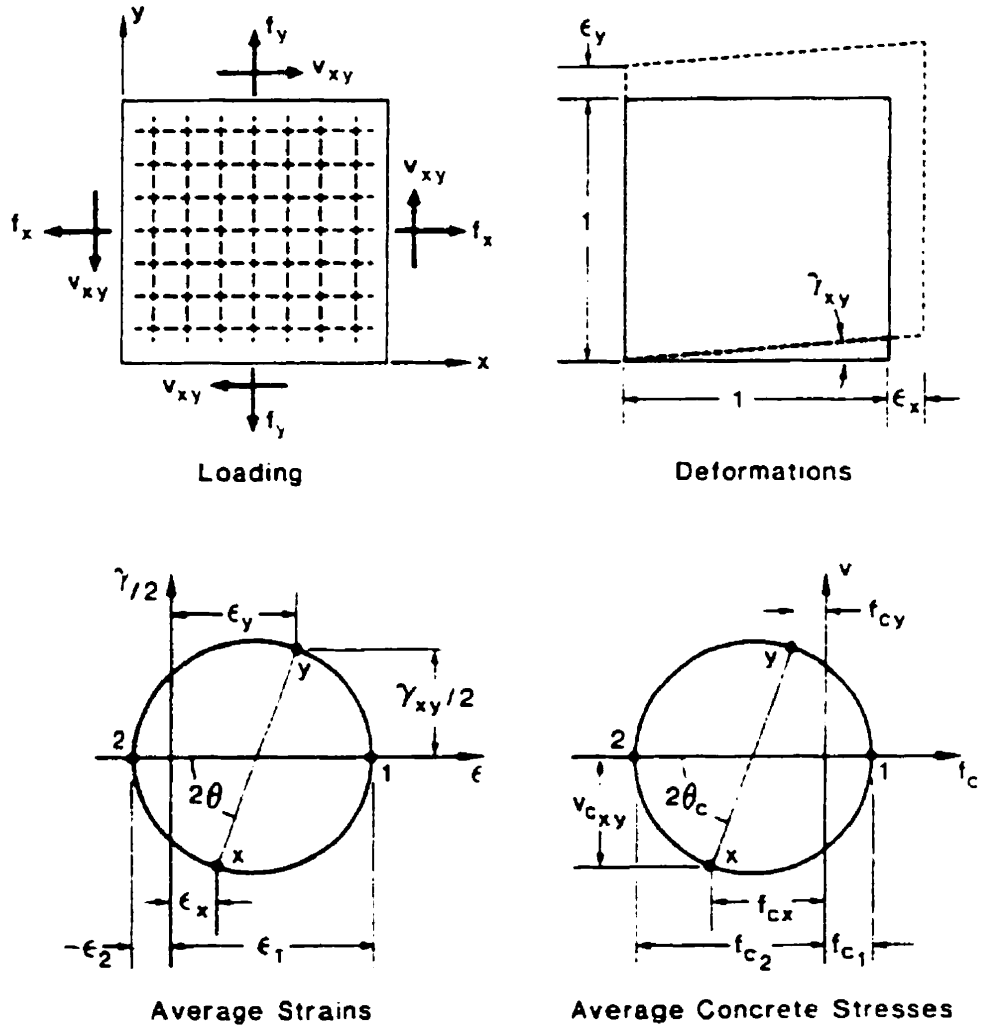

Figure 3.1: Average strains and stresses in a reinforced concrete element [68]

The principal tensile strain (ε_1), the principal compressive strain (ε_2) and the crack direction (θ_c) can be found as follows:

$$\varepsilon_1 = \frac{\varepsilon_x + \varepsilon_y}{2} + \frac{1}{2}\left[(\varepsilon_y - \varepsilon_x)^2 + \gamma_{xy}^2\right]^{1/2} \tag{3-1}$$

$$\varepsilon_2 = \frac{\varepsilon_x + \varepsilon_y}{2} - \frac{1}{2}\left[(\varepsilon_y - \varepsilon_x)^2 + \gamma_{xy}^2\right]^{1/2} \tag{3-2}$$

$$\theta_c = \frac{1}{2}\tan^{-1}\left[\frac{\gamma_{xy}}{\varepsilon_y - \varepsilon_x}\right] \tag{3-3}$$

where ε_x and ε_y are the normal strains and γ_{xy} is the shear strain. The stresses in the concrete and reinforcement are then determined from the strains using the MCFT constitutive relations described below.

For concrete in compression, the Hognestad parabola is used, with the maximum compressive strength reduced according to Eqn. 3-4, and as illustrated in Figure 3.2:

$$f_{c2} = f_p\left[2\left(\frac{\varepsilon_2}{\varepsilon_p}\right) - \left(\frac{\varepsilon_2}{\varepsilon_p}\right)^2\right] \tag{3-4}$$

where $f_p = \beta_d f'_c$, $\varepsilon_p = \beta_d \varepsilon_o$

$$\beta_d = \frac{1}{0.35\left(-\frac{\varepsilon_1}{\varepsilon_2} - 0.28\right)^{0.8}} \leq 1.0$$

in which f_{c2} is the concrete stress in the principal compressive stress direction, f'_c is the compressive cylinder strength, ε_o is the strain in the cylinder at f'_c, f_p is the maximum

compressive stress for cracked concrete in compression, ε_p is the strain corresponding to f_p, and β_d is the damage factor for cracked concrete.

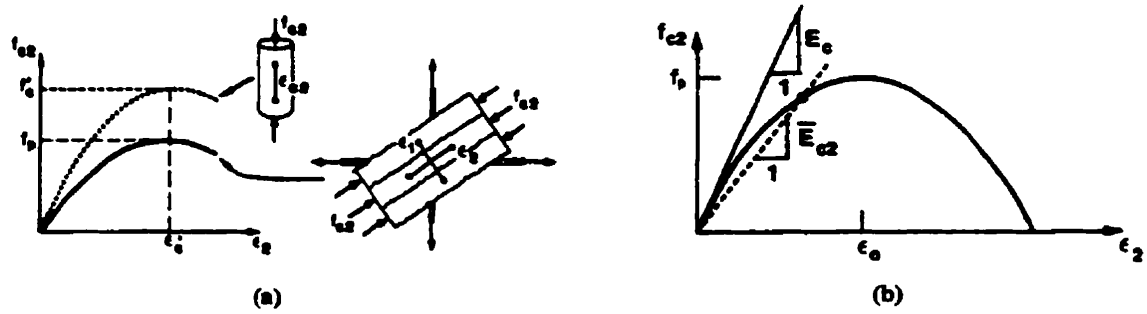

Figure 3.2: Constitutive relation for cracked concrete in compression [67, 69]

For concrete in tension, a linear response is used until cracking, with contribution from tension stiffening effects after cracking occurs, as represented by Eqn. 3.5 and Figure 3.3.

$$f_{c1} = E_c \varepsilon_1 \qquad \text{for } \varepsilon_1 \leq \varepsilon_{cr} \tag{3-5a}$$

$$f_{c1} = \frac{f'_t}{1+\sqrt{500\varepsilon_1}} \qquad \text{for } \varepsilon_1 > \varepsilon_{cr} \tag{3-5b}$$

where f_{c1} is the principal tensile stress, ε_1 is the principal tensile strain, E_c is the concrete's initial tangent modulus of elasticity (calculated as $2f'_c/\varepsilon_0$), ε_{cr} is the cracking strain, and f'_t is the tensile strength of concrete.

Steel reinforcement is assumed to behave in an elastic-plastic manner (Figure 3.4), but strain hardening effects can be included.

$$f_{sx} = E_s \varepsilon_x \leq f_{yx} \tag{3-6}$$

$$f_{sy} = E_s \, \varepsilon_y \leq f_{yy} \tag{3-7}$$

where f_{sx} and f_{sy} are average stresses in the x- and y-reinforcement, respectively, E_s is the elastic modulus of steel, and f_{yx} and f_{yy} are the yield strengths of the x- and y-reinforcement.

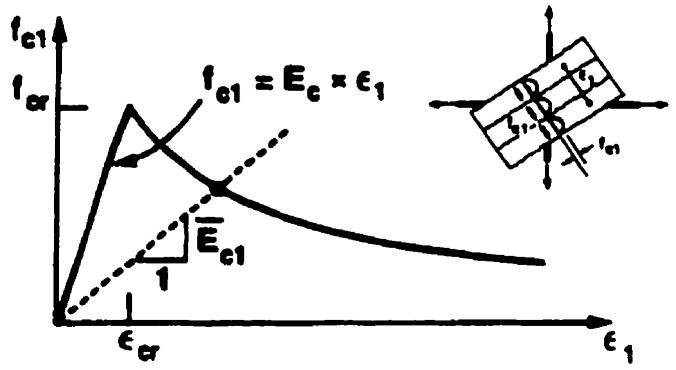

Figure 3.3: Constitutive relation for concrete in tension [67, 69]

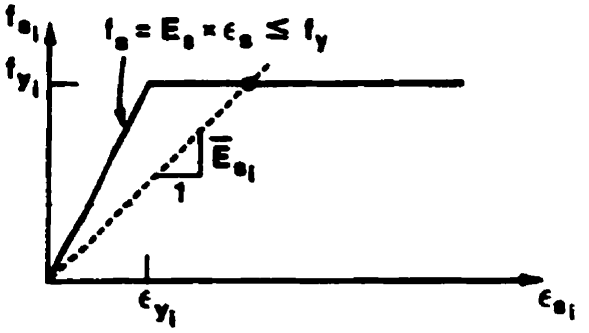

Figure 3.4: Constitutive relation for reinforcing steel [69]

The concrete stresses in the x- and y-directions (f_{cx} and f_{cy}) and the concrete normal shear stress (v_{cxy}) are then determined from the principal average stresses using the Mohr's circle (Figure 3.1):

$$f_{cx} = \frac{1}{2}(f_{c1} + f_{c2}) - \frac{1}{2}(f_{c1} - f_{c2})\cos 2\theta_c \tag{3-8}$$

$$f_{cy} = \frac{1}{2}(f_{c1} + f_{c2}) + \frac{1}{2}(f_{c1} - f_{c2})\cos 2\theta_c \tag{3-9}$$

$$v_{cxy} = \frac{1}{2}(f_{c1} - f_{c2})\sin 2\theta_c \tag{3-10}$$

For equilibrium conditions to be met, the stresses in the concrete and in the reinforcement must be equal to the applied loads:

$$f_{cx} + \rho_x f_{sx} = f_x \tag{3-11}$$

$$f_{cy} + \rho_y f_{sy} = f_y \tag{3-12}$$

$$v_{cxy} = v_{xy} \tag{3-13}$$

where ρ_x and ρ_y are the steel reinforcement ratios in the x and y directions, respectively. The strain values (ε_x, ε_y and γ_{xy}) assumed in Eqns. 3-1 to 3-3 are revised until Eqns. 3-11 to 3-13 are satisfied.

The stresses given above are average values; local conditions at a crack must also be considered. The transfer of stresses across the crack may be governed by the stresses in the reinforcement and the shear and compressive stresses acting at a crack:

$$f_{cl} \leq \Sigma_i \, \rho_i \left(f_{yi} - f_{si}\right)\cos^2 \theta_i \tag{3-14}$$

where f_{yi} and f_{si} are the yield and average stresses of the reinforcement in the i^{th} direction, respectively, and θ_i is the angle between the centreline of the rebars and the crack normal. The shear stress across the crack (v_{ci}) is related to the compressive stress on the crack (f_{ci}) in Walraven's equation:

$$v_{ci} = 0.18 v_{ci\max} + 1.64 f_{ci} - 0.82 \frac{f_{ci}^2}{v_{ci\max}} \tag{3-15}$$

where $$v_{ci\max} = \frac{\sqrt{f'_c}}{0.31 + 24 \frac{w}{a+16}}$$

in which v_{cimax} is the maximum transmissible shear stress across the crack, and is a function of the average crack width (w) and the maximum aggregate size (a).

3.3 FINITE ELEMENT PROCEDURE

Three input files are required for program VecTor2:

i) .job file – contains information on the files related to the current analysis, load factors, convergence requirements, and assumed material behaviour models

ii) .s2r file – contains information related to the material properties, finite element mesh definition, element state of activation, and restraints

iii) .l2r file – contains loading information, including imposed loads and displacements, temperature loads, concrete prestrains and ingress pressure

Once the input files have been created, the program can be executed. The flowchart for the nonlinear finite element procedure is depicted in Figure 3.5.

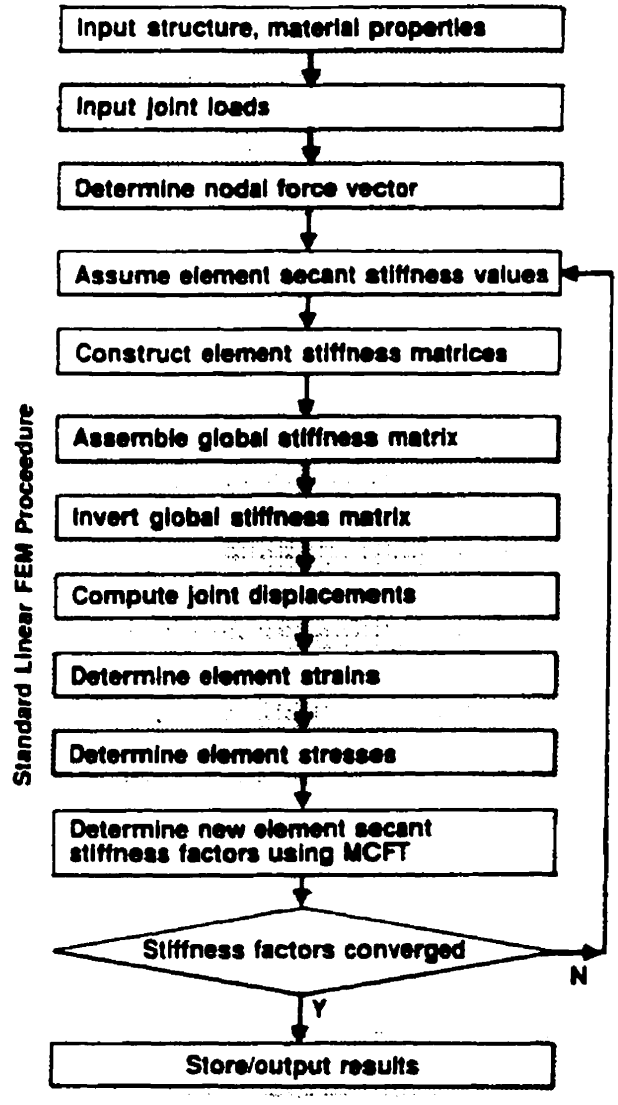

Figure 3.5: Flowchart for finite element procedure [69]

Definitions for the secant moduli are given as follows:

$$\overline{E}_{c1} = \frac{f_{c1}}{\varepsilon_1} \quad , \quad \overline{E}_{c2} = \frac{f_{c2}}{\varepsilon_2} \tag{3-16}$$

$$\overline{E}_{sx} = \frac{f_{sx}}{\varepsilon_x} \quad , \quad \overline{E}_{sy} = \frac{f_{sy}}{\varepsilon_y} \tag{3-17}$$

where $\overline{E}_{c1}$ and $\overline{E}_{c2}$ represent concrete behaviour in the principal directions, and $\overline{E}_{sx}$ and $\overline{E}_{sy}$ represent the behaviour of the reinforcement in the x and y directions, respectively. The secant stiffness values are then used to calculate the material stiffness matrix [D], composed of a concrete component $[D]_c$ and reinforcement components $[D]_{si}$:

$$[D] = [T]^T [D]_c [T] + \Sigma_i [T]^T [D]_{si} [T] \tag{3-18}$$

where [T] is an appropriate transformation matrix to account for the directions of the components. The material stiffness matrix for concrete is evaluated as:

$$[D]_c = \begin{bmatrix} \overline{E}_{c2} & 0 & 0 \\ 0 & \overline{E}_{c1} & 0 \\ 0 & 0 & \overline{G}_c \end{bmatrix} \tag{3-19}$$

where $$\overline{G}_c = \frac{\overline{E}_{c1}\overline{E}_{c2}}{\overline{E}_{c1} + \overline{E}_{c2}}$$

For each reinforcement component, a material stiffness matrix is determined as:

$$[D]_{si} = \begin{bmatrix} \rho_i \overline{E}_{si} & 0 & 0 \\ 0 & 0 & 0 \\ 0 & 0 & 0 \end{bmatrix} \tag{3-20}$$

The transformation matrix to be used in Eqn. 3-18 is calculated by:

$$[T]=\begin{bmatrix} \cos^2\phi & \sin^2\phi & \cos\phi\sin\phi \\ \sin^2\phi & \cos^2\phi & -\cos\phi\sin\phi \\ -2\cos\phi\sin\phi & 2\cos\phi\sin\phi & (\cos^2\phi-\sin^2\phi) \end{bmatrix} \tag{3-21}$$

where $\phi = 180° - \theta_c + \beta$ for the concrete component and $\phi = \alpha_i + \beta$ for the reinforcement components, in which β is the angle between the global and local x-axes and α_i is the orientation of the rebar with respect to the local x-axis.

After the material stiffness matrix [D] has been evaluated, the element stiffness matrix [k] can be determined from

$$[k]=\int [B]^T [D][B]dV \tag{3-22}$$

where [B] depends on the assumed element displacement functions. The structure stiffness matrix [K] is then assembled, inverted and used to calculate the unknown joint displacements. From the displacements, the strains and stresses in the element can be found. New secant moduli and material stiffness matrices are evaluated and compared with those from the previous step. This iterative procedure is continued until the specified convergence limit is met, at which time the final results can be obtained.

3.4 MODELLING OF REPAIRED STRUCTURES

The fact that most rehabilitation projects are carried out after the RC structures have been put into service for some time must be taken into account. This has been achieved in program VecTor2 with the plastic offset approach using a secant stiffness formulation. A schematic of the analysis procedure is shown in Figure 3.6. To begin the analysis, only the elements in the original RC member are activated. The repair materials, namely bond and FRP

elements (and concrete elements if damaged concrete is repaired), are included in the finite element mesh, but are initially disengaged. The disengaged elements experience strains equal to those of the activated elements, but these are kept as plastic offset strains (ε^{p}). These elements do not contribute to the stiffness or strength of the structure since their elastic strains (ε^{e}) are zero. At the load stage corresponding to the time of repair, the bond and FRP elements are activated. The repair elements start from a state of zero elastic strain, and their addition to the stiffness of the member is defined by the secant modulus calculated based on the net elastic strains. The plastic offset strains are updated as loading is incremented for the duration of the analysis.

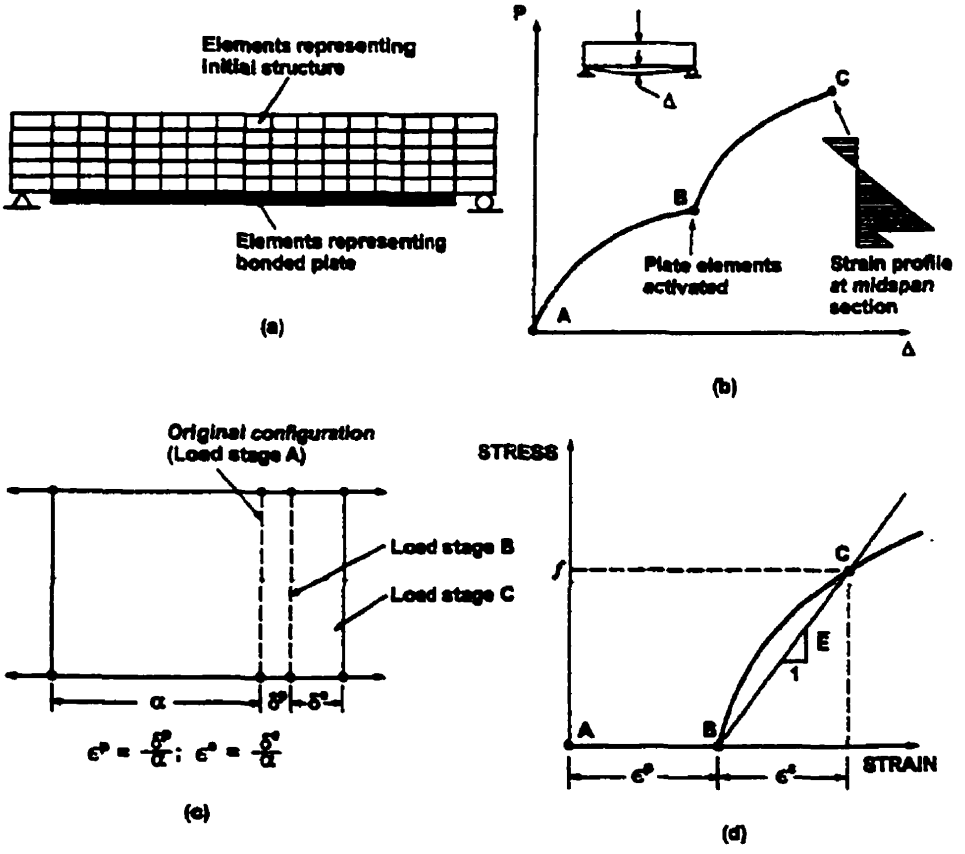

Figure 3.6: Analysis of beam bonded with FRP plate: (a) finite element mesh, (b) load history, (c) strains in FRP element, (d) determination of secant modulus [70]

3.5 MODELLING EXTERNALLY-BONDED FRP COMPOSITES

In a previous version of VecTor2 (formerly known as TRIX [69]), FRP composites were smeared into rectangular 'concrete' elements, as exemplified in Bucci's work [8]. This essentially means that the concrete mechanical properties were negligible as these elements were completely filled with FRP composites (i.e., the area ratio of the FRP was 100% in both directions). The FRP-filled rectangular elements were superimposed on top of the original concrete elements to simulate the repair, resulting in a double mesh for the FRP-bonded section of the member. This implied perfect bond conditions between the two adherents, assuming that no slip occurred between the concrete and FRP composites.

However, bond elements have since been implemented by Gan [71] into program TRIX. The goal of this undertaking was to model the bond-slip behaviour between rebars and concrete in members subjected to cyclic loading. The element formulations have been adopted in program VecTor2 and expanded to include the modelling of bond-slip response between FRP and concrete. Since the bond elements employed in the program are either dimensionless or one-dimensional (to be described later in this chapter), the FRP composites must now be modelled as two-noded truss elements.

3.5.1 *CONSTITUTIVE RELATION FOR FRP COMPOSITES*

FRP reinforcement is assumed to be linear elastic with brittle fracture in tension, as demonstrated by Figure 3.7. The ultimate tensile strength of the material is represented by $f_{f,u}$, while the corresponding strain at failure is $\varepsilon_{f,u}$.

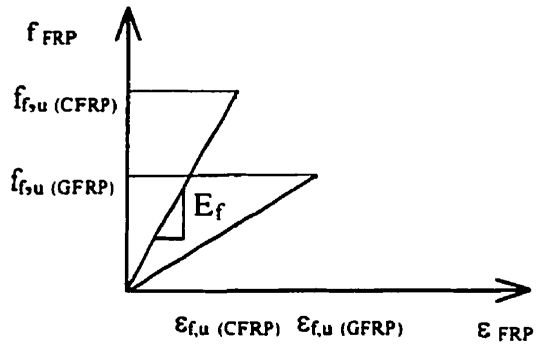

Figure 3.7: Constitutive relation for FRP reinforcement

3.5.2 *CONSTITUTIVE RELATIONS FOR BOND INTERFACE*

In the literature published up to now, various bond stress-slip relationships between concrete and FRP have been proposed, as previously described in section 2.4.4 of this report. This is mainly due to the many factors which influence the local behaviour, such as the concrete strength, FRP thickness and stiffness, the relative stiffness of flexural FRP and tension steel reinforcement, epoxy thickness, and the mechanical properties of the resin. At the time of implementation of the constitutive relation into the program, numerous researchers (Homam, Sato, Nanni and Lee) had noted that the relationship for the bond interface is either linear elastic or elastic-plastic. Therefore, a general shape of the elastic-plastic curve, as seen in Figure 3.8(a), has been adopted in the current research. The variables include the maximum shear stress that can be carried by the bond interface (U_{max}), the slip at the first occurrence of maximum bond stress (S_{max}), and the ultimate slip when the bond fails (S_{ult}). Therefore, a linear elastic relationship, shown in Figure 3.8(b), can also be specified by setting S_{max} equal to S_{ult}. The slope of the linear relationship is termed the "slip modulus" (E_b).

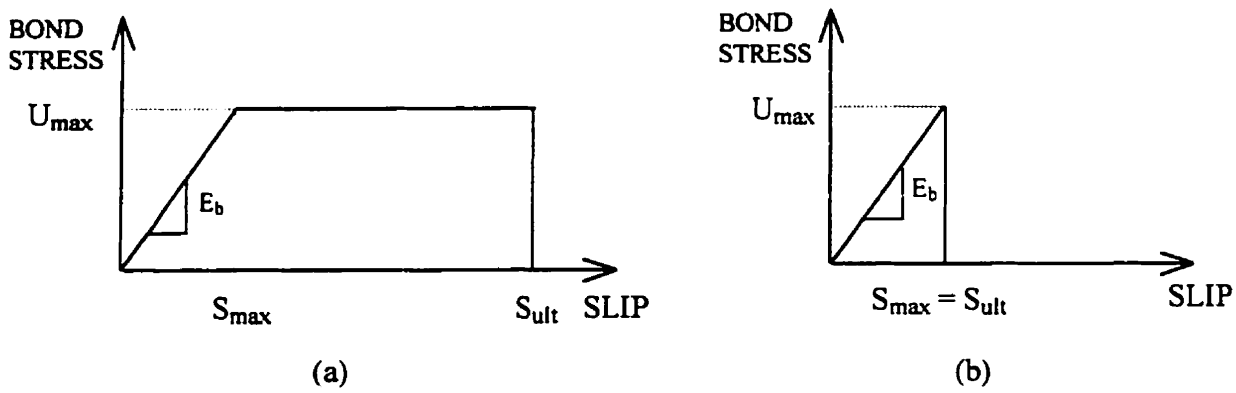

Figure 3.8: Constitutive relationship for bond interface: (a) elastic-plastic, (b) linear elastic

3.6 MODELLING BOND-SLIP BEHAVIOUR WITH BOND ELEMENTS

In order to simulate the slippage that occurs at the interface between two materials, interface or bond elements must be incorporated into the finite element program. Two appropriate bond element types are the link element and the one-dimensional contact element. Both of these elements have been used successfully in modelling bond-slip between concrete and internal steel reinforcement [71]. Similarly, these elements (with a modified constitutive relation) can represent the interface between concrete and externally-bonded FRP laminates, and will permit the debonding phenomenon to be modelled accurately.

To represent the bonding of FRP plates or sheets, the relevant concrete elements must be double-noded. One set of nodes is used for the concrete elements, while the second set is used for the FRP (represented as truss elements). The nodes of these two adherents are connected by bond elements, which allow relative displacement, or slip, to take place between concrete and FRP. The difference in displacement between the concrete node and the FRP node determines the nodal slip of the bond element. The bond stress is then calculated using

the specified constitutive relationship. Finally, the force transferred by the bond element is found by multiplying the bond stress and the bonded surface area represented by the element. The bond elements permit a certain amount of slippage to occur between concrete and FRP, while transferring load between the two components, until debonding failure occurs. Once the ultimate slip value has been attained, the bond fails and the corresponding FRP truss element is 'disconnected' from the concrete member by suppressing its load-carrying capacity.

3.6.1 *LINK ELEMENT*

3.6.1.1 GENERAL

The link element was developed by Ngo and Scordelis in their analysis of bond-slip between steel rebars and concrete in RC beams [72]. The link element has no physical dimensions, so the two nodes (i and j) that it connects have the same coordinates. A representation of the link element, shown in Figure 3.9, consists of two linear springs parallel to a set of orthogonal axes *h* and *v*. The link element can be oriented at any arbitrary angle θ with the horizontal axis of the RC member. Each spring has one degree of freedom (translation in *h* or *v* direction), and the displacement in each direction is independent of the other.

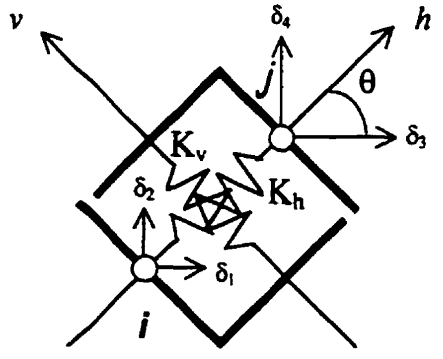

Figure 3.9: Representation of link element [adapted from 72]

Since only the mechanical properties of the link element are relevant to the formulation, it can be placed in any interface while using the appropriate spring stiffnesses. For the present analyses, link elements will be located at nodes where truss bars representing FRP are connected to the corner nodes of concrete elements. The springs represent the shear and normal stiffness of the adhesive connection, and transmit shear and normal forces between the nodes.

3.6.1.2 Element Stiffness Matrix

Let K_h and K_v represent the spring stiffnesses in the h and v directions. Displacements are considered positive in the directions shown in Figure 3.9. The stress-strain relationship is given by

$$\begin{Bmatrix} \sigma_h \\ \sigma_v \end{Bmatrix} = \begin{bmatrix} K_h & 0 \\ 0 & K_v \end{bmatrix} \begin{Bmatrix} \varepsilon_h \\ \varepsilon_v \end{Bmatrix} \tag{3-23}$$

where σ_h and σ_v are stresses in the h and v directions, and K_h and K_v are the respective stiffnesses. Relative displacements between nodes i and j in the h and v directions are represented by ε_h and ε_v, and are positive for tensile strains. The displacement transformation matrix [B] relates displacements to strains:

$$\begin{Bmatrix} \varepsilon_h \\ \varepsilon_v \end{Bmatrix} = \begin{bmatrix} -c & -s & c & s \\ s & -c & -s & c \end{bmatrix} \begin{Bmatrix} \delta_1 \\ \delta_2 \\ \delta_3 \\ \delta_4 \end{Bmatrix} \quad \text{or} \quad \{\varepsilon\} = [B]\{\delta\} \tag{3-24}$$

where $c = \cos\theta$ and $s = \sin\theta$. The force transformation matrix is equal to the transpose of the displacement transformation matrix [B], thus the stiffness of the link element can be obtained from

$$[k] = [B]^T \begin{bmatrix} K_h & 0 \\ 0 & K_v \end{bmatrix} [B] = \begin{bmatrix} K_{11} & K_{12} & -K_{11} & -K_{12} \\ K_{12} & K_{22} & -K_{12} & -K_{22} \\ -K_{11} & -K_{12} & K_{11} & K_{12} \\ -K_{12} & -K_{22} & K_{12} & K_{22} \end{bmatrix} \quad (3\text{-}25)$$

with $K_{11} = K_h \cos^2\theta + K_v \sin^2\theta$

$K_{12} = (K_h - K_v) \sin\theta \cos\theta$

$K_{22} = K_h \sin^2\theta + K_v \cos^2\theta$

The imperative quantities needed for this formulation are the spring stiffnesses K_h and K_v. The linear relationship between bond stress and slip assumed in this study is applicable in the *h*, or shear, direction, since the epoxy layer is primarily loaded in shear. In the normal, or *v*, direction, the spring stiffness may be related to the high tensile strength of the epoxy. However, most debonding failures with thin FRP plates or sheets are due to shear at the interface. Therefore, an artificially high value was assigned to K_v in order to focus on shear failure at the concrete-FRP interface, thus limiting the link element to having two degrees-of-freedom along the direction of the FRP truss element.

3.6.2 *CONTACT ELEMENT*

3.6.2.1 GENERAL

The one-dimensional contact element, developed by Hoshino and Schafer, provides a continuous connection between two adjoining elements [73]. It is an isoparametric element which, in its undeformed state, has no dimensions in the transverse direction. The simplest form has two double nodes, and is based on a linear displacement function. The double nodes of the contact element are independent. In each pair of double nodes, one node is connected to a concrete element while the other node is connected to the FRP element. In the unloaded

stage, the coordinates of the nodes at each end of the contact element are identical. However, once loading begins, the nodes behave independently, resulting in relative displacements between the two connected points, as illustrated in Figure 3.10.

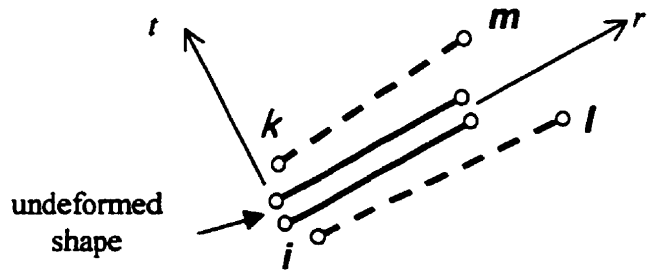

Figure 3.10: Representation of 1-D contact element [adapted from 73 and 74]

3.6.2.2 *Element Stiffness Matrix*

The interpolation functions which relate the displacements at each point of the element to the nodal displacements are given as:

$$N_1 = \frac{1-r}{2} \quad , \qquad N_2 = \frac{1+r}{2} \quad , \qquad N_3 = 1-r^2 \quad ,$$

$$N_4 = \frac{-27r^3 - 9r^2 + 27r + 9}{16} \tag{3-26}$$

Using appropriate relations between contact stresses and relative displacements [74], integration is carried out over the contact surface to obtain the element stiffness matrix. Assuming independent behaviour in the two coordinate directions, the relation between element forces and relative displacements is provided by

$$\begin{bmatrix} R_r^{ik} \\ R_r^{lm} \\ R_t^{ik} \\ R_t^{lm} \end{bmatrix} = \frac{\pi dL}{6} \begin{bmatrix} 2G_r & G_r & 0 & 0 \\ G_r & 2G_r & 0 & 0 \\ 0 & 0 & 2G_t & G_t \\ 0 & 0 & G_t & 2G_t \end{bmatrix} \begin{bmatrix} \Delta_r^{ik} \\ \Delta_r^{lm} \\ \Delta_t^{ik} \\ \Delta_t^{lm} \end{bmatrix} \tag{3-27}$$

where *i*, *k*, *l* and *m* are the nodes of the contact element, as shown in Figure 3.10, G_r and G_t are the bond moduli in the tangential (r) and normal (t) directions, respectively. R_r^{ik} and Δ_r^{ik} are the force and relative displacement between nodes *i* and *k* in the r direction, d is the diameter of the truss bar and L is the length of the element. Values for the bond moduli G_r and G_t can be derived from experiments in which local bond-slip and material strains are measured. Similar to the link element, a large stiffness value is chosen for the normal direction. Thus, the contact element has four degrees-of-freedom, each along the direction of the FRP element.

Comparing link and contact elements, the link element has been found to be inadequate in modelling non-constant slip curves [73]. Contact elements with a linear displacement function, on the other hand, can model linear slip curves exactly, and give good approximations to nonlinear slip curves with a few elements. The superiority of the contact element over the link element has also been demonstrated by Gan [71] in modelling the bond-slip between rebars and concrete.

CHAPTER 4 EXPERIMENTAL PROGRAM

4.1 INTRODUCTION

The RWOA beam series was fabricated and tested at the University of Toronto. The design of these three large-scale beams was based on the series of OA beams tested by Bresler and Scordelis [75], while using locally available materials. The original OA beams were shear critical, with no internal shear reinforcement. The RWOA beams were modelled after the OA beams, but were subsequently shear strengthened by bonding CFRP strips onto the side surfaces of the beams. Another student at the university tested specimens patterned after the Bresler-Scordelis beams, including a set of control specimens (TOA series) and three sets of specimens with internal steel stirrups. Among the series with stirrups, the dimensions of the TA series were identical to those of the TOA series, while two other series (TB and TC) were narrower in width.

4.2 PREPARATION OF SPECIMENS

4.2.1 *FABRICATION*

Each RWOA beam was cast in conjunction with a control beam from the TOA series, plus one beam from each of the TA, TB, and TC series. Therefore, the formwork was

constructed for the simultaneous casting of five beams. The cross-sections of the beams are shown in Figure 4.1 and their elevation views are given in Figure 4.2.

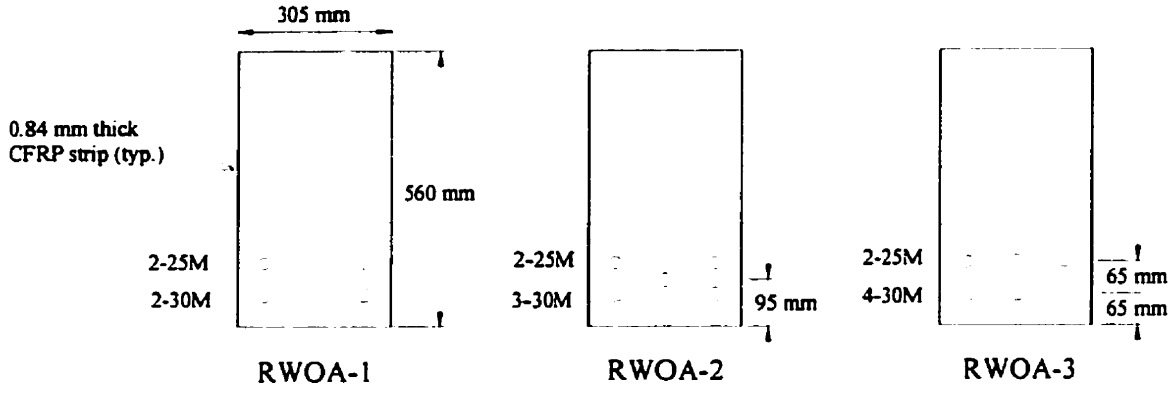

Figure 4.1: Cross-section details of RWOA beams

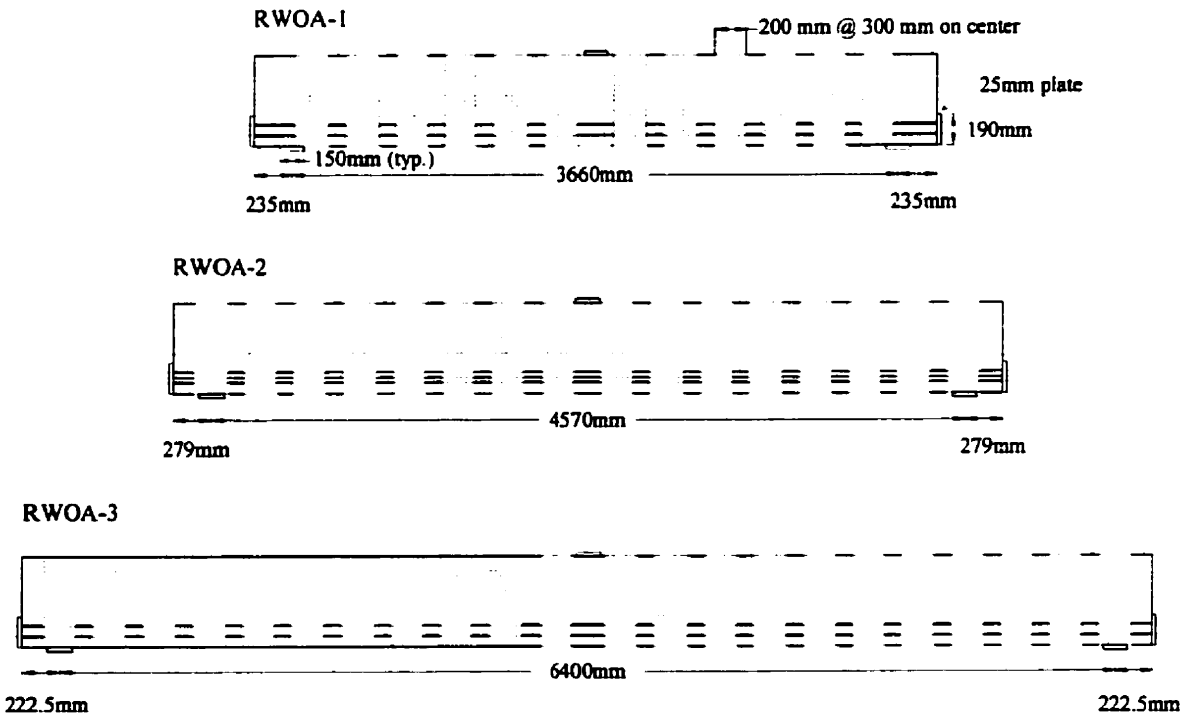

Figure 4.2: Elevation views of RWOA beams

Formwork was constructed with plywood and 2" × 4" timber, and the outer sides were reinforced with soldier piles. The plywood for the side surfaces of the beams was fixed to the base, while the planks for the ends of the beams were shifted after each cast to match the desired lengths of the beams. Smooth plywood was used for the sides of the beams to minimize the unevenness on the concrete surface which would be detrimental to the bond between concrete and FRP. The flexural steel reinforcement was cut into the required lengths, and 25 mm thick plates were welded to the ends of the rebars (at locations corresponding to the length of the beams). This was done to enhance anchorage of the rebars as flexural failure might ensue due to the presence of the CFRP strips. To prevent sagging of the rebars along the span, short pieces of 10M rebars were cut and tied to the flexural steel at 300 mm intervals. Small pieces of 2" × 4" timber were also used as spacers between the flexural steel until the time of casting. The formwork for the casting of concrete is depicted in Figure 4.3, while the newly-constructed beams are shown in Figure 4.4.

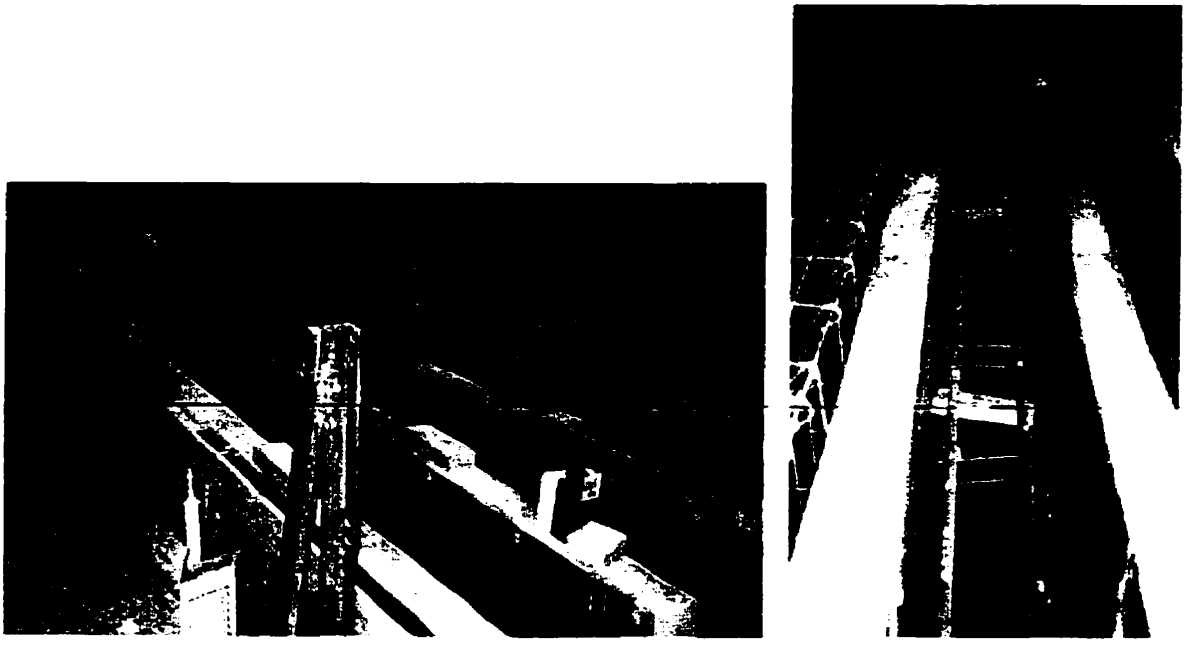

Figure 4.3: Formwork for casting of RWOA beam (along with other test beams)

Figure 4.4: Beams cast in formwork

4.2.2 *APPLICATION OF CFRP STRIPS*

Instead of using the common U-wrap configuration, the CFRP fabric was bonded only onto the sides of the beams. This method was preferred since exposing two free edges of the fabric would increase the probability of debonding. The roll of CFRP fabric was cut into strips of appropriate length (560 mm) and width (200 mm). The webs of the beams (spanning between the supports) were covered with the strips at 300 mm spacing (center-to-center), oriented perpendicularly to the axis of the beam, as shown in Figure 4.2. The exact locations of the FRP strips were chosen to avoid the rough edges that resulted from uneven joints in the formwork. Although it is common to use a continuous sheet in field applications to minimize the amount of manual labour, the use of strips would permit the observation of cracks in the laboratory. The strengthening with CFRP was performed without preloading the beams since it was desired to track the occurrences of debonding with the formation of cracks in the concrete. Also, the possibility of sudden shear failure prior to the bonding of CFRP was to be avoided.

After curing at room temperature for at least 28 days, the side surfaces of the beams were sprayed with a water jet to remove all loose particles. Bonding of the CFRP strips took place once the beams were air-dried. One coat of epoxy was applied, using paint-rollers, to the concrete surface to allow for some penetration into the concrete cover. Both sides of the CFRP strips were covered with epoxy to ensure saturation of the fibres. The beam and CFRP strips were left exposed to air for two hours until the epoxy thickened and became sticky. Epoxy was reapplied to parts of the concrete where the first coat had been absorbed from the surface. Then the strips of CFRP fabric were attached onto the beam, taking care to straighten the fibres as the fabric tended to fold under the weight of the epoxy. The thickness of the epoxy was not measured, but any excess was squeezed out when the CFRP strips were smoothed with a wallpaper smoother. This was done to remove air bubbles and to ensure complete epoxy coverage. It was recommended to apply a final coat of epoxy over the CFRP strips, but the weight of the added epoxy caused the strips to slide down the sides of the beam; therefore, the final coat was omitted. The photographs in Figure 4.5 show the steps involved in the bonding process.

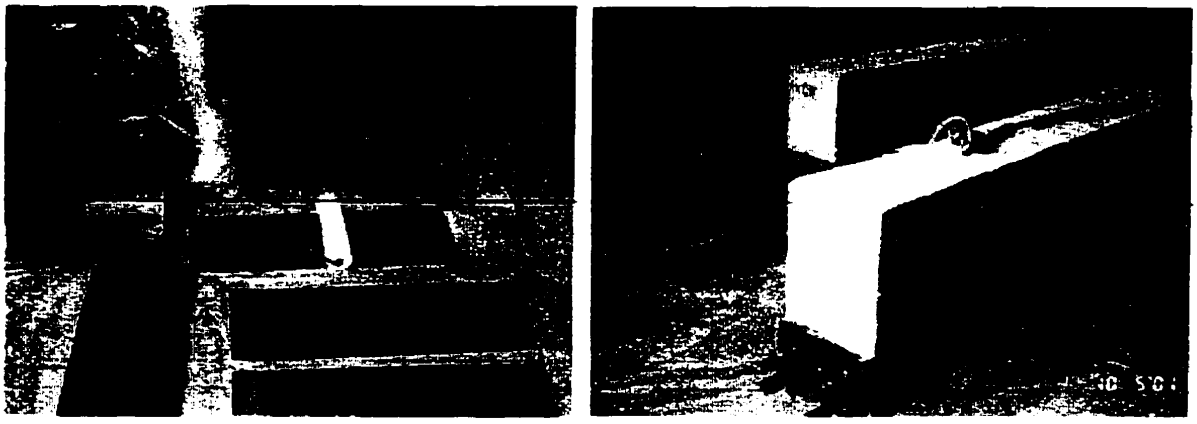

Figure 4.5: Application of CFRP strips to the sides of RWOA beams

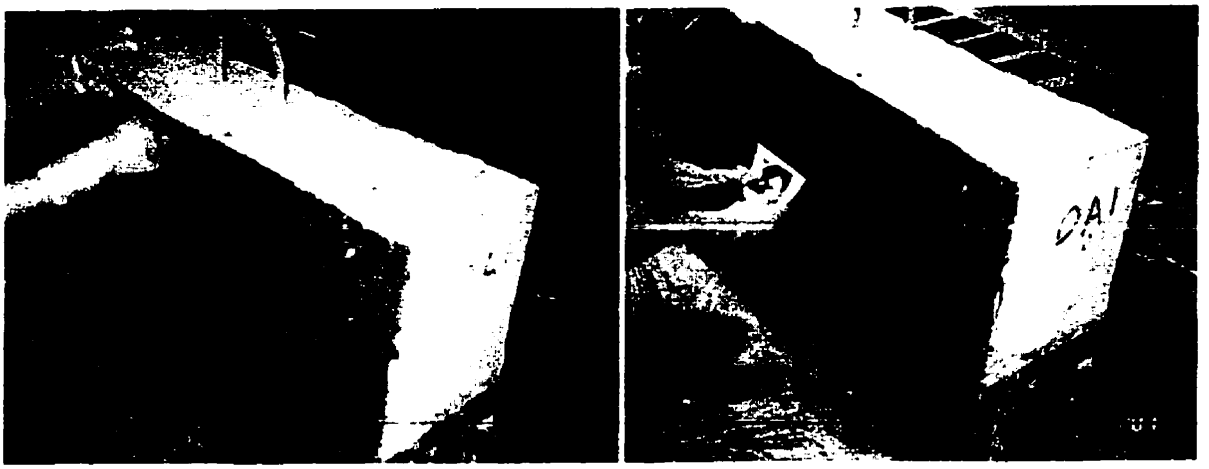

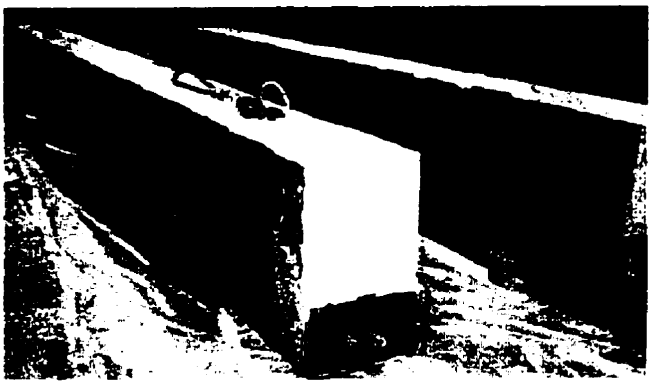

Figure 4.5 (continued): Application of CFRP strips to the sides of RWOA beams

4.3 MATERIAL PROPERTIES

Concrete was ordered from a local ready-mix plant, with f'_c of 20 MPa, 25 MPa and 30 MPa for RWOA-1, RWOA-2, and RWOA-3, respectively. Type 10 Portland cement, 10 mm maximum coarse aggregate size and 100 mm slump were specified. Prior to casting, the formwork was sprayed with form-oil to enable easy removal of the beams. The beam specimens were covered with wet burlap and polyethylene sheeting for at least 7 days after casting. For each batch of concrete, 20 concrete cylinders were cast to test for mechanical

properties. Cylinder compression tests and tensile splitting tests were performed, and compressive stress-strain curves were obtained (see Appendix A). Table 4.1 lists the measured material properties for the specimens.

Table 4.1: Measured Material Properties for RWOA Beam Specimens

Material	f'_c (MPa)	ε_o	f_{sp} (MPa)	E (GPa)
Concrete (RWOA-1)	22.6	0.0016	2.37	26
Concrete (RWOA-2)	25.9	0.0021	3.37	28
Concrete (RWOA-3)	43.5	0.0019	3.13	36
Material	**f_y (MPa)**	**f_u (MPa)**	**E (GPa)**	**ε_{ult}**
Steel (25M) (RWOA-2)	440	615	210	0.226
Steel (25M) (RWOA-1, 3)	445	680	220	0.224
Steel (30M)	436	700	200	0.183
Material	**f'_t (MPa)**	**E (GPa)**	**ε_{ult}**	**ν**
CFRP*	1090	100	0.011	-

* determined from tensile coupon tests (for fabric thickness of 0.84 mm)

Standard steel- and CFRP-tensile tests were conducted to determine their material properties. Steel rebar coupons were tested in tension to obtain their stress-strain curves, which have been included in Appendix A. CFRP coupons were fabricated according to ASTM D 3039/D 3039M [76], with adjustments made to suit the requirements of the testing machine. The geometry of the CFRP coupons is depicted in Figure 4.6. The length of the steel plate tabs was chosen to be longer than the grip length of the machine (146 mm) to disburse the pressure from the end of the grip. CFRP tabs were added between the steel plates and the main coupon to provide a cushioning effect in order to prevent gripping failure.

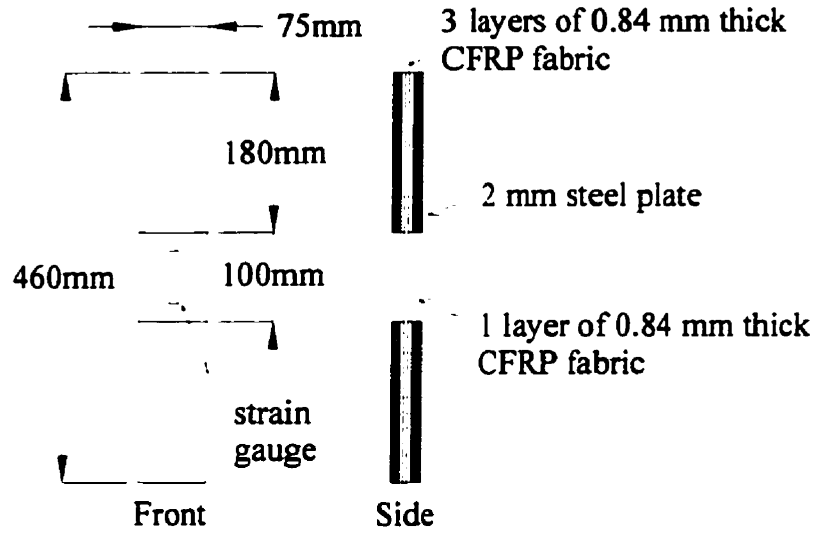

Figure 4.6: Geometry of CFRP coupons tested for RWOA beams

The type of CFRP used was SCH41, as part of the TYFO S® High Strength Graphite Fibrwrap® system, with graphite fibres oriented in the longitudinal direction and Kevlar 49 weft in the perpendicular direction (Figure 4.7). The thickness of this fabric was specified by the manufacturer as 1.04 mm (0.041 in) [77]. Measurements taken with a micrometer gave an average thickness value of 0.84 mm. This fabric was chosen over thinner sheets for the strengthening scheme in order to promote debonding failure. The epoxy resin used for the bonding of CFRP was a two-part epoxy adhesive (TYFO S®), which consisted of components A (Shell epoxy) and B (Texaco Hardener). The mixing ratio was 100 parts of A to 42 parts of B (by volume), and 1 L of epoxy was mixed for each square metre of area to be covered. A mechanical mixer was used to mix the two components together for 5 minutes at a speed of 400-600 RPM until uniform. The mechanical properties of the CFRP and epoxy, as given by the manufacturer, are presented in Table 4.2.

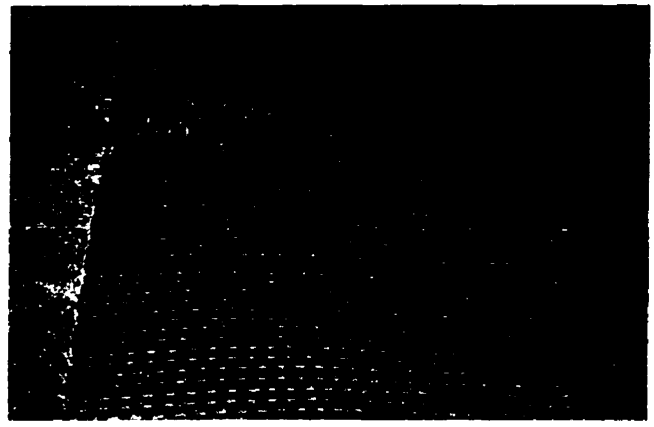

Figure 4.7: TYFO S® High Strength Graphite Fibrwrap® SCH41 CFRP fabric

Table 4.2: Mechanical Properties of CFRP and Epoxy for RWOA Beams

Material	f'_t (MPa)	E (GPa)	ε_{ult}
CFRP (SCH 41)*	1034	69	0.01
Material	**f'_t (MPa)**	**E (GPa)**	**Elongation at Break**
Epoxy (TYFO A/B)†	72.4	3.16	4.8%

*values given by manufacturer FYFE Company (for fabric thickness of 1.04 mm) [77]

†values obtained from material specifications supplied by Composite Retrofit International [78]

The CFRP fabric was delivered as a roll of approximately 600 mm width. In fabricating the coupons, one piece of 460 mm × 600 mm CFRP fabric was cut for the coupons, and four strips of 180 mm × 600 mm fabric were cut for the tabs. Both sides of the CFRP fabric were coated with epoxy, and the strips of tabs were bonded along both edges on each side, as shown in Figure 4.8. After curing for five days, the hardened panel was cut into 75 mm wide coupons. Steel plate tabs measuring 180 mm × 75 mm × 2 mm were glued onto the ends of the coupons using contact cement. Two strain gauges of type YL-60 (supplied by Tokyo Sokki Kenkyujo Co., Ltd.), oriented in the longitudinal direction, were glued onto each side of the coupon to measure the average strain experienced by the CFRP fibres.

Measurements were not recorded in the transverse direction since all carbon fibres were aligned in the longitudinal direction only. The completed coupons can be seen in Figure 4.9.

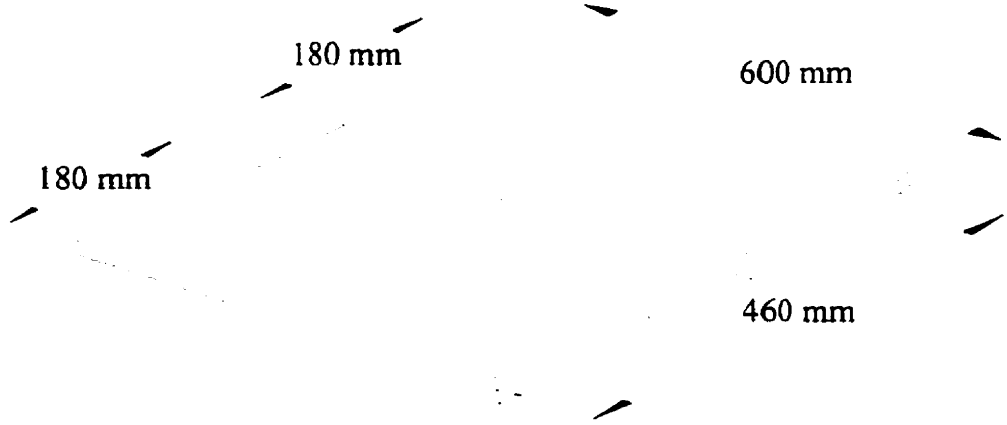

Figure 4.8: Fabrication of panel for CFRP coupons

Figure 4.9: Completed CFRP coupons

The coupons were subjected to tensile tests approximately 30 days after the initial bonding. Although eight coupons were made, three were not suitable to be tested due to an uneven curing surface. Thus, the test results of five coupons were used to determine average values. It was observed that the response measured by one strain gauge was consistently 50% higher than the readings from the gauge on the opposite side of the coupon. This was attributed to the fact that one side of the coupon did not have a smooth epoxy layer, but contained numerous voids caused by the plastic sheeting placed beneath the CFRP panel at the time of curing. The reduced amount of epoxy is thought to have lowered the stiffness on one side of the coupon. However, consistent data were obtained by averaging the readings from both gauges on all five coupons (Figure 4.10). The failure modes of the five coupons are summarized in Table 4.3, using the standard three-part code specified in ASTM D3039/D3039M [76]. While two coupons failed with the coupon separating neatly into two pieces, the failure of the remaining three coupons involved splitting of the CFRP, with several small pieces breaking off from the coupon. Photos depicting their failures and individual stress-strain curves are included in Appendix A.

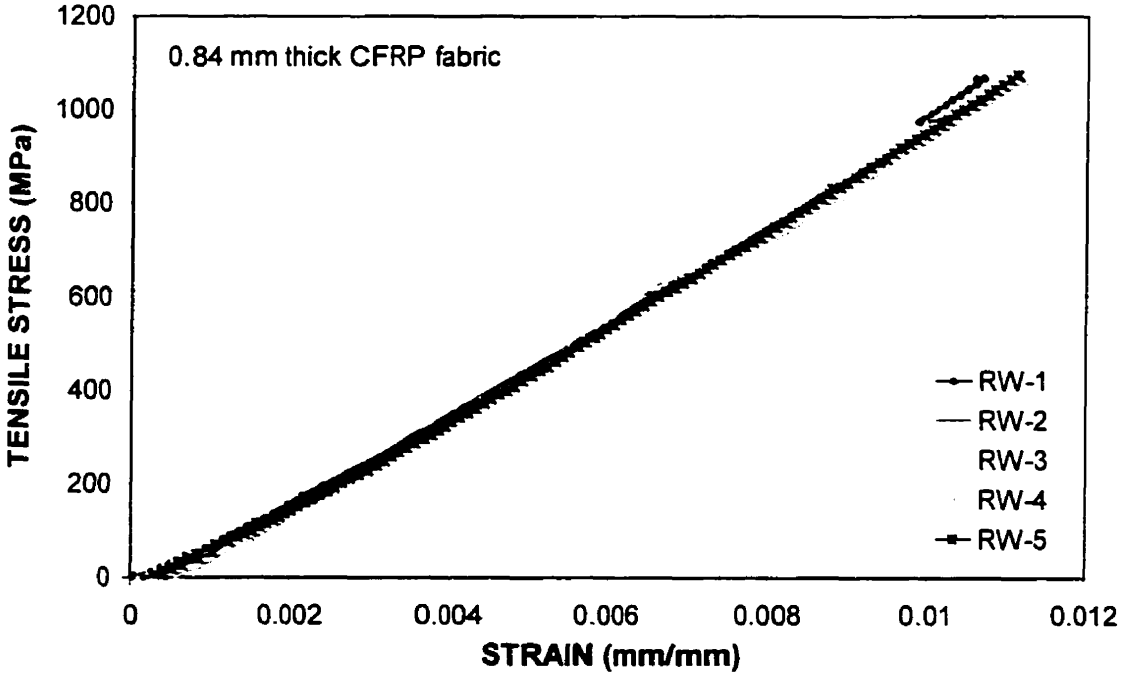

Figure 4.10: Stress-strain curves from CFRP coupon tests

Table 4.3: Failure Mode of CFRP Coupons

Coupon Number	Failure Mode Code
RW-1	AGM
RW-2	LAB
RW-3	SGR
RW-4	SGL
RW-5	XAB

First Letter: (failure type)	Second Letter: (failure area)	Third letter: (failure location)
A = Angled	A = At grip/tab	M = Middle
L = Lateral	G = Gage	B = Bottom
S = longitudinal Splitting		L = Left
		R = Right
X = eXplosive		

4.4 TESTING PROCEDURE

The beams were tested under monotonic three-point loading after the epoxy had cured at room temperature for at least 10 days. All specimens were tested using a hydraulic jack connected to a servo-hydraulic MTS testing machine frame. A load-cell connected to the data acquisition system measured the applied load. Mid-span deflection was measured using two linear variable differential transformers (LVDTs), one at the north face and the other at the south face. Two LVDTs were also set up at opposite faces of the two supports to detect any support settlements. Loading proceeded in increments of 20 kN until yielding of the longitudinal reinforcement, at which time loading was specified in terms of mid-span displacement. Surface strains at the level of the longitudinal reinforcement were recorded through the horizontal displacements of 12 Zurich targets bonded on each side of the beam. The set-up of the LVDTs and Zurich targets are depicted in Figure 4.11, and the measured displacements were directly recorded by the data acquisition system. Cracks noted on the

side concrete surfaces were marked and their widths were measured at every load stage. Figure 4.12 shows beam RWOA-3 ready to be tested.

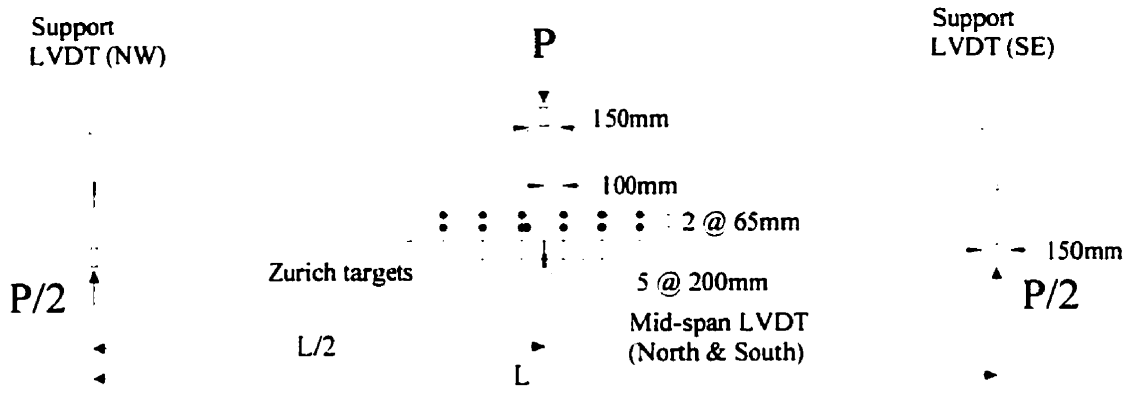

Figure 4.11: Typical test set-up for RWOA beams

Figure 4.12: Beam RWOA-3 set up in the MTS testing machine frame

4.5 EXPERIMENTAL OBSERVATIONS

4.5.1 *BEAM RWOA-1*

Due to the presence of the CFRP strips on the sides of the beam, the bottom surface had to be checked for the appearance of initial flexural cracks. They were first noted at 80 kN. The number and average width of flexural cracks increased as loading proceeded, and shear cracks first appeared at a load of 300 kN. Some cracks formed at the vertical edge of certain CFRP strips, and as these cracks widened, the CFRP strip appeared to be on the verge of peeling off from the beam. At 460 kN, yielding of the flexural reinforcement began, and the load increased as the steel entered the strain-hardening stage. Signs of concrete crushing under the loading plate were noted at 488 kN. Maximum load was reached at 493 kN, accompanied by a mid-span deflection of 35 mm. Prior to the peak load, the widest crack widths measured were 3.5 mm for flexural cracks and 0.20 mm for shear cracks.

After the peak load was reached, concrete crushing proceeded until ultimate failure. As concrete crushed under the loading platen, portions of four CFRP strips (two on the north and two on the south side of the beam) peeled off from the beam with a loud noise. These strips were closest to mid-span on the east half of the beam, where a large shear crack had formed, starting from the loading point. Figure 4.13(a) shows the debonding condition at failure. The section of the CFRP/concrete that peeled off from the beam was dependent on its position relative to the shear crack; the shorter length above or below the crack was critical. Under the strips that peeled above the crack, a thin layer of concrete and some aggregates were still attached. Once the CFRP strips had peeled away from the beam, the crushed concrete was exposed, the confinement effect was lost, and pieces of concrete spalled off. The strips that failed below the shear crack tore off with the concrete cover, causing the cover to split out from the beam. This behaviour was similarly observed on both sides (north and south) of the beam. At ultimate, after the stiff side surfaces were pulled outwards, the central section of the beam, now unreinforced in shear, punched out in shear. This failure mode is captured in Figure 4.13(b) (underside). The outward push of the concrete cover also

led to the partial splitting of a few CFRP strips. The overall crack pattern is depicted in Figure 4.13(c). N and S represent the north and south sides of the beam, respectively.

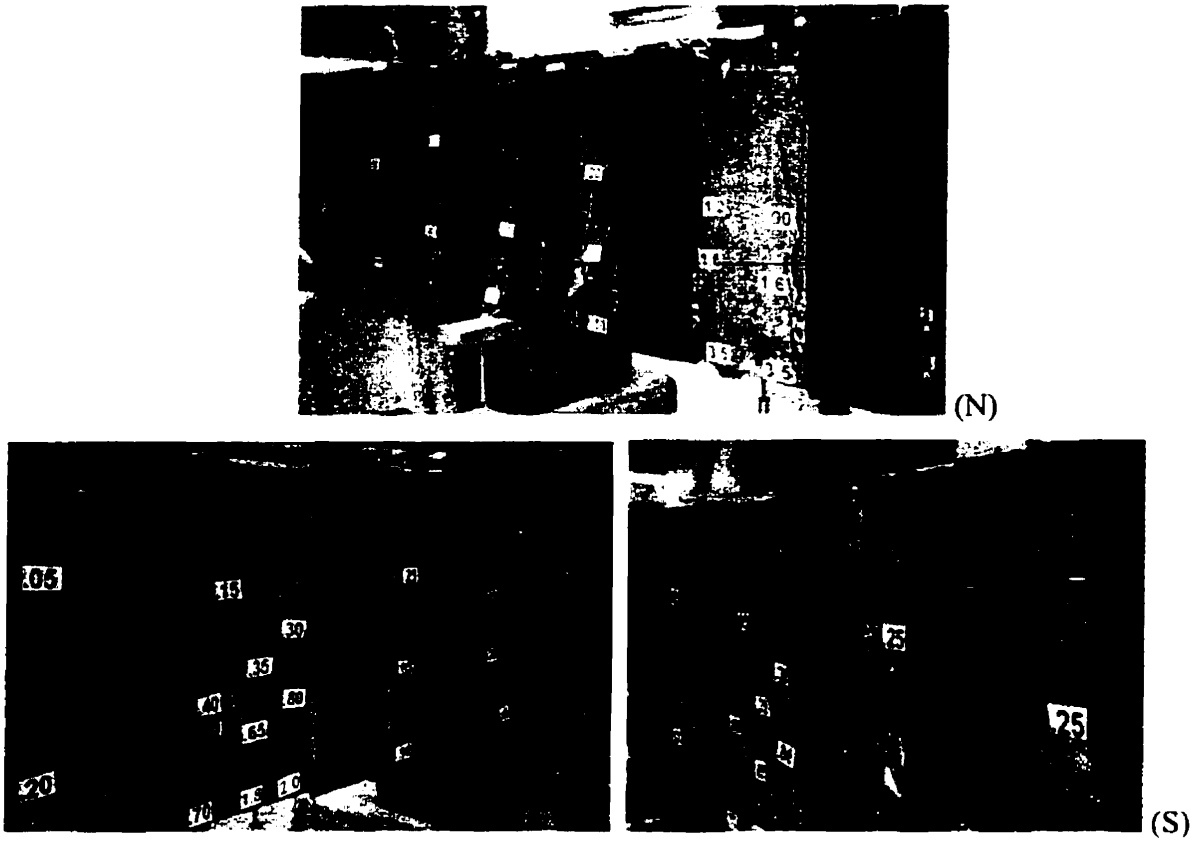

(a)

(b)

Figure 4.13: Beam RWOA-1 at failure: (a) debonding of CFRP strips, (b) concrete failure viewed from below

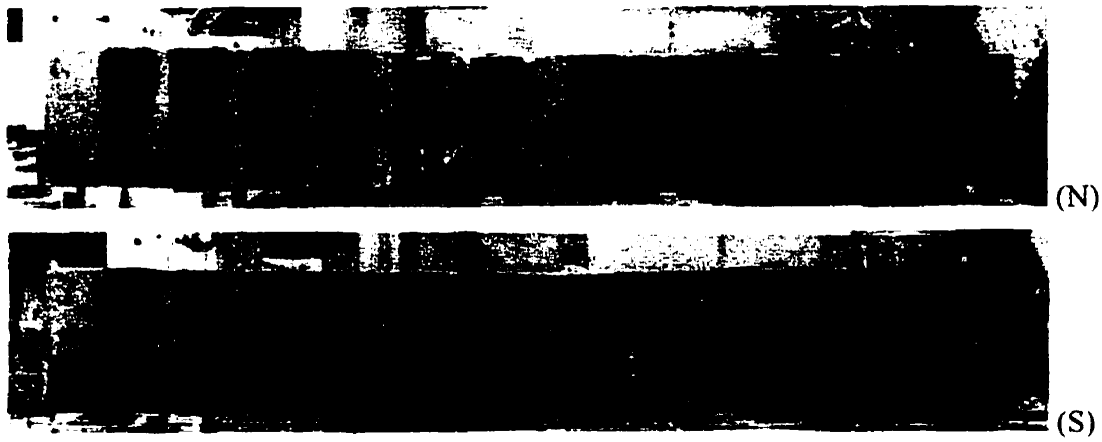

(c)

Figure 4.13 (continued): Beam RWOA-1 at failure: (c) overall crack pattern

4.5.2 *BEAM RWOA-2*

Similar to beam RWOA-1, the first flexural crack was observed at 80 kN on the underside of the beam. Shear cracks appeared at a load of 340 kN. Flexural crack widths increased to 0.55 mm until a load of 448 kN, when the flexural reinforcement started to yield. The maximum load attained was 457 kN, with a maximum mid-span deflection of 32 mm. Just before crushing, flexural crack widths were up to 2.0 mm and the widest shear cracks were 0.2 mm. Again, crushing of concrete at mid-span and a major shear crack on the west half of the beam led to ultimate failure. Similar to beam RWOA-1, the top half of a strip crossing the upper portion of the shear crack peeled off with a thin layer of concrete. The adjacent strip intersecting the lower end of the shear crack ripped off with the concrete, causing a triangular section of concrete cover below the shear crack (the base of which crossed three CFRP strips) to pop out from the beam. The debonding failure is evident in Figure 4.14(a). Again, the central section of the beam dropped down in shear after the side covers split out. The condition on the underside of the beam and the overall crack pattern are illustrated in Figures 4.14(b) and (c), respectively.

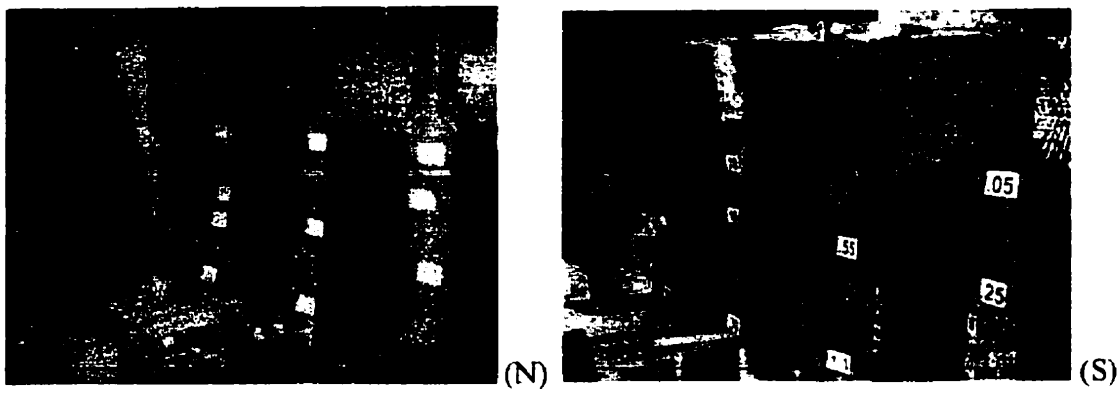

(a)

(b)

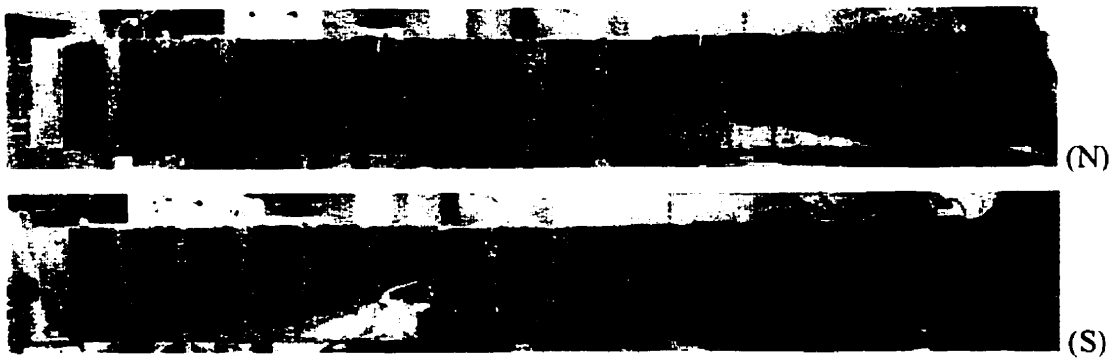

(c)

Figure 4.14: Beam RWOA-2 at failure: (a) debonding of CFRP strips, (b) concrete failure viewed from below, (c) overall crack pattern

4.5.3 *BEAM RWOA-3*

Similar to the two previous beams, the first flexural crack was noted at 80 kN on the bottom surface of the beam. As the spans of the beams increased for RWOA-1 to RWOA-3, the load at first cracking should have decreased. Although flexural cracks were first noted at approximately the same load level for all three beams, the CFRP strips and the darkened, epoxy-coated concrete surface made the cracks obscure. Therefore, cracks may have formed prior to 80 kN but remained undetected. At 180 kN, shear cracks started to form. At the onset of yielding of flexural reinforcement at 420 kN, flexural crack widths increased to 0.6 mm. Just before the peak load was reached, the maximum shear crack width was 0.15 mm, while the widest flexural crack was 1.6 mm. The maximum load sustained was 436 kN, with a mid-span deflection of 50 mm. The maximum displacement prior to failure was 73 mm. Although failure was initiated by flexural steel yielding and crushing of concrete under the load, final failure was caused by a shear crack starting from mid-span extending to the east side of the beam. As concrete was crushed, it spalled and forced the top sections of two CFRP strips (closest to mid-span on the east side) to bulge out. Once the force exceeded the bond (shear) strength of the concrete, the CFRP strips, along with a layer of concrete, debonded with a loud cracking sound. The top half of one of the strips split vertically into five pieces. The bottom sections of two CFRP strips crossing the lower end of the shear crack also debonded with a layer of concrete attached. Figure 4.15 shows the failure condition of this beam. Again, the peeling off of the CFRP strips allowed pieces of concrete to spall off from the beam. The punching out of the central portion of the beam, which was observed in beams RWOA-1 and RWOA-2, was not as evident for beam RWOA-3.

Photos depicting the progressive cracking of all three beams can be found in Appendix B. The debonding of the CFRP strips, along with the rupture of the side concrete cover that was noticed in this experiment, is similar to the test observations made by Khalifa and Nanni [38] regarding specimen BT5 (as reported in section 2.3.1). Also, the longitudinal cracking along the flexural steel on the bottom of the beam matched the results of Chaallal *et*

al. [30]. The high normal (peeling) forces at the ends of the strips led to the longitudinal cracking and subsequent separation of the concrete cover.

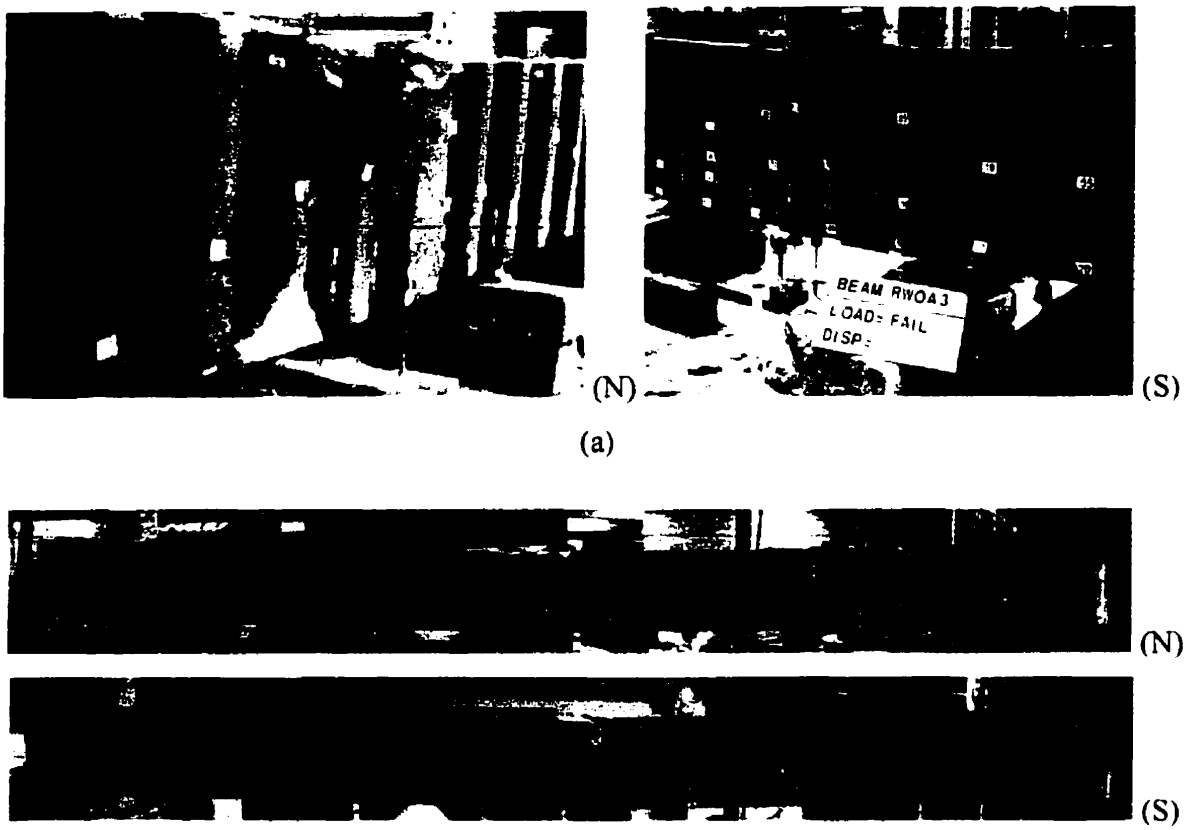

Figure 4.15: Beam RWOA-3 at failure: (a) debonding of CFRP strips, (b) overall crack pattern

4.6 TEST RESULTS

The load-deflection curves for all three RWOA beams are depicted in Figure 4.16. All three beams failed in shear-flexure while exhibiting ductile behaviour. Although no premature debonding of the CFRP strips was noted, part of the strips crossing the major shear

crack did peel off at ultimate. The shear-flexural dominated failures of the beams were accompanied by the rupture of the side concrete cover and the punching out of the beams' central sections. The mid-span deflections have been adjusted by subtracting the end settlement values from the displacements measured at mid-span.

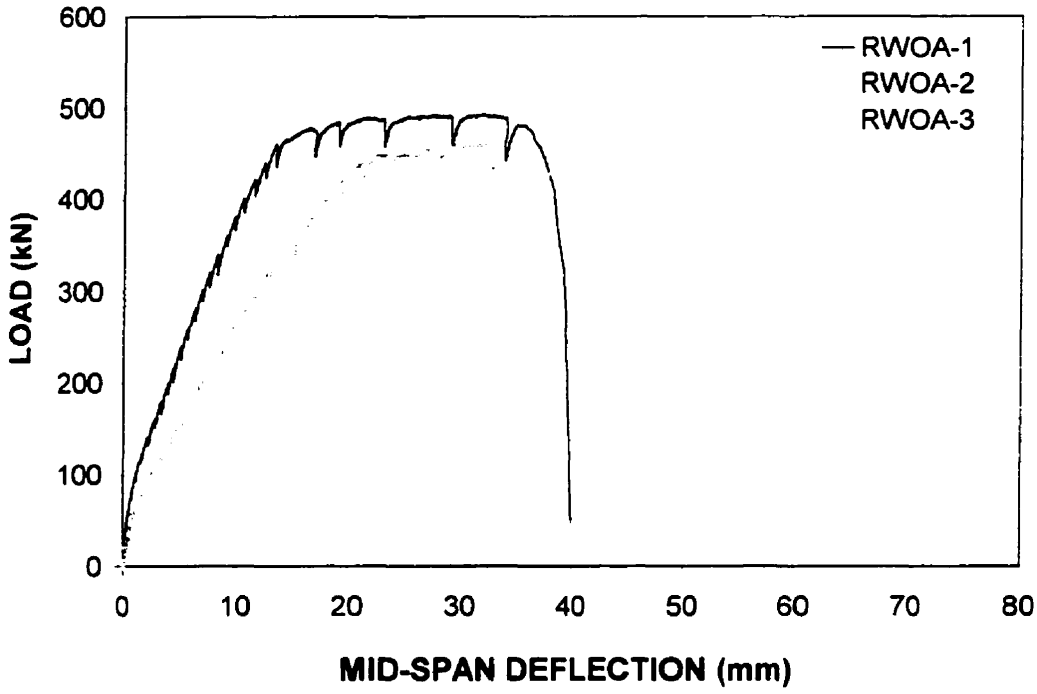

Figure 4.16: Experimental load-deflection response for RWOA beams

The mid-span surface strains at the level of the longitudinal reinforcement for all three RWOA beams are plotted in Figure 4.17. While the surface strains on RWOA-1 reached a maximum value of 0.02, the largest value measured for beams RWOA-2 and RWOA-3 was 0.01. Since the strains were determined from displacements between Zurich targets on the side surfaces of the beams, the measurements were affected by cracks along the beam and the subsequent movement of the CFRP strips. More accurate strain values at the level of the reinforcement would require strain gauges to be attached directly onto the rebars. Plots of surface strains measured along the beams have been included in Appendix B.

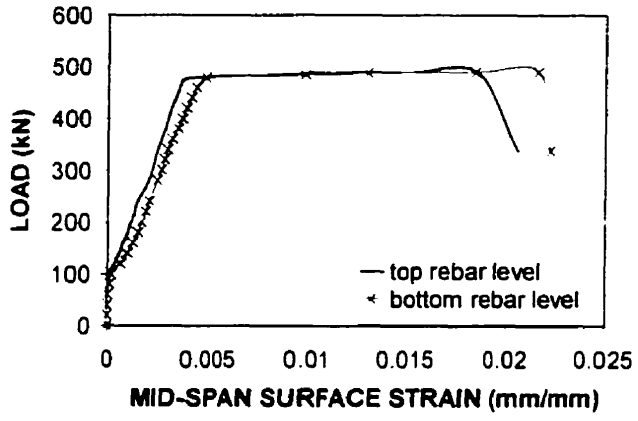

(a)

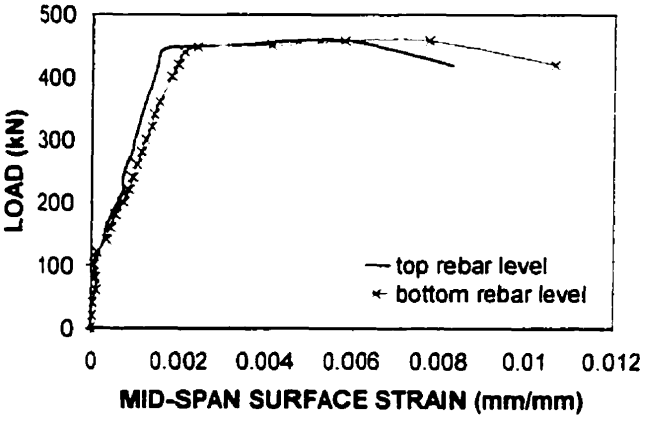

(b)

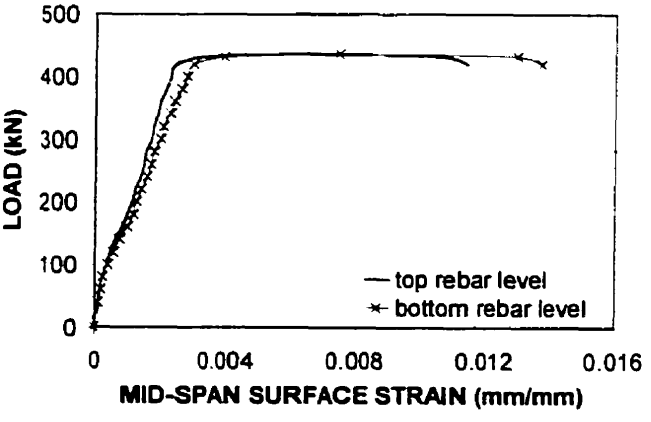

(c)

Figure 4.17: Mid-span surface strains at the level of longitudinal reinforcement: beam (a) RWOA-1, (b) RWOA-2, (c) RWOA-3

4.7 ANALYTICAL RESULTS

The ultimate loads of the RWOA beams were estimated using equations proposed by various researchers (previously presented in Chapter 2 of this report). These equations were formulated to calculate the shear contribution of FRP composites (V_f), applied either as strips or as continuous sheets. Expected failure modes include the debonding or fracture of the FRP laminates. Since FRP fracture is rarely observed in shear-strengthened beams, except in some cases of complete wrapping with the laminates, most of the equations focus on premature debonding failures. The experimental and predicted values for the shear contribution of the CFRP strips are listed in Table 4.4. The calculations are provided in Appendix C.

Table 4.4: Actual and Predicted Values of FRP Shear Contribution

Proposed Equation	V_f for RWOA-1 (kN)	V_f for RWOA-2 (kN)	V_f for RWOA-3 (kN)
Experimental Data*	81.5	69.5	25.5
Triantafillou (Eqns. 2-22 and 2-23)	238	238	238
Khalifa (Eqns. 2-24 and 2-26)	114.7	125.6	177.4
Triantafillou and Antonopoulos			
(Eqns. 2-22 and 2-29b)	106.1	111.7	135.5
(Eqn. 2-31, φ_f = 0.75 for debonding)	129.4	136.1	165.2
Schnerch (Eqns. 2-32 and 2-24)	150.8	167.0	246

*calculated by subtracting the shear capacity of the TOA beams from that of the RWOA beams

All of the predicted values were higher than the experimental data. However, this is consistent since all three beams were governed by shear-flexural failure rather than by debonding of the CFRP strips. Due to the high CFRP reinforcement ratio used in the RWOA beams, the validity of the proposed equations could not be adequately assessed.

4.8 DISCUSSION

The experimental results of the RWOA series of beams were compared with the TOA and TA series, where each series consisted of three beams, numbered 1, 2 and 3, respectively. The TOA series did not contain any stirrups, while the TA series had 0.1% of steel reinforcement in shear. Each beam number (1, 2 and 3) corresponded to a certain steel flexural reinforcement ratio (as given in Table 4.5), and the reinforcement properties of the beam series are also listed in the table. The purpose of the comparison is to determine the effect of the CFRP strengthening.

Table 4.5: Reinforcement Properties for the TOA, TA and RWOA Beam Series

Beam Series	Beam Number	Flexural Reinforcement Ratio	Flexural Steel Yield Strength* (MPa)	Shear (Steel) Reinforcement Ratio	CFRP Reinforcement Ratio
TOA	1	1.72 %	440, 436	-	-
	2	2.23 %	445, 436	-	-
	3	2.73 %	440, 436	-	-
TA	1	1.72 %	440, 465	0.1 %	-
	2	2.23 %	445, 465	0.1 %	-
	3	2.73 %	440, 465	0.1 %	-
RWOA	1	1.72 %	440, 436	-	0.367 %
	2	2.23 %	445, 436	-	0.367 %
	3	2.73 %	440, 436	-	0.367 %

* yield strengths of 25M and 30M rebars, respectively

The load-deflection response for each series of beams is plotted in Figure 4.18. Some general trends can be observed from these graphs. The TOA series of beams failed in shear in a brittle manner, while those shear-reinforced with steel stirrups (TA series) and CFRP strips (RWOA series) exhibited ductile behaviour and flexural failure. For the 1 and 2 series, after the shear capacity of concrete was reached, the response of the beams with CFRP strips was stiffer than those reinforced with stirrups. This can be attributed to the higher rigidity provided by the CFRP strips, where rigidity is defined as the shear reinforcement ratio

multiplied by the Young's modulus of the material. [The values of Young's modulus for CFRP and steel were 100 GPa and 200 GPa, respectively.] For the RWOA series, the rigidity is calculated as 0.367 GPa, while for the TA series, this value is 0.200 GPa. Also, the ultimate loads sustained by the RWOA series were higher than those of the TA series beams. However, since the reinforcement ratio provided by the CFRP strips was 3.7 times higher than that of the stirrups, no direct comparison can be made between their performance. In addition, the clamping force for the CFRP is 4.0 MPa while for the steel stirrups it is 0.4 MPa. The clamping force is determined as the shear reinforcement ratio multiplied by the yield strength of the material. [The yield strengths of CFRP and steel were 1090 MPa and 400 MPa, respectively.] The maximum load and displacement values, and the ratios of strength enhancement are summarized in Table 4.6.

Table 4.6: Maximum Load and Deflection for Beam Series TOA, TA and RWOA

Beam Series	**TOA**		**TA**		**RWOA**		**Ratio of RWOA to TOA**		**Ratio of RWOA to TA**	
Beam Number	P_{max} (kN)	Δ at P_{max} (mm)	P_{max} (kN)	Δ at P_{max} (mm)	P_{max} (kN)	Δ at P_{max} (mm)	P_{max}	Δ at P_{max}	P_{max}	Δ at P_{max}
1	331	9.0	459	20.8	493	31.8	1.49	3.53	1.07	1.53
2	320	13.2	441	28.5	459	31.3	1.43	2.37	1.04	1.10
3	385	31.8	420	50.3	436	48.6	1.13	1.53	1.04	0.97

As can be seen from the above graphs and table, the vertically-oriented CFRP strips prevented the brittle shear failure of the beams by acting in the same manner as stirrups. The strong fibres in the direction perpendicular to the beam axis provided resistance to tensile forces in the vertical direction arising due to shear. The CFRP strips exerted a closing effect on the shear cracks, limited their propagation, and increased the concrete's shear resistance by permitting more aggregate interlock to occur. This allowed the beam to sustain higher

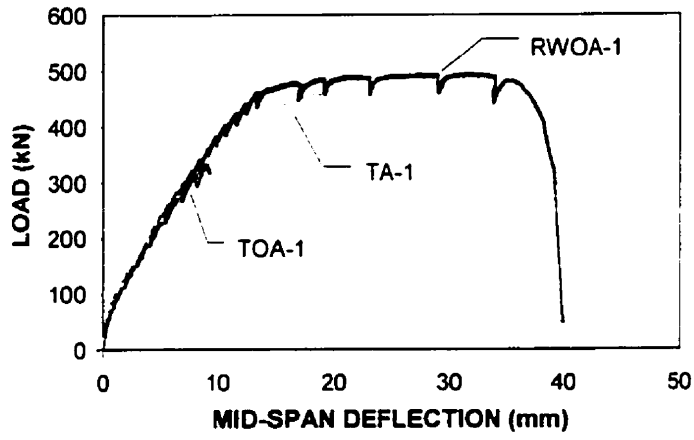

(a)

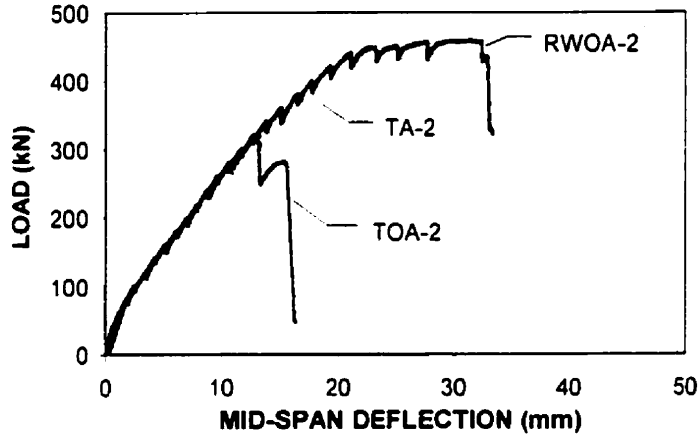

(b)

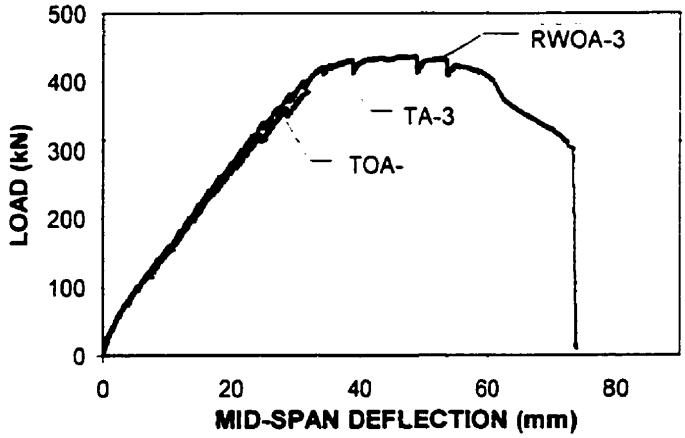

(c)

Figure 4.18: Load-deflection curves for beam series: (a) 1, (b) 2 and (c) 3 (comparison between TOA, TA and RWOA beams)

loads until the flexural steel bars yielded in tension, achieving loads up to 50% higher than the beams without shear reinforcement. It also resulted in a more ductile behaviour, with mid-span deflections up to 350% greater than the TOA beams. The strength enhancement of the RWOA series to the TA series beams was less than 10%, even though the shear reinforcement ratio was 3.7 times higher, and the clamping force was ten times greater. The degree of strength increase provided by the CFRP was limited by the yield strength of the flexural steel and the compressive capacity of the concrete.

Aside from the material properties, the main difference between the effect of the CFRP strips and steel stirrups lie in their configuration. Whereas the stirrups were closed loops enclosing all four surfaces of the beam, the CFRP strips were only bonded to the side surfaces. Thus, after concrete crushing occurred with shear failure at ultimate, the central section of the beam was unconfined, causing it to punch out in a downward direction as a result of shear forces. Some confinement could be provided if the CFRP strips were completely wrapped around the beam. However, since most beams are cast monolithically with a slab, forming a T-beam, it would be more practical to bond the CFRP strips or sheets in a U-shaped configuration. The top edges of the CFRP sheet should then be anchored into the concrete on both sides of the beam with steel plates and bolts, as has been investigated by Sato [63].

Overall, the presence of the CFRP strips was able to prevent brittle shear failure of the beams. Not only was the capacity of the beams increased, but the response was also more ductile. The excessive deformations at mid-span gave more warning as failure became imminent, making these beams safer to use in the field. No premature debonding of the CFRP strips was noted, which implies that the surface preparation of the beams was adequate, and that the bond strength of the epoxy used was sufficiently high. Debonding of the CFRP strips occurred only when concrete crushing had advanced and with the formation of a major shear crack near ultimate. It was observed that a thin layer of concrete was attached to the CFRP strips at the time of separation. This indicates that the lower shear strength of concrete had led to the debonding, rather than shear slippage within the epoxy

layer or at the FRP-adhesive interface. This is in correlation with the fact that the shear strength of epoxy is much higher than that of concrete.

For aging beams in which the stirrups have corroded or where the shear reinforcement ratio does not satisfy updated standards or is insufficient to meet current loading requirements, CFRP laminates present a viable and convenient method for upgrading their shear capacities. Sudden shear failures can also be converted to ductile flexural failures with more noticeable mid-span deflections.

CHAPTER 5 NUMERICAL ANALYSIS WITH FEM

5.1 INTRODUCTION

In order to verify the performance of the bond elements in the nonlinear finite element program VecTor2, the response of five sets of experimental specimens has been simulated, utilizing link or contact elements to model the concrete-FRP interface. These specimens are slabs or beams that have been strengthened in flexure or shear with FRP laminates. The external FRP reinforcement was successful in increasing the ultimate capacity of the specimens, while changing brittle shear failures to ductile flexural failures. In the current research, all of the specimens analyzed were subjected to monotonic loading conditions, hence, the bond-slip between rebars and concrete was not accounted for in the numerical modelling. The input files for all the specimens studied in this chapter are located in Appendix D, while the deflected shapes and crack patterns for the specimens can be found in Appendix E.

5.2 SPECIMENS STRENGTHENED IN FLEXURE WITH FRP COMPOSITES

Three sets of specimens strengthened in flexure with FRP laminates were analyzed. These flexural members had FRP plates or sheets bonded to their soffit for positive moment capacity or to the top surface to resist negative moments.

5.2.1 *ŽARNIĆ SPECIMENS*

The first set of flexural specimens modelled were the slab strips and beams tested at the University of Ljubljana, Slovenia, by Žarnić *et al.* [11]. Only the specimens repaired with CFRP plates have been analyzed in this study.

5.2.1.1 EXPERIMENTAL DETAILS

The cross sections and load application points for the slab strip and beam are shown in Figure 5.1. The slab strip specimens were 800 mm in width, 120 mm in depth, and 3250 mm in length. The beams were of the same length, but with cross sections 200 mm wide by 300 mm deep. For each type of flexural member, one specimen was kept as the control, while three were strengthened with CFRP plates. The CFRP plates were 50 mm wide and 1.2 mm thick, while the epoxy layer was 2 mm thick. External bonding was undertaken prior to the application of displacement-controlled, four-point loading on the beams. Table 5.1 lists the material properties for the specimens.

Table 5.1: Material Properties for Žarnić Slab Strips and Beams [11]

Material	f'_c (MPa)	f'_t (MPa)	E (GPa)	ν
Concrete	25	1.65	25	0.15
Epoxy	100	4	12.8	0.35
CFRP	100	2400	150	-
Material	**f_y (MPa)**	**f_u (MPa)**	**E (GPa)**	**ν**
Steel (slab strip)	500	560	210	0.30
Steel (beam)	450	550	210	0.30

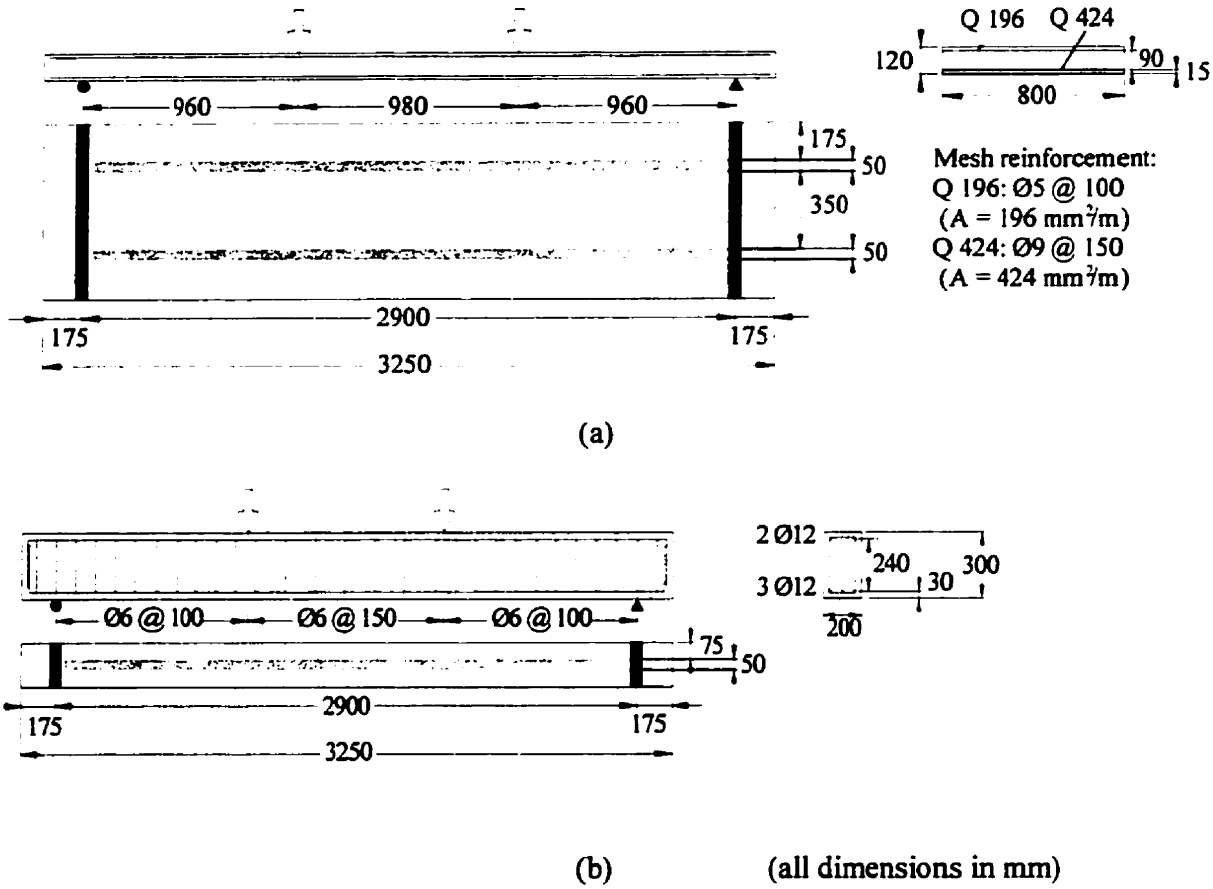

Figure 5.1: Geometry of Žarnić specimens: (a) slab strip and (b) beam [11]

In the experiment, the slab strip control specimen failed at a total load of 36.5 kN, while the CFRP plates increased its strength by 72.5% to 63 kN. For the control beam, the ultimate load was 86.5 kN, and the bonding of the CFRP plate raised this failure load by 35% to 116.8 kN. The presence of the CFRP plates delayed the development of cracks, resulting in higher post-cracking stiffnesses for the plated beams as compared to the control specimens. The linear elastic response of the CFRP plates dominated the behaviour of the specimens, culminating in the sudden failure due to delamination of the plates. In both the strengthened slab strip and beam specimens, the failures were caused by debonding or delamination of the plates below the concentrated load, in the region of extensive flexural deformation and cracking. The debonding initiated in the middle third of the beams and propagated to the free ends by peeling off a thin layer of concrete. Unlike most steel-plated

and some FRP-plated beams, these specimens were not sensitive to high normal and shear stresses at the plate ends. Similar to debonding failures observed by other researchers, the CFRP plates were under-utilized, as they were far from their ultimate tensile strength at failure.

5.2.1.2 NUMERICAL MODELLING

5.2.1.2.1 *Finite Element Mesh and Special Considerations in Analysis*

Due to the symmetrical nature of the Žarnić specimens, only one half of the beams was modelled. The finite element meshes used for both types of specimens are illustrated in Figure 5.2. For the Žarnić slab strip specimen, 847 rectangular elements were utilized for concrete, 154 truss elements were used for flexural steel, and the CFRP plates were modelled by 65 truss elements. For the bond interface, either 66 link elements or 65 contact elements were used. As for the Žarnić beam specimen, 588 rectangular concrete elements were defined, with the shear reinforcement smeared throughout them. 98 truss elements were employed for flexural steel, while 42 truss elements represented the CFRP plate. Either 43 link elements or 42 contact elements were used to model bond behaviour.

The truss elements representing flexural steel reinforcement were connected directly to the concrete elements since monotonic loading conditions were applied. Truss elements modelling the CFRP plates were joined to bond elements (either link or contact elements), which were in turn connected to the concrete elements. The diameter specified for truss elements is used in calculating tension stiffening effects. Thus, this value must be reduced to 1 mm for compression steel in thin slabs or to 0.1 mm for FRP laminates such that extra capacity will not be erroneously generated in the tensile zone.

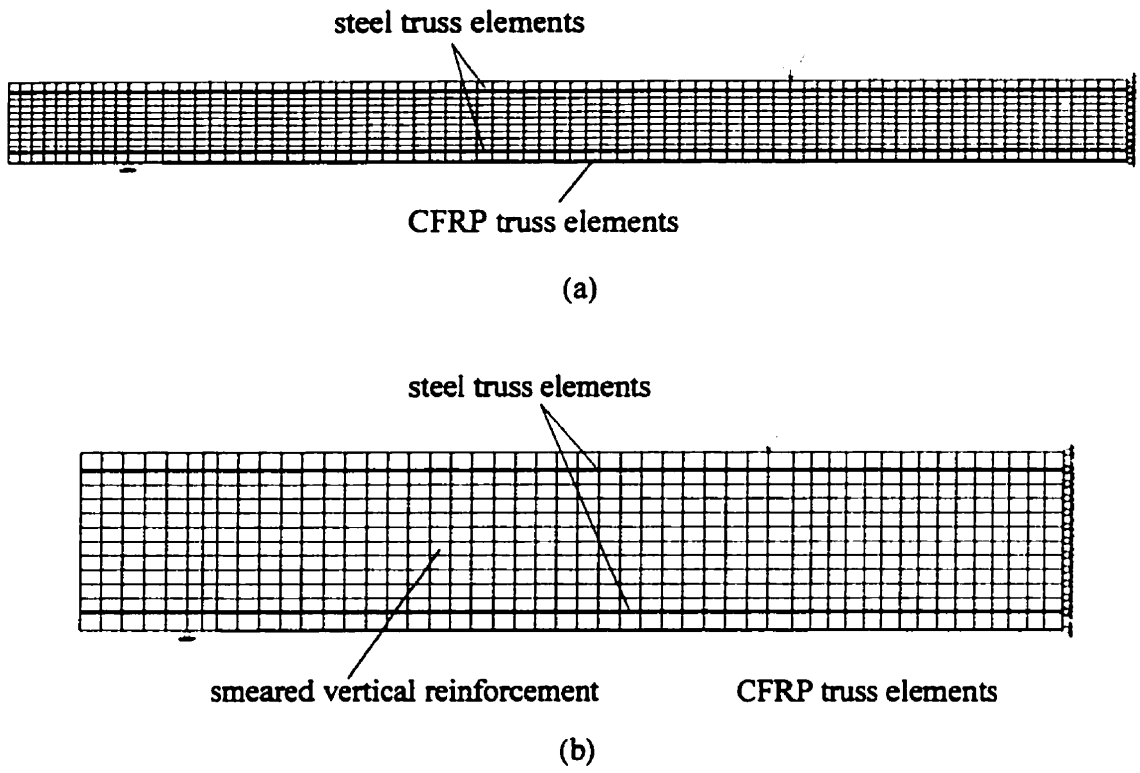

Figure 5.2: Finite element mesh for (a) Žarnić slab strip and (b) Žarnić beam

The most important parameter in capturing the debonding phenomenon observed in the tests is the characterization of the bond interface. The bond stress-slip law chosen for this analysis was linear elastic to failure. Since the experimental load-deflection curves exhibited sudden failures represented by sudden drops in load, and debonding failures were observed in the tests, a corresponding relationship with an abrupt drop in bond stress was selected for the initial trial. The stiffness E_b was based on the shear stiffness of the epoxy used, and was calculated according to (based on Eqn. 2-54):

$$E_b = \frac{G_a}{t_a} \qquad \text{where} \qquad G_a = \frac{E_a}{2(1+\nu_a)} \tag{5-1}$$

G is the shear modulus, E is the Young's modulus, ν is the Poisson's ratio, t is the thickness of the layer, and the subscript a refers to the adhesive (epoxy resin).

Various values ranging from 1 to 5 MPa were used for the maximum shear stress (U_{max}), and the corresponding maximum slip values (S_{max}) were calculated using E_b = 2370 MPa/mm (refer to Figure 3.8(b)). Numerous trials were conducted since it was found that the values used for the constitutive relation of the bond elements greatly influenced the response of the members. Both the failure load and deflection at failure were sensitive to the bond stress-slip law. If E_b was varied by modifying the maximum bond stress or maximum slip, the analysis results would be inaccurate. For comparison purposes, trials with perfect bond conditions and an elastic-plastic bond stress-slip relationship were also performed.

Since the CFRP plates were present from the onset of the tests, the elements representing the repair materials were activated from the first load stage of the analysis. Due to the low initial stiffness of both types of specimens, it was assumed that some time had elapsed from the time of casting to the time of testing. Thus, constant shrinkage strains of -0.4×10^{-3} and -0.2×10^{-3} were applied to the slab strip and beam, respectively, throughout the duration of the analyses. With the inclusion of shrinkage strains, it was found that the bond elements and horizontal FRP elements did not shrink with the concrete. This resulted in initial slips, but the concrete and FRP nodes were later reattached as the beam deflection increased. To resolve this problem, it was necessary to apply a prestressing strain ($\Delta\varepsilon p$) to the FRP truss elements. This strain value was slightly less than the absolute value of the shrinkage strain used. To match the experimental conditions, displacement-controlled loading was applied.

5.2.1.2.2 *Analysis Results and Discussion*

The load-deflection curves from the numerical analyses for the slab strip is shown in Figure 5.3. The perfect bond condition predicted a failure load 33% higher than the actual force sustained, at a mid-span deflection that was twice as large as the experimental value. For the cases including slip at the bond interface using the linear elastic bond law, it was found that a maximum shear stress of 3 MPa for the bond elements yielded the best results. The failure load of 58 kN and the corresponding mid-span deflection were within 5% of the average experimental values. With the elastic-plastic bond law, the peak load and deflection were overestimated by 22% and 73%, respectively. The effects of varying the maximum bond stress and of lowering the slip modulus are plotted in Figure 5.4, while the analytical results are summarized in Table 5.2.

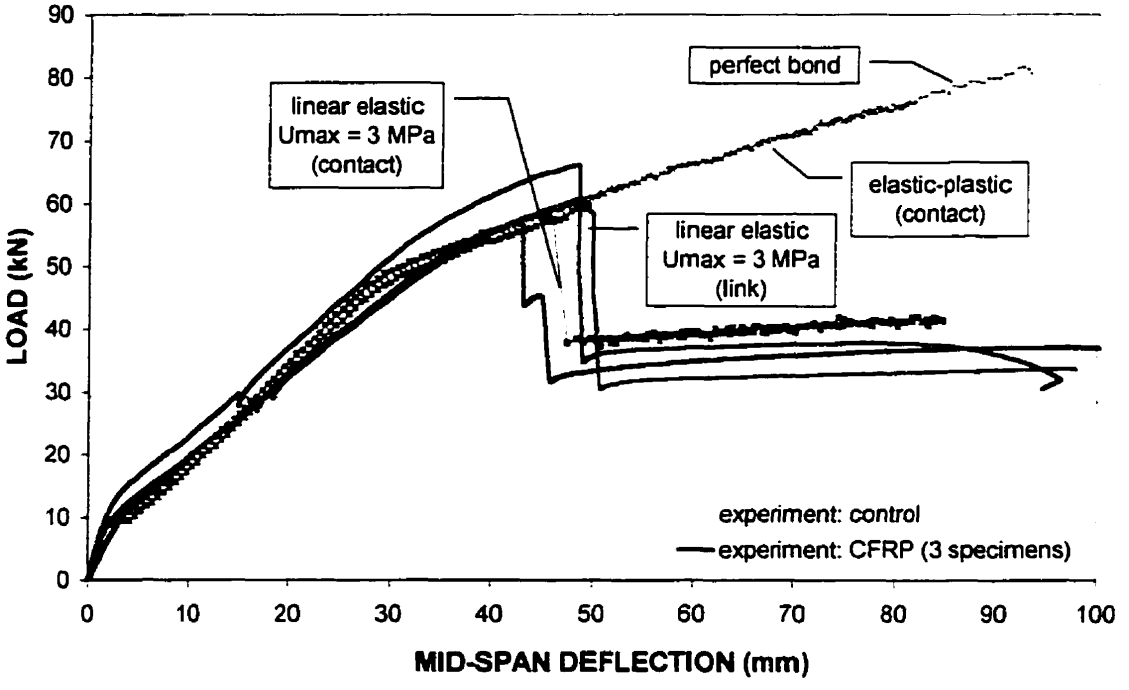

Figure 5.3: Load-deflection curves for Žarnić slab strip bonded with CFRP plate

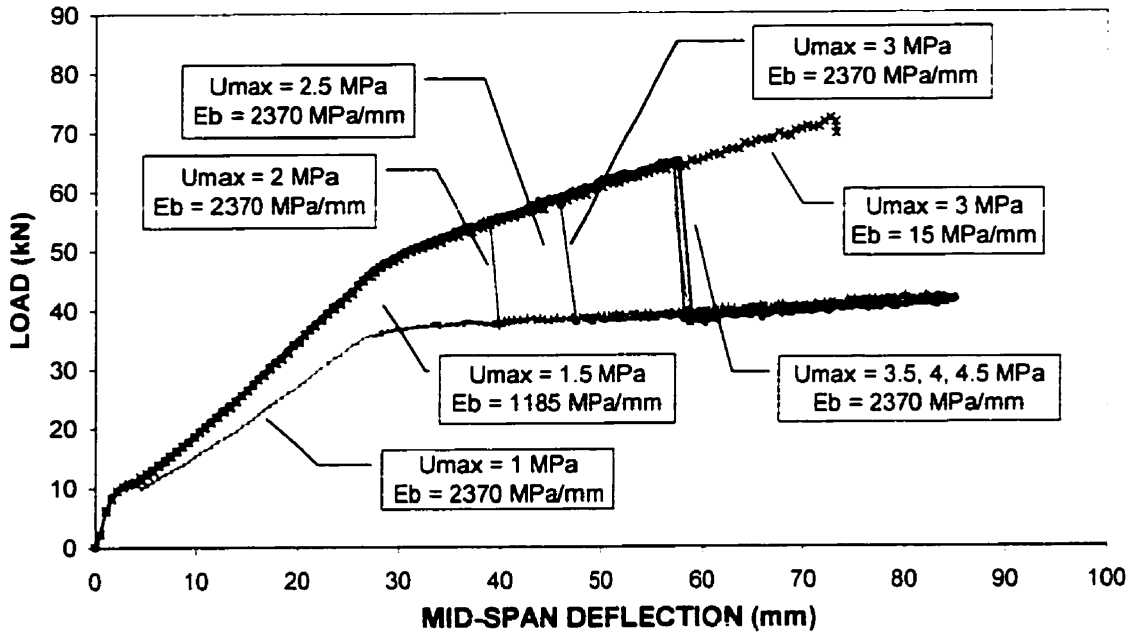

Figure 5.4: Effects of varying maximum bond stresses for Žarnić slab strip

Table 5.2: Predicted Results for Žarnić Slab Strip Bonded with CFRP Plate

Bond Element Type	Constitutive Relationship	U_{max} (MPa)	Maximum Load (kN)	Deviation from Exp. Load (%)	Mid-span Deflection at Maximum Load (mm)	Deviation from Exp. Deflection (%)
Contact	Linear elastic	2.0	55.0	-10.3	38.3	-17.4
		2.5	57.8	-5.72	44.3	-4.58
		3.0	58.2	-5.07	45.5	-1.99
		3.5	64.4	5.04	56.7	22.1
		4.0	65.2	6.35	57.6	24.1
		4.5	65.0	6.02	57.2	23.3
	Elastic-plastic	3.0	75.8	23.6	81.6	75.8
Link	Linear elastic	2.5	56.4	-8.01	44.3	-4.56
		3.0	59.2	-3.44	49.0	5.57
	Elastic-plastic	3.0	73.2	19.4	78.6	69.3
Perfect bond		∞	81.6	33.1	92.4	99.0

The mode of failure was by debonding of the CFRP plates, initiated under the loading point, as reported by Žarnić *et al.* Figure 5.5 shows the distribution of bond stress in the bond elements along the beam soffit at peak load and in the load stage immediately thereafter (for the case of U_{max} = 3 MPa). For the contact elements, the values are the average of the stresses calculated at the two ends of the element, while for the link elements, the average of two adjacent elements are plotted. At maximum load, peaks in the bond stress distribution were noted at approximately 100 mm from the free plate end, and also near the loading point and towards the mid-span of the beam. This is in agreement with the observations made by Aprile *et al.* [79] in their analysis of this member, using a displacement-based fibre beam model. The high shear stresses near the plate end are due to the change in the cross-section geometry and the lack of proper anchorage for the CFRP plate, and is similar to the plate-end shear stresses commonly noted in RC beams bonded with steel plates. Shear stresses near the end of the FRP plate were not as evident in the experiment, since the debonding failure initiated under the loading point. In the middle third of the beam span (to the right of the loading point in the analysis), the sign fluctuations of the bond stress can be attributed to the flexural cracks in this region. Immediately after the peak load, the bond stress in the link elements dropped to zero along the whole specimen. However, with the contact elements, the FRP plate was debonded over a length of 600 mm, with approximately 300 mm on each side of the loading point. In the following load stage, the plate became completely debonded. The prediction by the contact elements is closer to the actual failure mode of the specimens.

For the Žarnić beam, the perfect bond condition overestimated the failure load by 19% and the corresponding mid-span deflection was 66% larger than the experimental value. The mechanical properties of the bond elements in the beam were the same as those used for the slab strip analyses, since the same type of FRP and epoxy was used for both sets of specimens. However, having gained a better estimate of the maximum shear stress sustainable by the bond interface, fewer trials were performed for this specimen. As can be observed from Figure 5.6 and Table 5.3, a maximum bond stress of 3 MPa in the linear elastic relationship provided a reasonably accurate response. Applying the elastic-plastic

bond law gave values of ultimate load and deflection that were 17% and 59% higher than the test data, respectively.

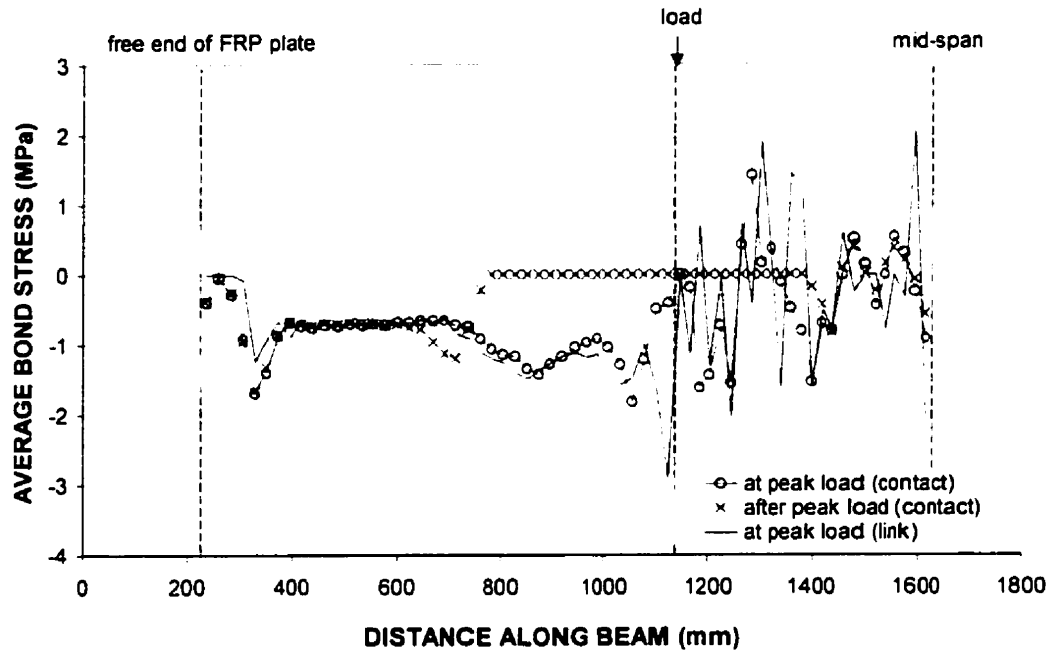

Figure 5.5: Bond stress distribution for Žarnić slab strip with bonded CFRP plate

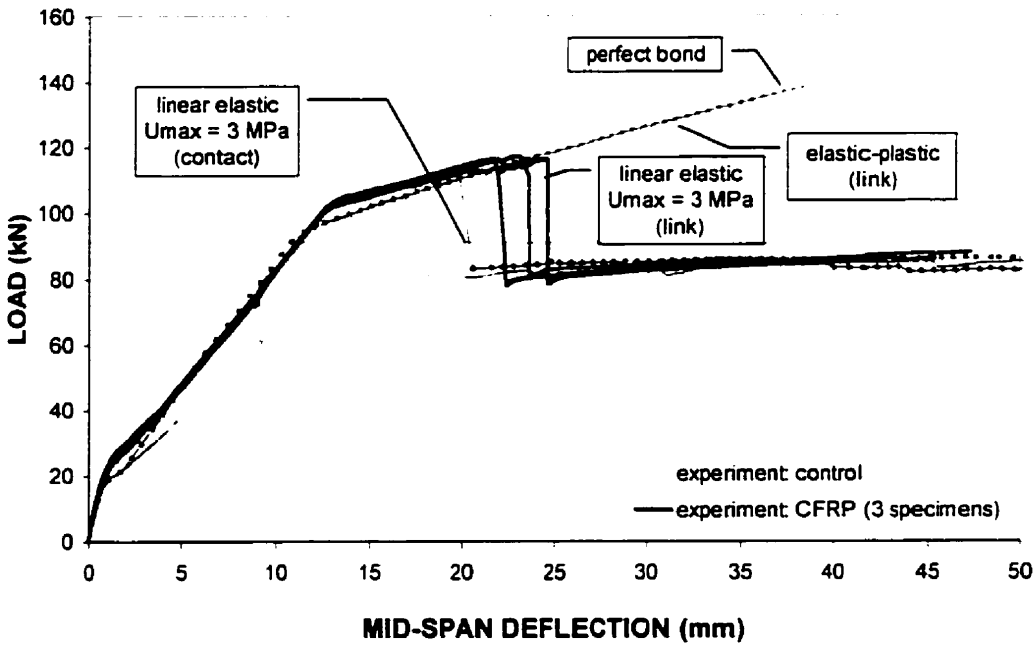

Figure 5.6: Load-deflection curves for Žarnić beam bonded with CFRP plate

Table 5.3: Predicted Results for Žarnić Beam Bonded with CFRP Plate

Bond Element Type	Constitutive Relationship	U_{max} (MPa)	Maximum Load (kN)	Deviation from Exp. Load (%)	Mid-span Deflection at Maximum Load (mm)	Deviation from Exp. Deflection (%)
Contact	Linear elastic	3.0	110.6	-4.38	19.9	-13.9
		3.25	112.4	-2.82	21.0	-8.70
		3.5	118.8	2.71	25.1	8.99
	Elastic-plastic	3.0	136.4	17.9	37.2	61.4
Link	Linear elastic	3.0	116.8	0.98	24.0	4.14
		3.25	120.6	4.27	26.3	14.1
		3.5	123.4	6.69	28.0	21.5
	Elastic-plastic	3.0	134.2	16.0	36.0	56.2
Perfect bond		∞	138.0	19.3	38.3	66.1

In the Žarnić beam, the bond stress is higher in the region near the loading point and towards mid-span, as shown in Figure 5.7. The average bond stress progressively increased from the free end of the plate, and fluctuations in sign were noted within the middle-third of the beam due to flexural cracks. The general trend observed is similar to that for the slab strip specimens, and the magnitude of the bond stresses are also comparable. However, immediately after the peak load, both types of bond elements predicted complete delamination of the CFPR plate. This is in agreement with the behaviour observed in the experimental and numerical load-deflection curves, where the load-carrying capacity of the repaired specimens dropped to that of the control specimen immediately after debonding of the CFRP plate.

After the analyses had been performed using various values for the maximum bond stress, it was realized that the most appropriate value (3.0 MPa) corresponded to the modulus of rupture for the concrete used in the test. Modulus of rupture is defined as $f_r = 0.6\ (f'_c)^{0.5}$, and f'_c of the concrete was 25 MPa. This rationale is supported by a thin layer of concrete that was found on the CFRP plate, indicating that failure had occurred within the concrete adjacent to the bond interface, rather than in the epoxy layer. The tensile properties of concrete must be considered since the stress transfer mechanism between concrete and FRP depends on the shear and tensile characteristics of the concrete.

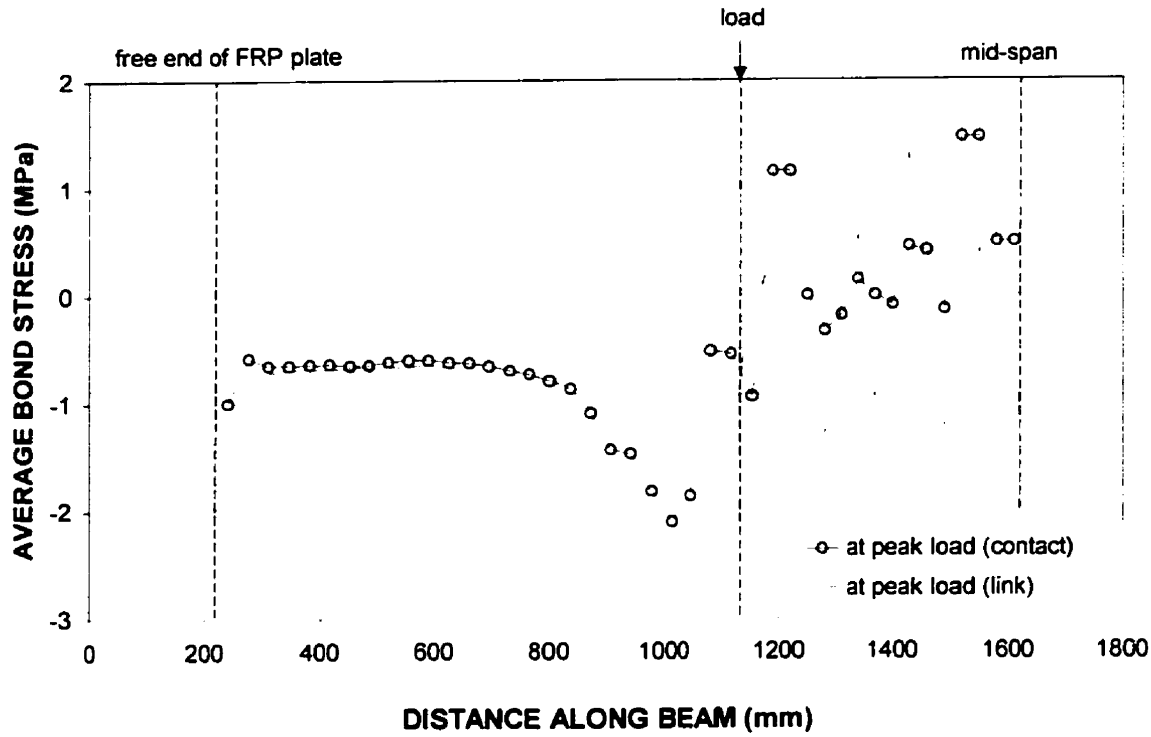

Figure 5.7: Bond stress distribution for Žarnić beam with bonded CFRP plate

5.2.2 *EL-REFAIE SPECIMENS*

The second set of specimens analyzed with program VecTor2 was a series of five continuous RC beams tested at the University of Bradford, UK [80]. Of the five two-span beams, one was tested as a control specimen, while the remaining four were strengthened with CFRP plates or sheets on the top and/or bottom surfaces of the beams.

5.2.2.1 EXPERIMENTAL DETAILS

The geometry of the beams were identical, each being 8500 mm long × 150 mm wide × 250 mm deep. Flexural steel was provided by four 16 mm diameter bars (two on the top and two on the bottom). Closed stirrups of 6 mm diameter were spaced at 100 mm along the

beam for shear reinforcement. The geometry, loading and support conditions are shown in Figure 5.8.

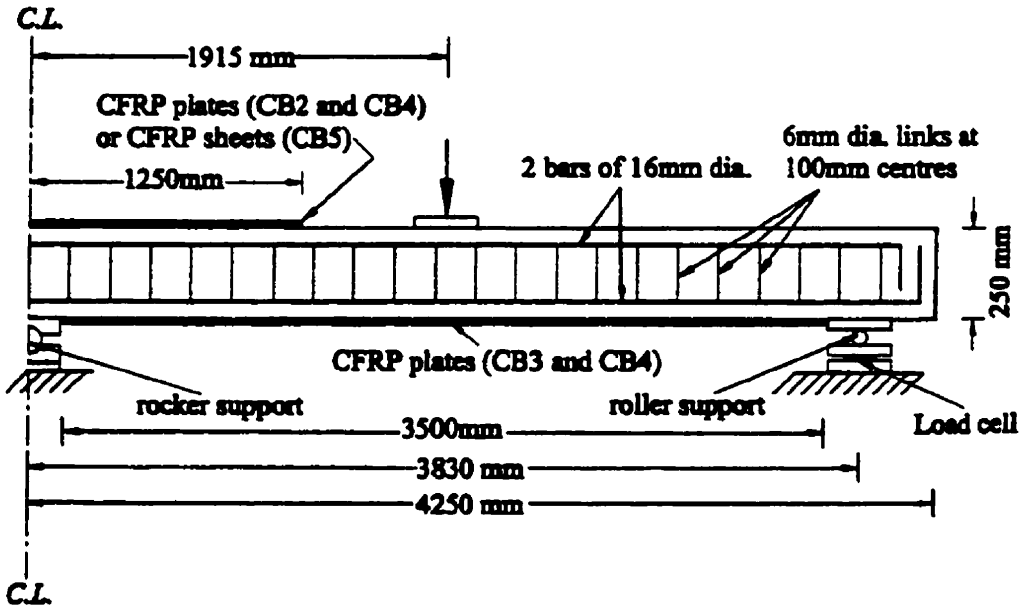

Figure 5.8: Details of El-Refaie specimens [80]

The main variables studied in the experiment were the position and type of CFRP reinforcement. Beam CB1 was kept as the control specimen, with no externally bonded CFRP. The strengthening scheme for beams CB2 to CB5, along with the material properties of the CFRP, are outlined in Table 5.4. The CFRP plates or sheets that were applied to the top surface of the beams were 2500 mm in length and were bonded symmetrically about the central support. For each of the plates (100 mm wide × 1.2 mm thick) that was attached to the beam soffit, the length was 3500 mm and its location was centered on each span of the beam. The strengthening scheme for beam CB2 was identical to that of beam CB5, the only difference being CFRP sheets were used for CB5. The total thickness of these sheets of 0.7 mm (110 mm in width) was designed to give the same strength and axial rigidity ($\rho_f \times E_f$) as the CFRP plate which was used for CB2.

Table 5.5 lists the properties of the concrete and the steel reinforcement used for the beams. Concrete cubes and prisms were tested to determine the concrete's cube strength and modulus of rupture.

Table 5.4: Strengthening Scheme and Properties of CFRP for El-Refaie Specimens [80]

Beam	Type of CFRP	Position of CFRP	f_f* (MPa)	E_f* (GPa)	Bonding Adhesive Used	f_a* (MPa)	E_a* (GPa)
CB1	none	none	-	-	none	-	-
CB2	plates	top face	2500	150	epoxy and structural adhesive	19	9.8
CB3		bottom face					
CB4		top and bottom faces					
CB5	sheets	top face	3900	240	epoxy and bonding adhesive	17	5

* subscripts f and a represent CFRP and adhesive, respectively

Table 5.5: Properties of Concrete and Steel Reinforcement for El-Refaie Specimens [80]

Beam	Concrete			Flexural Steel		Stirrups	
	f_{cu} (MPa)	f'_c* (MPa)	f_r (MPa)	f_y (MPa)	E_s (GPa)	f_y (MPa)	E_s (GPa)
CB1	24.0	20.4	3.0	520	201	308	200
CB2	43.6	37.1	4.6				
CB3	47.8	40.6	4.4				
CB4	46.1	39.2	4.4				
CB5	44.7	38.0	4.8				

• f'_c was calculated as $0.85 \times f_{cu}$

Sand blasting was used to roughen the concrete substrate, and the tensile strength was checked with pull-off bond tests prior to bonding of the CFRP laminates. Each span of 3830 mm was loaded at its midpoint (refer to Figure 5.8).

The load-deflection curves for all five beams are plotted in Figure 5.9. Prior to cracking, the stiffnesses for beams CB2 to CB4 were similar. Thereafter, beam CB4, which was reinforced with CFRP on both top and bottom surfaces, exhibited the highest stiffness and ultimate load, and beam CB3, whose soffit was strengthened, had the next highest stiffness and failure load. Although the CFRP sheets used for beam CB5 had a higher Young's modulus than the plates for beam CB2, the response of CB5 was less stiff than that of CB2. The researchers suggested that this was due to the lower stiffness of the epoxy adhesive used in CB5.

Failure loads, ultimate load and ultimate moment enhancement ratios for the CB beams are summarized in Table 5.6. Ultimate load enhancement ratios are the ratios of the strengthened beams' failure loads to that of the control beam. The ultimate moment enhancement ratios were calculated as the ultimate moment of the strengthened sections (sagging or hogging sections) divided by that of unstrengthened sections. Strengthening both top and bottom surfaces with CFRP laminates gave the best performance, while bonding CFRP to the soffit (beam CB3) was more effective than bonding over the top of the central support (beams CB2 and CB5). All of the strengthened beams saw an increase of about 50% in their moment capacities.

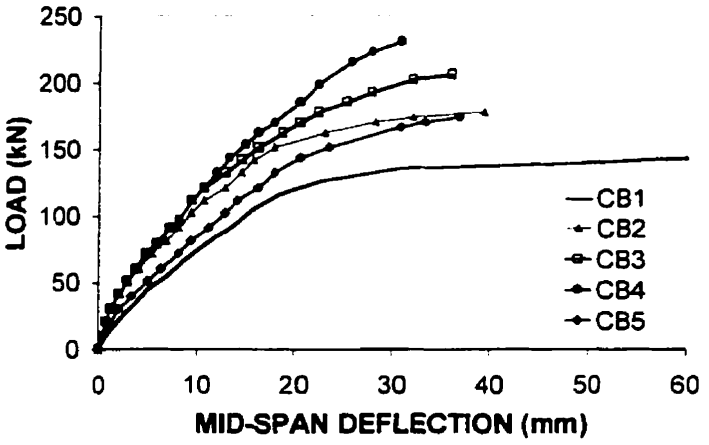

Figure 5.9: Experimental load-deflection curves for El-Refaie specimens [adapted from 80]

Table 5.6: Load and Moment Enhancement Ratios for El-Refaie Specimens [80]

Beam	Ultimate Load (kN)	Ultimate Load Enhancement Ratio	Ultimate Moment Enhancement Ratio	
			Sagging	Hogging
CB1	149.7	1.00	1.00	1.00
CB2	178.6	1.19	1.00	1.52
CB3	207.1	1.38	1.57	1.05
CB4	231.4	1.55	1.57	1.51
CB5	174.6	1.17	0.99	1.48

The control beam CB1 experienced a ductile failure, in which the tension steel yielded, accompanied by concrete crushing over the central support and at mid-span locations. The strengthened beams all failed by peeling of the concrete cover adjacent to the CFRP laminates. Failure was brittle and occurred suddenly with an explosively loud noise.

5.2.2.2 NUMERICAL MODELLING

5.2.2.2.1 *Finite Element Mesh and Special Considerations in Analysis*

The symmetry and identical geometry of the beams allowed one mesh to be defined for one span of all five beams. The mesh consisted of 1200 rectangular concrete elements with smeared shear reinforcement, while 240 truss elements modelled the flexural steel. The concrete elements adjacent to the loading plates were strengthened to prevent crushing failure at these locations. To facilitate the numbering of nodes, the extreme top and bottom rows were double-noded, enabling the connection of CFRP truss elements to the top or bottom surfaces as needed. When CFRP laminates were present, 35 truss elements represented those on the top surface and 100 truss elements were used for the CFRP bonded to the soffit. Nodes that were not joined to CFRP elements were connected by fictitious steel truss elements with minimal area and strength. All external truss elements were attached to the concrete using either 240 contact or 242 link elements. The finite element mesh defined for the beams is shown in Figure 5.10.

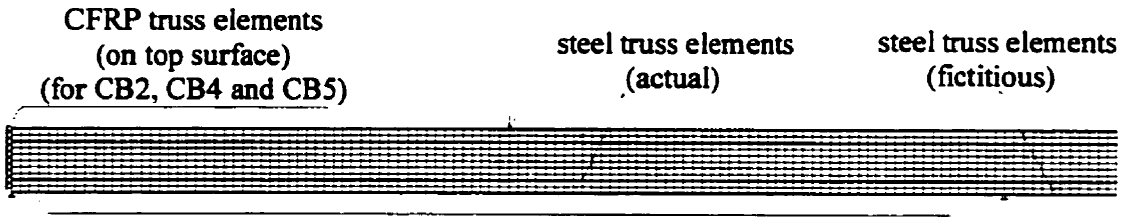

Figure 5.10: Finite element mesh for El-Refaie specimens

In modelling the concrete-CFRP bond interface, it was important to note that the mode of failure in the experiments was dominated by peeling of the concrete cover. Since this type of failure arises from shearing along a horizontal plane, the modulus of rupture was defined as the tensile strength for the concrete cover. This value is higher than $f'_t = 0.33\times(f'_c)^{0.5}$ which is usually used as the tensile strength for diagonal tension due to shear. Also, the modulus of rupture for the concrete was chosen as the maximum bond strength of the bond elements. This can be justified by fact that the higher tensile strength of the epoxy kept the CFRP composites intact with the concrete, while the lower modulus of rupture led to the failure of the concrete cover. To determine S_{max} for the bond elements, the slip modulus was calculated for each beam using Eqn. 5-1 (values of $\nu_a = 0.35$ and $t_a = 2$ mm were assumed). Table 5.7 lists the defining values of the elastic-plastic bond stress-slip relationship for the four strengthened beams. The value for the ultimate slip had to be assumed since no information was provided regarding bond tests for the CFRP composites. Trials using a linear elastic constitutive bond relationship in which S_{ult} was equal to S_{max} (keeping the lower of the two values) were also conducted.

Table 5.7: Bond Stress-Slip Values for El-Refaie Specimens

Beam	U_{max} (MPa)	S_{max} (mm)	S_{ult} (mm)
CB2	4.6	0.0025	0.10
CB3	4.4	0.0024	0.10
CB4	4.4	0.0024	0.10
CB5	4.8	0.005	0.10

Since the CFRP laminates were applied prior to loading, all elements were activated from the first load stage. Details of the loading method were not reported in the original paper; hence, displacement-controlled loading was assumed in the analyses.

5.2.2.2.2 *Analysis Results and Discussion*

The load-displacement curves from the analyses of all five beams are shown in Figure 5.11. The stiffness of the response, the ultimate loads and the mid-span deflections at maximum load were in good agreement with the experimental data. Only the stiffness for beam CB5 was slightly overestimated by the analysis. As can be seen from Figure 5.11, using contact or link elements to represent the bond interface produced almost identical results. Table 5.8 compares the peak loads and corresponding mid-span deflections recorded during the experiments and those obtained from the analyses (for elastic-plastic bond law and contact elements only). Overall, the analyses using the elastic-plastic bond law conservatively underestimated the maximum loads by up to 7% and the mid-span displacements by up to 19%. For beam CB1, the mode of failure was by yielding of the tension reinforcement, along with crushing of the concrete near the central support and the point of loading application, as was observed in the experiment. For beams CB2 to CB5, which were strengthened with CFRP laminates, the dominant failure mode in the analyses was by shearing of the concrete cover adjacent to the CFRP. This led to the delamination of the composites as the bond interface failed in shear. The predicted failure mode was in good agreement with the experimental results.

In the case of the elastic-plastic bond law, the slips at peak load were still in the elastic range, or just into the plastic range, for beams CB2 and CB5. The minimal slips can be ascribed to the smaller displacements experienced on the top surface of these beams, where the CFRP laminates were located. On the other hand, for beams CB3 and CB4, whose soffits were bonded with CFRP, the larger flexural deflections led to slips that were well into the plastic range. The bond-slip values calculated for these beams at maximum load were at least 16 times higher than the slip at peak load for beam CB2.

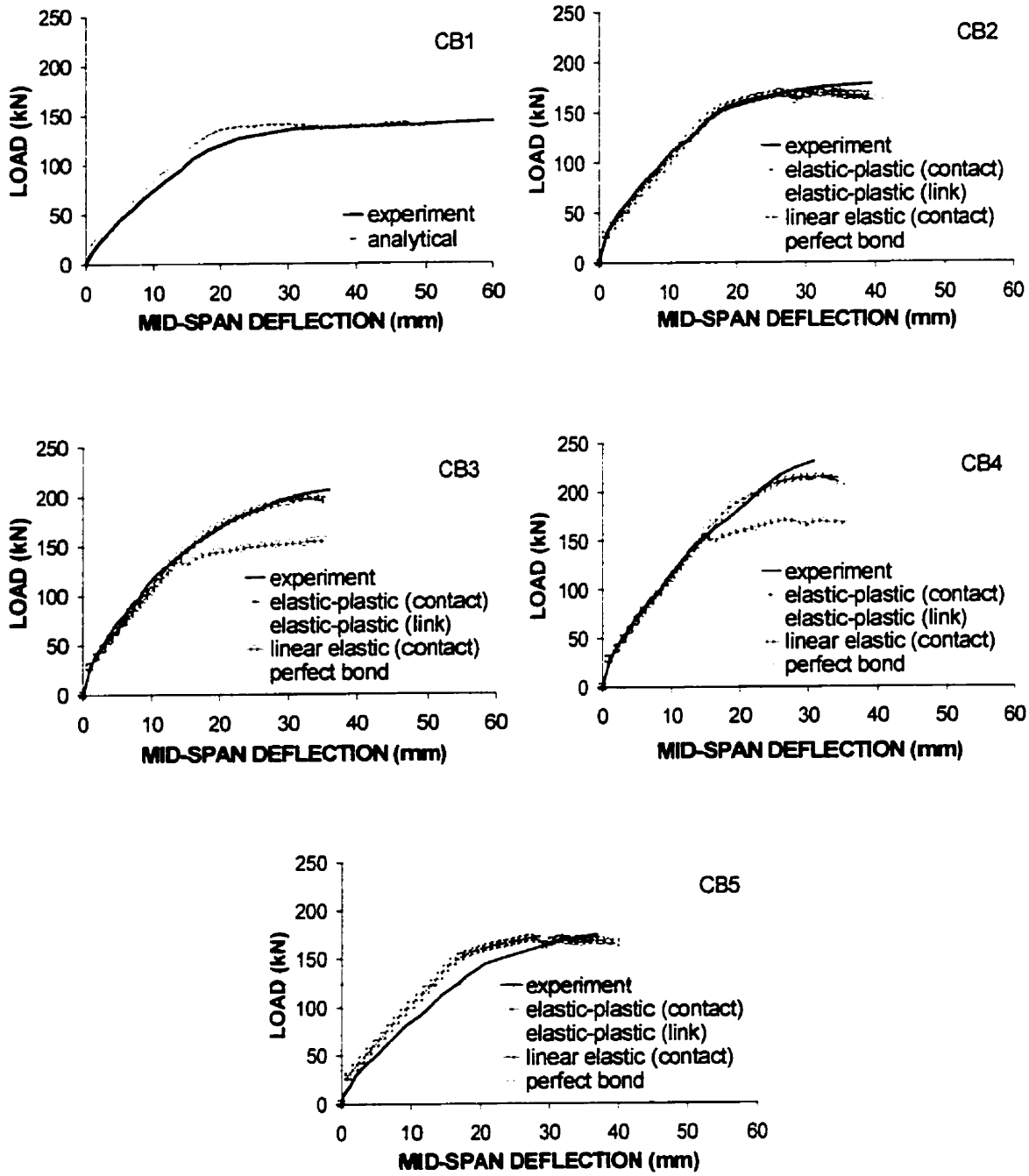

Figure 5.11: Load-displacement curves from numerical analyses of El-Refaie specimens

When the linear elastic bond law was applied, the response for beams CB2 and CB5 was almost identical to the elastic-plastic bond law case. At peak load, the highest bond-slip values were still within the elastic range, so none of the bond elements had reached their capacities yet. Thus, the failure loads were not affected. However, for beams CB3 and CB4, setting the ultimate slip value equal to the maximum slip value led to an underestimation of the failure loads by 20%. Early on in the analyses, the highest bond-slips had already surpassed the ultimate slip values specified for the bond elements. Since the linear elastic bond relationship was used, the load-transferring ability of bond elements with such high values of slip became negligible, hence reducing the load-carrying capacity of the beams.

Table 5.8: Comparison of Results from Experiments and Analyses of El-Refaie specimens

Beam	Peak Load (kN)			Mid-span Deflection at Peak Load (mm)		
	Experimental	Analysis*	% Difference	Experimental	Analysis*	% Difference
CB1	149.7	142	5.14	> 60	47.3	21.2
CB2	178.6	172	-3.72	39.4	32.2	-18.5
CB3	207.1	197.4	-4.67	36.0	32.5	-9.81
CB4	231.4	214.2	-7.44	30.9	31.7	269
CB5	174.6	171	-2.05	36.9	32.3	-12.5
Average			**-2.6**			**-3.4**

*analyses results using contact elements and elastic-plastic bond law

In the analyses, the maximum FRP strain at peak load was only 30% of the material's ultimate strain. Again, this shows that failure of the concrete cover leading to delamination under-utilizes the CFRP laminates. As for the bond stress distribution, in the beams with CFRP bonded on the top surface, the bond stress tended to be higher towards the center and the free end of the plate. For beams CB2 and CB5, the bond stress distributions predicted by the contact and link elements were in good agreement. Although the peak stresses in the link elements were slightly lower than those in the contact elements, the locations of the peaks were generally in the same region for both types of bond elements. The bond stress distribution for CB4 at 167 kN (near the peak load of beams CB2 and CB5) was plotted for comparison. As expected, the bond stress experienced by beam CB4 was lower than that in

beams CB2 and CB5, since the CFRP laminate on the soffit of CB4 alleviated some of the stress transferred to the top plate. In the beams with CFRP bonded to the bottom surface, bond stress peaked at the plate end near the central support, and also in the region to the left of the loading point. The estimates from contact and link elements were almost identical. Even though beam CB3 did not have CFRP laminates bonded on the top surface, the bond stress distribution along the bottom plate for beams CB3 and CB4 at peak load were very similar. This corresponds with the similarity in the average strains in the FRP plates on the soffit of these two beams. The bond stress distributions (in contact elements) for the El-Refaie specimens at peak load are plotted in Figure 5.12.

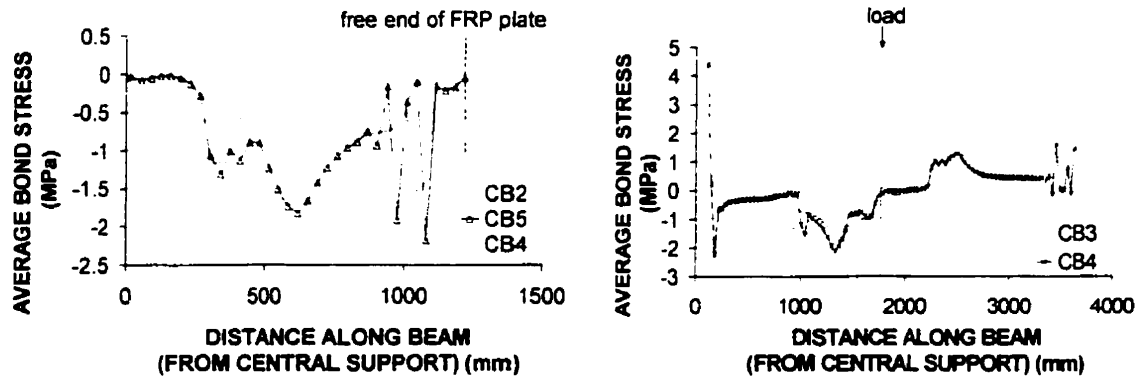

(a) (b)

Figure 5.12: Bond-stress distribution for El-Refaie specimens:
(a) FRP on top surface (near 170 kN), (b) FRP on bottom surface (near 200 kN)

5.2.3 *DE ROSE SLAB SPECIMENS*

The third set of specimens modelled numerically was the De Rose slab series tested at the University of Toronto [81]. The specimens were constructed to simulate a wall panel in a reinforced concrete parking structure. The condition survey indicated signs of distress, mostly exemplified by cracks, rendering the structure to be in need of repair. The objective of

the experimental study was to evaluate the effectiveness of repairing and strengthening the wall (hereafter referred to as the slab) with FRP.

5.2.3.1 EXPERIMENTAL DETAILS

Three slab specimens were fabricated and tested: one as a control specimen, one repaired with CFRP, and another repaired with GFRP. Figure 5.13 shows the slab dimensions and the details of the reinforcement. Along the span of the specimens, four 10M bars were used as tensile reinforcement, while three 10M bars were used as compression reinforcement. In the transverse direction, five 10M bars were employed as top and bottom bars. The properties of the materials are listed in Table 5.9. Figure 5.14 illustrates the loading and support conditions. The control specimen was tested as built to failure, while the other two specimens were preloaded and then repaired with the composite materials before loading to complete failure.

The carbon fabric used (SCH41) had fibres oriented in the longitudinal direction only. The glass fabric (SEH51) had glass fibres in the longitudinal direction and aramid fibres in the transverse direction. Transverse properties were not determined since there were substantially more glass fibres than aramid fibres. The type of epoxy adhesive used was TYFO S®, in accordance with the TYFO S® Fibrwrap® system.

The control specimen failed in flexure at a total load of approximately 193 kN. The specimen that was to be repaired with CFRP was loaded to 135 kN, at which time three strips of CFRP fabric, each 600 mm in width and about 1 mm in thickness, were applied to the slab as shown in Figure 5.15. The two outer strips were folded up and bonded to the sides of the specimen, providing some anchorage to the fabric on the soffit. Epoxy thickness was not controlled but excess epoxy was squeezed out.

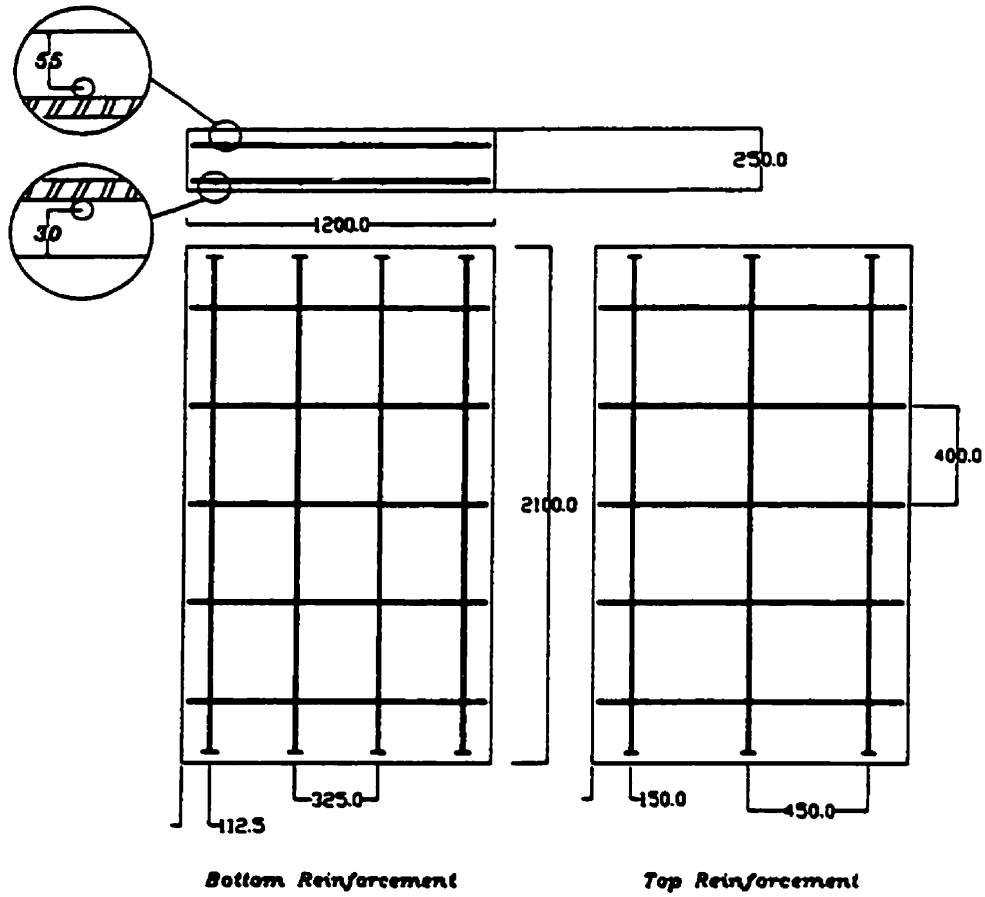

Figure 5.13: De Rose slab dimensions and reinforcement details [81]

Table 5.9: Material Properties for De Rose Slab Specimens [81]

Material	**f'_c (MPa)**	**f'_t (MPa)**	**E (GPa)**	**ν**
Concrete	53.9	2.42	40.4	0.15
Material	**f_y (MPa)**	**f_u (MPa)**	**E (GPa)**	**ε_{ult}**
Steel (10M)	458	692	200	0.168
Material	**Q (Force/unit width) (N/mm/layer)**	**E (GPa)**	**ε_{ult}**	**ν**
CFRP	850 – 956 (945*)	80.3	0.01422	-
GFRP	490 – 568 (518*)	27.2	0.01974	-
Kevlar 49 †	2758 MPa	117	0.025	-

* values used in analyses (average values from FRP coupon tests by De Rose)

† values obtained from [78]

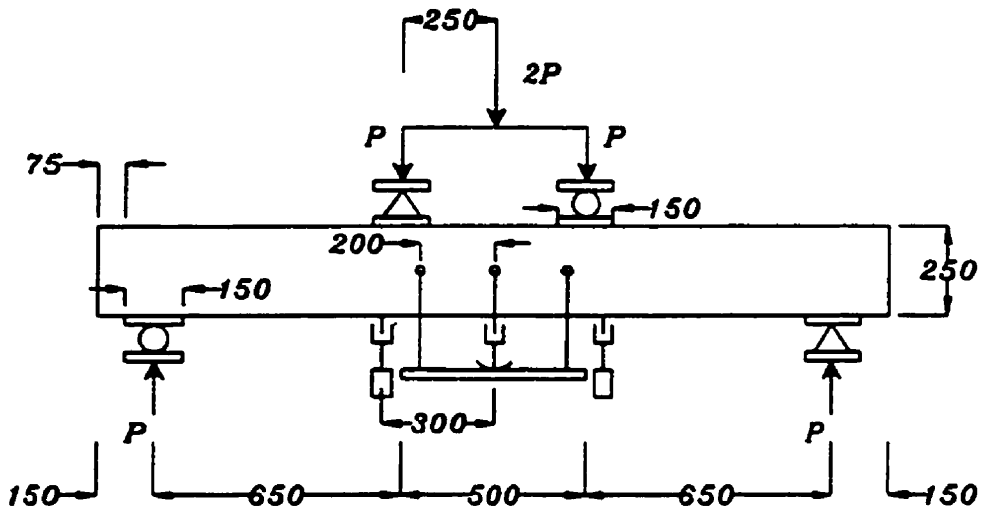

Figure 5.14: Loading and support conditions for De Rose slab [81]

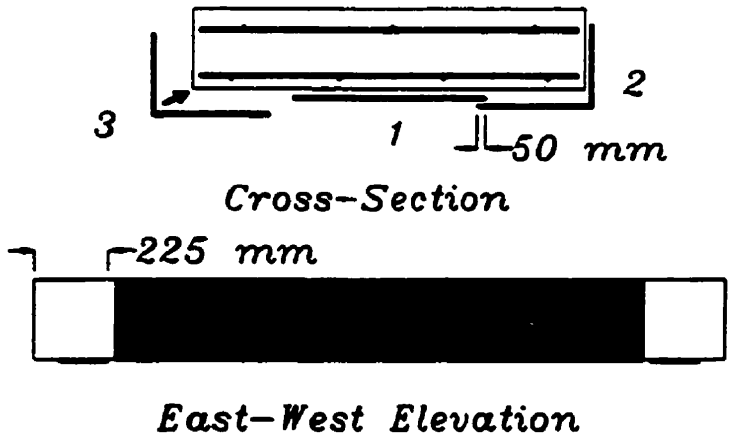

Figure 5.15: Application of FRP fabric to De Rose slab [81]

After curing for three days, loading on the slab continued until the specimen failed in shear at a total load of 478 kN, accompanied by large inclined cracks and delamination of CFRP. The third specimen was repaired and tested in a similar manner, except that GFRP was used. This slab also failed in shear, but at a lower load of 422 kN. Although the ultimate capacity of the slab was increased by 148% and 119% by the CFRP and GFRP, respectively, the full potential of the FRP fabric was not realized. The failure of the repaired slabs was

governed by their shear capacities, even though flexural strength was enhanced. There was no occurrence of premature FRP bond failure or peeling of FRP from the concrete surface. The load-deflection curves of all three specimens are shown in Figure 5.16. Immediately after the application of the FRP fabric, the stiffness of the slabs was restored to a value similar to the pre-cracking stiffness.

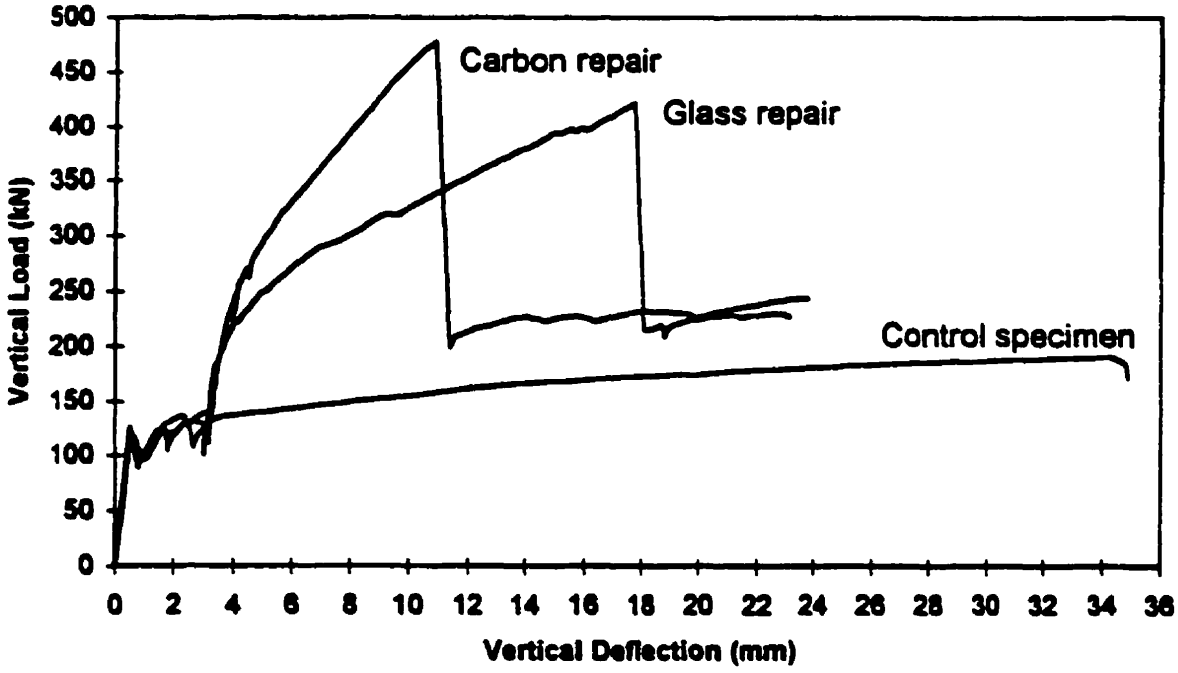

Figure 5.16: Experimental load-deflection curves for De Rose slab specimens [81]

5.2.3.2 NUMERICAL MODELLING

5.2.3.2.1 *Finite Element Mesh and Special Considerations in Analysis*

The symmetrical geometric and loading conditions of the De Rose slab permitted modelling of only one-half of the specimen. The finite element mesh used for the analysis is illustrated in Figure 5.17. Concrete was modelled with 474 rectangular elements, with 378 elements representing the original slab and 96 elements for the new concrete after repair. 84

truss elements were used to model steel reinforcement, while 320 horizontal and 297 vertical truss elements represented the FRP material. Although the FRP fabric is predominately unidirectional with a warp (0° orientation) of graphite or glass fibres, it is weaved with a weft (90° orientation) of Kevlar 49 twisted with a minimal amount of thermoplastic yarn or of aramid fibres. The Kevlar 49 or aramid fibres can provide a small amount of strength and stiffness for the sides of the slab where they are oriented perpendicularly to the longitudinal axis. As for the bond interface, 617 contact elements were used. From the two previous sets of analyses, it was noted that the overall member response predicted by contact and link elements was almost identical. Thus, contact elements were primarily used in the remaining analyses to model the concrete-FRP bond interface.

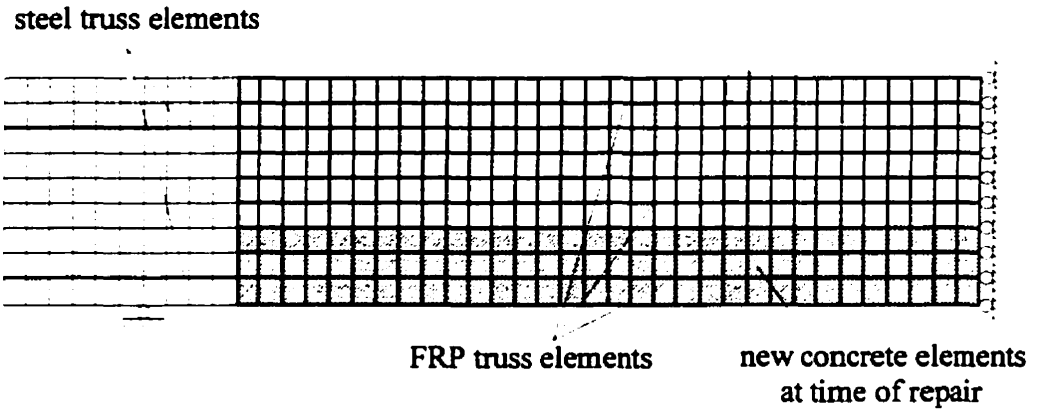

Figure 5.17: Finite element mesh for the De Rose slab specimen

Due to the current formulation of the link and contact elements, a horizontal and a vertical truss bar cannot be connected to the same corner node. Therefore, wherever these truss element connections occur in the finite element mesh, three nodes must be defined at the same location: one for the concrete element (and steel truss element if present), one for the horizontal FRP truss element, and the third for the vertical FRP truss element. Horizontal and vertical FRP truss elements were connected to the concrete elements through separate bond elements, as shown schematically in Figure 5.18.

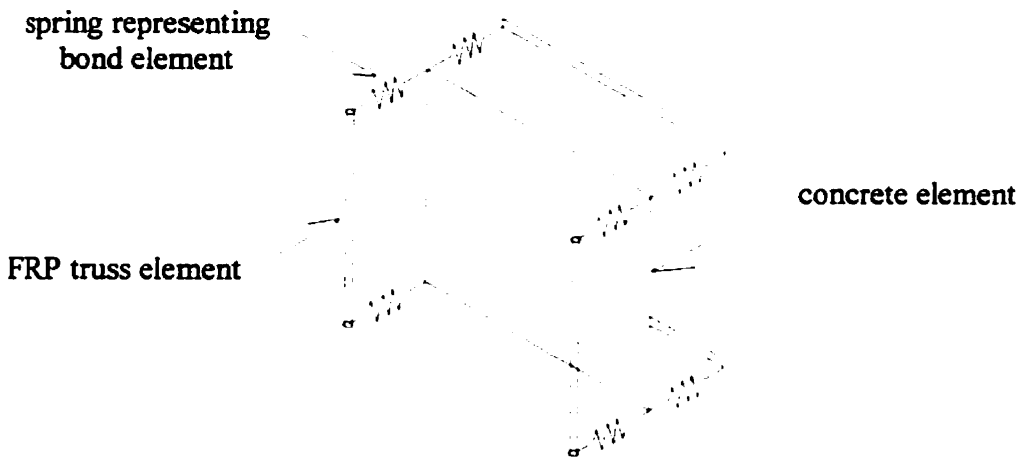

Figure 5.18: Schematic diagram of the connection between concrete and FRP truss elements

One set of analyses was carried out for the CFRP-repaired slab, while another set was performed for the slab strengthened with GFRP. For the bond stress-slip relationships, the maximum bond stress values were specified by the modulus of rupture of the concrete, and the corresponding maximum slips were calculated using the slip modulus E_b as defined in Eqn. 5.1. The properties of the epoxy were not measured in the experiment, but the elastic modulus of the epoxy was given as 3.16 GPa by the manufacturer. The Poisson's ratio and thickness of the epoxy were assumed to be 0.35 and 2 mm, respectively. Hence, the shear modulus of the epoxy was determined to be 1.17 GPa. The values for the ultimate slip were based on the experimental results of Homam [62], who used the same type of epoxy and FRP fabric in double-face shear tests. Table 5.10 lists the values used to define the bond stress-slip relationships for the two analyses. For comparison purposes, trials using the linear elastic bond law, in which the ultimate slip was reduced to the maximum slip value, were also conducted. Another difference between the two sets of analyses was the properties given to the horizontal FRP truss elements (representing the CFRP or GFRP fibres), as obtained from the coupon tests conducted by De Rose (refer to Table 5.9). For the vertical FRP truss elements modelling the Kevlar 49 or aramid fibres, values for the material properties were the same as those employed in Bucci's analyses (approximately equal to 5% of the values given by the manufacturer for homogeneous fibres tested in tension) [8].

Table 5.10: Elastic-Plastic Bond Law Values for De Rose Slab Analyses

Material	U_{max} (MPa)	S_{max} (mm)	S_{ult} (mm)
CFRP	4.4	0.0075	0.50
GFRP	4.4	0.0075	0.67

Since the slabs were preloaded to a specific load stage prior to the application of the FRP fabric, a two-stage analysis in which element strain histories are considered was required. In the first part of the analysis, only the concrete and steel elements in the original structure (as in the control specimen) were activated. Analysis was carried out to the load stage corresponding to the load at which the slab was repaired. Then the elements representing the repair materials (new concrete, bond and FRP elements) were activated, and the analysis was continued using the last load stage in the first portion of the analysis as the seed file. In the experiment, none of the concrete was actually repaired. However, at the time of FRP application, cracks had progressed one-third of the way up in the slab. It is presumed that the epoxy from the repair procedure would have penetrated and filled the cracks, thus stiffening the member. Therefore, in the FRP-repaired area of the slab, three bottom rows of new concrete elements were added. These new uncracked elements (starting in a stress-free condition) provided full tensile strength as found in the original slab, while their contribution to compressive strength was negligible.

Due to the thin nature of slabs, they are more prone to drying shrinkage, thus a shrinkage strain of -0.4×10^{-3} was applied to all the original concrete elements. Displacement-controlled monotonic loading was applied in order to match the experimental conditions. Since the slab specimens did not contain any shear reinforcement, the tension softening option of "linear with residual" was employed. The 10% residual tensile strength simulates the friction that exists along the fractured concrete surface. This option prevents the concrete tensile strength from dropping to zero, which usually leads to predictions of premature shear failures in long, flat beams. The crack width check and slip distortion options were de-activated to avoid premature shear failures.

5.2.3.2.2 *Analysis Results and Discussion*

The load-deflection curves for the CFRP-repaired slab are given in Figure 5.19, along with the original experimental results. The ultimate load calculated by the analysis (using the elastic-plastic bond law) was 436 kN, while the actual failure load was 478 kN. The mid-span deflection at peak load was overestimated by 8%. Although the stiffness of the member immediately after repair was underestimated by the analysis, the post-cracking stiffness and maximum load achieved were in close agreement with the experimental results.

As observed in the experiment, the numerical modelling predicted a shear failure for the CFRP-repaired slab. This was also exemplified by the similarity between the analysis with the perfect bond condition and the trial including bond-slip (using the elastic-plastic bond law). Since the failure of the slab was dominated by shear, the effect of the bond-slip behaviour at the interface did not affect the overall response of the slab. However, when the linear elastic bond relationship was applied, a premature debonding failure in which both the maximum load and the corresponding mid-span deflection were underestimated by 18% was predicted.

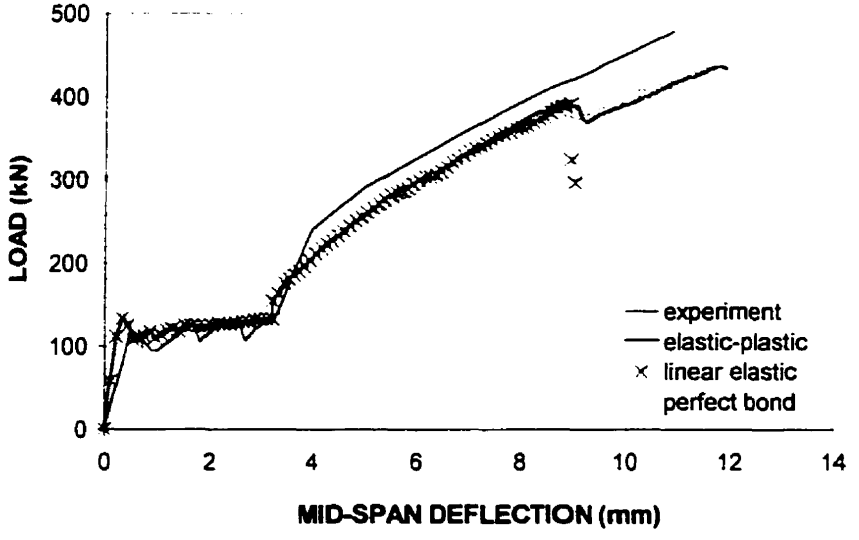

Figure 5.19: Predicted load-deflection curves for CFRP-repaired De Rose slab

The predicted average FRP strains and bond stresses for the CFRP-repaired slab is shown in Figure 5.20. [In the plots of FRP strain, bond stress or bond-slip presented in the remainder of this chapter, each curve represents the relative position of the elements in the member, as well as the parameter labelled on the axes. To illustrate the location of the elements, each curve is offset by the amount specified on the axes, while the magnitude of deviation from a horizontal line (for FRP oriented horizontally) or a vertical line (for FRP oriented vertically) indicates the value of the parameter.] As expected, the FRP strains are highest on the soffit of the slab (denoted by the bottommost curve) and near the mid-span. As for the bond stress distribution, the fluctuations in the central section of the slab are likely due to flexural cracking.

Figure 5.21 presents the response of the GFRP-repaired slab with the curve obtained from the test. Similar to the slab with CFRP, the program underestimated the failure load of the member. The slab was expected to fail at 395 kN (when the elastic-plastic bond law was utilized), whereas in the experiment, the ultimate load reached was 422 kN. Using the linear elastic bond relationship, the ultimate load was 15% lower than the test value, but the corresponding mid-span deflections were almost identical. Soon after repair, the predicted member stiffness was lower than expected, but the post-cracking stiffness increased to match that of the experimental response. Again, shear dominated the failure mode of this slab, so the results for the perfect bond condition were similar to those for the elastic-plastic bond law. The experimental and predicted global results are summarized in Table 5.11.

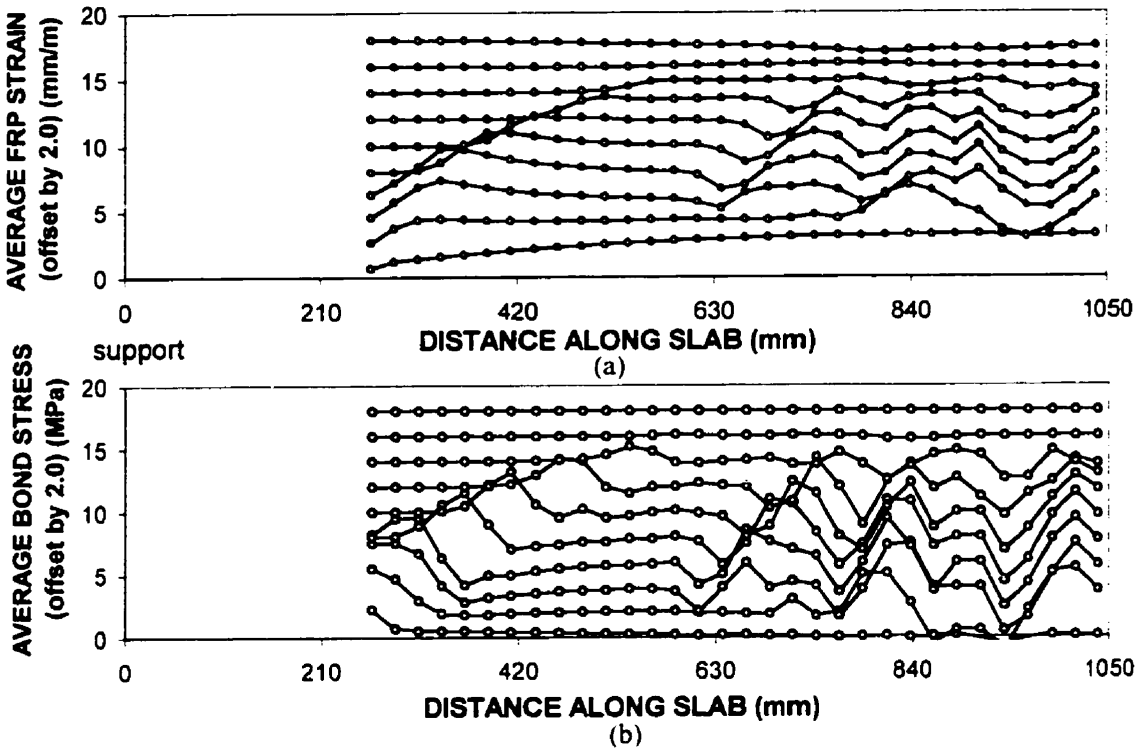

Figure 5.20: Predicted FRP strains and bond stresses for CFRP-repaired De Rose slab

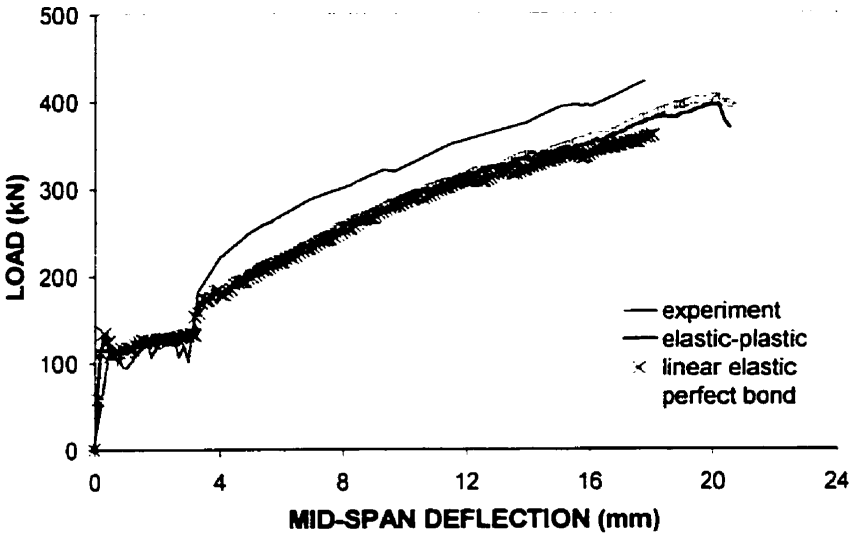

Figure 5.21: Predicted load-deflection curves for GFRP-repaired De Rose slab

Table 5.11: Experimental and Predicted Results for De Rose Slab Specimens

Type of FRP Used	Constitutive Relationship	Maximum Load (kN)	Deviation from Exp. Load (%)	Mid-span Deflection at Maximum Load (mm)	Deviation from Exp. Deflection (%)
CFRP	Experiment	478	0	10.9	0
	Elastic-plastic	436	-8.8	11.8	8.3
	Linear elastic	391	-18.2	8.92	-18.2
	Perfect bond	438	-8.4	11.6	6.4
GFRP	Experiment	422	0	17.8	0
	Elastic-plastic	395	-6.4	20.0	12.4
	Linear elastic	360	-14.7	18.0	1.1
	Perfect bond	403	-4.5	20.0	12.4

The FRP strains and bond stress distribution predicted for the GFRP-repaired slab are plotted in Figure 5.22. The general trends observed are similar to those for the CFRP-repaired slab. However, the magnitude of the FRP strains, especially those on the soffit of the slab (represented by the bottommost curve), are higher for the GFRP elements. This can be explained by the lower elastic modulus of GFRP as compared to CFRP (almost three times lower).

Previously, Bucci had analyzed the De Rose slab specimens with the former version of the FE program TRIX [8]. In those analyses, perfect bond conditions were implied as bond elements had not been incorporated into the program. FRP reinforcement was smeared into rectangular elements with minimal concrete strengths and stiffness. These FRP elements were connected directly to the actual concrete elements. Since bond-slip was not included in the numerical model, the failure loads were overestimated by 15 to 30% for these specimens, as shown in Figure 5.23. As well, compared to the present research, the post-repair stiffnesses of the beams predicted in Bucci's analyses were higher. The differences between Bucci's results and the perfect bond condition assumed in the current analyses can be attributed to the different method used in modelling the FRP composites (continuously distributed throughout rectangular elements as opposed to discrete truss elements) and to the modifications in the finite element program from its previous version (TRIX) to the current version (VecTor2).

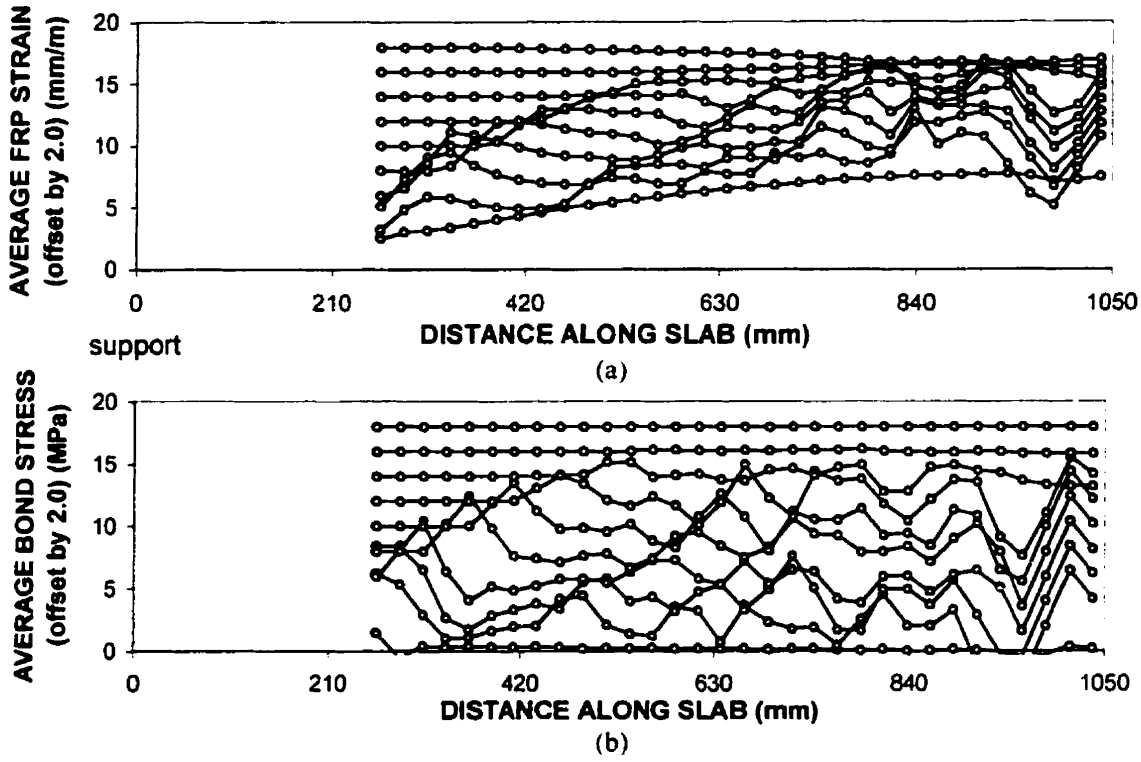

Figure 5.22: Predicted FRP strains and bond stresses for GFRP-repaired De Rose slab

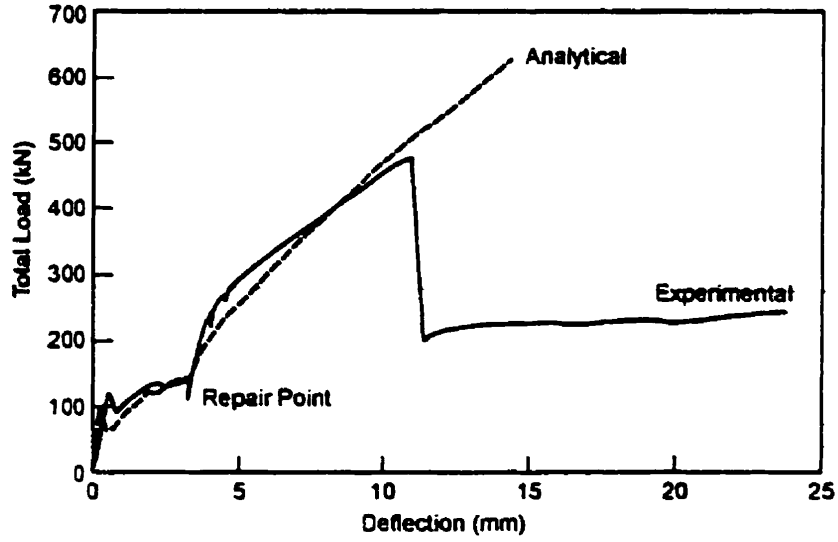

(a)

Figure 5.23: Analytical results for De Rose slab specimens (not accounting for bond-slip): (a) CFRP-repaired [8]

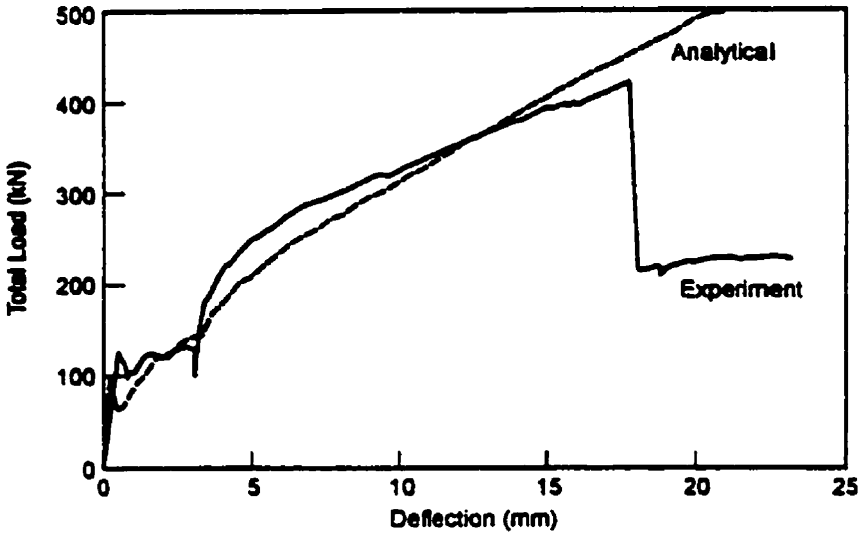

(b)

Figure 5.23 (continued): Analytical results for De Rose slab specimens (not accounting for bond-slip): (b) GFRP-repaired [8]

5.3 SPECIMENS STRENGTHENED IN SHEAR WITH FRP COMPOSITES

Besides the modelling of RC members strengthened in flexure with FRP composites, the program VecTor2 was also corroborated with the test results of two sets of RC beams externally bonded with FRP laminates as shear reinforcement.

5.3.1 *DE ROSE BEAM SPECIMEN*

The first FRP-shear-reinforced specimen analyzed with program VecTor2 was the De Rose beam. The specimen was designed to simulate a beam in the same reinforced concrete parking structure as the De Rose slabs and was also tested at the University of Toronto [81]. The objective of the experiment was to evaluate the effectiveness of repairing and shear strengthening the beam with CFRP.

5.3.1.1 EXPERIMENTAL DETAILS

The specimen represented a beam found in the parking structure that was framed into a wall. Thus, a haunched region was constructed on one half of the specimen to simulate this condition. Also, in this half of the beam, extra transverse reinforcement was added to promote the formation of shear cracks in the other half, as observed in the condition survey. Two beams were built: one was tested as a control specimen, while the second beam was strengthened with CFRP fabric. The specimen details are shown in Figure 5.24. The flexural reinforcement consisted of six 30M bars on the bottom and five 25M bars on the top. Shear reinforcement was provided by deformed U.S. No. 3 bars. The amount of shear reinforcement in Section B-B was less than that required by A23.3-94 [82]. The properties of the materials are given in Table 5.12. Figure 5.25 shows the loading and support locations.

Table 5.12: Material Properties for De Rose Beam Specimens [81]

Material	f'_c (MPa)	f'_t (MPa)	E (GPa)	ν
Concrete (beam)	45.7	2.23	37.2	0.15
Concrete (haunch)	41.2	2.12	35.3	0.15
Material	**f_y (MPa)**	**f_u (MPa)**	**E (GPa)**	**ε_{ult}**
Steel (25M)	490	688	200	0.147
Steel (30M)	492	650	200	0.150
Steel (No. 3)	507	778	200	0.121
Material	**Q (Force/unit width) (N/mm/layer)**	**E (GPa)**	**ε_{ult}**	**ν**
CFRP	850 – 956 (945*)	80.3	0.01422	-

* value used in analyses (average of FRP coupon tests by De Rose)

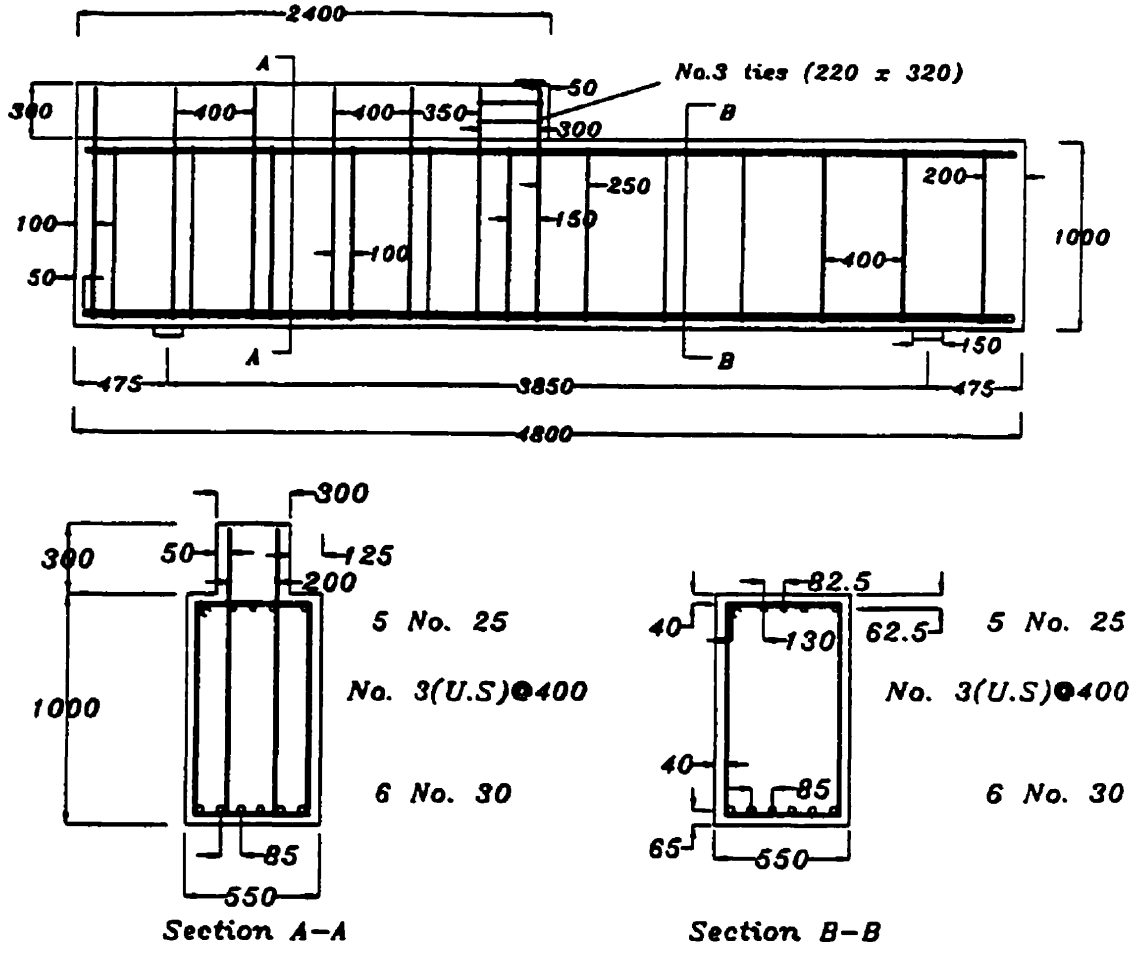

All dimensions in mm

Figure 5.24: De Rose beam details [81]

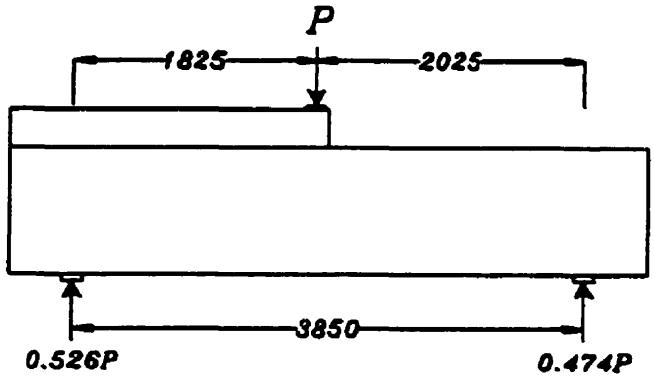

Figure 5.25: Loading and support locations for De Rose beam [81]

The control specimen failed suddenly in shear at a load of approximately 1700 kN. Similar to the slab specimens, the beam to be repaired with CFRP was preloaded prior to application of the FRP fabric. To ensure that the left side of the beam (with the haunched region) would not fail in shear after the repair, a beam-and-bar assembly was attached as a clamp prior to loading. The beam was loaded to 1180 kN, and this load was maintained while the CFRP was applied. Three strips of CFRP fabric (each approximately 610 mm wide) were wrapped around the specimen as indicated in Figure 5.26. A 200 mm overlap was provided on the top of the beam. Epoxy thickness was not controlled but excess epoxy was squeezed out.

Loading resumed after three days of curing, and continued until 1911 kN. At this time, a portion directly under the loading point experienced compression failure. The damaged concrete was removed and replaced with a high-strength mortar surrounded by a steel enclosure attached to the beam using threaded rods. After repairing this area, loading recommenced and reached 2528 kN. At this stage, the carbon fabric failed at a top corner near the load application point, and a substantial amount of concrete suddenly spalled off. Although the edges of the beam were rounded slightly by grinding prior to repair, the rupture of the fabric occurred at the top edge of the beam. The failure of the fabric may have been triggered by the large flexural deformations of the beam.

The load-deflection curves for the control and repaired beam specimens are depicted in Figure 5.27. The CFRP fabric enhanced the ultimate capacity of the beam by 49%. The premature shear failure observed in the control beam was changed to a ductile flexural failure in the repaired beam. This was demonstrated by the mid-span deflections at failure: 14 mm for the control beam as opposed to 143 mm for the repaired beam.

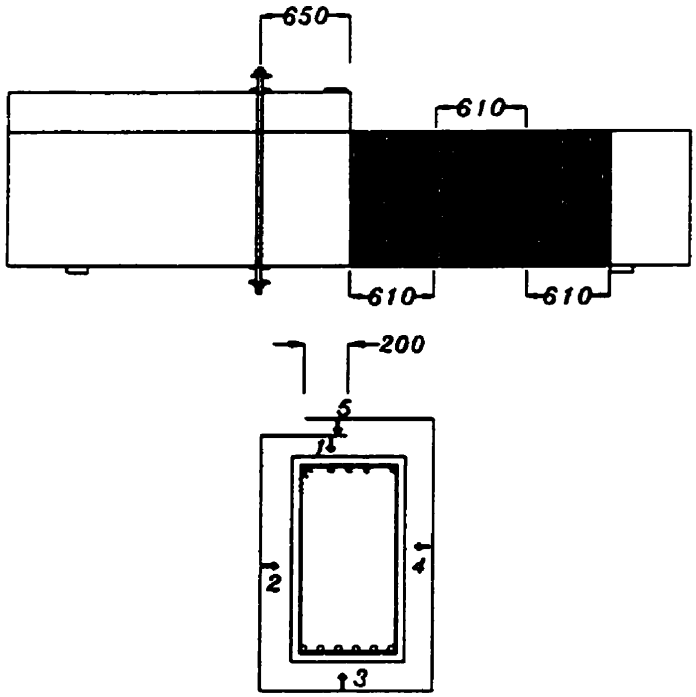

Figure 5.26: Layout for De Rose beam repaired with CFRP [81]

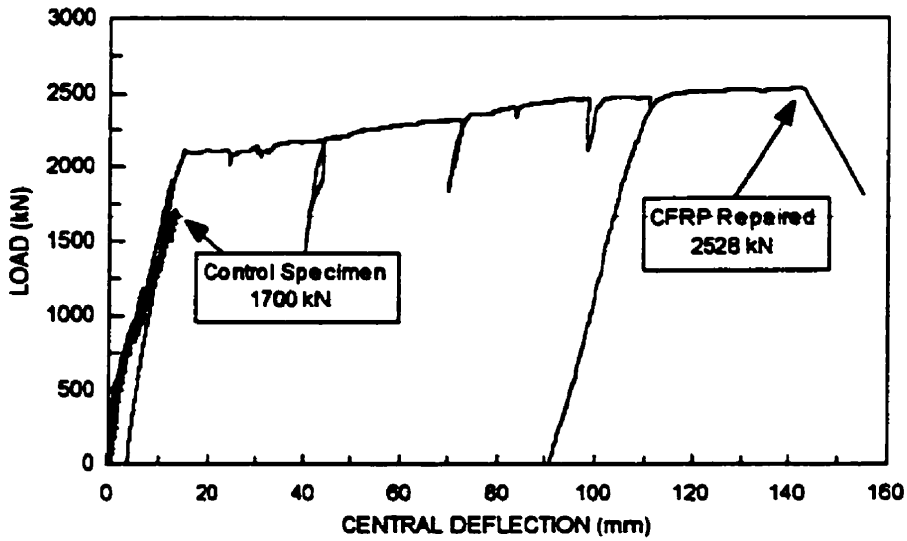

Figure 5.27: Experimental load-deflection behaviour of De Rose beam specimens [81]

5.3.1.2 NUMERICAL MODELLING

5.3.1.2.1 *Finite Element Mesh and Special Considerations in Analysis*

The asymmetrical geometry and loading conditions of the De Rose beam specimen made it necessary to model the entire beam in the finite element analysis. The mesh for the beam analysis is drawn in Figure 5.28. In total, 764 rectangular elements were used, with 675 elements modelling the original beam, 80 elements for new concrete at the time of repair, and 9 elements representing the plates of the steel enclosure. The internal shear reinforcement was smeared among the concrete elements. 630 truss elements were employed, with 100 modelling the flexural reinforcement, 15 for the steel bar used for clamping the haunched region, and three for the side steel enclosure plate. As for the CFRP, 252 truss elements represented the fabric in the vertical direction, while the bond interface was modelled by 252 contact elements. As the CFRP fabric was mainly used for shear reinforcement, the horizontally-oriented Kevlar 49 fibres were not modelled.

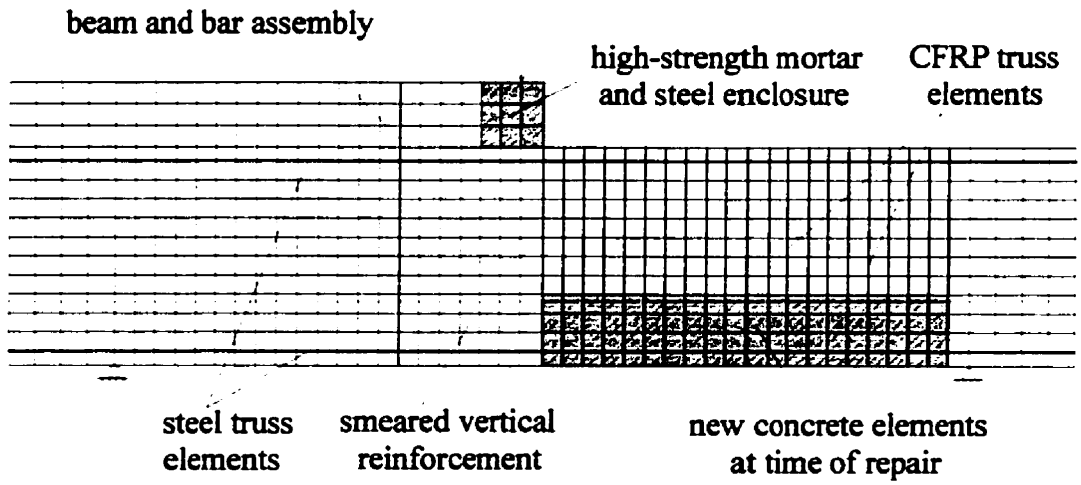

Figure 5.28: Finite element mesh for the De Rose beam specimen

For the De Rose beam, the type of epoxy and CFRP fabric used were the same as those employed in the De Rose slabs. The maximum bond stress (modulus of rupture of the concrete) was 4.1 MPa, while the corresponding slip was 0.007 mm, using the same slip modulus as in the De Rose slab analyses. The ultimate slip was obtained from Homam's report to be 0.50 mm. Again, trials utilizing a linear elastic bond law and perfect bond conditions were also conducted.

As was done for the De Rose slab, the beam analysis was divided into two parts. The first portion consisted of loading the control specimen, with only the original concrete and internal steel reinforcement elements activated. At the load stage corresponding to the time of repair, all remaining elements (representing the new concrete, CFRP, bond and the external steel reinforcement) were activated, after which analysis was continued.

5.3.1.2.2 *Analysis Results and Discussion*

The predicted response of the CFRP-repaired beam is compared to the test data in Figure 5.29.

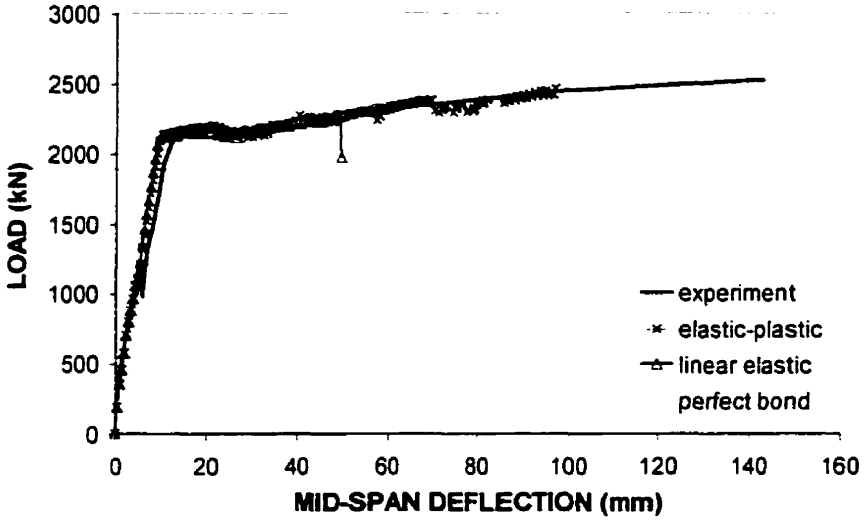

Figure 5.29: Predicted load-deflection response of CFRP-repaired De Rose beam

The estimated mode of failure for the De Rose beam was a shear-flexural failure. Concrete crushing occurred at mid-span near the base of the haunch, with wide cracks fanning out from this point to the quarter point of the beam on the side wrapped with CFRP. Similar results were obtained whether perfect bond conditions, the linear elastic bond law, or the elastic-plastic bond law was applied, although the latter produced the most stable response. The predicted failure took place at a mid-span deflection of 97 mm under a load of 2465 kN. Although the actual failure load of 2528 kN was reached when the beam deflected to 143 mm, the estimated response was in good agreement with the test results in terms of the post-cracking and post-yielding stiffnesses. A previous analysis by Bucci (without the presence of bond elements and bond law, as described before) predicted a maximum load of approximately 2400 kN at 35 mm mid-span deflection, as shown in Figure 5.30.

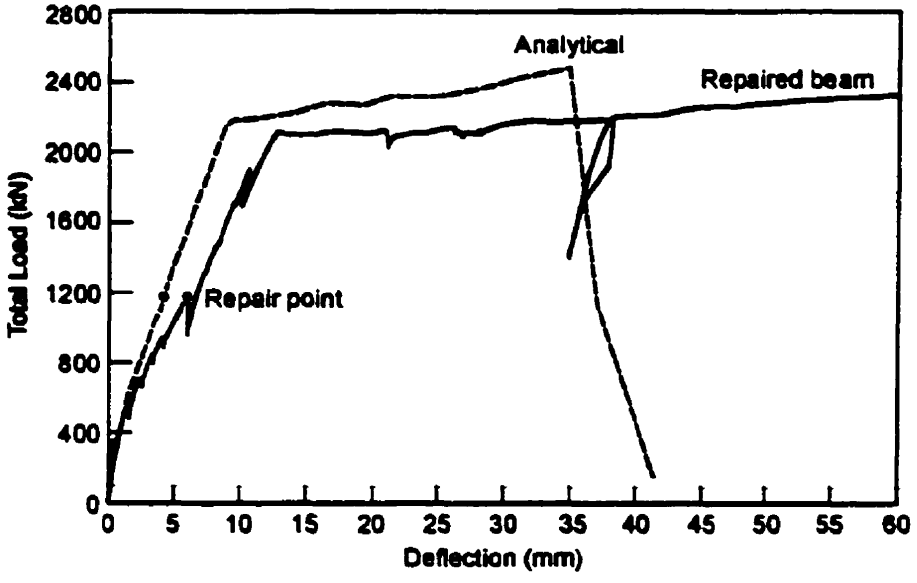

Figure 5.30: Analytical results for De Rose beam specimen (not accounting for bond-slip)[8]

The calculated FRP strains and bond stress distribution for the repaired De Rose beam are depicted in Figure 5.31. The excessive FRP strains are due to the major shear cracks that dictated the failure of the beam. In the CFRP elements near the top of the beam close to mid-span (on the top left side of the graph), the average strains in the CFRP reached values of 0.0085, which is 60% of the ultimate strain of the material. In the experiment, this

is the location where the CFRP fabric ruptured. The lower end of the shear cracks is also marked by high estimates of FRP strains. Similarly, the large fluctuations in the bond stress distribution are also the result of the diagonal shear cracks.

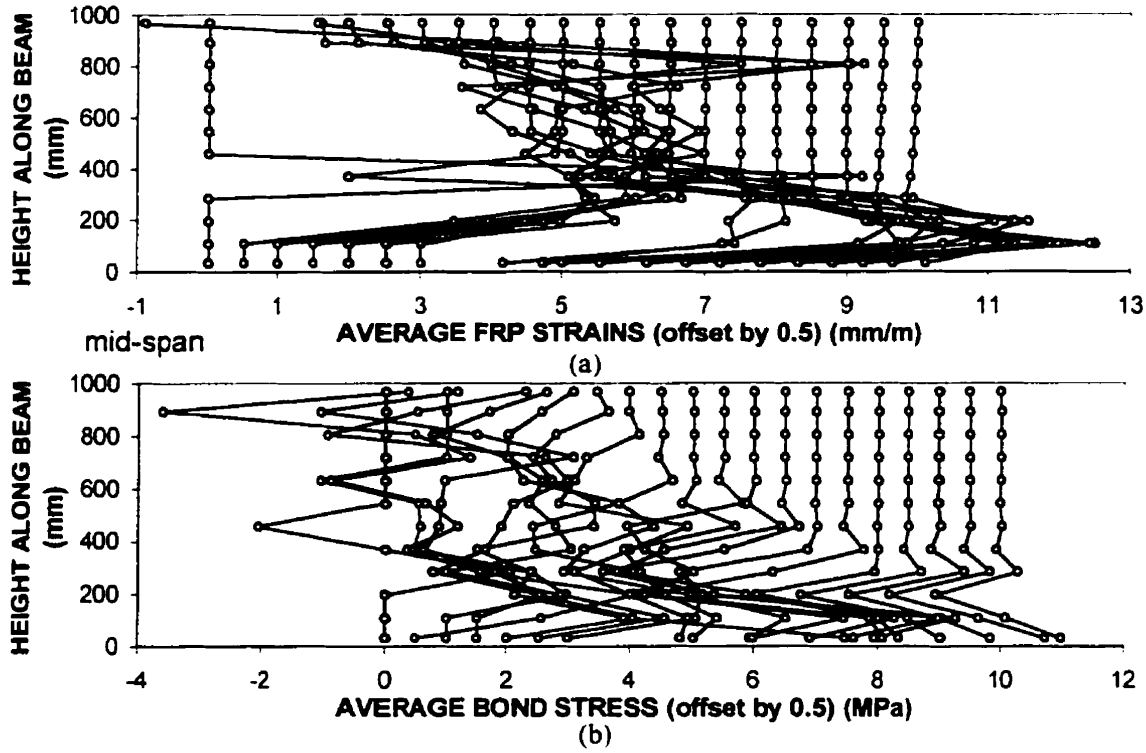

Figure 5.31: Predicted FRP strains and bond stresses for CFRP-repaired De Rose beam

5.3.2 *RWOA BEAM SPECIMENS*

The experimental details for the RWOA beam series, in which CFRP strips were used as shear reinforcement, have been presented in Chapter 4 of this report. In this section, only the numerical modelling of the three beams will be described.

5.3.2.1 FINITE ELEMENT MESH AND SPECIAL CONSIDERATIONS IN ANALYSIS

All three beams were symmetrical, thus only half of the beam was modelled. The CFRP strips were bonded prior to loading of the beams, so only one set of analysis was required starting from zero load. Longitudinal reinforcement was represented by truss elements, and each CFRP strip was divided into five columns of truss elements in the finite element mesh. Similar to the De Rose beam specimen, the Kevlar 49 fibres in the CFRP fabric were not modelled as the strips were loaded primarily in the direction of the carbon fibres. The steel plate at the end of the beam was included in the mesh to provide anchorage for the rebars. However, the loading plate was not modelled since it implied a contribution to the beam stiffness from a fixed plate, while in reality slippage of the plate most likely occured. The finite element mesh for the three beams are given in Figure 5.32.

For the bond stress-slip relationships, the maximum bond stress values were specified by the modulus of rupture of the concrete, and the corresponding maximum slips were calculated using the slip modulus E_b as defined in Eqn 5.1. The elastic modulus of the epoxy was given by the manufacturer as 3.16 GPa, while values of 0.35 and 2 mm were assumed for the Poisson's ratio and thickness of the epoxy, respectively. Thus, the shear modulus of the epoxy was determined to be 1.17 GPa (values measured by Bizindavyi and Neale [59] for the same type of epoxy were: $\nu_a = 0.4$ and $G = 1.18$ GPa). The ultimate slip value was obtained from Homam's bond test as the same type of CFRP fabric was used. The bond law values used for the RWOA beams are summarized in Table 5.13.

Table 5.13: Bond Stress-Slip Values for RWOA Beams

Beam	U_{max} (MPa)	S_{max} (mm)	S_{ult} (mm)
RWOA-1	2.85	0.005	0.50
RWOA-2	3.05	0.005	0.50
RWOA-3	3.50	0.006	0.50

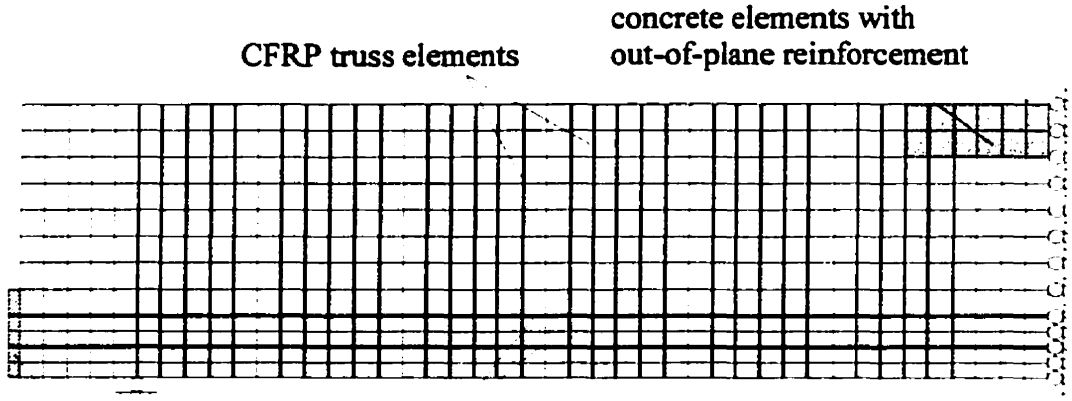

(a)

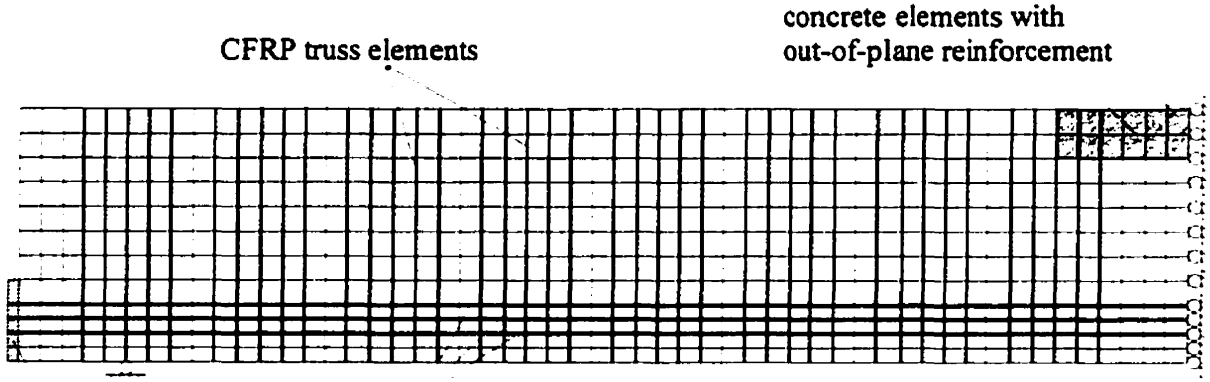

(b)

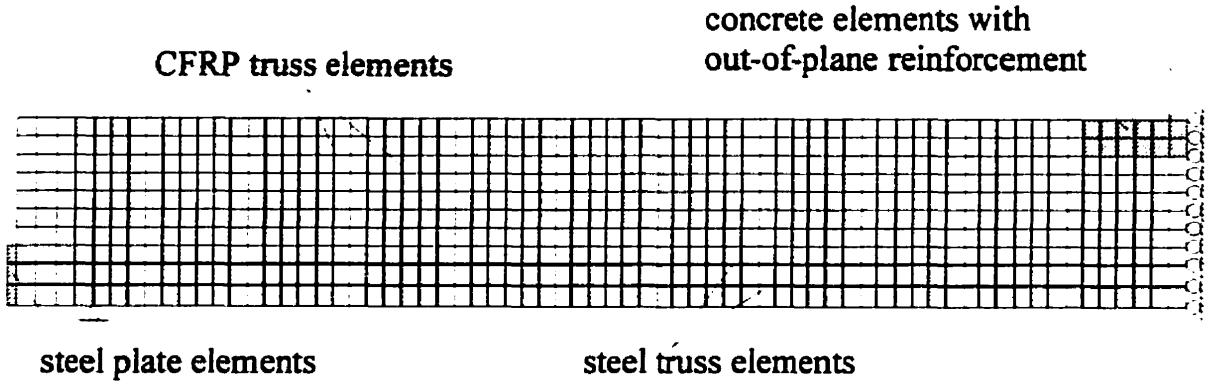

(c)

Figure 5.32: Finite element mesh for beams: (a) RWOA-1, (b) RWOA-2, (c) RWOA-3

Initially, all three beams were predicted to fail abruptly prior to yielding of the longitudinal reinforcement, contradicting the experimental observations of ductile failures. The discrepancy was traced to the crushing of several concrete elements near the loading point. A first attempt to remedy this situation was by strengthening the elements that suffered premature crushing. The compressive strength of those elements were doubled, while the strain at peak stress and the parabolic shape of the concrete stress-strain curve were maintained. However, this only shifted the crushing zone further away from the point load, and did not enhance the ductility of the beam response. A second attempt, which proved to be successful, was by adding out-of-plane reinforcement to the concrete elements near the load (up to three times the width of the loading plate and two layers down). The addition of such reinforcement is based on the confinement effects that the loading plate imparts onto the concrete. These effects simulate triaxial compression, where the crushing strength of concrete is increased and the ductility of the concrete response is augmented. The out-of-plane reinforcement was able to prevent early crushing failure by confining the lateral expansion of the concrete elements due to Poisson's effect. After the addition of the out-of-plane reinforcement, the analyses predicted more ductile behaviour for the beams.

Although this series of beams did not contain any internal shear reinforcement, the CFRP strips acted as external shear reinforcement. Therefore, the linear tension softening model with no residual was used in these analyses. With the predominant crushing failure, it was found that a lower averaging factor of 0.2 gave a more stable response.

5.3.2.2 ANALYSIS RESULTS AND DISCUSSION

The analytical results for the three RWOA beams are summarized in Table 5.14, and will be discussed in the following sections.

Table 5.14: Experimental and Analytical Results for RWOA Beams

Beam	Constitutive Relationship	Maximum Load (kN)	Deviation from Exp. Load (%)	Mid-span Deflection at Maximum Load (mm)	Deviation from Exp. Deflection (%)
RWOA-1	Experiment	493	0	31.8	0
	Elastic-plastic	551	11.9	34.5	8.6
	Linear elastic	437	-11.4	11.2	-64.7
	Perfect bond	548	11.2	33.6	5.7
RWOA-2	Experiment	459	0	31.3	0
	Elastic-plastic	526	14.7	36.4	16.2
	Linear elastic	452	-1.5	17.8	-43.0
	Perfect bond	525	14.4	45.5	45.4
RWOA-3	Experiment	436	0	48.6	0
	Elastic-plastic	492	12.8	92.9	91.0
	Linear elastic	426	-2.3	32.6	-33.0
	Perfect bond	487	11.7	79.5	63.6

5.3.2.1.1 *Beam RWOA-1*

The predicted load-deflection curve for beam RWOA-1 is plotted against the experimental results in Figure 5.33. The pre-cracking and initial post-cracking stiffness of the response were well matched with those recorded in the test, but starting at about 70% of the maximum load, the predicted behaviour was stiffer than that observed. With the elastic-plastic bond law, the estimated yielding and ultimate loads were 7% and 12% higher than the test data, and the mid-span deflection at maximum load was overestimated by 9%. The linear elastic bond assumption led to a premature shear failure.

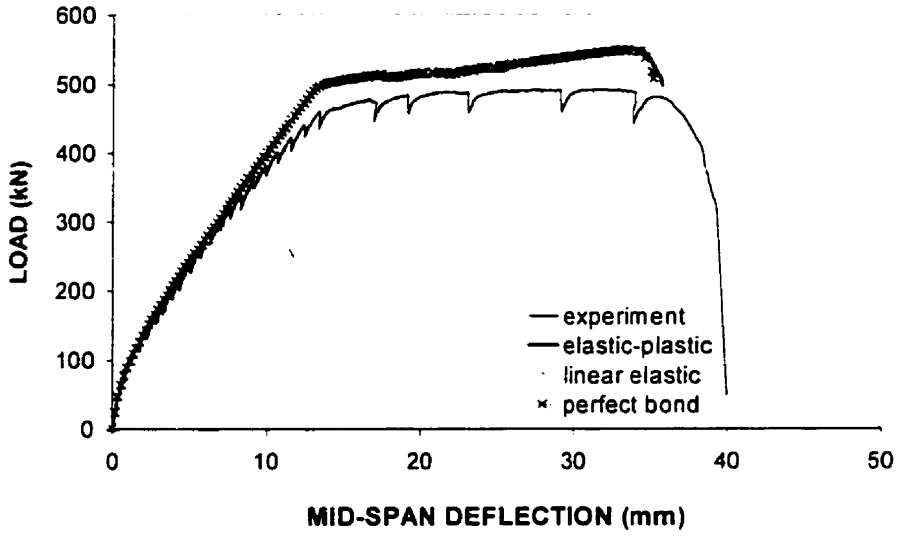

Figure 5.33: Analytical and experimental load-deflection curves for beam RWOA-1

The predicted mode of failure was marked by yielding of both layers of flexural reinforcement near mid-span, along with concrete crushing in compression near the loading point. A major shear crack initiated from just below the loading point and extended to a distance approximately one-tenth of the beam span. This is in accordance with the experimental observation, as shown in Figure 4.13(c).

The predicted FRP strains and average bond-slip values for beam RWOA-1 are graphed in Figure 5.34. The formation of the shear crack in the beam at ultimate is reflected in the progressively increasing FRP strains toward the loading point. The distribution of the FRP strains matches the shape of the diagonal shear cracks in the beam. Large bond-slip values are noted in the CFRP strip closest to mid-span, which correlates with the experimental location of debonding at ultimate.

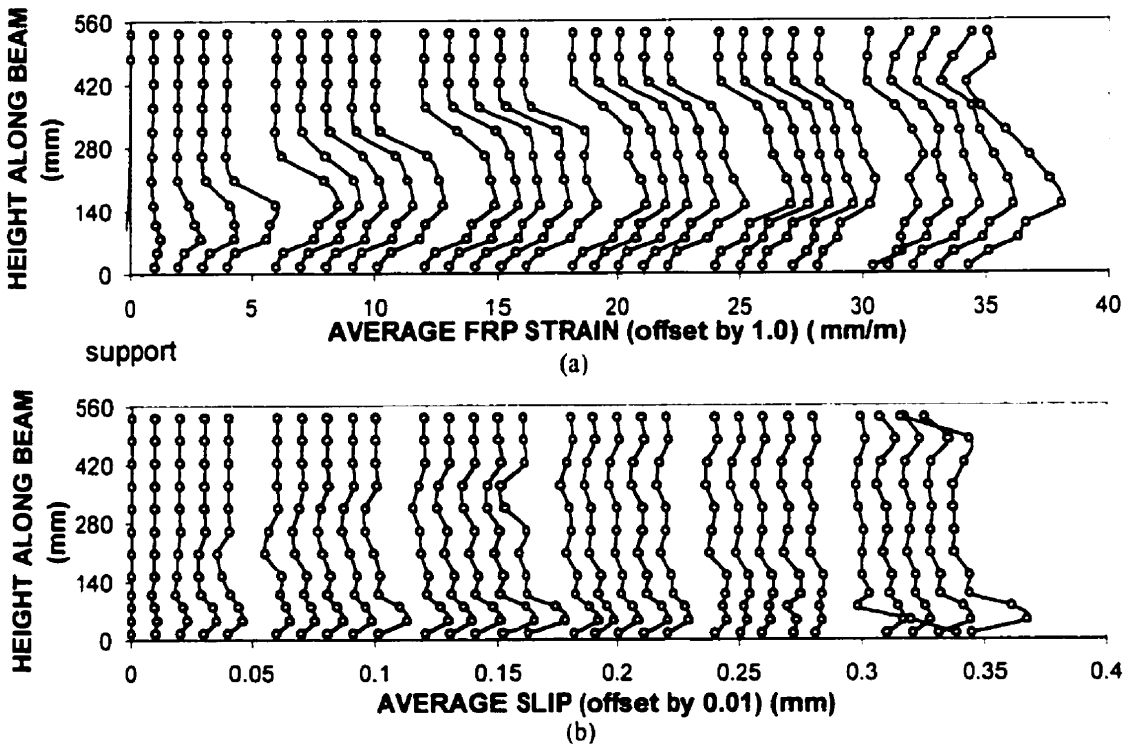

Figure 5.34: Predicted FRP strains and bond-slip distribution for beam RWOA-1 at peak load

5.3.2.1.2 *Beam RWOA-2*

The analytical response for beam RWOA-2 is plotted against the test data in Figure 5.35. The pre-cracking stiffness of the response was in agreement with that measured in the test, but the post-cracking stiffness was slightly overestimated. Again, the linear elastic bond relationship produced an early shear failure, while the elastic-plastic assumption gave a more accurate response. The calculated yielding and ultimate loads were 10% and 15% higher than the test data, respectively. The mid-span deflection at peak load was overestimated by 16%.

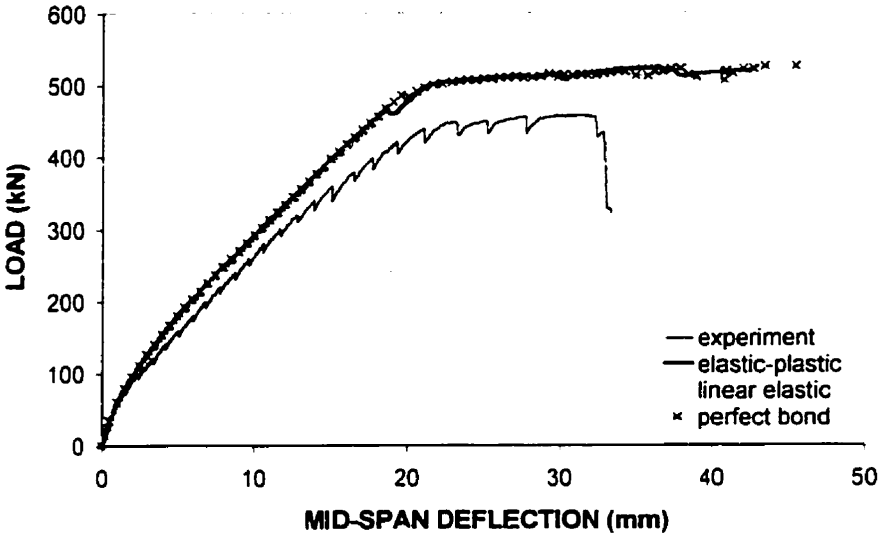

Figure 5.35: Analytical and experimental load-deflection curves for beam RWOA-2

Similar to beam RWOA-1, the predicted failure of beam RWOA-2 was marked by yielding of all three layers of flexural reinforcement near mid-span, accompanied by concrete crushing in compression near the loading point. A major shear crack also initiated from just below the point of load application. This agrees with the experimental observation, as shown in Figure 4.14(c).

The FRP strains and slips at the interface calculated by VecTor2 for beam RWOA-2 are plotted in Figure 5.36. Again, the distributions correspond to the location of shear cracks found in the beam. Similar to beam RWOA-1, the maximum bond-slip is anticipated to be experienced by the CFRP strip closest to mid-span.

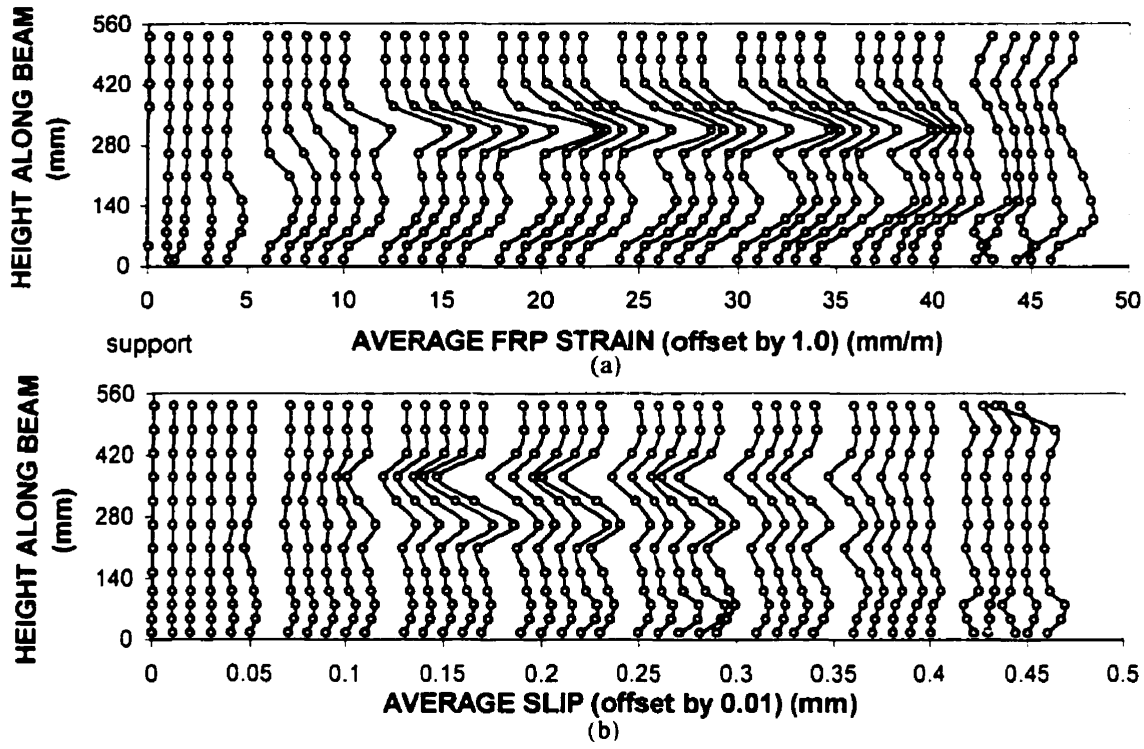

Figure 5.36: Predicted FRP strains and bond-slip distribution for beam RWOA-2 at peak load

5.3.2.1.3 *Beam RWOA-3*

The expected behaviour of beam RWOA-3 is plotted against the experimental data in Figure 5.37. The pre-cracking and post-cracking stiffness of the response compared well with the test curve, but the strain-hardening effects were overestimated. Although the yield load was very close to the actual value, the predicted peak load and corresponding mid-span deflection both exceeded the test results.

Again, the predicted failure of beam RWOA-3 was marked by concrete crushing in compression near the loading point and by yielding of both layers of flexural reinforcement near mid-span. A major shear crack initiating from just below the loading point extended

across the width of two CFRP strips. This corresponds with the experimental observation, as depicted in Figure 4.15(b).

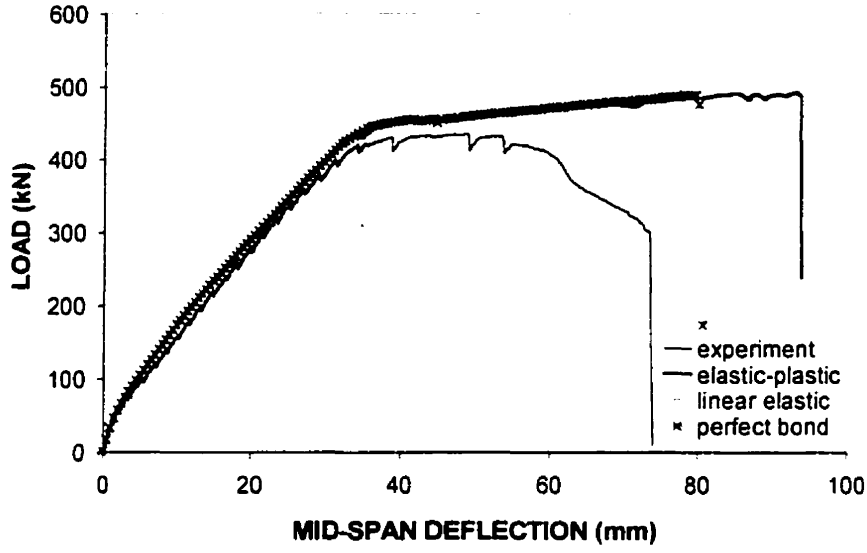

Figure 5.37: Analytical and experimental load-deflection curves for beam RWOA-3

Figure 5.38 shows the predicted FRP strains and bond-slip distribution for beam RWOA-3. The general trends resemble those for the two previous beams. Average bond-slip values of up to -0.1 mm were predicted for the top of the CFRP strip near the point of load application.

Overall, the general responses of all three RWOA beams were reasonably well predicted by the program VecTor2. The yielding loads were estimated to be higher than those recorded from the experiment since the program cannot recognize the downwards shearing of the beam's central portion containing the flexural steel. Predictions with the elastic-plastic bond law and the perfect bond conditions were similar since the failure of the beams was governed by shear-flexural failure rather than by debonding of the CFRP strips. The overestimation of ductility in the analytical results can be attributed to the fact that the 2-D program is not able to simulate the splitting out and downwards punching of the central concrete beam section. This mode of failure led to the sudden drop in load-carrying capacity

and a loss of ductility in the experiment. Also, correct modelling of confinement around the loading plate is a factor contributing to the excess ductility.

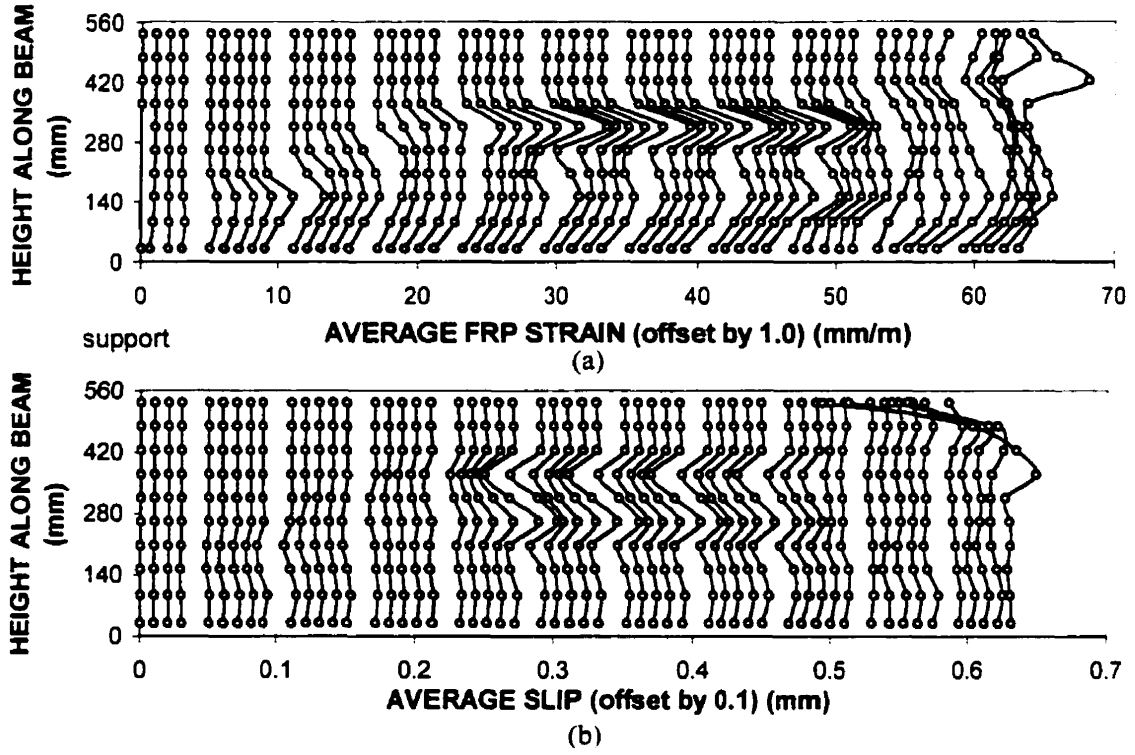

Figure 5.38: Predicted FRP strains and bond-slip distribution for beam RWOA-3 at peak load

The maximum FRP strains in the RWOA beams predicted by program VecTor2 are compared to those estimated by the various proposed models in Table 5.15 (refer to section 2.3.2 of this report and Appendix C). It can be seen that the strains from the finite element analyses are similar to those from the earlier models for effective FRP strains. These values are higher than the results from the more recently proposed equations, which were calibrated with more experimental data, and thus, should be more accurate. However, since the actual FRP strains were not measured in the RWOA beam tests, the predicted strain values cannot be verified. Therefore, it is not possible to ascertain the range of effective strains at which FRP composites can be expected to debond from the concrete surface. Nonetheless, the

increase of FRP strain with an increase in concrete strength, as implied in the proposed models, is reflected in the values obtained from the numerical analyses.

Table 5.15: Predicted and Calculated Effective FRP Strains

Proposed Equation	Effective FRP Strain (mm/m)		
	Beam RWOA-1	Beam RWOA-2	Beam RWOA-3
VecTor2	4.1	5.0	5.1
Chajes [41]	5.0	5.0	5.0
Triantafillou (Eqn. 2-23)	5.8	5.8	5.8
Khalifa ($\varepsilon_{f,e}$= R×$\varepsilon_{f,u}$, R from Eqn. 2-26)	2.2	2.4	3.2
Triantafillou and Anotonopoulos (Eqn. 2-29b)	3.7	3.9	4.5
Triantafillou - ACI ($\varepsilon_{f,e,A}$ = 0.9×$\varepsilon_{f,e}$)	3.3	3.5	4.0
Schnerch (Eqn. 2-32)	2.9	3.2	4.3

At peak load, the magnitude of the predicted maximum bond-slip in the three RWOA beams was on the order of 0.05 mm, 0.06 mm, and 0.20 mm, respectively. These values are much lower than the ultimate slip value (0.5 mm) specified for the bond interface. Thus, debonding was not expected to occur in the analyses. Since debonding was observed in the experiment at failure, this suggests that the ultimate slip in the bond law needs to be re-evaluated. However, it can be concluded that the elastic-plastic bond law was suitable for the concrete-FRP interface of these beams, as the linear elastic bond relationship produced premature shear failures.

After the analyses for the RWOA beams had been completed, a double-shear bond test was conducted by a post-doctorate researcher at the university. The specimen used is depicted in Figure 5.39, where the CFRP strips (50 mm wide) and epoxy tested were the same as those for the RWOA beams. The average concrete strength was 32 MPa, while the CFRP bond lengths were varied as 100 mm, 200 mm, and 400 mm. The specimen was subjected to tensile forces applied to the embedded rebars, and relative displacements between the prisms were measured by a LVDT on each of the four faces. All six specimens failed by peeling of the CFRP strips. Whereas larger pieces of concrete were attached to the

underside of the strips near the central section of the specimen, only small amounts of fine aggregates and cement paste were found under the remainder of the peeled strip.

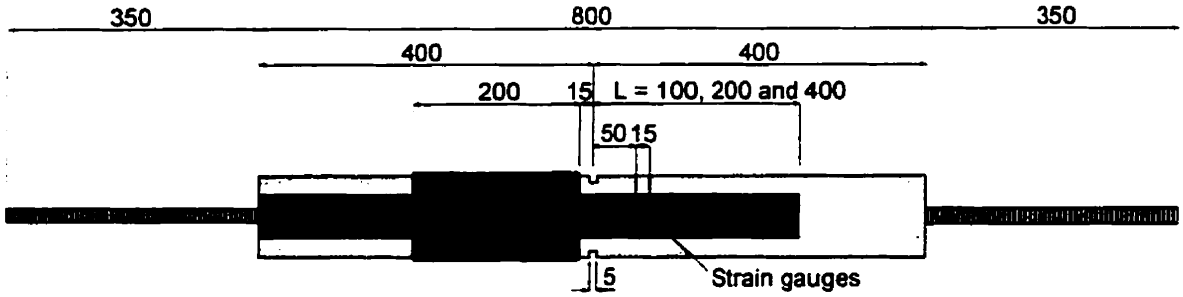

Figure 5.39: Bond test specimen utilized by Sato [83]

The fracture energy of the bond interface (G_f), or the area under the bond stress-slip curve, was estimated to be 0.34 N/mm. The bond length for attaining the maximum bond capacity was determined to be at least 150 mm. It was found that the bond stress-slip relationships could be fitted with Popovics' equation (Figure 5.40(a)), as reported by Nakaba *et al.* [50], but a triangular distribution (Figure 5.40(b)) was recommended for the FE analysis. However, the values from the bond test have not been adopted in the analyses as the concrete strength did not match those of the RWOA beams.

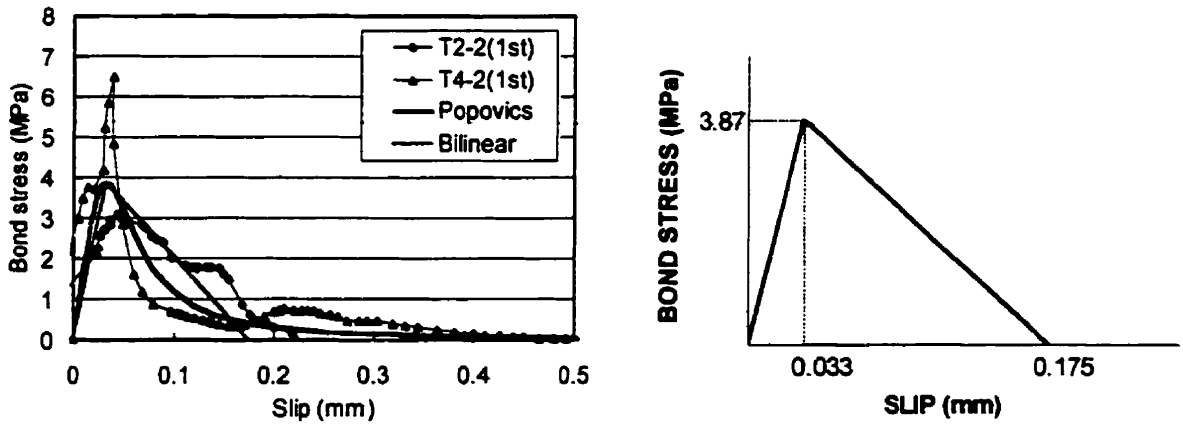

Figure 5.40: (a) Bond stress-slip curves [83] and (b) equivalent bilinear relationship

CHAPTER 6 DISCUSSION

6.1 TRENDS IN EXPERIMENTAL BEHAVIOUR

Numerous behavioural trends have been noted in the tests of RC members strengthened with FRP composites. These will be grouped according to the purpose of the strengthening scheme.

6.1.1 *FLEXURAL STRENGTHENING WITH FRP COMPOSITES*

In members that are strengthened for flexure, their stiffness and load-carrying capacity can be greatly enhanced, but is usually accompanied by a reduction in ductility. The brittle behaviour observed in these beams is usually attributed to the delamination of the FRP plate or to the ripping-off of the concrete cover. The mechanical and geometrical properties of the FRP plate, epoxy resin and concrete determine which mode of failure dominates, and the amount of slip that can be sustained at the concrete-FRP interface. FRP plate delamination, the principal factor in lowering beam ductility, can be triggered by failure within the concrete cover or by the separation of the concrete cover from the flexural reinforcement. Long and thin FRP laminates are prone to the first failure mode, which is exemplified by peeling at shear cracks along the beam. Short and thick FRP plates will likely cause failure of the second type, where high shear and normal stresses exist at the plate ends. Thus, it is highly recommended

that FRP laminates bonded onto the soffits of beams be well anchored into the beam in order to impede debonding failures.

6.1.2 *SHEAR STRENGTHENING WITH FRP COMPOSITES*

For beams strengthened in shear with FRP composites, their stiffnesses are usually the same or just slightly higher than the control specimens since the load-carrying fibres are usually oriented perpendicularly to the beam axis. The strength enhancement experienced by these beams is usually less significant than that commonly seen in members strengthened in flexure. However, the main improvement noted in these beams is in the change of the failure mode from brittle shear to ductile flexural failure. By acting as external shear reinforcement, the FRP composites work to limit the propagation of cracks and to increase the shear capacity of the concrete. The member will be able to sustain higher shear forces until the flexural steel reinforcement yields and concrete crushing occurs near the loading point.

Although premature debonding of FRP laminates has been reported by other researchers, this behaviour was not observed in the two sets of tests carried out at the University of Toronto (by De Rose and the author). Whereas the De Rose beam was completely wrapped with CFRP fabric, the series of RWOA beams were bonded with CFRP strips on the sides only. The absence of premature debonding may be due to the strong epoxy used in the bonding process. Also, the CFRP reinforcement ratio used was sufficiently high to restrict the widening of the shear cracks, thus limiting the strains in the CFRP and preventing premature debonding failure of the strips.

For beams with FRP bonded to the sides only, peeling of the FRP (after shear-flexural failure) tended to occur below the main shear crack, pulling the stiff side cover outwards, which enabled the central portion of the beam to punch down in shear. This behaviour can be avoided through the use of FRP in the shape of U-wraps, where the FRP is likely to peel off

above the shear crack. The peeling-off can be further mitigated by some form of anchorage system along the top edge of the FRP laminates.

6.2 NEED FOR FUTURE EXPERIMENTAL WORK

Since an extensive amount of published research has been related to flexural strengthening with FRP, more attention should be directed to its application for shear strengthening.

6.2.1 *GLOBAL RESPONSE*

The RWOA beam series should be viewed as a set of pilot tests. More tests should be conducted to develop a deeper understanding of the failure mechanisms involved. Nevertheless, the tests performed in this study showed that CFRP strips are capable of enhancing a beam's shear strength by 50% and can change a brittle shear failure to a more ductile flexural response. In order to study the premature debonding phenomenon prior to shear-flexural failure, the percentage of CFRP shear reinforcement should be reduced so that shear cracks can propagate and widen. This can be achieved by bonding narrower CFRP strips or using a wider spacing between the vertical strips. Achieving premature debonding failures in experiments will enable the verification of bond constitutive relationships assumed in FE analyses, and also of equations for predicting the ultimate strengths of beams governed by debonding failure, as proposed by several researchers. To gain a better understanding of the maximum slip that can be sustained at the bond interface, strain gauges should be bonded onto the CFRP strips and on the concrete surface near the edge of the strips. Measuring the strain distribution in the CFRP fabric will also allow the determination of the strips' contribution to the beam's shear capacity when stirrups are included. To study the behaviour of beams more likely to be encountered in the field, tests should be performed on beams with internal steel

stirrups. It has been reported that the shear force carried by FRP laminates is higher when the stirrup ratio is low, so these two components of shear reinforcement should be considered simultaneously.

Different beam geometries, such as various shear span-to-depth ratios, should also be analyzed. Full-scale specimens such as the RWOA beams should be tested to eliminate problems associated with size effects and to observe the true failure modes of real-life members. Although the capacity and ductility of the beams were increased through the bonding of the CFRP strips onto the side surfaces, further enhancement may be attained by using a U-wrap configuration. Some confinement can be provided to the concrete in the central section of the beam, and anchorage of the strips to the concrete will further delay debonding. The influence of the strip spacing on the inclination and location of the shear cracks should also be investigated. This can help determine the optimal spacing that should be used, although continuous sheets would be more convenient in field applications. Various orientations of the CFRP strips may also be studied to find an optimum angle, but at 90° to the beam axis seems to be the most practical.

6.2.2 *LOCAL BEHAVIOUR*

As for the local bond behaviour, bond tests should be conducted in which strips of FRP fabric bonded to a concrete prism are subjected to a tensile force (double-face shear test). Strain gauges should be mounted on both the FRP and the concrete surface to measure the slip that can be endured before debonding failure. The maximum bond stress should also be determined to confirm its dependence on the relative mechanical properties of the FRP, concrete and epoxy resin. This type of test has been performed by many researchers, as described in Chapter 2 of this report. Rather than simply plotting the strain distribution along the bond length and finding the effective bond length, a parametric study should be used to determine the effects of various factors on the bond stress-strain relationship. More attempts

should be made to establish the shape of the bond stress-strain curve, and equations should be developed to estimate the values needed to define this curve. Although general design equations mostly rely on the mechanical properties and configuration of the FRP and the RC member, a constitutive relationship for the concrete-FRP bond interface is required for a detailed FE analysis. An attempt has been made by Sato to measure the maximum bond stress and characteristic slip values for the CFRP and epoxy used in the current research [83]. However, the concrete strength of the bond test specimens differed from those of the beam specimens. Therefore, the values obtained by Sato are specific to the type of concrete, CFRP and epoxy resin used in the bond test. Nevertheless, the test conducted has produced preliminary results and has paved the way for future bond tests. The epoxy resin used should be tested in tension according to ASTM D638 [84] to determine its Poisson's ratio and shear modulus. Other variables that should be studied as related to FRP composites include their durability under aggressive environmental conditions and cyclical loads.

6.3 STRENGTHS/WEAKNESSES IN ANALYTICAL METHODS

The incorporation of bond elements into the FE program enabled better predictions of the response of members strengthened in flexure or shear with FRP. However, the accuracy of these estimations depended on the bond stress-slip relationship that was chosen for the analyses. So far, only two types of bond law have been tested: linear elastic and elastic-plastic, although several other forms have since been proposed by various researchers. From the current research, it was found that the linear elastic bond law was appropriate only when the failure was dominated by sudden delamination of the FRP plate, accompanied by a thin layer of concrete (as in the Žarnić specimens). This situation is expected to occur when the shear strength of the epoxy is low. Since all of the reported strengths for the epoxy were the tensile strengths, these values will be used for comparison, as the shear and tensile properties are related. For the Žarnić specimens, the tensile strength of the epoxy was 4 MPa. On the other hand, the tensile strength for the epoxy used in the El-Refaie specimens was approximately 18

MPa, while for the De Rose and RWOA specimens, the epoxy strength was given to be 72 MPa. Therefore, in the specimens utilizing stronger epoxies, the failure was predominantly through the peeling of the concrete cover, which was critical due to its lower shear strength (represented by the concrete's modulus of rupture). For these specimens, the analyses were more accurate when the elastic-plastic bond relationship was applied. This is due to the fact that peeling of the concrete cover progresses gradually along the member, whereas the debonding of FRP laminates (as in the Žarnić specimens) occurs suddenly, corresponding to the sudden drop of bond stress in the linear elastic bond law once the ultimate slip is reached. An in-depth review of published experiments should be conducted to determine the range of epoxy strengths that distinguishes sudden plate debonding failures from those involving failure of the concrete cover. The shear strength (and indirectly, the tensile strength) of the epoxy is thought to have a larger role than its elastic modulus in determining the failure mode. This is supported by the observation that the elastic moduli of the epoxies used in the Žarnić specimens (12.8 GPa) and in some of the El-Refaie specimens (10 GPa) were similar, but the failure conditions were different, as discussed above.

After performing FE analyses of several sets of specimens, it can be suggested that the maximum bond stress is a function of the concrete strength (the modulus of rupture of concrete), the maximum slip is a function of the shear modulus (and the elastic modulus) of the epoxy, and the existence of the plastic range in the bond law depends on the shear (or tensile) strength of epoxy. The maximum bond stress is usually limited by the shear strength of the concrete, as it is typically lower than the strength of the epoxy resin. As for the ultimate slip that can be sustained, more work is needed to estimate its value. Since many interrelated factors influence the bond stress-slip relationship, further studies are required. Despite some minor uncertainties regarding the bond constitutive relationship, the program VecTor2 can give fairly accurate predictions of the overall behaviour of RC members strengthened with externally-bonded FRP composites.

One weakness noted in the analyses is associated with the simulation of precracked members repaired while loaded. Some discrepancies were noted in the response of such members immediately after repair (as observed for the De Rose slabs presented in section 5.2.3.2.2). Another weakness in the FE program is related to the premature shear failures predicted for some slabs and shear-critical beams. Therefore, several trials may be required to determine the most suitable behaviour models and modelling assumptions in defining the finite element mesh.

6.4 NEED FOR FUTURE ANALYTICAL WORK

Currently, in the FE program VecTor2, FRP strips or sheets can only be represented by one-dimensional truss elements if bond-slip is to be considered. Also, two FRP truss elements that meet at the same coordinates cannot be connected to a single node due to the formulation of the link and contact elements. Thus, three nodes are required at the same location in order to account for both longitudinal and transverse properties of the FRP laminates. The properties of the bond interface can only be simulated with dimensionless link elements or one-dimensional contact elements. This forces the bond stress distribution to be discrete at the nodes or along the FRP truss elements. Only uni-directional slip at the FRP-concrete interface is permissible, while experimental observations suggest that debonding of FRP due to shear is a two-directional phenomenon. Therefore, it is recommended that a two-dimensional isoparametric contact element, as presented by Mehlhorn and Keuser [74], be incorporated into the FE program. Such an element will permit slippage in the global x- and y-directions, and allow for a continuous bond stress distribution across the FRP-concrete interface. Correspondingly, using rectangular elements rather than truss elements for side-bonded FRP sheets will give a more accurate response for the externally-strengthened member. In terms of the bond constitutive model, corroboration with more specimens is needed to confirm the determination of the values used in the bond law, and other formulations of the bond stress-slip relationship should be examined.

Aside from the bond elements and associated bond models, more work is required in the area of sequential analyses where repair or strengthening takes place after initial loading. The difference between the estimated and actual response reported in the current research may be related to the inclusion of strain history considerations. Previous loading must be accounted for in this type of analysis, but the accuracy of such considerations for bond elements must be confirmed.

As for analytical work related to design equations for shear strengthening, more independent test results are required to truly validate the equations proposed by various researchers. If these are found to be inadequate, then more test variables and their effects should be studied. Before the design of RC members shear strengthened with FRP can be adopted in the design codes, the equations must be verified for a wider range of specimens and test conditions.

CHAPTER 7 CONCLUSIONS

Before FRP composites can be widely utilized in field applications, engineers must be confident about the performance of RC members externally reinforced with this material. As well, they must be able to predict the behaviour of such members using simple analytical equations for preliminary design, or with finite element analysis for more detailed studies. Although the experimental database for RC members strengthened in flexure with FRP composites is extensive, further investigations are imperative in the domain of shear strengthening. The failure modes of flexural-strengthened members have been analyzed thoroughly by numerous researchers, but the complexities involved with shear behaviour requires more attention.

The experimental program conducted in the current research points the way to additional work in this area. The set of pilot test beams showed that CFRP strips are capable of increasing the load-carrying capacity of shear-critical members, while changing the failure mode from brittle shear to ductile flexural failure. However, it did not meet the aim of producing premature debonding failures due to the high FRP shear reinforcement ratio used. Nevertheless, it provided a first-hand observation into the failure mode involving the peeling of the side concrete cover leading to the punching failure of the beam's central section. The experiment also supplied valuable information for the design of the next test series, in which the FRP reinforcement ratio should be lowered to promote widening of shear cracks, strain

gauges should be applied to detect slip, and steel stirrups should be included in some specimens to obtain more comprehensive results. Attainment of premature debonding failures will also enable the validation of proposed design equations, which have been primarily verified with data used to calibrate the models. As well, bond tests involving FRP-bonded prisms subjected to shear should be performed to clarify the local behaviour at the interface.

As for analytical work, it can be concluded from the current research that the behaviour of the bond interface must be considered for an accurate prediction of the member's response. Neglecting the bond-slip at the interface would lead to overestimated stiffness and ultimate loads. Modelling of the bond interface for the critical force transfer between the concrete and FRP is dependent on the characterization of the bond zone. While experimental and analytical work has been undertaken in this regard, verification of the proposed bond stress-slip relationships is needed. A clearly defined constitutive relationship must be adopted for the bond elements representing the bond interface. In this first attempt of applying a linear elastic or elastic-plastic bond law, the analytical response of flexural- or shear-strengthened members were in good accord with the experimental results. Not only were the failure loads and corresponding deflections accurate, but the stiffness of the response and the failure modes were also well matched. In terms of the bond element types, the dimensionless link element and the one-dimensional contact element have proved sufficient in modelling the bond interface. Nonetheless, improvements in the numerical predictions could be achieved by implementing a higher order element, such as a two-dimensional contact element. This type of element would permit slippage in two directions, while providing a continuous stress distribution along the interface between the concrete and FRP laminates.

Although FRP composites have shown potential in enhancing the strength and stiffness of RC members, reductions in ductility must be avoided through the use of proper anchorage systems. In addition, other properties of this advanced material must be examined, such as their long-term durability in aggressive environments and their behaviour in cyclical loading conditions.

REFERENCES

1. Rizkalla, S. and Labossiere, P. "Structural Engineering with FRP - in Canada", *Concrete International*, Vol. 21, No. 10, 1999, pp. 25-28.
2. Alkhrdaji, T., Nanni, A., Chen, G., and Barker, M. "Solid RC Decks Strengthened with FRP", *Concrete International*, Vol. 21, No. 10, 1999, pp. 37-41.
3. Katsumata, H., Kobayashi, K., Morita, S., and Matsuzaki, Y. "Japanese State of the Art on Seismic Retrofit by Fiber Wrapping for Building Structures: Technologies and Research and Development Activities", *Fiber Reinforced Polymer Reinforcement for Reinforced Concrete Structures*, Fourth International Symposium, Michigan, USA, 1999, pp. 865-878.
4. Taerwe, L. R. and Matthys, S. "FRP for Concrete Construction: Activities in Europe", *Concrete International*, Vol. 21, No. 10, 1999, pp. 33-36.
5. Ross, C. A., Jerome, D. M., Tedesco, J. W., and Hughes, M. L. "Strengthening of Reinforced Concrete Beams with Externally Bonded Composite Laminates", *ACI Structural Journal*, Vol. 96, No. 2, 1999, pp. 212-220.
6. Nitereka, C. and Neale, K. W. "Analysis of Reinforced Concrete Beams Strengthened in Flexure with Composite Laminates", *Canadian Journal of Civil Engineering*, Vol. 26, 1999, pp. 646-654.
7. Arduini, M. and Nanni, A. "Behavior of Precracked RC Beams Strengthened with Carbon FRP Sheets", *Journal of Composites for Construction*, Vol. 1, No. 2, 1997, pp. 63-70.
8. Bucci, F. "Finite Element Analysis of Repaired Concrete Structures", *M.A.Sc Thesis*, University of Toronto, Canada, 1998, 185 p.
9. Arduini, M., Di Tommaso, A., and Nanni, A. "Brittle Failure in FRP Plated and Sheet Bonded Beams", *ACI Structural Journal*, Vol. 94, No. 4, 1997, pp. 363-370.
10. Bokan-Bosiljkov, V.,Bosiljkov, V., Gostič S., and Žarnić, R. "Critical Local Failure of Externally Strengthened Concrete Elements Loaded in Flexure", *Specialist Techniques and Materials for Concrete Construction*, Proceedings of the International Conference 'Creating with Concrete', Dundee, Scotland, UK, 1999, pp. 123-129.

11. Žarnić, R., Gostič, S., Bosiljkov, V., and Bokan-Bosiljkov, V. "Improvement of Bending Load-Bearing Capacity by Externally Bonded Plates", *Specialist Techniques and Materials for Concrete Construction*, Proceedings of the International Conference 'Creating with Concrete', Dundee, Scotland, UK, 1999, pp. 433-442.
12. Rahimi, H. and Hutchinson, A. "Concrete Beams Strengthened with Externally Bonded FRP Plates", *Journal of Composites for Construction*, Vol. 5, No. 1, 2001, pp. 44-56.
13. Limam, A. and Hamelin, P. "On the Extending Performance of an RC Beam with a CFRP Sheet: Experiments and Simulations", *Proceedings of the 6th International Conference on Computer Methods in Composite Materials*, CADCOMP'98, Montreal, Canada, 1998, pp. 569-578.
14. Buyukozturk, O. and Hearing, B. "Failure Behavior of Precracked Concrete Beams Retrofitted with FRP", *Journal of Composites for Construction*, Vol. 2, No. 3, 1998, pp. 138-144.
15. Karbhari, V. M. "Characteristics of Adhesion Between Composites and Concrete as Related to Infrastructure Rehabilitation", *Diversity into the Next Century*, 27th International Technical Conference, Society for the Advancement of Material and Process Engineering, 1995, pp. 1083-1094.
16. Triantafillou, T. and Plevris, N. "Post-Strengthening of R/C Beams with Epoxy-Bonded Fiber Composite Materials", *Advanced Composites Materials in Civil Engineering Structures*, Proceedings of the Specialty Conference, ASCE Materials Engineering Division, Nevada, USA, 1991, pp. 245-256.
17. Nguyen, D. M., Chan, T. K., and Cheong, H. K. "Brittle Failure and Bond Development Length of CFRP-Concrete Beams", *Journal of Composites for Construction*, Vol. 5, No. 1, 2001, pp. 12-17.
18. Blaschko, M., Niedermeier, R., and Zilch, K. "Bond Failure Modes of Flexural Members Strengthened with FRP", *Fiber Composites in Infrastructure*, Proceedings of the Second International Conference on Composites in Infrastructure, Vol. 1, Tucson, Arizona, USA, 1998, pp. 315-327.

19. Malek, A. M., Saadatmanesh, H., and Ehsani, M. R. "Prediction of Failure Load of R/C Beams Strengthened with FRP Plate Due to Stress Concentration at the Plate End", *ACI Structural Journal*, Vol. 95, No. 1, 1998, pp. 142-152.
20. Mukhopadhyaya, P. and Swamy, N. "Interface Shear Stress: A New Design Criterion for Plate Debonding", *Journal of Composites for Construction*, Vol. 5, No. 1, 2001, pp. 35-43.
21. Varastehpour, H. and Hamelin, P. "Analysis and Study of Failure Mechanism of RC Beam Strengthened with FRP Plate", *Advanced Composite Materials in Bridges and Structures*, Montreal, Quebec, 1996, pp. 527-536.
22. Wang, C.-Y. and Ling, F.-S. "Prediction Model for the Debonding Failure of Cracked RC Beams with Externally Bonded FRP Sheets", *Fiber Composites in Infrastructure*, Proceedings of the Second International Conference on Composites in Infrastructure, Vol. 1, Tucson, Arizona, USA, 1998, pp. 548-562.
23. Colotti, V. and Spadea, G. "Shear Strength of RC Beams Strengthened with Bonded Steel or FRP Plates", *Journal of Structural Engineering*, Vol. 127, No. 4, 2001, pp. 367-373.
24. Li, A., Assih, J., and Delmas, Y. "Shear Strengthening of RC Beams with Externally Bonded CFRP Sheets", *Journal of Structural Engineering*, Vol. 127, No. 4, 2001, pp. 374-380.
25. Khalifa, A., Gold, W. J., Nanni, A., and Aziz, A. M. I. "Contribution of Externally Bonded FRP to Shear Capacity of RC Flexural Members", *Journal of Composites for Construction*, Vol. 2, No. 4, 1998, pp. 195-202.
26. Triantafillou, T. C. "Shear Strengthening of Concrete Members Using Composites", *Non-Metallic (FRP) Reinforcement for Concrete Structures*, Proceedings of the Third International Symposium, Vol. 1, Japan, 1997, pp. 523-530.
27. Taerwe, L., Khalil, H., and Matthys, S. "Behaviour of RC Beams Strengthened in Shear by External CFRP Sheets", *Non-Metallic (FRP) Reinforcement for Concrete Structures*, Proceedings of the Third International Symposium, Vol. 1, Japan, 1997, pp. 483-490.
28. Funakawa, I., Shimono, K., Watanabe, T., Asada, S., and Ushijima, S. "Experimental Study on Shear Strengthening with Continuous Fiber Reinforcement Sheet and Methyl

Methacrylate Resin", *Non-Metallic (FRP) Reinforcement for Concrete Structures*, Proceedings of the Third International Symposium, Vol. 1, Japan, 1997, pp. 475-482.

29. Sato, Y., Ueda, T., and Kakuta, Y. "Shear Reinforcing Effect of Carbon Fiber Sheet Attached to Side of Reinforced Concrete Beams", *Advanced Composite Materials in Bridges and Structures*, Canadian Society for Civil Engineering, Montreal, Quebec, Canada, 1996, pp. 621-628.
30. Chaallal, O., Nollet, M.-J., and Perraton, D. "Shear Strengthening of RC Beams by Externally Bonded Side CRFP Strips", *Journal of Composites for Construction*, Vol. 2, No. 2, 1998, pp. 111-113.
31. Kage, T., Abe, M., Lee, H.-S., and Tomosawa, F. "Effect of CFRP Sheets on Shear Strengthening of RC Beams Damaged by Corrosion of Stirrup", *Non-Metallic (FRP) Reinforcement for Concrete Structures*, Proceedings of the Third International Symposium, Vol. 1, Japan, 1997, pp. 443-450.
32. Norris, T., Saadatmanesh, H., and Ehsani, M. "Shear and Flexural Strengthening of R/C Beams with Carbon Fiber Sheets", *Journal of Structural Engineering*, Vol. 123, No. 7, 1997, pp. 903-911.
33. Arduini, M., Nanni, A., Di Tommaso, A., and Focacci, F. "Shear Response of Continuous RC Beams Strengthened with Carbon FRP Sheets", *Non-Metallic (FRP) Reinforcement for Concrete Structures*, Proceedings of the Third International Symposium, Vol. 1, Japan, 1997, pp. 459-466.
34. Araki, N., Matsuzaki, Y., Nakano, K., Kataoka, T., and Fukuyama, H. "Shear Capacity of Retrofitted RC Members with Continuous Fiber Sheets", *Non-Metallic (FRP) Reinforcement for Concrete Structures*, Proceedings of the Third International Symposium, Vol. 1, Japan, 1997, pp. 515-522.
35. Grace, N. F., Sayed, G. A., Soliman, A. K., and Saleh, K. R. "Strengthening Reinforced Concrete Beams Using Fiber Reinforced Polymer (FRP) Laminates", *ACI Structural Journal*, Vol. 96, No. 5, 1999, pp. 865-874.
36. Sato, Y., Ueda, T., Kakuta, Y., and Ono, S. "Ultimate Shear Capacity of Reinforced Concrete Beams with Carbon Fiber Sheet", *Non-Metallic (FRP) Reinforcement for*

Concrete Structures, Proceedings of the Third International Symposium, Vol. 1, Japan, 1997, pp. 499-506.

37. Sato, Y., Katsumata, H., and Kobatake, Y. "Shear Strengthening of Existing Reinforced Concrete Beams by CFRP Sheet", *Non-Metallic (FRP) Reinforcement for Concrete Structures*, Proceedings of the Third International Symposium, Vol. 1, Japan, 1997, pp. 507-514.
38. Khalifa, A. and Nanni, A. "Improving Shear Capacity of Existing RC T-Section Beams Using CFRP Composites", *Cement & Concrete Composites*, Vol. 22, 2000, pp. 165-174.
39. Deniaud, C. and Cheng, J. J. R. "Shear Behavior of Reinforced Concrete T-Beams with Externally Bonded Fiber-Reinforced Polymer Sheets", *ACI Structural Journal*, Vol. 98, No. 3, 2001, pp. 386-394.
40. Triantafillou, T. C. "Shear Strengthening of Reinforced Concrete Beams Using Epoxy-Bonded FRP Composites", *ACI Structural Journal*, Vol. 95, No. 2, 1998, pp. 107-115.
41. Chajes, M. J., Januszka, T. F., Mertz, D. F., Thomson, T. A., and Finch, W. W. "Shear Strengthening of Reinforced Concrete Beams Using Externally Applied Composite Fabrics", *ACI Structural Journal*, Vol. 92, No. 3, 1995, pp. 295-302.
42. Gendron, G., Picard, A., and Guerin, M.-C. "A Theoretical Study on Shear Strengthening of Reinforced Concrete Beams Using Composite Plates", *Composite Structures*, Vol. 45, 1999, pp. 303-309.
43. Malek, A. M. and Saadatmanesh, H. "Analytical Study of Reinforced Concrete Beams Strengthened with Web-Bonded Fiber Reinforced Plastic Plates or Fabrics", *ACI Structural Journal*, Vol. 95, No. 3, 1998, pp. 343-351.
44. Malek, A. M. and Saadatmanesh, H. "Ultimate Shear Capacity of Reinforced Concrete Beams Strengthened with Web-Bonded Fiber-Reinforced Plastic Plates", *ACI Structural Journal*, Vol. 95, No. 4, 1998, pp. 391-399.
45. Khalifa, A. and Nanni, A. "Improving Shear Capacity of Existing RC T-Section Beams Using CFRP Composites", *Cement & Concrete Composites*, Vol. 22, 2000, pp. 165-174.

46. Maeda, T., Asano, Y., Sato, Y., Ueda, T., and Kakuta, Y. "A Study on Bond Mechanism of Carbon Fiber Sheet", *Non-Metallic (FRP) Reinforcement for Concrete Structures*, Proceedings of the Third International Symposium, Vol. 1, Japan, 1997, pp. 279-286.

47. Triantafillou, T. C. and Antonopoulos, C. P. "Design of Concrete Flexural Members Strengthened in Shear with FRP", *Journal of Composites for Construction*, Vol. 4, No. 4, 2000, pp. 198-205.

48. Schnerch, D. A. "Shear Behaviour of Large-Scale Concrete Beams Strengthened with Fibre Reinforced Polymer (FRP) Sheets," *Masters Thesis*, University of Manitoba, Winnipeg, Canada, 2001, 163 p.

49. Kamiharako, A., Maruyama, K., and Shimomura, T. "Evaluation Systems of Shear Capacity of Reinforced Concrete Members Retrofitted with Carbon Fiber reinforced Polymer Sheets in Consideration of Bond-Peeling Characteristics", *Fiber Reinforced Polymer Reinforcement for Reinforced Concrete Structures*, Fourth International Symposium, ACI SP-188, Michigan, USA, 1999, pp. 973-983.

50. Nakaba, K., Kanakubo, T., Furuta, T. and Yoshizawa, H. "Bond Behavior Between Fiber-Reinforced Polymer Laminates and Concrete", *ACI Structural Journal*, Vol. 98, No. 3, 2001, pp. 359-367.

51. Chajes, M. J., Finch, Jr., W. W., Januszka, T. F., and Thomson, Jr., T. A. "Bond and Force Transfer of Composite Material Plates Bonded to Concrete", *ACI Structural Journal*, Vol. 93, No. 2, 1996, pp. 208-217.

52. Ueda, T., Sato, Y., and Asano, Y. "Experimental Study on Bond Strength of Continuous Carbon Fiber Sheet", *Fiber Reinforced Polymer Reinforcement for Reinforced Concrete Structures*, Fourth International Symposium, ACI SP-188, Michigan, USA, 1999, pp. 407-416.

53. Chen, J. F. and Teng, J. G. "Anchorage Strength Models for FRP and Steel Plates Bonded to Concrete", *Journal of Structural Engineering*, Vol. 127, No. 7, 2001, pp. 784-791.

54. Horiguchi, T. and Saeki, N. "Effect of Test Methods and Quality of Concrete on Bond Strength of CFRP Sheet", *Non-Metallic (FRP) Reinforcement for Concrete Structures*, Proceedings of the Third International Symposium, Vol. 1, Japan, 1997, pp. 265-270.

55. Brosens, K. and Van Gemert, D. "Anchoring Stresses Between Concrete and Carbon Fibre Reinforced Laminates", *Non-Metallic (FRP) Reinforcement for Concrete Structures*, Proceedings of the Third International Symposium, Vol. 1, Japan, 1997, pp. 271-278.

56. Miller, B. and Nanni, A. "Bond Between CFRP Sheets and Concrete", *Materials and Construction: Exploring the Connection*, Proceedings of the Fifth ASCE Materials Engineering Congress, Cincinnati, Ohio, USA, pp. 240-247.

57. Yoshizawa, H., Myojo, T., Okoshi, M., Mizukoshi, M. and Kliger, H. "Effect of Sheet Bonding Condition on Concrete Members Having Externally Bonded Carbon Fiber Sheet", *Materials for the New Millennium*, Proceedings of the Fourth Materials Engineering Conference, Vol. 2, Washington, D.C., USA, 1996, pp. 1608-1616.

58. Tripi, J. M., Bakis, C. E., Boothby, T. E., and Nanni, A. "Deformation in Concrete with External CFRP Sheet Reinforcement", *Journal of Composites for Construction*, Vol. 4, No. 2, 2000, pp. 85-94.

59. Bizindavyi, L. and Neale, K. W. "Transfer Length and Bond Strengths for Composites Bonded to Concrete", *Journal of Composites for Construction*, Vol. 3, No. 4, 1999, pp. 153-160.

60. Wu, Z. S. and Yoshizawa, H. "Analytical/Experimental Study on Composite Behavior in Strengthening Structures with Bonded Carbon Fiber Sheets", *Journal of Reinforced Plastics and Composites*, Vol. 18, No. 12, 1999, pp. 1131-1155.

61. Yoshizawa, H. and Wu, Z. S. "Analysis of Debonding Fracture Properties of CFS Strengthened RC Member Subject to Tension", *Non-Metallic (FRP) Reinforcement for Concrete Structures*, Proceedings of the Third International Symposium, Vol. 1, Japan, 1997, pp. 287-294.

62. Homam, S. M., Sheikh, S. A., Pernica, G., and Mukherjee, P. K. "Durability of Fibre Reinforced Polymers (FRP) Used in Concrete Structures", *Research Report*, Department of Civil Engineering, University of Toronto, Toronto, Canada, January 2000, 202 p.

63. Sato, Y. "Shear Strengthening of Reinforced Concrete Beam Using Continuous Fiber Sheet", *Ph.D. Dissertation*, Kyoto University, Japan, 2000, 213 p.

64. Nanni, A., Bakis, C. E., and Boothby, T. E. "Externally Bonded FRP Composites for Repair of RC Structures", *Non-Metallic (FRP) Reinforcement for Concrete Structures*, Proceedings of the Third International Symposium, Vol. 1, Japan, 1997, pp. 303-310.

65. Lee, Y.-J., Tripi, J. M., Boothby, T. E. Bakis, C. E., and Nanni, A. "Tension Stiffening Model for FRP Sheets Bonded to Concrete", *Fiber Composites in Infrastructure*, Proceedings of the Second International Conference on Composites in Infrastructure, Vol. 1, Tucson, Arizona, USA, 1998, pp. 175-186.

66. Lee, Y.-J., Boothby, T. E., Bakis, C. E., and Nanni, A. "Slip Modulus of FRP Sheets Bonded to Concrete", *Journal of Composites for Construction*, Vol. 3, No. 4, 1999, pp. 161-167.

67. Vecchio, F. J. and Collins, M. P. "The Modified Compression Field Theory for Reinforced Concrete Elements Subjected to Shear", *ACI Journal*, Vol. 83, No. 2, 1986, pp. 219-231.

68. Vecchio, F. J. and Collins, M. P. "Predicting the Response of Reinforced Concrete Beams Subjected to Shear Using Modified Compression Field Theory", *ACI Structural Journal*, Vol. 85, No. 3, 1988, pp. 258-268.

69. Vecchio, F. J. "Nonlinear Finite Element Analysis of Reinforced Concrete Membranes", *ACI Structural Journal*, Vol. 86, No. 1, 1989, pp. 26-35.

70. Vecchio, F. J. and Bucci, F. "Analysis of Repaired Reinforced Concrete Structures", *Journal of Structural Engineering*, Vol. 125, No. 6, 1999, pp. 644-652.

71. Gan, Y. "Bond Stress and Slip Modeling in Nonlinear Finite Element Analysis of Reinforced Concrete Structures", *M.A.Sc Thesis*, University of Toronto, Canada, 2000, 250 p.

72. Ngo, D. and Scordelis, A. C. "Finite Element Analysis of Reinforced Concrete Beams", *ACI Journal*, Proceedings Vol. 64, No. 3, 1967, pp. 152-163.

73. Keuser, M. and Mehlhorn, G. "Finite Element Models for Bond Problems", *Journal of Structural Engineering*, Vol. 113, No. 10, 1987, pp. 2160-2173.

74. Mehlhorn, G. and Keuser, M. "Isoparametric Contact Elements for Analysis of Reinforced Concrete Structures", *Finite Element Analysis of Reinforced Concrete Structures*, Proceedings of Seminar, Tokyo, Japan, 1985, pp. 329-347.

75. Bresler, B. and Scordelis, A. C. "Shear Strength of Reinforced Concrete Beams", *Journal of the American Concrete Institute*, January 1963, pp. 51-72.

76. American Society for Testing and Materials. ASTM D 3039/D 3039M "Standard Test Method for Tensile Properties of Polymer Matrix Composite Materials", 2000.

77. Composite Retrofit International website: www.tyfosfibrwrap.com

78. Composite Retrofit International. Technical Data Sheets for TYFO S® Fibrwrap® System. (Supplied to the University of Toronto, 1998.)

79. Aprile, A., Spacone, E., and Limkatanyu, S. "Role of Bond in RC Beams Strengthened with Steel and FRP Plates", *Journal of Structural Engineering*, 2001 (in press).

80. El-Refaie, S. A., Ashour, A. F., and Garrity, S. W. "Strengthening of Reinforced Concrete Continuous Beams with CFRP Composites", *Structural Engineering, Mechanics and Computation*, Proceedings of the International Conference on Structural Engineering, Mechanics and Computation, Vol. 2, Cape Town, Africa, April 2001, pp. 1591-1598.

81. DeRose, D. and Sheikh, S. A. "Rehabilitation of a Concrete Structure Using Fibre Reinforced Plastics", *Research Report*, Department of Civil Engineering, University of Toronto, Toronto, Canada, 1997, 170 p.

82. CSA Standard A23.3-94. CPCA Concrete Design Handbook, 1995.

83. Sato, Y. "Report of FRP Sheet Bond Test", University of Toronto, 2001, 15 p.

84. American Society for Testing and Materials. ASTM D638 "Standard Test Method for Tensile Properties of Plastics", 1999.

APPENDIX A

CONCRETE

COMPRESSIVE STRESS-STRAIN CURVES

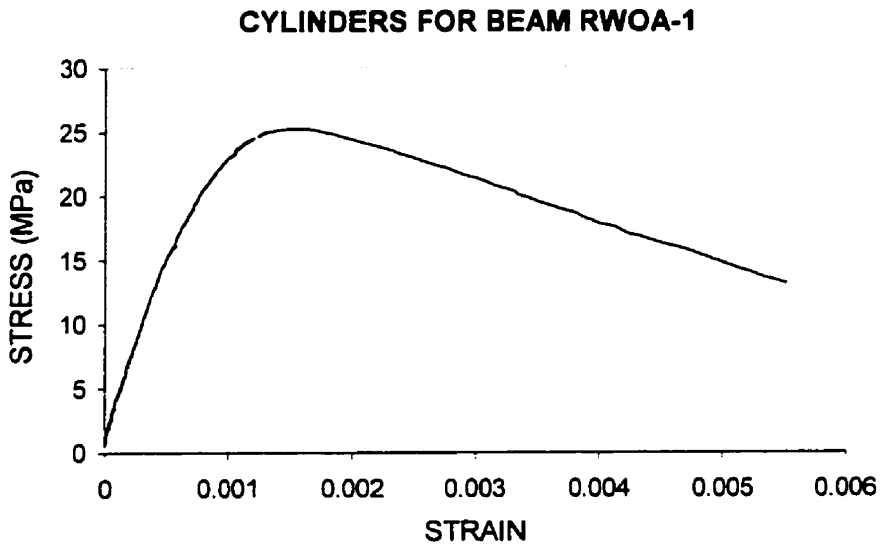

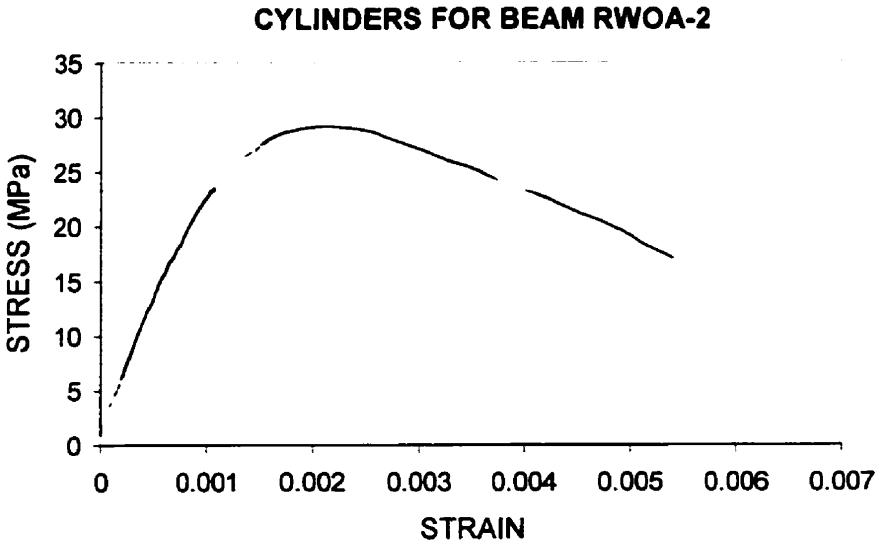

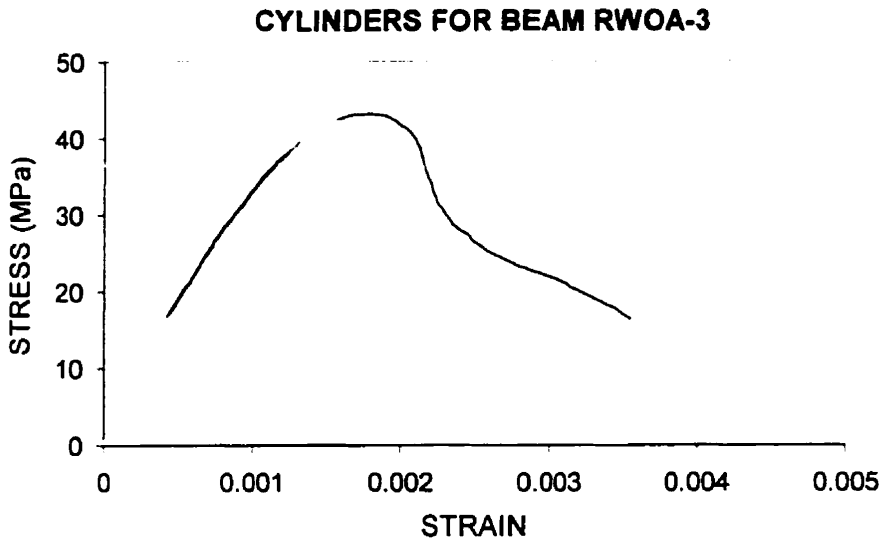

RAW DATA FROM CONCRETE CYLINDER COMPRESSION TESTS

Beam	Days After Casting	Peak Load (kN)	Concrete Strength (MPa)
RWOA-1	3	192	10.5
		195	10.7
	7	263	14.4
		250	13.7
	28	407	22.3
		416	22.8
RWOA-2	3	159	8.72
		166	9.10
	7	277	15.2
		276	15.2
	28	473	25.9
		472	25.9
RWOA-3	3	396	21.7
		384	21.1
	7	542	29.7
		522	28.6
	28	788	43.2
		800	43.9

*cross-sectional area of concrete cylinder = 18242mm^2

RAW DATA FROM CONCRETE CYLINDER TENSILE SPLITTING TESTS

Beam	Peak Load (kN)	Tensile Splitting Strength (MPa)
RWOA-1	160.6	2.27
	180.4	2.55
	136.1	1.92
	192.9	2.73
RWOA-2	272.1	3.85
	228.4	3.23
	211.4	2.99
	240.4	3.40
RWOA-3	249.2	3.53
	232.1	3.28
	197.1	2.79
	207.9	2.94

* length of cylinder (L) = 300 mm, diameter of cylinder (D) = 150 mm
* tensile splitting strength calculated as $2 \times P/(\pi \times L \times D)$

STEEL

TENSILE STRESS-STRAIN CURVES

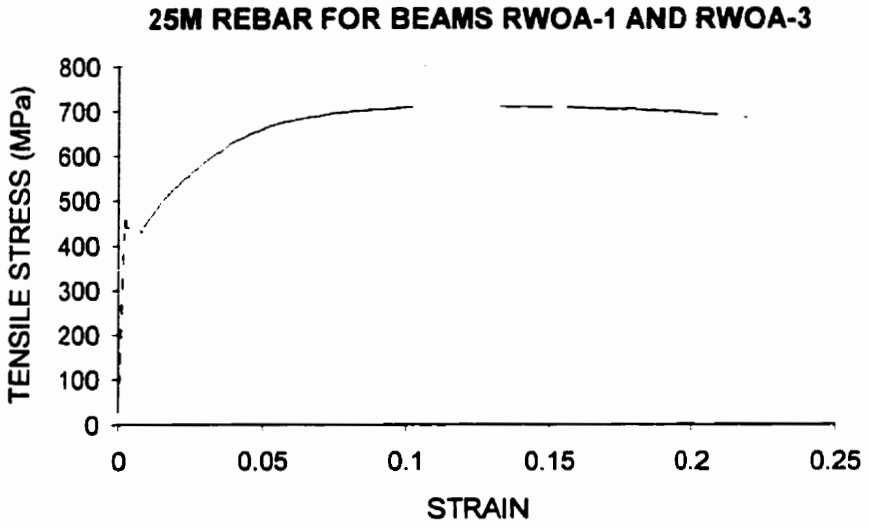

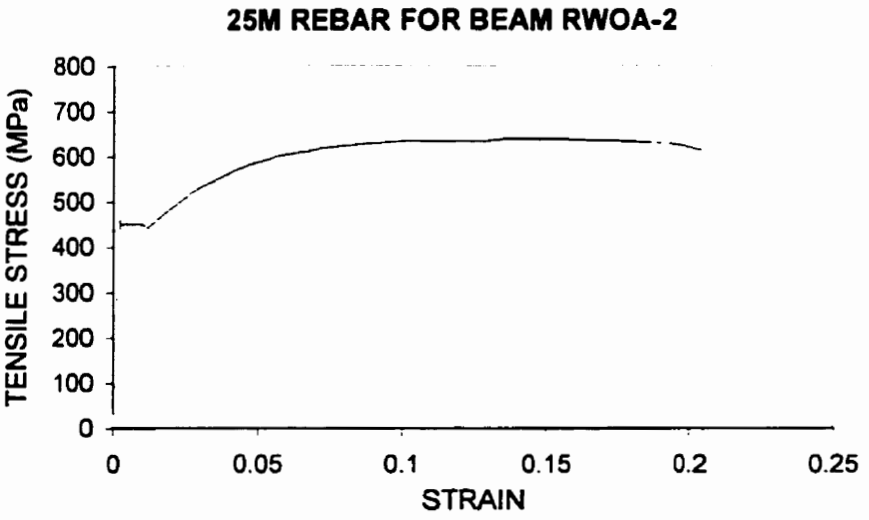

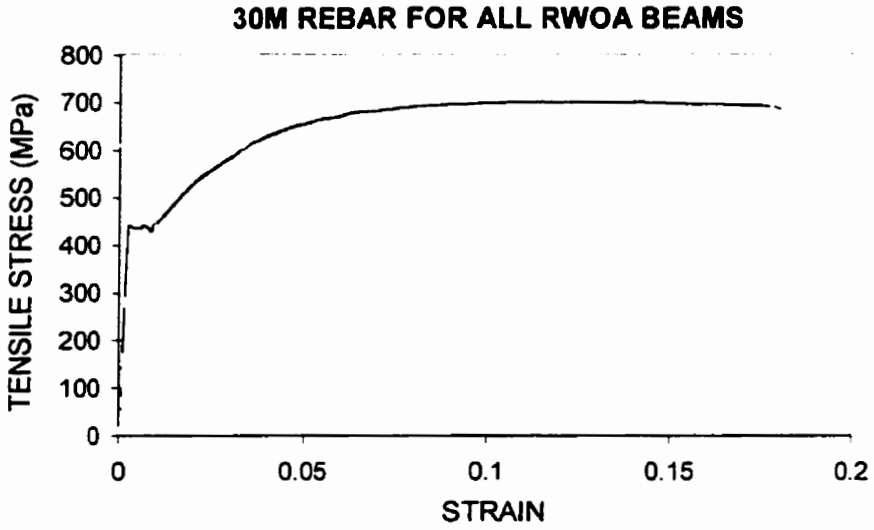
30M REBAR FOR ALL RWOA BEAMS
TENSILE STRESS (MPa)
800
700
600
500
400
300
200
100
0
0
0.05
0.1
0.15
0.2
STRAIN

CFRP

TENSILE STRESS-STRAIN CURVES

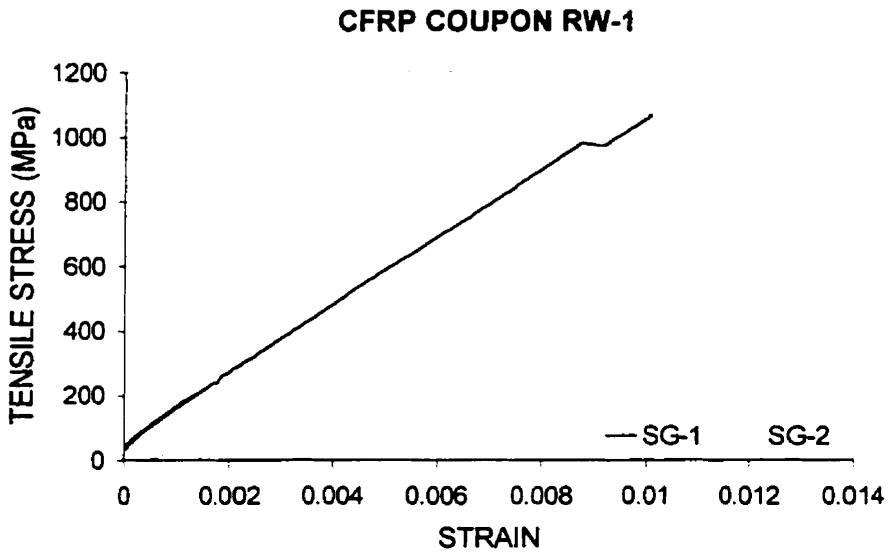

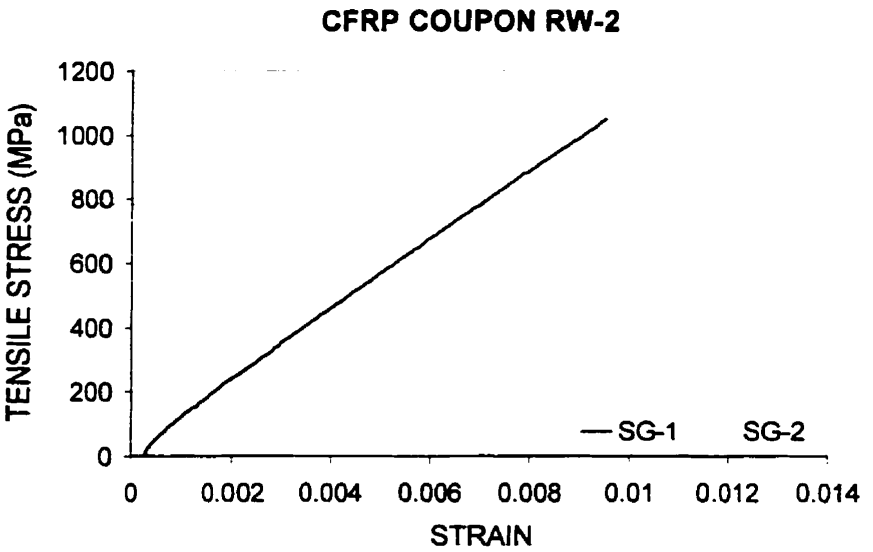

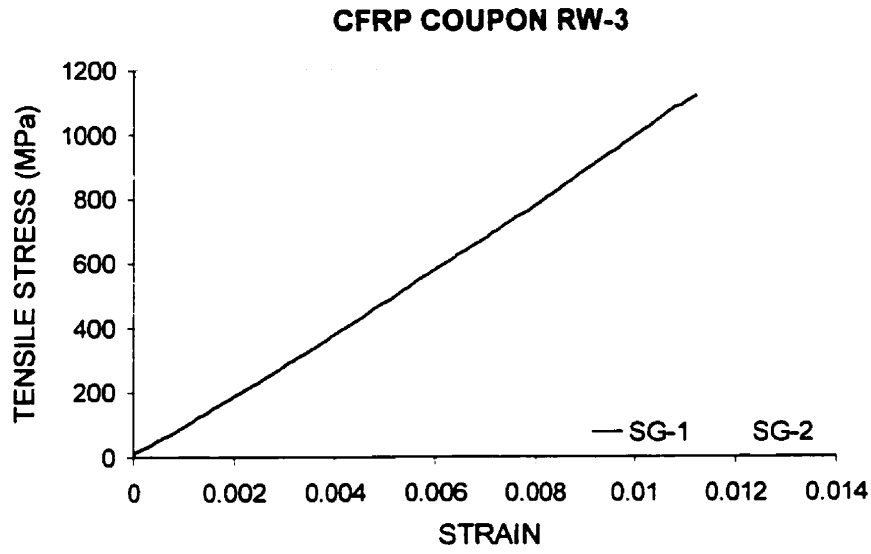
CFRP COUPON RW-3
TENSILE STRESS (MPa)
1200
1000
800
600
400
200
0
0
0.002
0.004
0.006
0.008
0.01
0.012
0.014
STRAIN
SG-1
SG-2

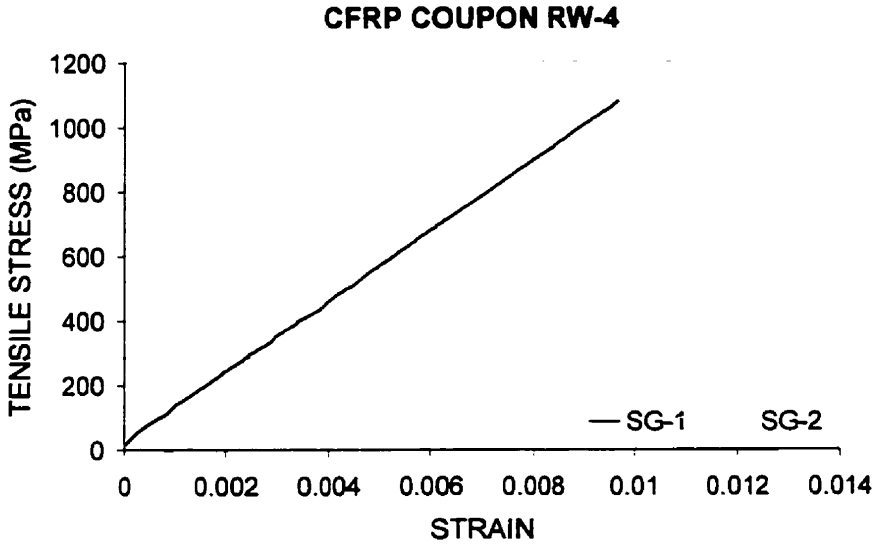
CFRP COUPON RW-4
TENSILE STRESS (MPa)
1200
1000
800
600
400
200
0
0
0.002
0.004
0.006
0.008
0.01
0.012
0.014
STRAIN
SG-1
SG-2

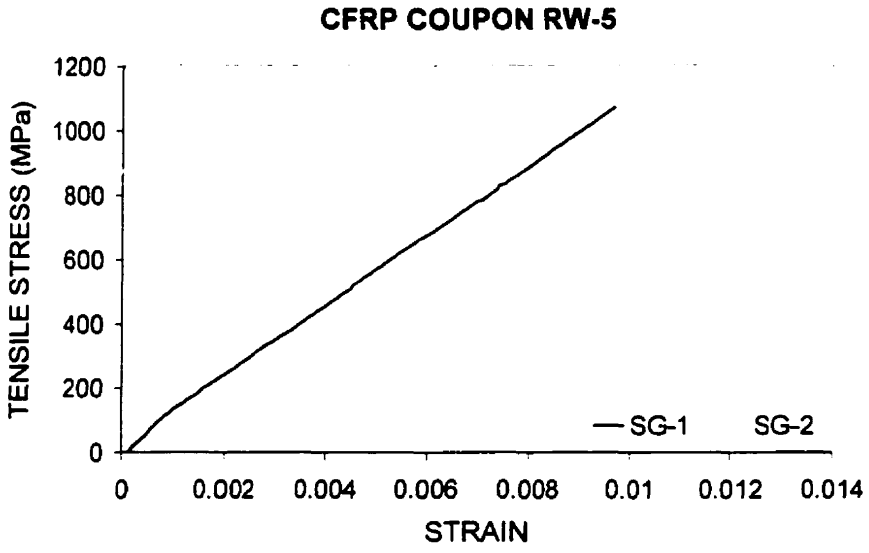

RAW DATA FROM CFRP COUPON TENSILE TESTS

Coupon	Failure Load (kN)	Force/Unit Width (N/mm)	Tensile Strength° (MPa)	Ultimate Strain*	Elastic Modulus† (GPa)
RW-1	68.2	897	1073	0.010675	98.5
RW-2	67.2	886	1060	0.010963	98.5
RW-3	71.8	948	1134	0.011322	100.4
RW-4	68.7	918	1098	0.011375	99.4
RW-5	68.2	905	1083	0.011119	100.8
Average	68.8	911	1090	0.011091	99.5

°based on average fabric thickness of 0.84 mm
*average of values measured by two strain gauges
†based on best linear fit of average strain values

PHOTOS FROM CFRP COUPON TENSILE TESTS

Coupon tested in MTS machine

Coupon RW-1

Coupon RW-2

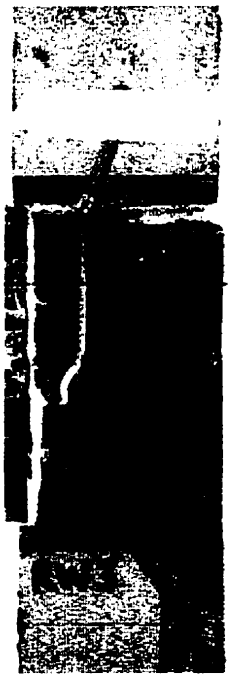

Coupon RW-3

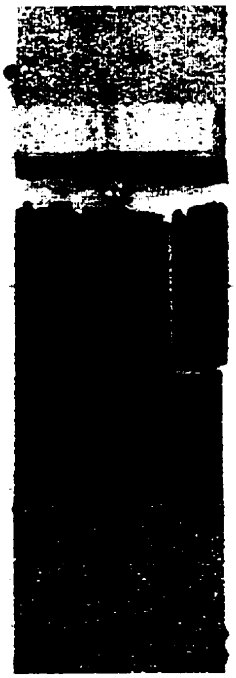

Coupon RW-4

Coupon RW-5

APPENDIX B

RWOA BEAMS: EXPERIMENTAL RESULTS

PHOTOS OF RWOA BEAMS AS TESTING PROGRESSED

BEAM RWOA-1:

Load = 340 kN (maximum load of beam TOA-1), mid-span displacement = 9.0 mm

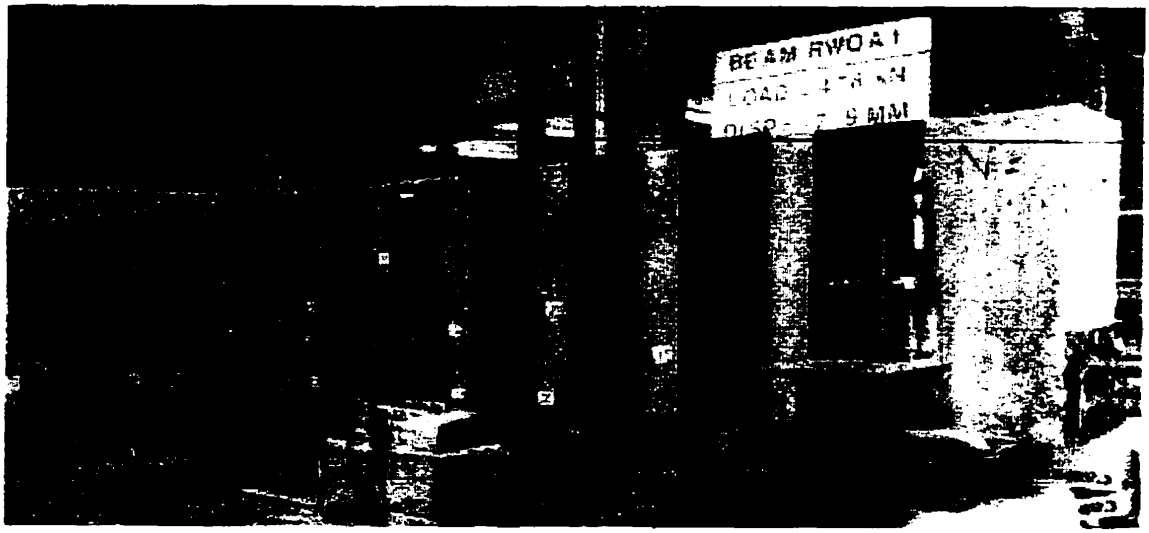

Load = 478 kN (just after yielding of flexural steel), mid-span displacement = 17.9 mm

BEAM RWOA-1 (continued):

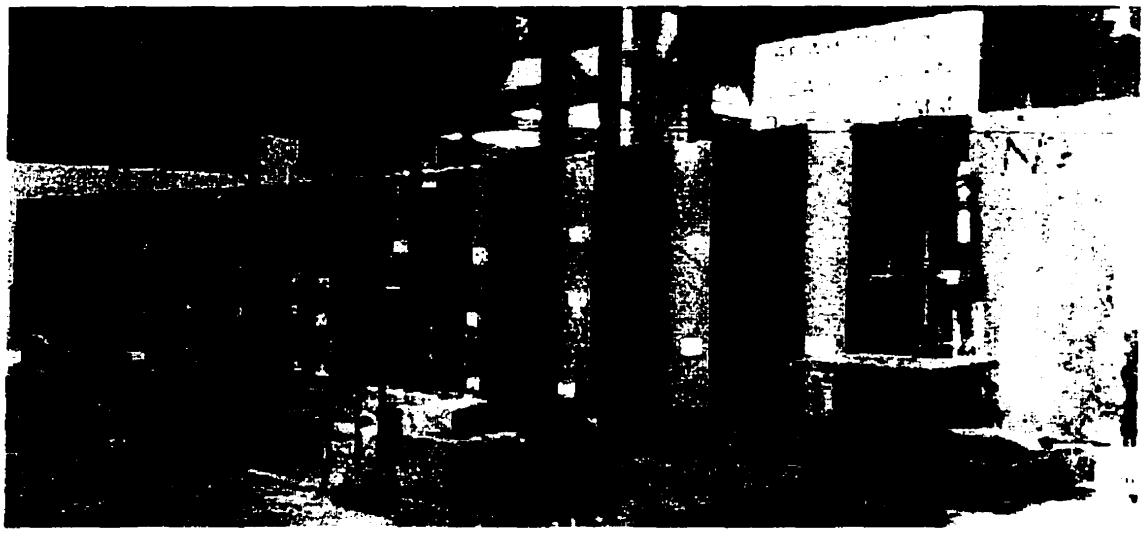

Load = 489 kN (just prior to failure), mid-span deflection = 35.0 mm

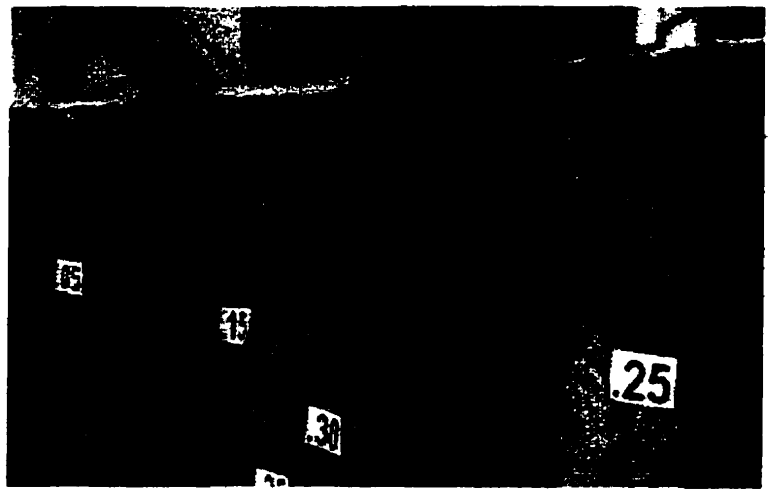

Concrete crushing and debonding near loading point, load = 489 kN (just prior to failure)

BEAM RWOA-2:

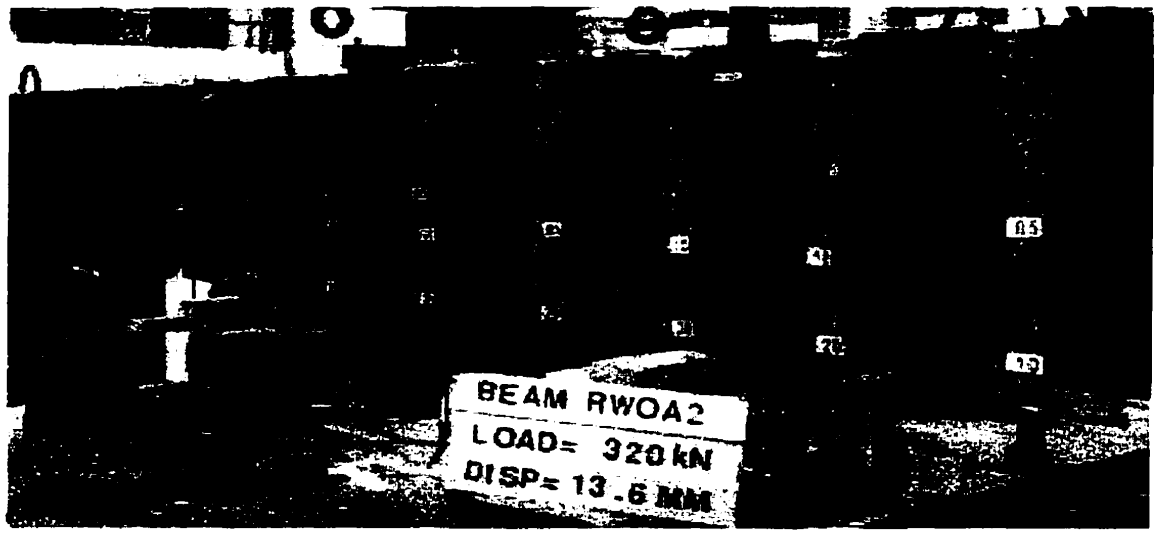

Load = 320 kN (maximum load of beam TOA-2), mid-span deflection = 13.6 mm

Load = 448 kN (just after yielding of flexural steel), mid-span displacement = 23.6 mm

BEAM RWOA-2 (continued):

Load = 457 kN (maximum load), mid-span deflection = 33.6 mm

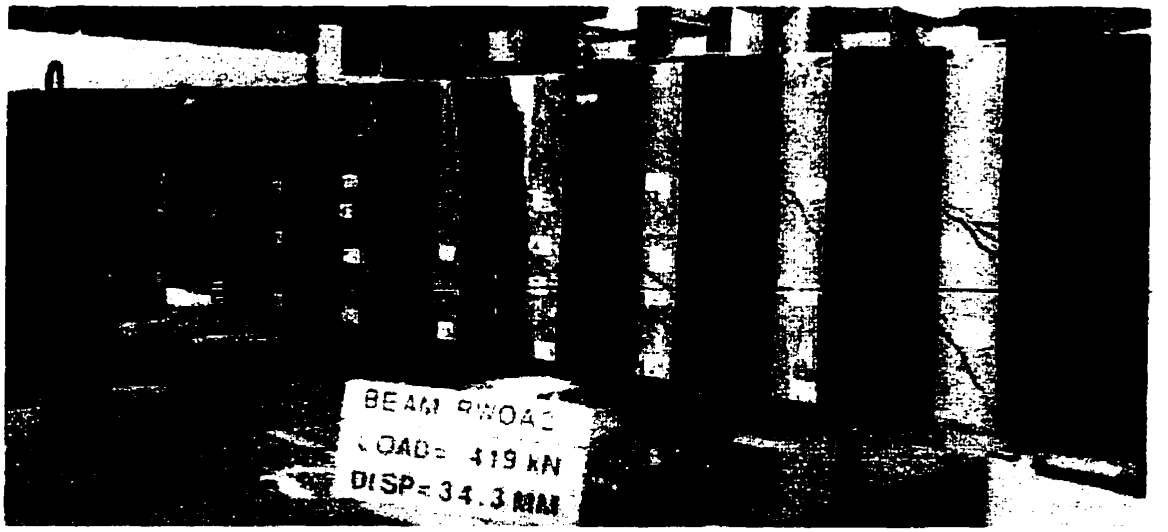

Load = 419 kN (just prior to failure), mid-span deflection = 34.3 mm

BEAM RWOA-3:

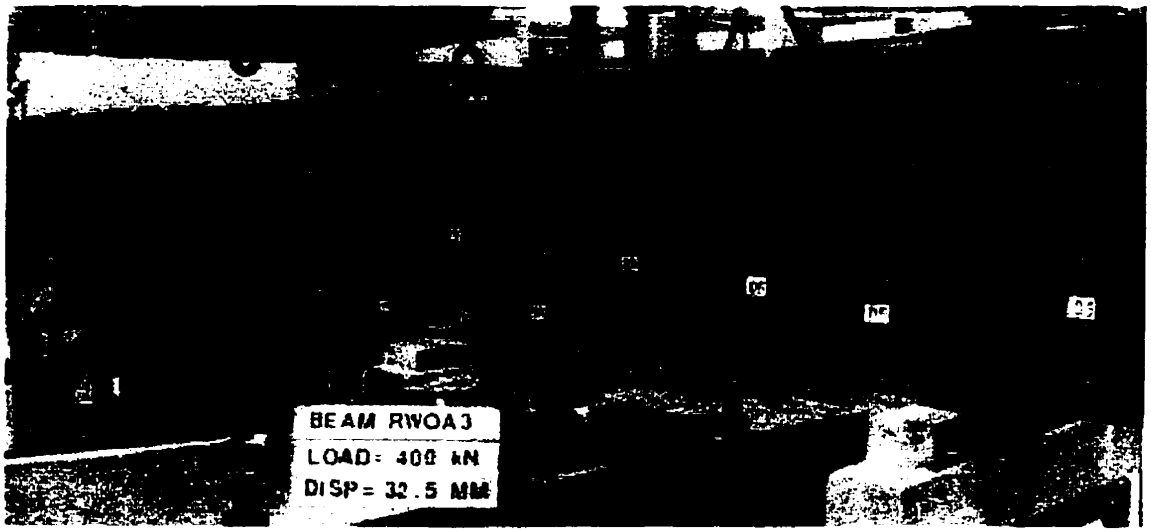

Load = 400 kN (near maximum load of beam TOA-3), mid-span deflection = 32.5 mm

Load = 420 kN (just after yielding of flexural steel), mid-span displacement = 35.5 mm

BEAM RWOA-3 (continued):

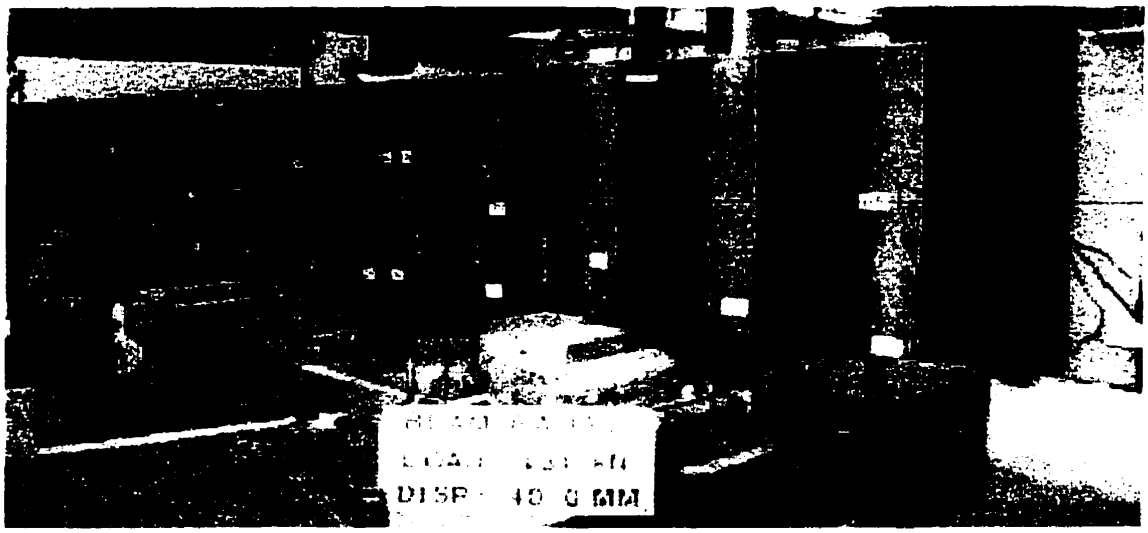

Load = 431 kN (approaching maximum load), mid-span deflection = 40.0 mm

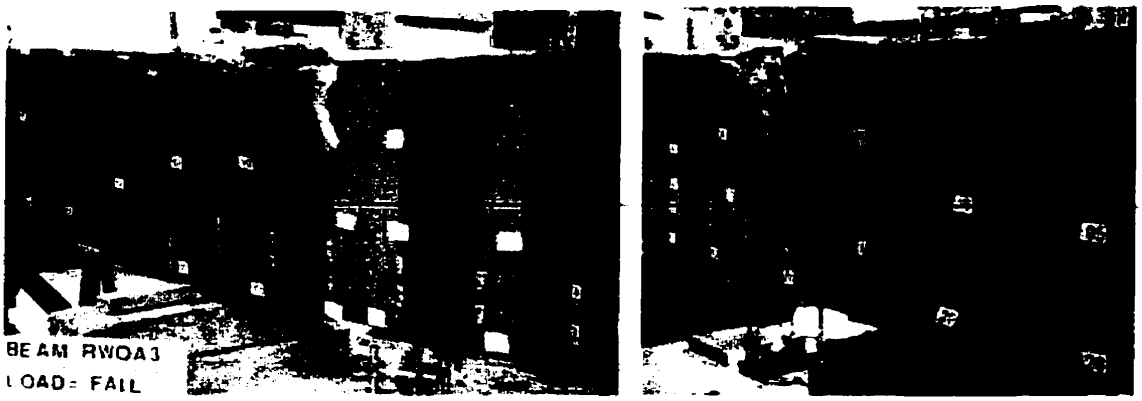

Concrete crushing and debonding of CFRP strips near loading point at failure

CRACK PATTERNS OF BEAMS

RWOA-1

RWOA-2

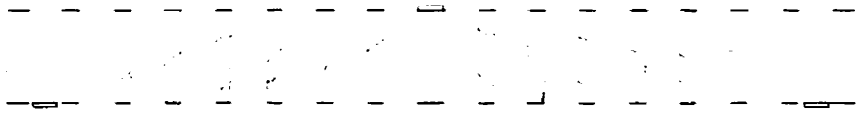

RWOA-3

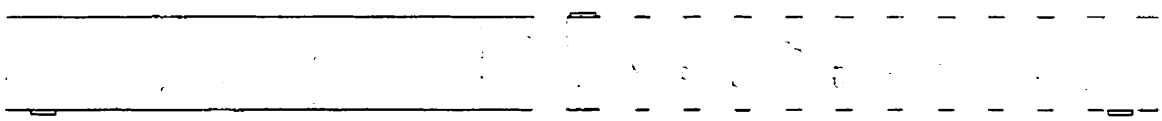

SURFACE STRAINS AT VARIOUS LOAD STAGES

- strains determined from displacements measured by 12 Zurich targets along the beam (6 at the top rebar level, 6 at the bottom rebar level)

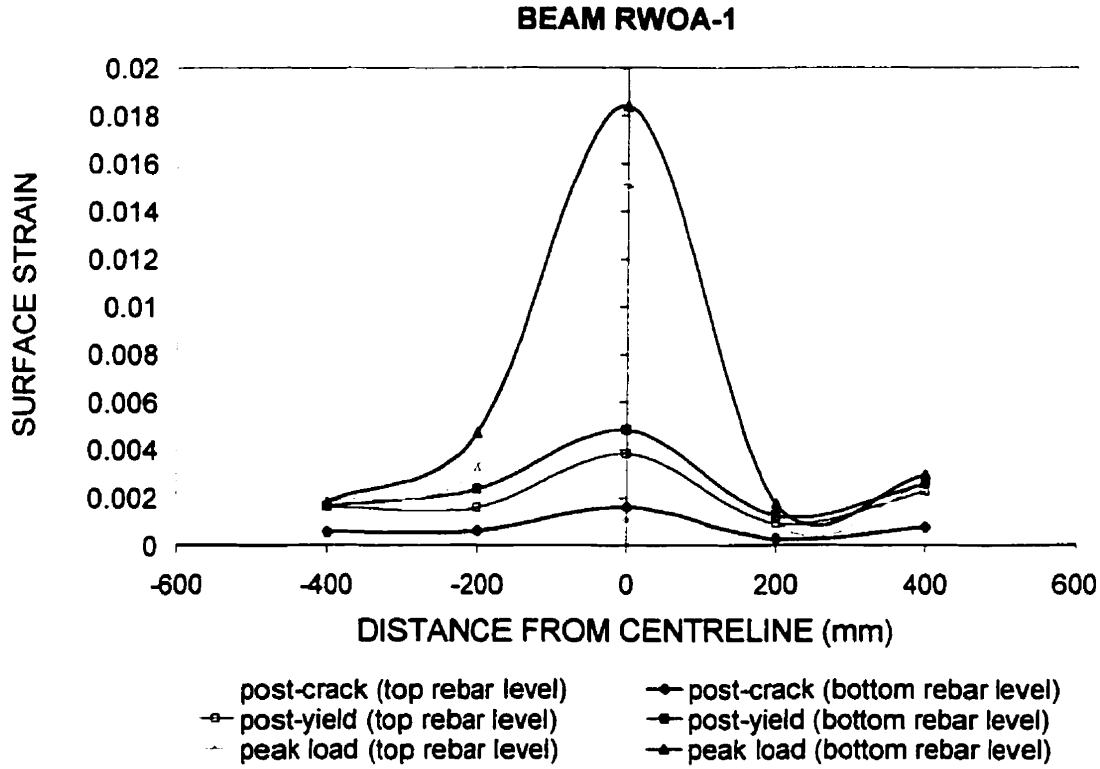

BEAM RWOA-2

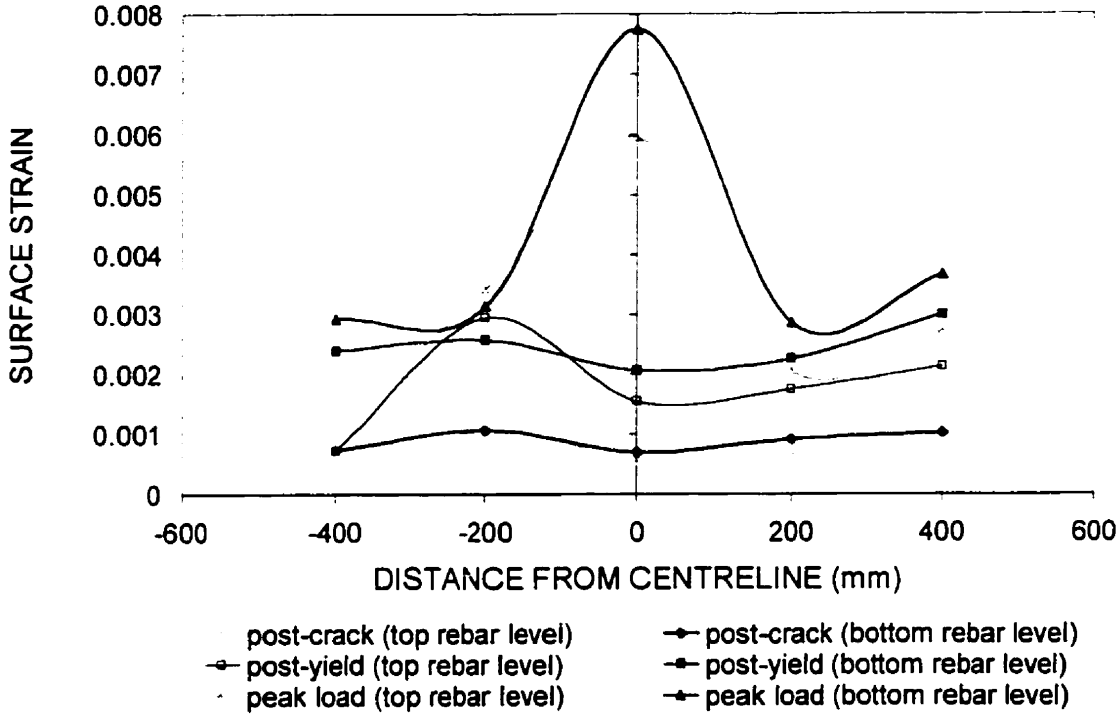

BEAM RWOA-3

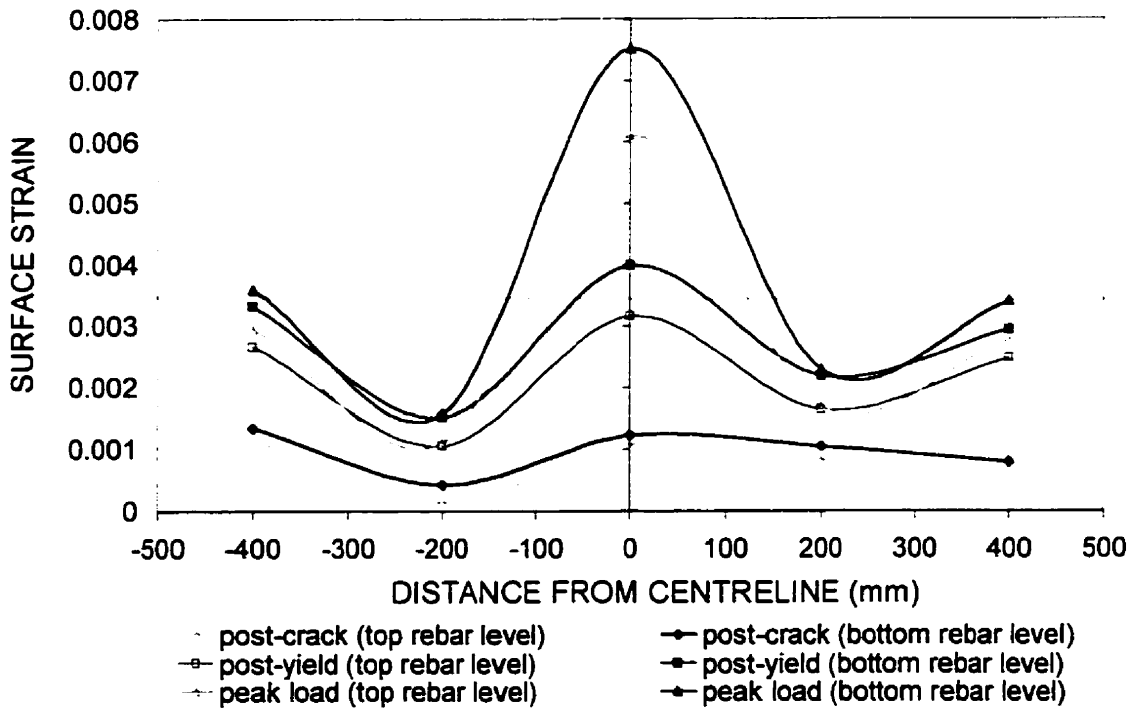

APPENDIX C

PREDICTED VALUES OF SHEAR CONTRIBUTION BY CFRP STRIPS IN RWOA BEAMS

Beam RWOA-1: $f'_c = 22.6$ MPa
Beam RWOA-2: $f'_c = 25.9$ MPa
Beam RWOA-2: $f'_c = 43.5$ MPa
Beam width (b) = 305 mm

FRP properties for all three beams:

$f_{fu} = 1090$ MPa
$E_f = 99.5$ GPa
$\varepsilon_{fu} = 0.011$
$t_f = 0.84$ mm
$w_f = 200$ mm
$s_f = 300$ mm

$d_f = 470$ mm
$d_s = 470$ mm
$A_f = 2 \times t_f \times w_f = 2 \times 0.84 \times 200 = 336$ mm^2
$\rho_f = A_f / (b \times s_f) = 336/(305 \times 300) = 0.00367$
$\rho_f \times E_f = 0.365 < 1.1$ GPa

Sample calculations will be given for beam RWOA-1:

Triantafillou:

$$\varepsilon_f = 0.0119 - 0.0205 \times 0.365 + 0.0104 \times 0.365^2 = 0.0058 \qquad \text{(Eqn. 2-23)}$$

$$V_f = \frac{0.9}{1.15} \times 0.365 \times 0.0058 \times 305 \times 470 \times \sin 90^\circ = \underline{238\text{kN}} \qquad \text{(Eqn. 2-22)}$$

Khalifa:

Effective stress method:

$$R = 0.5622 \times 0.365^2 - 1.2188 \times 0.365 + 0.778 = 0.408 \quad \leq 0.50 \qquad \text{(Eqn. 2-25)}$$

Bond mechanism:

$$L_e = e^{\left[6.134 - 0.58 \ln (0.84 \times 99.5)\right]} = 35.4 \text{ mm} \qquad \text{(Eqn. 2-27)}$$

$$w_{fe} = d_f - 2L_e = 470 - 2(35.4) = 399 \text{ mm} \qquad \text{(Fig. 2.42)}$$

$$R = \frac{0.0042 \times (22.6)^{2/3} \times 399}{(99.5 \times 0.84)^{0.58} \times 0.011 \times 470} = 0.199 \qquad \text{(governs)} \qquad \text{(Eqn. 2-26)}$$

$$f_{f,e} = R f_{f,u} = 0.199 \times 1090 = 217 \text{MPa}$$

$$V_f = \frac{336 \times 217 \times \sin 90^\circ \times 470}{300 \times 1000} = \underline{\underline{114.7 \text{kN}}} \qquad \text{(Eqn. 2-24)}$$

Triantafillou and Antonopoulos:

Debonding:

$$\varepsilon_{f,e} = 0.65 \left(\frac{22.6^{2/3}}{0.00367 \times 99.5} \right)^{0.56} \times 10^{-3} = 0.00366 \quad \text{(governs)} \qquad \text{(Eqn. 2-29b)}$$

FRP fracture:

$$\varepsilon_{f,e} = 0.17 \left(\frac{22.6^{2/3}}{0.00367 \times 99.5} \right)^{0.30} \times 0.011 = 0.0047 \qquad \text{(Eqn. 2-29b)}$$

$$\varepsilon_{k\,f,e} = 0.8 \times 0.00366 = 0.00293 \quad \leq 0.005$$

$$V_f = \frac{0.9}{1.3}(0.365 \times 0.00293 \times 305 \times 470) = \underline{106.1\text{kN}} \qquad \text{(Eqn. 2-22)}$$

ACI format:

$$\varepsilon_{f,e,A} = 0.9 \times \varepsilon_{f,e} = 0.9 \times 0.00366 = 0.00329 < 0.006$$

Debonding:

$$V_f = 0.75 \times 0.00329 \times 0.365 \times \sin 90^\circ \times 305 \times 470 = \underline{129.4\text{kN}} \qquad \text{(Eqn. 2-31)}$$

FRP fracture:

$$V_f = 0.80 \times 0.00329 \times 0.365 \times \sin 90^\circ \times 305 \times 470 = \underline{138\text{kN}} \qquad \text{(Eqn. 2-31)}$$

Schnerch:

$$\varepsilon_{f,e} = 0.0012 \frac{1}{0.0065}\left(\frac{22.6}{0.365}\right)^{0.75} \sqrt{\frac{\sin 90^\circ \times 470}{2 \times 470}} \times 10^{-3} = 0.00288 \qquad \text{(Eqn. 2-32)}$$

$$f_{f,e} = E_f \varepsilon_{f,e} = 99520 \times 0.00288 = 286\text{MPa}$$

$$V_f = \frac{336 \times 286 \times \sin 90^\circ \times 470}{300 \times 1000} = \underline{150.8\text{kN}} \qquad \text{(Eqn. 2-24)}$$

APPENDIX D

INPUT FILES FOR NUMERICAL ANALYSES WITH PROGRAM VECTOR2

The files provided herein are for analyses employing contact elements for the concrete-FRP interface. Notes for the .job, .s2r, and .l2r files are included with the files for the Žarnić slab strip only.

ŽARNIĆ SLAB STRIP (named as FLAT BEAM in the files):

```
************
* VECTOR   *
* JOB DATA *
************
```

Job Title (30 char. max.) : ZARNIC FLAT BEAM
Job File Name (8 char. max.) : ZFBCD
Date (30 char. max.) : Feb 7, 2001

STRUCTURE DATA

Structure Type : 2
File Name (8 char. max.) : ZFBC

LOADING DATA

No. of Load Stages : 141
Starting Load Stage No. : 1
Load Series ID (5 char. max.) : ZFBC

Load Case	File Name (8 char. max.)	Factors Initial	Final	LS-Inc	Type	Reps	C-Inc
1	ZFBD	0.000	70.000	0.500	1	1	0.000
2	SHRINK	1.000	1.000	0.000	1	1	0.000
3	NULL	0.000	40.000	0.500	1	1	0.000

ANALYSIS PARAMETERS

Seed File Name (8 char. max.) : NULL
Convergence Limit (factor > 1.0) : 1.000010
Averaging Factor (0.0 to 1.0) : 0.30
Maximum No. of Iterations : 100
Convergence Criteria : 1
Results Files : 2
Output Format : 1

MATERIAL BEHAVIOUR MODELS

Concrete Compression Base Curve (0-3) : 1
Concrete Compression Post-Peak (0-3) : 1

Concrete Compression Softening	(0-8) : 1
Concrete Tension Stiffening	(0-3) : 1
Concrete Tension Softening	(0-3) : 1
Concrete Tension Splitting	(0-1) : 1
Concrete Confined Strength	(0-2) : 1
Concrete Dilatation	(0-1) : 1
Concrete Cracking Criterion	(0-4) : 1
Concrete Crack Slip Check	(0-2) : 1
Concrete Crack Width Check	(0-2) : 1
Concrete Bond or Adhesion	(0-3) : 1
Concrete Hysteresis	(0-2) : 1
Reinforcement Hysteresis	(0-3) : 1
Reinforcement Dowel Action	(0-1) : 1
Reinforcement Buckling	(0-1) : 1
Element Strain Histories	(0-1) : 0
Element Slip Distortions	(0-4) : 1
Geometric Nonlinearity	(0-1) : 1

<<<NOTES>>> [As of Nov 14, 2000]

Structure Type:
1. Beam Section (2-D)
2. Plane Membrane (2-D)
3. Solid (3-D)
4. Shell
5. Plane Frame (2-D)
6. Space Frame (3-D)
7. Axisymmetric Solid
8. Axisymmetric Shell
9. Mixed Type

Concrete Compression Pre-Peak Response:
0. Linear
1. Nonlinear - Hognestad (Parabola)
2. Nonlinear - Popovics (High Strength)
3. Nonlinear - Hoshikuma Et Al

Concrete Compression Post-Peak Response:
0. Base Curve
1. Modified Park-Kent
2. Popovics
3. Hoshikuma Et Al

Concrete Compression Softening Model:
0. No compression softening
1. Vecchio 1992-A (e1/e2-Form)
2. Vecchio 1992-B (e1/e0-Form)
3. Vecchio-Collins 1982
4. Vecchio-Collins 1986

Concrete Tension Stiffening Model:
0. No tension stiffening
1. Modified Bentz
2. Vecchio 1982
3. Collins-Mitchell 1987
4. Bentz 1999
5. Izumo, Maekawa Et Al

Concrete Tension Softening:
0. Not Considered
1. Linear - No Residual
2. Linear - w/ Residual

3. Residual Only (10%)
4. Yamamoto 1999

Concrete Tension Splitting:
1. Not Considered
2. DeRoo 1995

Concrete Confinement Strength:
0. Strength enhancement neglected
1. Kupfer / Richart Model
2. Selby Model

Concrete Lateral Expansion:
0. Constant Poisson's ratio
1. Variable Poisson's ratio

Concrete Cracking Criterion:
0. Uniaxial cracking stress
1. Mohr-Coulomb (Stress)
2. Mohr-Coulomb (Strain)
3. CEB-FIP Model
4. Gupta 1998 Model

Concrete Crack Slip Check:
0. Crack shear check omitted
1. Vecchio-Collins 1986
2. Gupta 1998 Model

Concrete Crack Width Check:
0. Stability check omitted
1. Check based on 5 mm max crack width
2. Check based on 2 mm max crack width

Concrete Bond:
0. Perfect bond
1. Eligehausen Model
2. Gan Model
3. Harjli Model

Concrete Hysteretic Response:
0. No plastic offsets
1. Plastic offsets; linear loading/unloading
2. Plastic offsets; nonlinear loading/unloading
3. Plastic offsets; nonlinear w/ cyclic decay
4. Mander Model - Version 1
5. Mander Model - Version 2

Reinforcement Hysteretic Response:
0. Linear
1. Elastic-Plastic
2. Elastic-Plastic w/ Hardening
3. Seckin Model w/ Bauschinger Effect

Element Strain Histories:
0. Previous loading neglected
1. Previous loading considered

Element Slip Distortion:
0. Not considered
1. Stress Model (Walraven)
2. Stress Model (Maekawa)
3. Stress Model (Vecchio/Lai)
4. Hydrid-I Model
5. Hydrid-II Model
6. Hybrid-III Model
7. Rotation lag of 5 degrees
8. Rotation lag of 7.5 degrees
9. Rotation lag of 10 degrees

10. Rotation lag of 15 degrees

Convergence Criteria:

1. Secant Moduli - Weighted Average
2. Displacements - Weighted Average
3. Displacements - Maximum Value
4. Reactions - Weighted Average
5. Reactions - Maximum Value

Results File Storage:

1. ASCII and binary files
2. ASCII files only
3. Binary files only
4. Last load stage only

```
**************
* STRUCTURE  *
*   DATA     *
**************
```

STRUCTURAL PARAMETERS

Structure Title (30 char. max.)	: ZARNIC FLAT BEAM
Structure File Name (8 char. max.)	: ZFBC
No. of R.C. Material Types	: 1
No. of Steel Material Types	: 3
No. of Bond Material Types	: 2
No. of Rectangular Elements	: 847
No. of Triangular Elements	: 0
No. of Truss Bar Elements	: 219
No. of Linkage Elements	: 0
No. of Contact Elements	: 65
No. of Joints	: 1002
No. of Restraints	: 14

MATERIAL SPECIFICATIONS

(A) REINFORCED CONCRETE

<NOTE:> TO BE USED IN RECTANGULAR AND TRIANGULAR ELEMENTS ONLY

CONCRETE

MAT	Ns	T	fc	[ft	Ec	e0	Mu	Cc	Agg][	Sx	Sy]
TYP	#	mm	MPa	MPa	MPa	me		/C	mm	mm	mm
1	1	800	25.0	1.65	25000	2.0	0.15	0	10	300	120

/

REINFORCEMENT COMPONENTS

MAT	REF	DIR	As	Db	Fy	Fu	Es	Esh	esh	Cs	Dep
TYP	TYP	deg	%	mm	MPa	MPa	MPa	MPa	me	/C	me
1	1	90	0.05	6	400	550	210000	100	10.0	0	0

/

(B) STEEL

```
<NOTE:> TO BE USED FOR TRUSS ELEMENTS ONLY
MAT REF  AREA  Db   Fy   Fu   Es     Esh    esh  Cs  Dep
TYP TYP  mm2   mm   MPa  MPa  MPa    MPa    me   /C  me
1   1  339.0  9.0  500  560  210000 1000   10.0  0   0
2   1  157.0  1.0  500  560  210000 1000   10.0  0   0
3   3  120.0  0.1  2400 2400 150000 150000 16.0  0   0.385
/
```

(C) BOND

```
<NOTE:> TO BE USED FOR EXTERIOR/INTERIOR BONDED ELEMENTS
MAT REF [ Ao   Umax  Sm    Su ] [ CPF  Cmin  No.  HOOK ]
TYP TYP mm^2  MPa   mm    mm    0-1   mm    LYR  0/1
1   3   2275.0 3.0 0.001266 0.001266 0 0    0    0/
2   3   1960.0 3.0 0.001266 0.001266 0 0    0    0/
/
```

ELEMENT INCIDENCES

(A) RECTANGULAR ELEMENTS

```
<<<<< FORMAT >>>>>
ELMT INC1 INC2 INC3 INC4 [#ELMT d(ELMT) d(INC)] [#ELMT d(ELMT) d(INC)]/
  1   1  13  14   2  11  11  12  11  1  1/
122 133 146 147 134  11   1   1/
133 146 159 160 147  65  11  13  11  1  1/
/
```

(B) TRIANGULAR ELEMENTS

```
<<<<< FORMAT >>>>>
ELMT INC1 INC2 INC3  [ #ELMT d(ELMT) d(INC) ] [ #ELMT d(ELMT) d(INC)] /
/
```

(C) TRUSS ELEMENTS

```
<<<<< FORMAT >>>>>
ELMT INC1 INC2 [ #ELMT d(ELMT) d(INC)] [#ELMT d(ELMT) d(INC) ]/
 848   2  14 11 1 12  2  77 9/
 859 134 147 66 1 13  2  77 9/
1002 145 158 65 1 13/
/
```

(D) LINKAGE ELEMENTS

```
<<<<< FORMAT >>>>
ELMT INC1 INC2 [ #ELMT d(ELMT) d(INC) ] [ #ELMT d(ELMT) d(INC) ]
/
```

(E) CONTACT ELEMENTS

```
<<<<< FORMAT >>>>
ELMT INC1 INC2 INC3 INC4 [ #ELMT d(ELMT) d(INC) ] [ #ELMT d(ELMT) d(INC) ]
1067  145  146  158  159  65  1  13/
/
```

MATERIAL TYPE ASSIGNMENT

```
<<<<< FORMAT >>>>>
ELMT MAT ACT [ #ELMT d(ELMT)] [ #ELMT d(ELMT) ] /
  1   1   1  847  1/
848   1   1   77  1/
925   2   1   77  1/
```

```
1002 3  1  65 1/
1067 1  1  40 1/
1107 2  1  25 1/
/
                COORDINATES
                ***********
<NOTE:> UNITS: in OR mm
<<<<< FORMAT >>>>>
NODE X Y [ #NODES d(NODES)  d(X) d(Y) ] [ #NODES d(NODES)  d(X) d(Y) ] /
 1   0.0  0.0  10 12  17.5 0.0/
 2   0.0  15.0  10 12  17.5 0.0  10  1 0.0  10.0/
 12   0.0 120.0  10 12  17.5 0.0/
121  175.0  0.0   2 12  25.0 0.0/
122  175.0  15.0   2 12  25.0 0.0  10  1 0.0  10.0/
132  175.0 120.0   2 12  25.0 0.0/
145  225.0  0.0  40 13  22.75 0.0/
146  225.0  0.0  40 13  22.75 0.0/
147  225.0  15.0  40 13  22.75 0.0  10  1 0.0  10.0/
157  225.0 120.0  40 13  22.75 0.0/
665 1135.0  0.0  26 13  19.6  0.0/
666 1135.0  0.0  26 13  19.6  0.0/
667 1135.0  15.0  26 13  19.6  0.0  10  1 0.0  10.0/
677 1135.0 120.0  26 13  19.6  0.0/
/
              SUPPORT RESTRAINTS
              ******************
<NOTE:> CODE:  '0' FOR NOT RESTRAINED NODES AND '1' FOR RESTRAINED ONES
<<<<< FORMAT >>>>>
NODE  X-RST  Y-RST [ #NODE d(NODE) ] /
121  0  1/
990  1  0 13  1/
/

<<< STRUCTURE FILE NOTES >>>  [As of Nov 14, 2000]

(1)  DO NOT INSERT OR DELETE ANY LINE. EXCEPTION: INSERTION OF LINES IN
     THE SPACE PROVIDED FOR INPUT OF DATA. IN THIS CASE, LEAVE LINE WITH
     SLASH AFTER LAST DATA LINE

(2)  TABS, BLANKS OR COMMAS CAN BE USED TO SEPARATE DATA. DO NOT ENCLOSE
     ANY DATUM IN QUOTATION MARKS

(3)  NUMBER ELEMENTS IN THE STRUCTURE ACCORDING TO TYPE IN THE FOLLOWING
     ORDER: RECTANGULAR, TRIANGULAR, TRUSS, LINKAGE, CONTACT

(4)  DIMENSIONED FOR: 25 REINFORCED CONCRETE MATERIAL TYPES WITH 4
     POSSIBLE REINFORCEMENT COMPONENTS EACH, 25 STEEL MATERIAL TYPES,
     2000 ELEMENTS AND 2400 JOINTS

(5)  REINFORCEMENT/STEEL REFERENCE TYPES:
     '1' FOR DUCTILE STEEL REINFORCEMENT
     '2' FOR PRESTRESSING STEEL
     '3' FOR TENSION ONLY REINFORCEMENT
     '4' FOR COMPRESSION ONLY REINFORCEMENT

(6)  BOND MATERIAL REFERENCE TYPES:
     '1' FOR EMBEDDED DEFORMED REBARS
```

'2' FOR EMBEDDED SMOOTH REBARS
'3' FOR EXTERNALLY BONDED PLATES OR SHEETS

(7) INPUT DATA FOR BOND MATERIAL:
FOR EMBEDDED BARS:
CPF - Confinement Pressure Factor (0.0 < CPF < 1.0)
A confinement pressure of 7.5 MPa produces CPF of 1.0
Cmin - Minumum of clear cover or spacing between bars
LYR - Number of layers of reinforcement through depth
HOOK - '0' for no hook; '1' if bar has hook
FOR SURFACE BONDED PLATES/SHEETS:
Ao - Bonded surface area
Umax - Maximum bond stress
Sm - Slip at maximum bond stress
Su - Slip at ultimate

(8) ELEMENT ACTIVATION
'0' FOR DEACTIVATED ELEMENT
'1' FOR ACTIVATED ELEMENT

```
**************
* LOAD CASE  *
*    DATA    *
**************
```

LOAD CASE PARAMETERS
****

Structure Title (30 char. max.)	: ZARNIC
Load Case Title (30 char. max.)	: VERT DISP
Load Case File Name (8 char. max.)	: ZFBD
No. of Loaded Joints	: 0
No. of Prescribed Support Displacements	: 1
No. of Elements with Temperature Loads	: 0
No. of Elements with Concrete Prestrain	: 0
No. of Elements with Ingress Pressure	: 0

JOINT LOADS
****

<NOTE:> UNITS: KIPS OR KN
<<<<< FORMAT >>>>>
NODE Fx Fy [#NODE d(NODE) d(Fx) d(Fy)] /
/

SUPPORT DISPLACEMENTS
****

<NOTE:> UNITS: MM OR IN
<<<<< FORMAT >>>>>
JNT DOF DISPL [#JNT d(JNT)] /
677 2 -1.00/
/

TEMPERATURE LOADS
****

<NOTE:> UNITS: F OR C
<<<<< FORMAT >>>>>
ELMT TEMP [#ELMT d(ELMT) d(TEMP)] [#ELMT d(ELMT) d(TEMP)] /
/

CONCRETE PRESTRAINS
****
<NOTE:> UNITS: me
<<<<< FORMAT >>>>>
ELMT STRAIN [#ELMT d(ELMT) d(STRAIN)] [#ELMT d(ELMT) d(STRAIN)] /
/
INGRESS PRESSURES
****
<NOTE:> UNITS: MPa
<<<<< FORMAT >>>>>
ELMT PRESSURE [#ELMT d(ELMT) d(PRS)] [#ELMT d(ELMT) d(PRS)] /
/

<<< LOAD FILE NOTES >>> [As of Nov 14, 2000]

(1) DO NOT INSERT OR DELETE ANY LINE. EXCEPTION: INSERTION OF LINES IN THE SPACE PROVIDED FOR INPUT OF DATA. IN THIS CASE, LEAVE LINE WITH SLASH AFTER LAST DATA LINE

(2) TABS, BLANKS OR COMMAS CAN BE USED TO SEPARATE DATA. DO NOT ENCLOSE ANY DATUM IN QUOTATION MARKS

****
* LOAD CASE *
* DATA *
****

LOAD CASE PARAMETERS
****

Structure Title (30 char. max.) : ZARNIC
Load Case Title (30 char. max.) : SHRINKAGE
Load Case File Name (8 char. max.) : SHRINK
No. of Loaded Joints : 0
No. of Prescribed Support Displacements : 0
No. of Elements with Temperature Loads : 0
No. of Elements with Concrete Prestrain : 847
No. of Elements with Ingress Pressure : 0

JOINT LOADS
****
<NOTE:> UNITS: KIPS OR KN
<<<<< FORMAT >>>>>
NODE Fx Fy [#NODE d(NODE) d(Fx) d(Fy)] /
/
SUPPORT DISPLACEMENTS
****
<NOTE:> UNITS: MM OR IN
<<<<< FORMAT >>>>>
JNT DOF DISPL [#JNT d(JNT)] /
/
TEMPERATURE LOADS
****
<NOTE:> UNITS: F OR C

<<<<< FORMAT >>>>>
ELMT TEMP [#ELMT d(ELMT) d(TEMP)] [#ELMT d(ELMT) d(TEMP)] /
/

CONCRETE PRESTRAINS
****

<NOTE:> UNITS: me
<<<<< FORMAT >>>>>
ELMT STRAIN [#ELMT d(ELMT) d(STRAIN)] [#ELMT d(ELMT) d(STRAIN)] /
1 -0.4 847 1 0/
/

INGRESS PRESSURES
****

<NOTE:> UNITS: MPa
<<<<< FORMAT >>>>>
ELMT PRESSURE [#ELMT d(ELMT) d(PRS)] [#ELMT d(ELMT) d(PRS)] /
/

ŽARNIĆ BEAM:

****
* VECTOR *
* JOB DATA *
****

Job Title (30 char. max.) : ZARNIC BEAM
Job File Name (8 char. max.) : ZBCD
Date (30 char. max.) : Feb 19, 2001

STRUCTURE DATA

Structure Type : 2
File Name (8 char. max.) : ZBC

LOADING DATA

No. of Load Stages : 121
Starting Load Stage No. : 1
Load Series ID (5 char. max.) : ZBC

Load Case	File Name (8 char. max.)	Factors Initial	Final	LS-Inc	Type	Reps	C-Inc
1	ZBD	0.000	60.000	0.500	1	1	0.000
2	SHRINK	1.000	1.000	0.000	1	1	0.000
3	NULL	0.000	0.000	0.000	1	1	0.000

ANALYSIS PARAMETERS

Seed File Name (8 char. max.) : NULL
Convergence Limit (factor > 1.0) : 1.000010
Averaging Factor (0.0 to 1.0) : 0.50
Maximum No. of Iterations : 75
Convergence Criteria : 1
Results Files : 2
Output Format : 1

MATERIAL BEHAVIOUR MODELS

Concrete Compression Base Curve	(0-3) : 1
Concrete Compression Post-Peak	(0-3) : 1
Concrete Compression Softening	(0-8) : 1
Concrete Tension Stiffening	(0-3) : 1
Concrete Tension Softening	(0-3) : 1
Concrete Tension Splitting	(0-1) : 1
Concrete Confined Strength	(0-2) : 1
Concrete Dilatation	(0-1) : 1
Concrete Cracking Criterion	(0-4) : 1
Concrete Crack Slip Check	(0-2) : 1
Concrete Crack Width Check	(0-2) : 1
Concrete Bond or Adhesion	(0-3) : 1
Concrete Hysteresis	(0-2) : 1
Reinforcement Hysteresis	(0-3) : 1
Reinforcement Dowel Action	(0-1) : 1
Reinforcement Buckling	(0-1) : 1
Element Strain Histories	(0-1) : 0
Element Slip Distortions	(0-4) : 1
Geometric Nonlinearity	(0-1) : 1

STRUCTURE DATA

STRUCTURAL PARAMETERS

Structure Title (30 char. max.)	: ZARNIC BEAM
Structure File Name (8 char. max.)	: ZBC
No. of R.C. Material Types	: 2
No. of Steel Material Types	: 3
No. of Bond Material Types	: 3
No. of Rectangular Elements	: 588
No. of Triangular Elements	: 0
No. of Truss Bar Elements	: 140
No. of Linkage Elements	: 0
No. of Contact Elements	: 42
No. of Joints	: 693
No. of Restraints	: 15

MATERIAL SPECIFICATIONS

(A) REINFORCED CONCRETE

<NOTE:> TO BE USED IN RECTANGULAR AND TRIANGULAR ELEMENTS ONLY

CONCRETE

MAT Ns T fc [ft Ec e0 Mu Cc Agg][Sx Sy]

```
TYP #  mm  MPa  MPa  MPa  me      /C  mm  mm  mm
1  1 200  25.0  1.65 25000 2.0  0.15  0   10  0  0
2  1 200  25.0  1.65 25000 2.0  0.15  0   10  0  0
/
REINFORCEMENT COMPONENTS
----------
MAT REF DIR  As  Db  Fy  Fu  Es  Esh  esh  Cs  Dep
TYP TYP deg  %  mm  MPa MPa MPa MPa  me  /C  me
1   1  90 0.283 6.0 450 500 210000 1000 10.0 0  0
2   1  90 0.188 6.0 450 500 210000 1000 10.0 0  0
/
                (B) STEEL
                ---------
<NOTE:> TO BE USED FOR TRUSS ELEMENTS ONLY
MAT REF  AREA Db  Fy  Fu  Es  Esh  esh  Cs  Dep
TYP TYP  mm2  mm  MPa MPa MPa MPa  me  /C  me
1   1  339.0  12.0  450  550 210000  1000 10.0  0   0
2   1  226.0  12.0  450  550 210000  1000 10.0  0   0
3   3  60.0   0.1  2400 2400 150000 150000 16.0  0   0.193
/
                (C) BOND
                --------
<NOTE:> TO BE USED FOR EXTERIOR/INTERIOR BONDED ELEMENTS
MAT REF [ Ao  Umax  Sm  Su ] [ CPF  Cmin  No.  HOOK ]
TYP TYP mm^2  MPa  mm  mm  0-1  mm  LYR  0/1
1  3  1750.0  3.0 0.001266 0.001266  0   0   0/
2  3  2000.0  3.0 0.001266 0.001266  0   0   0/
3  3  1500.0  3.0 0.001266 0.001266  0   0   0/
/
              ELEMENT INCIDENCES
              ******************

            (A) RECTANGULAR ELEMENTS
            ------------------------
<<<<< FORMAT >>>>>
ELMT INC1 INC2 INC3 INC4 [#ELMT d(ELMT) d(INC)] [#ELMT d(ELMT) d(INC)]/
 1  1 14  15  2 6  12  13  12  1  1/
73  79  93  94  80 12  1  1/
85  93 107 108  94 42  12  14  12  1  1/
/
            (B) TRIANGULAR ELEMENTS
            -----------------------
<<<<< FORMAT >>>>>
ELMT INC1 INC2 INC3  [ #ELMT d(ELMT) d(INC) ] [ #ELMT d(ELMT) d(INC)] /
/
              (C) TRUSS ELEMENTS
              ------------------
<<<<< FORMAT >>>>>
ELMT INC1 INC2 [ #ELMT d(ELMT) d(INC)] [#ELMT d(ELMT) d(INC) ]/
589  2  15  6 1 13  2  49 10/
595  80  94 43 1 14  2  49 10/
687  92 106 42 1 14/
/
              (D) LINKAGE ELEMENTS
              --------------------
<<<<< FORMAT >>>>
ELMT INC1 INC2 [ #ELMT d(ELMT) d(INC) ] [ #ELMT d(ELMT) d(INC) ]
```

```
/
                (E) CONTACT ELEMENTS
                ____________________

<<<<< FORMAT >>>>
ELMT INC1 INC2 INC3 INC4 [ #ELMT d(ELMT) d(INC) ] [ #ELMT d(ELMT) d(INC) ]
729  92  93 106 107  42   1  14/
/
                MATERIAL TYPE ASSIGNMENT
                ************************
<<<<< FORMAT >>>>>
ELMT MAT ACT [ #ELMT d(ELMT)] [ #ELMT d(ELMT) ] /
  1   1   1  408  1/
409   2   1  180  1/
589   1   1   49  1/
638   2   1   49  1/
687   3   1   42  1/
729   1   1   26  1/
755   2   1/
756   3   1   15  1/
/
                  COORDINATES
                  ***********
<NOTE:> UNITS: in OR mm
<<<<< FORMAT >>>>>
NODE X Y [ #NODES d(NODES)  d(X) d(Y) ] [ #NODES d(NODES)  d(X) d(Y) ] /
  1   0   0   6  13  35   0/
  2   0  30   6  13  35   0  11   1   0  24/
 13   0 300   6  13  35   0/
 79 200   0/
 80 200  30  11   1   0  24/
 91 200 300/
 92 225   0  27  14  35   0   2   1   0   0/
 94 225  30  27  14  35   0  11   1   0  24/
105 225 300  27  14  35   0/
470 1175   0  16  14  30   0   2   1   0   0/
472 1175  30  16  14  30   0  11   1   0  24/
483 1175 300  16  14  30   0/
/
                SUPPORT RESTRAINTS
                ******************
<NOTE:> CODE:  '0' FOR NOT RESTRAINED NODES AND '1' FOR RESTRAINED ONES
<<<<< FORMAT >>>>>
NODE  X-RST  Y-RST [ #NODE d(NODE) ] /
  66   0   1/
 680   1   0  14  1/
/


                * * * * * * * * * * * * *
                *  L O A D   C A S E  *
                *     D A T A         *
                * * * * * * * * * * * * *

                 LOAD CASE PARAMETERS
                 ********************

Structure Title    (30 char. max.)              : ZARNIC BEAM
```

```
Load Case Title    (30 char. max.)          : VERT DISP
Load Case File Name  (8 char. max.)         : ZBD
No. of Loaded Joints                        : 0
No. of Prescribed Support Displacements     : 1
No. of Elements with Temperature Loads      : 0
No. of Elements with Concrete Prestrain     : 0
No. of Elements with Ingress Pressure       : 0

                  JOINT LOADS
                  ***********
<NOTE:> UNITS:  KIPS OR KN
<<<<< FORMAT >>>>>
NODE   Fx   Fy   [ #NODE d(NODE) d(Fx) d(Fy) ] /
/
               SUPPORT DISPLACEMENTS
               **********************
<NOTE:> UNITS: MM OR IN
<<<<< FORMAT >>>>>
JNT  DOF  DISPL  [ #JNT d(JNT) ] /
469  2   -1.00/
/
               TEMPERATURE LOADS
               *****************
<NOTE:> UNITS:  F OR C
<<<<< FORMAT >>>>>
ELMT   TEMP   [ #ELMT d(ELMT) d(TEMP) ] [ #ELMT d(ELMT) d(TEMP) ] /
/
               CONCRETE PRESTRAINS
               *******************
<NOTE:> UNITS:  me
<<<<< FORMAT >>>>>
ELMT  STRAIN   [ #ELMT d(ELMT) d(STRAIN) ] [ #ELMT d(ELMT) d(STRAIN) ]  /
/
               INGRESS PRESSURES
               *****************
<NOTE:> UNITS:  MPa
<<<<< FORMAT >>>>>
ELMT PRESSURE  [ #ELMT d(ELMT) d(PRS) ] [ #ELMT d(ELMT) d(PRS) ]  /
/


              *************
              * LOAD CASE *
              *   DATA    *
              *************

               LOAD CASE PARAMETERS
               ********************

Structure Title    (30 char. max.)          : ZARNIC BEAM
Load Case Title    (30 char. max.)          : SHRINKAGE
Load Case File Name  (8 char. max.)         : SHRINK
No. of Loaded Joints                        : 0
No. of Prescribed Support Displacements     : 0
No. of Elements with Temperature Loads      : 0
No. of Elements with Concrete Prestrain     : 588
No. of Elements with Ingress Pressure       : 0
```

```
                JOINT LOADS
                ***********
<NOTE:> UNITS: KIPS OR KN
<<<<< FORMAT >>>>>
NODE   Fx   Fy   [ #NODE d(NODE) d(Fx) d(Fy) ] /
/
              SUPPORT DISPLACEMENTS
              **********************
<NOTE:> UNITS: MM OR IN
<<<<< FORMAT >>>>>
JNT  DOF  DISPL   [ #JNT d(JNT) ] /
/
               TEMPERATURE LOADS
               *****************
<NOTE:> UNITS:  F OR C
<<<<< FORMAT >>>>>
ELMT   TEMP   [ #ELMT d(ELMT) d(TEMP) ] [ #ELMT d(ELMT) d(TEMP) ] /
/
              CONCRETE PRESTRAINS
              *******************
<NOTE:> UNITS:  me
<<<<< FORMAT >>>>>
ELMT  STRAIN   [ #ELMT d(ELMT) d(STRAIN) ] [ #ELMT d(ELMT) d(STRAIN) ] /
1   -0.2  588  1  0/
/
               INGRESS PRESSURES
               *****************
<NOTE:> UNITS:  MPa
<<<<< FORMAT >>>>>
ELMT PRESSURE  [ #ELMT d(ELMT) d(PRS) ] [ #ELMT d(ELMT) d(PRS) ]  /
/
```

EL-REFAIE SPECIMENS: (The structure file is provided for beam CB3 only.)

```
            ************
            *   VECTOR *
            * JOB DATA *
            ************

Job Title     (30 char. max.)       : CB3
Job File Name  ( 8 char. max.)      : CB3
Date          (30 char. max.)       : Nov 08, 2000

STRUCTURE DATA
--------------
Structure Type                      : 2
File Name     ( 8 char. max.)       : CB3

LOADING DATA
------------
No. of Load Stages                  : 51
Starting Load Stage No.             : 1
Load Series ID  ( 5 char. max.)     : CB3
```

Load Case	File Name (8 char. max.)	Factors Initial	Final	LS-Inc	Type	Reps	C-Inc
1	CBD	0.000	60.000	1.000	1	2	1.000
2	NULL	0.000	0.000	1.000	1	1	0.000
3	NULL	0.000	0.000	0.000	1	1	0.000

ANALYSIS PARAMETERS

Seed File Name (8 char. max.)	: NULL
Convergence Limit (factor > 1.0)	: 1.000010
Averaging Factor (0.0 to 1.0)	: 0.25
Maximum No. of Iterations	: 100
Convergence Criteria	: 2
Results Files	: 2
Output Format	: 1

MATERIAL BEHAVIOUR MODELS

Concrete Compression Base Curve	(0-3) : 1
Concrete Compression Post-Peak	(0-3) : 1
Concrete Compression Softening	(0-8) : 1
Concrete Tension Stiffening	(0-3) : 1
Concrete Tension Softening	(0-3) : 1
Concrete Tension Splitting	(0-1) : 1
Concrete Confined Strength	(0-2) : 1
Concrete Dilatation	(0-1) : 1
Concrete Cracking Criterion	(0-4) : 1
Concrete Crack Slip Check	(0-2) : 1
Concrete Crack Width Check	(0-2) : 1
Concrete Bond or Adhesion	(0-4) : 1
Concrete Hysteresis	(0-2) : 1
Reinforcement Hysteresis	(0-3) : 1
Reinforcement Dowel Action	(0-1) : 1
Reinforcement Buckling	(0-1) : 1
Element Strain Histories	(0-1) : 1
Element Slip Distortions	(0-4) : 1
Geometric Nonlinearity	(0-1) : 1

****
* STRUCTURE *
* DATA *
****

STRUCTURAL PARAMETERS
****

Structure Title (30 char. max.)	: BEAM CB3
Structure File Name (8 char. max.)	: CB3
No. of R.C. Material Types	: 3
No. of Steel Material Types	: 4
No. of Bond Material Types	: 1
No. of Rectangular Elements	: 1200
No. of Triangular Elements	: 0
No. of Truss Elements	: 480
No. of Linkage Elements	: 0

```
No. of Contact Elements                 : 240
No. of Joints                           : 1573
No. of Restraints                       : 15

                MATERIAL SPECIFICATIONS
                ***********************

                (A) REINFORCED CONCRETE
                -----------------------

<NOTE:> TO BE USED IN RECTANGULAR AND TRIANGULAR ELEMENTS ONLY

CONCRETE
--------
MAT Ns  T   fc [ ft   Ec    e0   Mu   Cc   Agg ][ Sx   Sy ]
TYP #   mm  MPa  MPa  MPa   me        /C   mm    mm   mm
 1  0 150. 40.6  4.40 35000 2.00  0.15   0    12   0.0  0.0
 2  1 150. 40.6  2.10 35000 2.00  0.15   0    12   0.0  0.0
 3  2 150. 80.0  80.0 40000 4.00  0.15   0    12   0.0  0.0
/
REINFORCEMENT COMPONENTS
-----------------------
MAT SRF DIR  As   Db  Fy   Fu   Es     Esh   esh  Cs  Dep
TYP TYP deg  %    mm  MPa  MPa  MPa    MPa   me   /C  me
 2   1  90. 0.377 6.0 308  600  200000 2000  5    0   0
 3   1   0. 10.0  6.0 400  600  200000 2000  5    0   0
 3   1  90. 10.0  6.0 400  600  200000 2000  5    0   0
/
                (B) STEEL
                ---------
<NOTE:> TO BE USED FOR TRUSS ELEMENTS ONLY
MAT REF  AREA  Db   Fy   Fu   Es     Esh  esh  Cs  Dep
TYP TYP  mm2   mm   MPa  MPa  MPa    MPa  me   /C  me
1   1    400.  16.  520  650  201000 5000 2.6  0   0
2   1    120.  1.2  2500 2501 150000 1500 16.7 0   0
3   1    77.2  0.7  3900 3901 240000 2400 16.3 0   0
4   1    0.01  1    10   10   200000 2000 5    0   0
/
                (C) BOND
                --------
<NOTE:> TO BE USED FOR EXTERIOR/INTERIOR BONDED ELEMENTS
MAT REF [ Ao   Umax  Sm   Su ] [ CPF  Cmin  No.  HOOK ]
TYP TYP mm^2  MPa   mm   mm   0-1   mm    LYR  0/1
1   3   3545  4.4  0.0024 0.0024 0    0.    1    0
/
                ELEMENT INCIDENCES
                ******************

                (A) RECTANGULAR ELEMENTS
                ------------------------
<<<<< FORMAT >>>>>
ELMT INC1 INC2 INC3 INC4  [ #ELMT d(ELMT) d(INC) ] [ #ELMT d(ELMT) d(INC) ] /
 1   2   15   16   3     120  1  13    10  120  1 /
/
                (B) TRIANGULAR ELEMENTS
                -----------------------
<<<<< FORMAT >>>>>
ELMT INC1 INC2 INC3  [ #ELMT d(ELMT) d(INC)] [ #ELMT d(ELMT) d(INC) ] /
```

```
/
                (C) TRUSS ELEMENTS
                ------------------
<<<<< FORMAT >>>>>
ELMT INC1 INC2 [ #ELMT d(ELMT) d(INC)] [ #ELMT d(ELMT) d(INC) ] /
1201  4 17 120 1 13 /
1321 10 23 120 1 13 /
1441  1 14 120 1 13 /
1561 13 26 120 1 13 /
/
                (D) LINKAGE ELEMENTS
                --------------------
<<<<< FORMAT >>>>
ELMT INC1 INC2 [ #ELMT d(ELMT) d(INC) ] [ #ELMT d(ELMT) d(INC) ]
/
                (E) CONTACT ELEMENTS
                --------------------
<<<<< FORMAT >>>>
ELMT INC1 INC2 INC3 INC4 [ #ELMT d(ELMT) d(INC) ] [ #ELMT d(ELMT) d(INC) ]
1681  1  2 14 15  120 1  13 /
1801 12 13 25 26  120 1  13 /
/
                MATERIAL TYPE ASSIGNMENT
                ************************
<<<<< FORMAT >>>>>
ELMT  MAT  ACT  [ #ELMT d(ELMT)] [ #ELMT d(ELMT) ] /
  4  1  1  119 1 /
 121  2  1  120 1  8  120 /
1081  1  1   52 1 /
1137  1  1   64 1 /
  1  3  1    3 1 /
1133  3  1    4 1 /

1201  1  1  120 1  2  120 /

1441  4  1    3 1 /
1444  2  1  100 1 /
1544  4  1   17 1 /
1561  4  1   35 1 /
1596  4  1   85 1 /

1681  1  1  120 1  2  120 /
/
                COORDINATES
                ***********
<NOTE:> UNITS: in OR mm
<<<<< FORMAT >>>>>
NODE X Y  [ #NODES d(NODES)  d(X) d(Y) ] [ #NODES d(NODES)  d(X) d(Y) ] /
  1   0.   0.  121  13  35.45  0. /
  2   0.   0.  121  13  35.45  0.   2  1  0.0  20.00 /
  4   0.  40.  121  13  35.45  0.   6  1  0.0  28.33 /
 10   0. 210.  121  13  35.45  0.   3  1  0.0  20.00 /
 13   0. 250.  121  13  35.45  0. /
/
                SUPPORT RESTRAINTS
                ******************
<NOTE:> CODE:  '0' FOR NOT RESTRAINED NODES AND '1' FOR RESTRAINED ONES
```

```
<<<<< FORMAT >>>>>
NODE  X-RST  Y-RST [ #NODE d(NODE) ] /
  1 1 0 /
  2 1 1 /
  3 1 0 11 1 /
1406 0 1 /
/
```

LOAD CASE DATA

LOAD CASE PARAMETERS

Structure Title (30 char. max.)	: CB Beams
Load Case Title (30 char. max.)	: 1 MM
Load Case File Name (8 char. max.)	: CBD
No. of Loaded Joints	: 0
No. of Prescribed Support Displacements	: 1
No. of Elements with Temperature Loads	: 0
No. of Elements with Concrete Prestrain	: 0
No. of Elements with Ingress Pressure	: 0

JOINT LOADS

```
<NOTE:> UNITS:  KIPS OR KN
<<<<< FORMAT >>>>>
NODE   Fx   Fy   [ #NODE d(NODE) d(Fx) d(Fy) ] /
/
```

SUPPORT DISPLACEMENTS

```
<NOTE:> UNITS: MM OR IN
<<<<< FORMAT >>>>>
JNT  DOF  DISPL   [ #JNT d(JNT) ] /
714   2   -1.0 /
/
```

TEMPERATURE LOADS

```
<NOTE:> UNITS:  F OR C
<<<<< FORMAT >>>>>
ELMT   TEMP   [ #ELMT d(ELMT) d(TEMP) ] [ #ELMT d(ELMT) d(TEMP) ] /
/
```

CONCRETE PRESTRAINS

```
<NOTE:> UNITS:  me
<<<<< FORMAT >>>>>
ELMT  STRAIN   [ #ELMT d(ELMT) d(STRAIN) ] [ #ELMT d(ELMT) d(STRAIN) ] /
/
```

INGRESS PRESSURES

```
<NOTE:> UNITS:  MPa
<<<<< FORMAT >>>>>
ELMT PRESSURE  [ #ELMT d(ELMT) d(PRS) ] [ #ELMT d(ELMT) d(PRS) ]  /
/
```

DE ROSE SLAB: (The structure file is provided for the CFRP-repaired slab only; CFRP properties are replaced with GFRP properties for the GFRP-repaired slab.)

Control slab:

```
************
* VECTOR   *
* JOB DATA *
************
```

Job Title (30 char. max.) : DEROSE SLAB
Job File Name (8 char. max.) : DRS
Date (30 char. max.) : MAR 7, 2001

STRUCTURE DATA

Structure Type : 2
File Name (8 char. max.) : DRS

LOADING DATA

No. of Load Stages : 61
Starting Load Stage No. : 1
Load Series ID (5 char. max.) : DRS

Load Case	File Name (8 char. max.)	Factors Initial	Final	LS-Inc	Type	Reps	C-Inc
1	DRS	0.000	6.000	0.100	1	1	0.000
2	SHRINK	1.000	1.000	0.000	1	1	0.000
3	NULL	0.000	0.000	0.500	1	1	0.000

ANALYSIS PARAMETERS

Seed File Name (8 char. max.) : NULL
Convergence Limit (factor > 1.0) : 1.00001
Averaging Factor (0.0 to 1.0) : 0.30
Maximum No. of Iterations : 100
Convergence Criteria : 1
Results Files : 1
Output Format : 1

MATERIAL BEHAVIOUR MODELS

Concrete Compression Base Curve (0-3) : 1
Concrete Compression Post-Peak (0-3) : 1
Concrete Compression Softening (0-8) : 1
Concrete Tension Stiffening (0-3) : 1
Concrete Tension Softening (0-3) : 1
Concrete Tension Splitting (0-1) : 1
Concrete Confined Strength (0-2) : 1
Concrete Dilatation (0-1) : 1
Concrete Cracking Criterion (0-4) : 1
Concrete Crack Slip Check (0-2) : 1
Concrete Crack Width Check (0-2) : 1
Concrete Bond or Adhesion (0-3) : 1

Concrete Hysteresis	(0-2) : 1
Reinforcement Hysteresis	(0-3) : 1
Reinforcement Dowel Action	(0-1) : 1
Reinforcement Buckling	(0-1) : 1
Element Strain Histories	(0-1) : 0
Element Slip Distortions	(0-4) : 0
Geometric Nonlinearity	(0-1) : 1

STRUCTURE DATA

STRUCTURAL PARAMETERS

Structure Title (30 char. max.)	: DEROSE SLAB
Structure File Name (8 char. max.)	: DRS
No. of R.C. Material Types	: 2
No. of Steel Material Types	: 8
No. of Bond Material Types	: 6
No. of Rectangular Elements	: 474
No. of Triangular Elements	: 0
No. of Truss Bar Elements	: 701
No. of Linkage Elements	: 0
No. of Contact Elements	: 617
No. of Joints	: 1090
No. of Restraints	: 31

MATERIAL SPECIFICATIONS

(A) REINFORCED CONCRETE

<NOTE:> TO BE USED IN RECTANGULAR AND TRIANGULAR ELEMENTS ONLY

CONCRETE

MAT	Ns	T	fc	[ft	Ec	e0	Mu	Cc	Agg][	Sx	Sy]
TYP	#	mm	MPa	MPa	MPa	me		/C	mm	mm	mm
1	0	1200	53.9	2.42	40400	2.67	0.15	0	20	250	250
2	0	1200	0.1	2.42	2000	0.1	0.15	0	20	250	250

/

REINFORCEMENT COMPONENTS

MAT	REF	DIR	As	Db	Fy	Fu	Es	Esh	esh	Cs	Dep
TYP	TYP	deg	%	mm	MPa	MPa	MPa	MPa	me	/C	me

/

(B) STEEL

<NOTE:> TO BE USED FOR TRUSS ELEMENTS ONLY

MAT	REF	AREA	Db	Fy	Fu	Es	Esh	esh	Cs	Dep
TYP	TYP	mm2	mm	MPa	MPa	MPa	MPa	me	/C	me
1	1	400	11.3	458	692	200000	2000	15.0	0	0/
2	1	300	1.0	458	692	200000	2000	15.0	0	0/
3	3	1200	0.1	945	945	80300	80300	11.8	0	0/

```
4  3   87.5   0.1  945 945 80300  80300 11.8 0   0/
5  3    55    0.1  945 945 80300  80300 11.8 0   0/
6  3   27.5   0.1  945 945 80300  80300 11.8 0   0/
7  3    25    0.1  90  90  5500   5500 16.4 0   0/
8  3    50    0.1  90  90  5500   5500 16.4 0   0/
/
```

(C) BOND

```
<NOTE:> TO BE USED FOR EXTERIOR/INTERIOR BONDED ELEMENTS
MAT REF [ Ao   Umax  Sm   Su ] [ CPF  Cmin   No.  HOOK ]
TYP TYP mm^2  MPa   mm   mm    0-1   mm    LYR   0/1
1   3  30000   4.4 0.0075 0.50   0   0   0  0
2   3 2187.5   4.4 0.0075 0.50   0   0   0  0
3   3   1375   4.4 0.0075 0.50   0   0   0  0
4   3  687.5   4.4 0.0075 0.50   0   0   0  0
5   3    750   4.4 0.0075 0.50   0   0   0  0
6   3   1500   4.4 0.0075 0.50   0   0   0  0
/
```

ELEMENT INCIDENCES

(A) RECTANGULAR ELEMENTS

```
<<<<< FORMAT >>>>>
ELMT INC1 INC2 INC3 INC4 [#ELMT d(ELMT) d(INC)] [#ELMT d(ELMT) d(INC)]/
  1   1  11  12  2   9  9   10 9  1  1/
 82  91 101 104 92/
 83  92 104 107 93/
 84  93 107 110 94/
 85  94 110 113 95/
 86  95 113 116 96/
 87  96 116 119 97/
 88  97 119 122 98/
 89  98 122 125 99/
 90  99 125 128 100/
 91 101 131 134 104  32  9  30  9  1  3/
379 101 131 134 104  32  1  30  3 32  3/
/
```

(B) TRIANGULAR ELEMENTS

```
<<<<< FORMAT >>>>>
ELMT INC1 INC2 INC3  [ #ELMT d(ELMT) d(INC) ] [ #ELMT d(ELMT) d(INC)] /
/
```

(C) TRUSS ELEMENTS

```
<<<<< FORMAT >>>>>
ELMT INC1 INC2 [ #ELMT d(ELMT) d(INC)] [#ELMT d(ELMT) d(INC) ]/
475  2 12  9  1 10  2 42  6/
484 92 104/
526 98 122/
485 104 134 32  1 30  2 42 18/
559 102 132 32  1 30 10 32  3/
879 103 106  9  1  3 33  9 30/
/
```

(D) LINKAGE ELEMENTS

```
<<<<< FORMAT >>>>
```

```
ELMT INC1 INC2 [ #ELMT d(ELMT) d(INC) ] [ #ELMT d(ELMT) d(INC) ]
/
```

(E) CONTACT ELEMENTS

```
<<<<< FORMAT >>>>
ELMT INC1 INC2 INC3 INC4 [ #ELMT d(ELMT) d(INC) ] [ #ELMT d(ELMT) d(INC) ]
1176 101 102 131 132  32  1  30  10 32  3/
1496 101 103 104 106   9  1   3  33  9 30/
/
```

MATERIAL TYPE ASSIGNMENT

```
<<<<< FORMAT >>>>>
ELMT MAT ACT [ #ELMT d(ELMT)] [ #ELMT d(ELMT) ] /
  1   1 1   90  1/
 91   1 1    3  1 32   9/
 94   1 1    6  1 32   9/
379   2 0   96  1/
475   1 1   42  1/
517   2 1   42  1/
559   3 0   32  1/
591   4 0   32  1/
623   5 0   32  1  8  32/
847   6 0   32  1/
879   7 0    9  i  2 288/
888   8 0    9  1 31   9/
1176  1 0   32  1/
1208  2 0   32  1/
1240  3 0   32  1  7  32/
1464  4 0   32  1/
1496  5 0    2 288/
1497  4 0    8  1  2 288/
1505  6 0   31  9/
1506  3 0    8  1 31   9/
/
```

COORDINATES

```
<NOTE:> UNITS: in OR mm
<<<<< FORMAT >>>>>
NODE X Y [ #NODES d(NODES)  d(X) d(Y) ] [ #NODES d(NODES)  d(X) d(Y) ] /
  1   0  0   10  10  25  0/
  2   0 30   10  10  25  0  9  1  0  27.5/
101 250  0   33  30  25  0/
102 250  0   33  30  25  0/
103 250  0   33  30  25  0/
104 250 30   33  30  25  0  9  3  0  27.5/
105 250 30   33  30  25  0  9  3  0  27.5/
106 250 30   33  30  25  0  9  3  0  27.5/
/
```

SUPPORT RESTRAINTS

```
<NOTE:> CODE:  '0' FOR NOT RESTRAINED NODES AND '1' FOR RESTRAINED ONES
<<<<< FORMAT >>>>>
NODE  X-RST  Y-RST [ #NODE d(NODE) ] /
61    0      1/
1061  1      0     30     1/
/
```

```
**************
* LOAD CASE *
*   DATA     *
**************

LOAD CASE PARAMETERS
********************

Structure Title     (30 char. max.)          : DeRose Slab
Load Case Title     (30 char. max.)          : Disp (1.00mm)
Load Case File Name  ( 8 char. max.)         : DRS
No. of Loaded Joints                         : 0
No. of Prescribed Support Displacements      : 1
No. of Elements with Temperature Loads       : 0
No. of Elements with Concrete Prestrain      : 0
No. of Elements with Ingress Pressure        : 0

JOINT LOADS
***********
<NOTE:> UNITS: KIPS OR KN
<<<<< FORMAT >>>>>
NODE Fx Fy [ #NODE d(NODE) d(Fx) d(Fy) ] /
/
SUPPORT DISPLACEMENTS
*********************
<NOTE:> UNITS: MM OR IN
<<<<< FORMAT >>>>>
JNT DOF DISPL [ #JNT d(JNT) ] /
788 2 -1.00/
/
TEMPERATURE LOADS
*****************
<NOTE:> UNITS: F OR C
<<<<< FORMAT >>>>>
ELMT TEMP [ #ELMT d(ELMT) d(TEMP) ] [ #ELMT d(ELMT) d(TEMP) ] /
/
CONCRETE PRESTRAINS
*******************
<NOTE:> UNITS: me
<<<<< FORMAT >>>>>
ELMT STRAIN [ #ELMT d(ELMT) d(STRAIN) ] [ #ELMT d(ELMT) d(STRAIN) ] /
/
INGRESS PRESSURES
*****************
<NOTE:> UNITS: mpA
<<<<< FORMAT >>>>>
ELMT PRESSURE [ #ELMT d(ELMT) d(PRS) ] [ #ELMT d(ELMT) d(PRS) ] /
/

**************
* LOAD CASE *
*   DATA     *
**************

LOAD CASE PARAMETERS
********************
Structure Title     (30 char. max.)          : DeRose Slab
```

```
Load Case Title     (30 char. max.)        : SHRINK
Load Case File Name  ( 8 char. max.)       : SHRINK
No. of Loaded Joints                       : 0
No. of Prescribed Support Displacements    : 0
No. of Elements with Temperature Loads     : 0
No. of Elements with Concrete Prestrain    : 378
No. of Elements with Ingress Pressure      : 0

                  JOINT LOADS
                  ***********
<NOTE:> UNITS: KIPS OR KN
<<<<< FORMAT >>>>>
NODE Fx Fy [ #NODE d(NODE) d(Fx) d(Fy) ] /
/
               SUPPORT DISPLACEMENTS
               **********************
<NOTE:> UNITS: MM OR IN
<<<<< FORMAT >>>>>
JNT DOF DISPL [ #JNT  d(JNT) ] /
/
                TEMPERATURE LOADS
                *****************
<NOTE:> UNITS:  F OR C
<<<<< FORMAT >>>>>
ELMT TEMP  [ #ELMT d(ELMT) d(TEMP) ] [ #ELMT d(ELMT) d(TEMP) ] /
/
               CONCRETE PRESTRAINS
               *******************
<NOTE:> UNITS:  me
<<<<< FORMAT >>>>>
ELMT STRAIN  [ #ELMT d(ELMT) d(STRAIN) ] [ #ELMT d(ELMT) d(STRAIN) ]  /
1  -0.4  378  1  0/
/
               INGRESS PRESSURES
               *****************
<NOTE:> UNITS:  mpA
<<<<< FORMAT >>>>>
ELMT PRESSURE  [ #ELMT d(ELMT) d(PRS) ] [ #ELMT d(ELMT) d(PRS) ]  /
/
```

CFRP-repaired slab: (The load and shrinkage files are the same as those for the control slab.)

```
            ************
            *  VECTOR  *
            * JOB DATA *
            ************

Job Title     (30 char. max.)     : DEROSE SLAB
Job File Name  ( 8 char. max.)    : DRSC
Date          (30 char. max.)     : MAR 7, 2001

STRUCTURE DATA
--------------
Structure Type                    : 2
```

File Name (8 char. max.) : DRSC

LOADING DATA

No. of Load Stages : 90
Starting Load Stage No. : 1
Load Series ID (5 char. max.) : DRSC

Load Case	File Name (8 char. max.)	Factors Initial	Final	LS-Inc	Type	Reps	C-Inc
1	DRS	2.900	20.000	0.100	1	1	0.000
2	SHRINK	1.000	1.000	0.000	1	1	0.000
3	NULL	0.000	0.000	0.500	1	1	0.000

ANALYSIS PARAMETERS

Seed File Name (8 char. max.) : DRS_30
Convergence Limit (factor > 1.0) : 1.00001
Averaging Factor (0.0 to 1.0) : 0.30
Maximum No. of Iterations : 100
Convergence Criteria : 1
Results Files : 2
Output Format : 1

MATERIAL BEHAVIOUR MODELS

Concrete Compression Base Curve (0-3) : 1
Concrete Compression Post-Peak (0-3) : 1
Concrete Compression Softening (0-8) : 1
Concrete Tension Stiffening (0-3) : 1
Concrete Tension Softening (0-3) : 2
Concrete Tension Splitting (0-1) : 1
Concrete Confined Strength (0-2) : 1
Concrete Dilatation (0-1) : 1
Concrete Cracking Criterion (0-4) : 1
Concrete Crack Slip Check (0-2) : 1
Concrete Crack Width Check (0-2) : 0
Concrete Bond or Adhesion (0-3) : 1
Concrete Hysteresis (0-2) : 1
Reinforcement Hysteresis (0-3) : 1
Reinforcement Dowel Action (0-1) : 1
Reinforcement Buckling (0-1) : 1
Element Strain Histories (0-1) : 1
Element Slip Distortions (0-4) : 0
Geometric Nonlinearity (0-1) : 1

****
* STRUCTURE *
* DATA *
****

STRUCTURAL PARAMETERS
****

Structure Title (30 char. max.) : DEROSE SLAB
Structure File Name (8 char. max.) : DRSC
No. of R.C. Material Types : 2

No. of Steel Material Types	: 8
No. of Bond Material Types	: 6
No. of Rectangular Elements	: 474
No. of Triangular Elements	: 0
No. of Truss Bar Elements	: 701
No. of Linkage Elements	: 0
No. of Contact Elements	: 617
No. of Joints	: 1090
No. of Restraints	: 31

MATERIAL SPECIFICATIONS

(A) REINFORCED CONCRETE

<NOTE:> TO BE USED IN RECTANGULAR AND TRIANGULAR ELEMENTS ONLY

CONCRETE

MAT	Ns	T	f'c	[ft	Ec	e0	Mu	Cc	Agg][	Sx	Sy]
TYP	#	mm	MPa	MPa	MPa	me		/C	mm	mm	mm
1	0	1200	53.9	2.42	40400	2.67	0.15	0	20	250	250
2	0	1200	0.1	2.42	2000	0.1	0.15	0	20	250	250

/

REINFORCEMENT COMPONENTS

MAT	REF	DIR	As	Db	Fy	Fu	Es	Esh	esh	Cs	Dep
TYP	TYP	deg	%	mm	MPa	MPa	MPa	MPa	me	/C	me

/

(B) STEEL

<NOTE:> TO BE USED FOR TRUSS ELEMENTS ONLY

MAT	REF	AREA	Db	Fy	Fu	Es	Esh	esh	Cs	Dep
TYP	TYP	mm2	mm	MPa	MPa	MPa	MPa	me	/C	me
1	1	400	11.3	458	692	200000	2000	15.0	0	0/
2	1	300	1.0	458	692	200000	2000	15.0	0	0/
3	3	1200	0.1	945	945	80300	80300	11.8	0	0/
4	3	87.5	0.1	945	945	80300	80300	11.8	0	0/
5	3	55	0.1	945	945	80300	80300	11.8	0	0/
6	3	27.5	0.1	945	945	80300	80300	11.8	0	0/
7	3	25	0.1	90	90	5500	5500	16.4	0	0/
8	3	50	0.1	90	90	5500	5500	16.4	0	0/

/

(C) BOND

<NOTE:> TO BE USED FOR EXTERIOR/INTERIOR BONDED ELEMENTS

MAT	REF	[Ao	Umax	Sm	Su] [	CPF	Cmin	No.	HOOK]
TYP	TYP	mm^2	MPa	mm	mm	0-1	mm	LYR	0/1
1	3	30000	4.4	0.0075	0.50	0	0	0	0
2	3	2187.5	4.4	0.0075	0.50	0	0	0	0
3	3	1375	4.4	0.0075	0.50	0	0	0	0
4	3	687.5	4.4	0.0075	0.50	0	0	0	0
5	3	750	4.4	0.0075	0.50	0	0	0	0
6	3	1500	4.4	0.0075	0.50	0	0	0	0

/

ELEMENT INCIDENCES

(A) RECTANGULAR ELEMENTS

```
<<<<< FORMAT >>>>>
ELMT INC1 INC2 INC3 INC4 [#ELMT d(ELMT) d(INC)] [#ELMT d(ELMT) d(INC)]/
  1   1  11  12  2   9  9  10 9  1  1/
 82  91 101 104 92/
 83  92 104 107 93/
 84  93 107 110 94/
 85  94 110 113 95/
 86  95 113 116 96/
 87  96 116 119 97/
 88  97 119 122 98/
 89  98 122 125 99/
 90  99 125 128 100/
 91 101 131 134 104  32  9  30  9  1  3/
379 101 131 134 104  32  1  30  3 32  3/
/
```

(B) TRIANGULAR ELEMENTS

```
<<<<< FORMAT >>>>>
ELMT INC1 INC2 INC3  [ #ELMT d(ELMT) d(INC) ] [ #ELMT d(ELMT) d(INC)] /
/
```

(C) TRUSS ELEMENTS

```
<<<<< FORMAT >>>>>
ELMT INC1 INC2 [ #ELMT d(ELMT) d(INC)] [#ELMT d(ELMT) d(INC) ]/
475  2 12  9 1 10  2 42  6/
484 92 104/
526 98 122/
485 104 134 32  1 30  2 42 18/
559 102 132 32  1 30 10 32  3/
879 103 106  9  1  3 33  9 30/
/
```

(D) LINKAGE ELEMENTS

```
<<<<< FORMAT >>>>
ELMT INC1 INC2 [ #ELMT d(ELMT) d(INC) ] [ #ELMT d(ELMT) d(INC) ]
/
```

(E) CONTACT ELEMENTS

```
<<<<< FORMAT >>>>
ELMT INC1 INC2 INC3 INC4 [ #ELMT d(ELMT) d(INC) ] [ #ELMT d(ELMT) d(INC) ]
1176 101 102 131 132  32  1 30  10 32  3/
1496 101 103 104 106  9  1  3 33  9 30/
/
```

MATERIAL TYPE ASSIGNMENT

```
<<<<< FORMAT >>>>>
ELMT MAT ACT [ #ELMT d(ELMT)] [ #ELMT d(ELMT) ] /
  1  1 1  90 1/
 91  1 1   3 1 32   9/
 94  1 1   6 1 32   9/
379  2 1  96 1/
475  1 1  42 1/
517  2 1  42 1/
559  3 1  32 1/
591  4 1  32 1/
```

```
623  5 1  32 1  8  32/
847  6 1  32 1/
879  7 1   9 1  2 288/
888  8 1   9 1 31   9/
1176 1 1  32 1/
1208 2 1  32 1/
1240 3 1  32 1  7  32/
1464 4 1  32 1/
1496 5 1   2 288/
1497 4 1   8 1  2 288/
1505 6 1  31 9/
1506 3 1   8 1 31   9/
/
                COORDINATES
                ***********
<NOTE:> UNITS: in OR mm
<<<<< FORMAT >>>>>
NODE X Y [ #NODES d(NODES)  d(X) d(Y) ] [ #NODES d(NODES)  d(X) d(Y) ] /
 1   0  0   10  10 25  0/
 2   0 30   10  10 25  0  9  1  0  27.5/
101 250  0   33  30 25  0/
102 250  0   33  30 25  0/
103 250  0   33  30 25  0/
104 250 30   33  30 25  0  9  3  0  27.5/
105 250 30   33  30 25  0  9  3  0  27.5/
106 250 30   33  30 25  0  9  3  0  27.5/
/
              SUPPORT RESTRAINTS
              ******************
<NOTE:> CODE: '0' FOR NOT RESTRAINED NODES AND '1' FOR RESTRAINED ONES
<<<<< FORMAT >>>>>
NODE  X-RST  Y-RST [ #NODE d(NODE) ] /
61    0     1/
1061  1     0     30     1/
/
```

DEROSE BEAM:

Control beam:

```
            ************
            *  VECTOR  *
            * JOB DATA *
            ************
```

Job Title (30 char. max.) : DEROSE BEAM (CONTROL)
Job File Name (8 char. max.) : DRB
Date (30 char. max.) : APR 2, 2001

STRUCTURE DATA

Structure Type : 2
File Name (8 char. max.) : DRB

LOADING DATA

No. of Load Stages : 41
Starting Load Stage No. : 1
Load Series ID (5 char. max.) : DRB

Load Case	File Name (8 char. max.)	Factors Initial	Final	LS-Inc	Type	Reps	C-Inc
1	DRB	0.000	20.000	0.500	1	1	0.000
2	SHRINK	1.000	1.000	0.000	1	1	0.000
3	NULL	0.000	40.000	0.500	1	1	0.000

ANALYSIS PARAMETERS

Seed File Name (8 char. max.) : NULL
Convergence Limit (factor > 1.0) : 1.00001
Averaging Factor (0.0 to 1.0) : 0.40
Maximum No. of Iterations : 90
Convergence Criteria : 1
Results Files : 1
Output Format : 1

MATERIAL BEHAVIOUR MODELS

Concrete Compression Base Curve (0-3) : 1
Concrete Compression Post-Peak (0-3) : 1
Concrete Compression Softening (0-8) : 1
Concrete Tension Stiffening (0-3) : 1
Concrete Tension Softening (0-3) : 1
Concrete Tension Splitting (0-1) : 1
Concrete Confined Strength (0-2) : 1
Concrete Dilatation (0-1) : 1
Concrete Cracking Criterion (0-4) : 1
Concrete Crack Slip Check (0-2) : 1
Concrete Crack Width Check (0-2) : 1
Concrete Bond or Adhesion (0-3) : 1
Concrete Hysteresis (0-2) : 1
Reinforcement Hysteresis (0-3) : 1
Reinforcement Dowel Action (0-1) : 1
Reinforcement Buckling (0-1) : 1
Element Strain Histories (0-1) : 1
Element Slip Distortions (0-4) : 1
Geometric Nonlinearity (0-1) : 1

****
* STRUCTURE *
* DATA *
****

STRUCTURAL PARAMETERS

Structure Title (30 char. max.) : DEROSE BEAM
Structure File Name (8 char. max.) : DRB

No. of R.C. Material Types : 9
No. of Steel Material Types : 10
No. of Bond Material Types : 9
No. of Rectangular Elements : 764
No. of Triangular Elements : 0
No. of Truss Bar Elements : 630
No. of Linkage Elements : 0
No. of Contact Elements : 512
No. of Joints : 1287
No. of Restraints : 3

MATERIAL SPECIFICATIONS

(A) REINFORCED CONCRETE

<NOTE:> TO BE USED IN RECTANGULAR AND TRIANGULAR ELEMENTS ONLY

CONCRETE

MAT TYP	Ns #	T mm	fc MPa	[ft MPa	Ec MPa	e0 MPa	Mu me	Cc	Agg /C	][Sx mm	Sy] mm
1	1	550	45.7	2.23	37200	2.46	0.15	0	20	0	0
2	1	300	41.2	2.12	35300	2.33	0.15	0	20	0	0
3	1	550	45.7	2.23	37200	2.46	0.15	0	20	0	0
4	1	300	41.2	2.12	35300	2.33	0.15	0	20	0	0
5	1	550	45.7	2.23	37200	2.46	0.15	0	20	0	0
6	1	300	41.2	2.12	35300	2.33	0.15	0	20	0	0
7	1	550	45.7	2.23	37200	2.46	0.15	0	20	0	0
8	0	550	0.1	2.23	2000	0.1	0.15	0	20	0	0
9	2	30	41.2	2.12	35300	2.33	0.15	0	20	0	0

/

REINFORCEMENT COMPONENTS

MAT TYP	REF TYP	DIR deg	As %	Db mm	Fy MPa	Fu MPa	Es MPa	Esh MPa	esh me	Cs /C	Dep me
1	1	90	0.1836	9.5	507	778	200000	6000	10.0	0	0
2	1	90	0.1188	9.5	507	778	200000	6000	10.0	0	0
3	1	90	0.201	9.5	507	778	200000	6000	10.0	0	0
4	1	90	0.1358	9.5	507	778	200000	6000	10.0	0	0
5	1	90	0.223	9.5	507	778	200000	6000	10.0	0	0
6	1	90	0.1584	9.5	507	778	200000	6000	10.0	0	0
7	1	90	0.0648	9.5	507	778	200000	6000	10.0	0	0
9	1	0	100.0	3.0	492	650	200000	2000	15.0	0	0
9	1	90	100.0	3.0	492	650	200000	2000	15.0	0	0

/

(B) STEEL

<NOTE:> TO BE USED FOR TRUSS ELEMENTS ONLY

MAT TYP	REF TYP	AREA mm2	Db mm	Fy MPa	Fu MPa	Es MPa	Esh MPa	esh me	Cs /C	Dep me
1	1	4200	29.9	492	650	200000	2000	15.0	0	0/
2	1	2500	25.2	490	688	200000	3500	13.0	0	0/
3	1	1400	30.0	492	650	200000	2000	15.0	0	0/
4	1	4500	3.0	492	650	200000	2000	15.0	0	0/
5	3	91.5	0.1	945	945	80300	80300	11.8	0	0/
6	3	183	0.1	945	945	80300	80300	11.8	0	0/

```
7  3   550  0.1  90  90  5500  5500 16.4  0  0/
8  3 108.63  0.1  90  90  5500  5500 16.4  0  0/
9  3  87.25  0.1  90  90  5500  5500 16.4  0  0/
10 3 106.13  0.1  90  90  5500  5500 16.4  0  0/
/
```

(C) BOND

<NOTE:> TO BE USED FOR EXTERIOR/INTERIOR BONDED ELEMENTS

```
MAT REF [ Ao   Umax  Sm   Su ] [ CPF  Cmin  No.  HOOK ]
TYP TYP mm^2  MPa   mm   mm    0-1   mm   LYR   0/1
1   3  5947.5  4.1 0.007 0.50   0   0   0   0
2   3  7983.4  4.1 0.007 0.50   0   0   0   0
3   3  5718.8  4.1 0.007 0.50   0   0   0   0
4   3   11895  4.1 0.007 0.50   0   0   0   0
5   3 15966.8  4.1 0.007 0.50   0   0   0   0
6   3 11437.6  4.1 0.007 0.50   0   0   0   0
7   3   50325  4.1 0.007 0.50   0   0   0   0
8   3 19878.4  4.1 0.007 0.50   0   0   0   0
9   3 19420.9  4.1 0.007 0.50   0   0   0   0
/
```

ELEMENT INCIDENCES

****

(A) RECTANGULAR ELEMENTS

```
<<<<< FORMAT >>>>>
ELMT INC1 INC2 INC3 INC4 [#ELMT d(ELMT) d(INC)] [#ELMT d(ELMT) d(INC)]/
 1   1  17  18   2  15 1  1  24 15 16/
361 385 401 404 386/
362 386 404 407 387/
363 387 407 410 388/
364 388 410 413 389/
365 389 413 416 390/
366 390 416 419 391/
367 391 419 422 392/
368 392 422 425 393/
369 393 425 428 394/
370 394 428 431 395/
371 395 431 434 396/
372 396 434 437 397/
373 397 437 440 398/
374 398 440 441 399  2  1  1/
376 401 443 446 404 12  1  3/
388 443 482 485 446 12  1  3  19 12 39/
616 1184 1223 1224 1187/
617 1187 1224 1225 1190/
618 1190 1225 1226 1193/
619 1193 1226 1227 1196/
620 1196 1227 1228 1199/
621 1199 1228 1229 1202/
622 1202 1229 1230 1205/
623 1205 1230 1231 1208/
624 1208 1231 1232 1211/
625 1211 1232 1233 1214/
626 1214 1233 1234 1217/
627 1217 1234 1235 1220/
628 1223 1236 1237 1224 12  1  1  4 12 13/
```

```
676 401 443 446 404  4  1  3/
680 443 482 485 446  4  1  3 19  4 39/
756 365 381 382 366  3  1  1  2  3 16/
762 397 437 440 398/
763 398 440 441 399  2  1  1/
/
```

(B) TRIANGULAR ELEMENTS

```
<<<<< FORMAT >>>>>
ELMT INC1 INC2 INC3  [ #ELMT d(ELMT) d(INC) ] [ #ELMT d(ELMT) d(INC)] /
/
```

(C) TRUSS ELEMENTS

```
<<<<< FORMAT >>>>>
ELMT INC1 INC2 [ #ELMT d(ELMT) d(INC)] [#ELMT d(ELMT) d(INC) ]/
765   2  18 24  1 16   2 50  10/
789 386 404/
839 396 434/
790 404 446  2 50  30/
791 446 485  2 50  30/
792 485 524 18  1 39   2  50  30/
810 1187 1224/
860 1217 1234/
811 1224 1237  4  1 13   2  50  10/
865 289 290 15  1  1/
880 437 440/
881 440 441  2  1  1/
883 402 405 12  1  3   2 12  42/
907 483 486 12  1  3  19 12  39/
1135 403  445 13 20   3/
1136 445  484 13 20   3 19  1 39/
/
```

(D) LINKAGE ELEMENTS

```
<<<<< FORMAT >>>>
ELMT INC1 INC2 [ #ELMT d(ELMT) d(INC) ] [ #ELMT d(ELMT) d(INC) ]
/
```

(E) CONTACT ELEMENTS

```
<<<<< FORMAT >>>>
ELMT INC1 INC2 INC3 INC4 [ #ELMT d(ELMT) d(INC) ] [ #ELMT d(ELMT) d(INC) ]
1395  401  402  404  405 12  1 3   2  12  42/
1419  482  483  485  486 12  1 3  19  12  39/
1647  401  403  443  445 13 20  3/
1648  443  445  482  484 19  1 39 13  20   3/
/
```

MATERIAL TYPE ASSIGNMENT

```
<<<<< FORMAT >>>>>
ELMT MAT ACT [ #ELMT d(ELMT)] [ #ELMT d(ELMT) ] /
  1  1  1   12  1  17  15/
 13  2  1    3  1  17  15/
256  3  1   12  1   4  15/
268  4  1    3  1   4  15/
316  5  1   12  1   4  15/
328  6  1    3  1   4  15/
376  7  1   12  1  25  12/
```

```
 676 8 0   4 1 20  4/
 756 9 0   3 1  3  3/
 765 1 1  50 1/
 815 2 1  50 1/
 865 3 0  15 1/
 880 4 0   3 1/
 883 5 0  12 1  2 240/
 895 6 0  12 1 19  12/
1135 7 0  20 1  2 240/
1155 8 0  20 1/
1175 9 0  20 1  9 20/
1355 10 0  20 1/
1395 1 0   2 240/
1396 2 0  10 1  2 240/
1406 3 0   2 240/
1407 4 0  19 12/
1408 5 0  10 1 19 12/
1418 6 0  19 12/
1647 7 0  20 1  2 240/
1667 8 0  20 1/
1687 5 0  20 1  9 20/
1867 9 0  20 1/
/
```

COORDINATES

****

```
<NOTE:> UNITS: in OR mm
<<<<< FORMAT >>>>>
NODE X Y [ #NODES d(NODES)  d(X) d(Y) ] [ #NODES d(NODES)  d(X) d(Y) ] /
  1   0    0  4  16  118.75  0/
  2   0   65  4  16  118.75  0   11  1  0   87.25/
 13   0 1000  4  16  118.75  0    4  1  0  100/
 65 475    0 21  16  91.25  0/
 66 475   65 21  16  91.25  0   11  1  0   87.25/
 77 475 1000 21  16  91.25  0    4  1  0  100/
401 2400    0/
402 2400    0/
403 2400    0/
404 2400   65 11   3   0   87.25/
405 2400   65 11   3   0   87.25/
406 2400   65 11   3   0   87.25/
437 2400 1000/
438 2400 1000/
439 2400 1000  4   1   0  100/
443 2491.5   0 20  39  91.5  0/
444 2491.5   0 20  39  91.5  0/
445 2491.5   0 20  39  91.5  0/
446 2491.5  65 20  39  91.5  0   11  3  0   87.25/
447 2491.5  65 20  39  91.5  0   11  3  0   87.25/
448 2491.5  65 20  39  91.5  0   11  3  0   87.25/
479 2491.5 1000 20  39  91.5  0/
480 2491.5 1000 20  39  91.5  0/
481 2491.5 1000 20  39  91.5  0/
1223 4325    0  5  13  118.75  0/
1224 4325   65  5  13  118.75  0   11  1  0   87.25/
1235 4325 1000  5  13  118.75  0/
```

```
                SUPPORT RESTRAINTS
                ******************
<NOTE:> CODE: '0' FOR NOT RESTRAINED NODES AND '1' FOR RESTRAINED ONES
<<<<< FORMAT >>>>>
NODE  X-RST  Y-RST [ #NODE d(NODE) ] /
65    0      1/
1223  1      1/
/

                **************
               * LOAD CASE    *
               *   DATA       *
                **************

                LOAD CASE PARAMETERS
                ********************

Structure Title     (30 char. max.)          : DeRose Beam
Load Case Title     (30 char. max.)          : Disp (1.00mm)
Load Case File Name  ( 8 char. max.)         : DRB
No. of Loaded Joints                         : 0
No. of Prescribed Support Displacements      : 1
No. of Elements with Temperature Loads       : 0
No. of Elements with Concrete Prestrain      : 0
No. of Elements with Ingress Pressure        : 0

                  JOINT LOADS
                  ***********
<NOTE:> UNITS:  KIPS OR KN
<<<<< FORMAT >>>>>
NODE Fx Fy [ #NODE d(NODE) d(Fx) d(Fy) ] /
/
                SUPPORT DISPLACEMENTS
                *********************
<NOTE:> UNITS: MM OR IN
<<<<< FORMAT >>>>>
JNT  DOF  DISPL  [ #JNT  d(JNT) ] /
400  2    -1.00/
/
                TEMPERATURE LOADS
                *****************
<NOTE:> UNITS:  F OR C
<<<<< FORMAT >>>>>
ELMT TEMP  [ #ELMT d(ELMT) d(TEMP) ] [ #ELMT d(ELMT) d(TEMP) ] /
/
                CONCRETE PRESTRAINS
                *******************
<NOTE:> UNITS:  me
<<<<< FORMAT >>>>>
ELMT STRAIN  [ #ELMT d(ELMT) d(STRAIN) ] [ #ELMT d(ELMT) d(STRAIN) ]  /
/
                INGRESS PRESSURES
                *****************
<NOTE:> UNITS:  mpA
<<<<< FORMAT >>>>>
ELMT PRESSURE  [ #ELMT d(ELMT) d(PRS) ] [ #ELMT d(ELMT) d(PRS) ]  /
/
```

```
**************
* LOAD CASE  *
*   DATA     *
**************

 LOAD CASE PARAMETERS
 ********************

Structure Title     (30 char. max.)          : DeRose Beam
Load Case Title     (30 char. max.)          : SHRINK
Load Case File Name  ( 8 char. max.)         : SHRINK
No. of Loaded Joints                         : 0
No. of Prescribed Support Displacements      : 0
No. of Elements with Temperature Loads       : 0
No. of Elements with Concrete Prestrain      : 675
No. of Elements with Ingress Pressure        : 0

                JOINT LOADS
                ***********
<NOTE:> UNITS:  KIPS OR KN
<<<<< FORMAT >>>>>
NODE Fx Fy [ #NODE d(NODE) d(Fx) d(Fy) ] /
/
              SUPPORT DISPLACEMENTS
              *********************
<NOTE:> UNITS: MM OR IN
<<<<< FORMAT >>>>>
JNT  DOF  DISPL  [ #JNT  d(JNT) ] /
/
               TEMPERATURE LOADS
               *****************
<NOTE:> UNITS:  F OR C
<<<<< FORMAT >>>>>
ELMT TEMP  [ #ELMT d(ELMT) d(TEMP) ] [ #ELMT d(ELMT) d(TEMP) ] /
/
               CONCRETE PRESTRAINS
               *******************
<NOTE:> UNITS:  me
<<<<< FORMAT >>>>>
ELMT STRAIN  [ #ELMT d(ELMT) d(STRAIN) ] [ #ELMT d(ELMT) d(STRAIN) ]  /
1  -0.4  675  1  0/
/
               INGRESS PRESSURES
               *****************
<NOTE:> UNITS:  mpA
<<<<< FORMAT >>>>>
ELMT PRESSURE  [ #ELMT d(ELMT) d(PRS) ] [ #ELMT d(ELMT) d(PRS) ]  /
/
```

CFRP-repaired beam: (The load and shrinkage files are the same as those for the control beam.)

```
************
* VECTOR   *
* JOB DATA *
************
```

Job Title (30 char. max.) : DEROSE BEAM (CFRP)
Job File Name (8 char. max.) : DRBC
Date (30 char. max.) : APR 2, 2001

STRUCTURE DATA

Structure Type : 2
File Name (8 char. max.) : DRBC

LOADING DATA

No. of Load Stages : 269
Starting Load Stage No. : 1
Load Series ID (5 char. max.) : DRBC

Load Case	File Name (8 char. max.)	Factors Initial	Final	LS-Inc	Type	Reps	C-Inc
1	DRB	6.000	140.000	0.500	1	1	0.000
2	SHRINK	1.000	1.000	0.000	1	1	0.000
3	NULL	0.000	40.000	0.500	1	1	0.000

ANALYSIS PARAMETERS

Seed File Name (8 char. max.) : DRB_13
Convergence Limit (factor > 1.0) : 1.00001
Averaging Factor (0.0 to 1.0) : 0.40
Maximum No. of Iterations : 100
Convergence Criteria : 1
Results Files : 2
Output Format : 1

MATERIAL BEHAVIOUR MODELS

Concrete Compression Base Curve (0-3) : 1
Concrete Compression Post-Peak (0-3) : 1
Concrete Compression Softening (0-8) : 1
Concrete Tension Stiffening (0-3) : 1
Concrete Tension Softening (0-3) : 1
Concrete Tension Splitting (0-1) : 1
Concrete Confined Strength (0-2) : 1
Concrete Dilatation (0-1) : 1
Concrete Cracking Criterion (0-4) : 1
Concrete Crack Slip Check (0-2) : 1
Concrete Crack Width Check (0-2) : 0
Concrete Bond or Adhesion (0-3) : 1
Concrete Hysteresis (0-2) : 1
Reinforcement Hysteresis (0-3) : 1
Reinforcement Dowel Action (0-1) : 1

Reinforcement Buckling (0-1) : 1
Element Strain Histories (0-1) : 1
Element Slip Distortions (0-4) : 1
Geometric Nonlinearity (0-1) : 1

****
* STRUCTURE *
* DATA *
****

STRUCTURAL PARAMETERS
****

Structure Title (30 char. max.) : DEROSE BEAM
Structure File Name (8 char. max.) : DRBC
No. of R.C. Material Types : 9
No. of Steel Material Types : 10
No. of Bond Material Types : 9
No. of Rectangular Elements : 764
No. of Triangular Elements : 0
No. of Truss Bar Elements : 630
No. of Linkage Elements : 0
No. of Contact Elements : 512
No. of Joints : 1287
No. of Restraints : 3

MATERIAL SPECIFICATIONS
****

(A) REINFORCED CONCRETE

<NOTE:> TO BE USED IN RECTANGULAR AND TRIANGULAR ELEMENTS ONLY

CONCRETE

MAT TYP	Ns #	T mm	fc MPa	ft MPa	Ec MPa	e0	Mu	Cc	Agg /C	Sx mm	Sy mm
1	1	550	45.7	2.23	37200	2.46	0.15	0	20	0	0
2	1	300	41.2	2.12	35300	2.33	0.15	0	20	0	0
3	1	550	45.7	2.23	37200	2.46	0.15	0	20	0	0
4	1	300	41.2	2.12	35300	2.33	0.15	0	20	0	0
5	1	550	45.7	2.23	37200	2.46	0.15	0	20	0	0
6	1	300	41.2	2.12	35300	2.33	0.15	0	20	0	0
7	1	550	45.7	2.23	37200	2.46	0.15	0	20	0	0
8	0	550	0.1	2.23	2000	0.1	0.15	0	20	0	0
9	2	30	41.2	2.12	35300	2.33	0.15	0	20	0	0

/

REINFORCEMENT COMPONENTS

MAT TYP	REF TYP	DIR deg	As %	Db mm	Fy MPa	Fu MPa	Es MPa	Esh MPa	esh	Cs /C	Dep me
1	1	90	0.1836	9.5	507	778	200000	6000	10.0	0	0
2	1	90	0.1188	9.5	507	778	200000	6000	10.0	0	0
3	1	90	0.201	9.5	507	778	200000	6000	10.0	0	0
4	1	90	0.1358	9.5	507	778	200000	6000	10.0	0	0
5	1	90	0.223	9.5	507	778	200000	6000	10.0	0	0

```
6   1  90 0.1584 9.5  507  778  200000 6000 10.0  0   0
7   1  90 0.0648 9.5  507  778  200000 6000 10.0  0   0
9   1   0  100.0 3.0  492  650  200000 2000 15.0  0   0
9   1  90  100.0 3.0  492  650  200000 2000 15.0  0   0
/
```

(B) STEEL

```
<NOTE:> TO BE USED FOR TRUSS ELEMENTS ONLY
MAT REF   AREA  Db   Fy   Fu    Es    Esh  esh  Cs  Dep
TYP TYP   mm2   mm   MPa  MPa   MPa   MPa  me   /C  me
1   1    4200  29.9  492  650  200000  2000 15.0  0   0/
2   1    2500  25.2  490  688  200000  3500 13.0  0   0/
3   1    1400  30.0  492  650  200000  2000 15.0  0   0/
4   1    4500   3.0  492  650  200000  2000 15.0  0   0/
5   3    91.5   0.1  945  945  80300  80300 11.8  0   0/
6   3     183   0.1  945  945  80300  80300 11.8  0   0/
7   3     550   0.1   90   90   5500   5500 16.4  0   0/
8   3  108.63   0.1   90   90   5500   5500 16.4  0   0/
9   3   87.25   0.1   90   90   5500   5500 16.4  0   0/
10  3  106.13   0.1   90   90   5500   5500 16.4  0   0/
/
```

(C) BOND

```
<NOTE:> TO BE USED FOR EXTERIOR/INTERIOR BONDED ELEMENTS
MAT REF [ Ao   Umax  Sm   Su ] [ CPF  Cmin  No.  HOOK ]
TYP TYP mm^2  MPa   mm   mm    0-1   mm    LYR   0/1
1   3  5947.5  4.1 0.007 0.50   0   0   0   0
2   3  7983.4  4.1 0.007 0.50   0   0   0   0
3   3  5718.8  4.1 0.007 0.50   0   0   0   0
4   3   11895  4.1 0.007 0.50   0   0   0   0
5   3 15966.8  4.1 0.007 0.50   0   0   0   0
6   3 11437.6  4.1 0.007 0.50   0   0   0   0
7   3   50325  4.1 0.007 0.50   0   0   0   0
8   3 19878.4  4.1 0.007 0.50   0   0   0   0
9   3 19420.9  4.1 0.007 0.50   0   0   0   0
/
```

ELEMENT INCIDENCES

****

(A) RECTANGULAR ELEMENTS

```
<<<<< FORMAT >>>>>
ELMT INC1 INC2 INC3 INC4 [#ELMT d(ELMT) d(INC)] [#ELMT d(ELMT) d(INC)]/
 1   1  17  18   2  15 1  1  24 15  16/
361 385 401 404 386/
362 386 404 407 387/
363 387 407 410 388/
364 388 410 413 389/
365 389 413 416 390/
366 390 416 419 391/
367 391 419 422 392/
368 392 422 425 393/
369 393 425 428 394/
370 394 428 431 395/
371 395 431 434 396/
372 396 434 437 397/
373 397 437 440 398/
```

```
374 398 440 441 399  2  1  1/
376 401 443 446 404 12  1  3/
388 443 482 485 446 12  1  3  19 12 39/
616 1184 1223 1224 1187/
617 1187 1224 1225 1190/
618 1190 1225 1226 1193/
619 1193 1226 1227 1196/
620 1196 1227 1228 1199/
621 1199 1228 1229 1202/
622 1202 1229 1230 1205/
623 1205 1230 1231 1208/
624 1208 1231 1232 1211/
625 1211 1232 1233 1214/
626 1214 1233 1234 1217/
627 1217 1234 1235 1220/
628 1223 1236 1237 1224 12  1  1  4 12 13/
676 401 443 446 404  4  1  3/
680 443 482 485 446  4  1  3 19  4 39/
756 365 381 382 366  3  1  1  2  3 16/
762 397 437 440 398/
763 398 440 441 399  2  1  1/
/
```

(B) TRIANGULAR ELEMENTS

```
<<<<< FORMAT >>>>>
ELMT INC1 INC2 INC3  [ #ELMT d(ELMT) d(INC) ] [ #ELMT d(ELMT) d(INC)] /
/
```

(C) TRUSS ELEMENTS

```
<<<<< FORMAT >>>>>
ELMT INC1 INC2 [ #ELMT d(ELMT) d(INC)] [#ELMT d(ELMT) d(INC) ]/
765  2  18 24 1 16  2 50 10/
789 386 404/
839 396 434/
790 404 446  2 50 30/
791 446 485  2 50 30/
792 485 524 18 1 39  2 50 30/
810 1187 1224/
860 1217 1234/
811 1224 1237  4 1 13  2 50 10/
865 289 290 15 1  1/
880 437 440/
881 440 441  2 1  1/
883 402 405 12 1  3  2 12 42/
907 483 486 12 1  3 19 12 39/
1135 403 445 13 20  3/
1136 445 484 13 20  3 19  1 39/
/
```

(D) LINKAGE ELEMENTS

```
<<<<< FORMAT >>>>
ELMT INC1 INC2 [ #ELMT d(ELMT) d(INC) ] [ #ELMT d(ELMT) d(INC) ]
/
```

(E) CONTACT ELEMENTS

```
<<<<< FORMAT >>>>
ELMT INC1 INC2 INC3 INC4 [ #ELMT d(ELMT) d(INC) ] [ #ELMT d(ELMT) d(INC) ]
```

```
1395 401 402 404 405 12 1 3  2 12 42/
1419 482 483 485 486 12 1 3 19 12 39/
1647 401 403 443 445 13 20 3/
1648 443 445 482 484 19 1 39 13 20  3/
/
```

MATERIAL TYPE ASSIGNMENT

```
<<<<< FORMAT >>>>>
ELMT MAT ACT [ #ELMT d(ELMT)] [ #ELMT d(ELMT) ] /
  1 1 1  12 1 17 15/
 13 2 1   3 1 17 15/
256 3 1  12 1  4 15/
268 4 1   3 1  4 15/
316 5 1  12 1  4 15/
328 6 1   3 1  4 15/
376 7 1  12 1 25 12/
676 8 1   4 1 20  4/
756 9 1   3 1  3  3/
765 1 1  50 1/
815 2 1  50 1/
865 3 1  15 1/
880 4 1   3 1/
883 5 1  12 1  2 240/
895 6 1  12 1 19 12/
1135 7 0  20 1  2 240/
1155 8 0  20 1/
1175 9 0  20 1  9 20/
1355 10 0  20 1/
1395 1 1   2 240/
1396 2 1  10 1  2 240/
1406 3 1   2 240/
1407 4 1  19 12/
1408 5 1  10 1 19 12/
1418 6 1  19 12/
1647 7 0  20 1  2 240/
1667 8 0  20 1/
1687 5 0  20 1  9 20/
1867 9 0  20 1/
/
```

COORDINATES

```
<NOTE:> UNITS: in OR mm
<<<<< FORMAT >>>>>
NODE X Y  [ #NODES d(NODES)  d(X) d(Y) ] [ #NODES d(NODES)  d(X) d(Y) ] /
 1   0    0  4  16 118.75 0/
 2   0   65  4  16 118.75 0   11  1  0   87.25/
13   0 1000  4  16 118.75 0    4  1  0  100/
65  475    0 21  16  91.25 0/
66  475   65 21  16  91.25 0   11  1  0   87.25/
77  475 1000 21  16  91.25 0    4  1  0  100/
401 2400    0/
402 2400    0/
403 2400    0/
404 2400   65 11   3   0   87.25/
405 2400   65 11   3   0   87.25/
406 2400   65 11   3   0   87.25/
437 2400 1000/
```

```
438 2400  1000/
439 2400  1000  4   1   0  100/
443 2491.5   0 20  39  91.5  0/
444 2491.5   0 20  39  91.5  0/
445 2491.5   0 20  39  91.5  0/
446 2491.5  65 20  39  91.5  0   11  3  0   87.25/
447 2491.5  65 20  39  91.5  0   11  3  0   87.25/
448 2491.5  65 20  39  91.5  0   11  3  0   87.25/
479 2491.5 1000 20  39  91.5  0/
480 2491.5 1000 20  39  91.5  0/
481 2491.5 1000 20  39  91.5  0/
1223 4325    0  5  13 118.75 0/
1224 4325   65  5  13 118.75 0   11  1  0   87.25/
1235 4325  1000  5  13 118.75 0/
/
```

SUPPORT RESTRAINTS
****

<NOTE:> CODE: '0' FOR NOT RESTRAINED NODES AND '1' FOR RESTRAINED ONES
<<<<< FORMAT >>>>>
NODE X-RST Y-RST [#NODE d(NODE)] /
65 0 1/
1223 1 1/
/

RWOA BEAMS:

Beam RWOA-1:

****
* VECTOR *
* JOB DATA *
****

Job Title (30 char. max.) : RWOA1
Job File Name (8 char. max.) : RWOA1
Date (30 char. max.) : Apr 25, 2001

STRUCTURE DATA

Structure Type : 2
File Name (8 char. max.) : RWOA1

LOADING DATA

No. of Load Stages : 201
Starting Load Stage No. : 1
Load Series ID (5 char. max.) : COA1

Load Case	File Name (8 char. max.)	Factors Initial	Final	LS-Inc	Type	Reps	C-Inc
1	RWOA1	0.000	40.000	0.200	1	1	1.000
2	NULL	0.000	0.000	1.000	2	1	0.000
3	NULL	0.000	40.000	0.500	1	1	0.000

ANALYSIS PARAMETERS

Seed File Name (8 char. max.)	: NULL
Convergence Limit (factor > 1.0)	: 1.000010
Averaging Factor (0.0 to 1.0)	: 0.20
Maximum No. of Iterations	: 150
Convergence Criteria	: 1
Results Files	: 2
Output Format	: 1

MATERIAL BEHAVIOUR MODELS

Concrete Compression Base Curve (0-3)	: 1
Concrete Compression Post-Peak (0-3)	: 1
Concrete Compression Softening (0-8)	: 1
Concrete Tension Stiffening (0-3)	: 1
Concrete Tension Softening (0-3)	: 1
Concrete Tension Splitting (0-1)	: 1
Concrete Confined Strength (0-2)	: 1
Concrete Dilatation (0-1)	: 1
Concrete Cracking Criterion (0-4)	: 1
Concrete Crack Slip Check (0-2)	: 1
Concrete Crack Width Check (0-2)	: 1
Concrete Bond or Adhesion (0-4)	: 1
Concrete Hysteresis (0-2)	: 1
Reinforcement Hysteresis (0-3)	: 1
Reinforcement Dowel Action (0-1)	: 1
Reinforcement Buckling (0-1)	: 1
Element Strain Histories (0-1)	: 1
Element Slip Distortions (0-4)	: 1
Geometric Nonlinearity (0-1)	: 1

STRUCTURE DATA

STRUCTURAL PARAMETERS

Structure Title (30 char. max.)	: RWOA1 beam
Structure File Name (8 char. max.)	: RWOA1
No. of R.C. Material Types	: 4
No. of Steel Material Types	: 5
No. of Bond Material Types	: 4
No. of Rectangular Elements	: 518
No. of Triangular Elements	: 0
No. of Truss Elements	: 506
No. of Linkage Elements	: 0
No. of Contact Elements	: 420
No. of Joints	: 1030
No. of Restraints	: 15

MATERIAL SPECIFICATIONS

(A) REINFORCED CONCRETE

<NOTE:> TO BE USED IN RECTANGULAR AND TRIANGULAR ELEMENTS ONLY

CONCRETE

```
MAT Ns  T   fc [ ft   Ec    e0   Mu   Cc   Agg ][ Sx   Sy ]
TYP #   mm  MPa  MPa  MPa   me        /C   mm    mm   mm
 1  0 305  22.6  1.57 26000 2.00  0.15  0    10  0.0  0.0
 2  1 305  22.6  1.57 26000 2.00  0.15  0    10  0.0  0.0
 3  1 305  22.6  1.57 26000 2.00  0.15  0    10  0.0  0.0
 4  1 305   1.0  1.0   500 4.00  0.15  0    10  0.0  0.0
/
```

REINFORCEMENT COMPONENTS

```
MAT SRF DIR  As  Db  Fy   Fu   Es     Esh  esh  Cs  Dep
TYP TYP deg  %   mm  MPa  MPa  MPa    MPa  me   /C  me
2   1 400.  2.5  6.0 400  600  200000 2000 5    0 0
3   1 400.  5.0  6.0 400  600  200000 2000 5    0 0
4   1 400. 10.0  6.0 400  600  200000 2000 5    0 0
/
```

(B) STEEL

<NOTE:> TO BE USED FOR TRUSS ELEMENTS ONLY

```
MAT REF  AREA  Db   Fy   Fu   Es     Esh  esh  Cs  Dep
TYP TYP  mm2   mm   MPa  MPa  MPa    MPa  me   /C  me
1   1    1400  29.9 436  700  200000  5000  8.0 0 0
2   1    1000  25.2 440  680  200000  7500  7.0 0 0
3   3    48.2  0.1  1090 1090  99520 99520 11.0 0 0
4   3    96.3  0.1  1090 1090  99520 99520 11.0 0 0
5   3    0.01  1    10   10 200000  2000  5    0 0
/
```

(C) BOND

<NOTE:> TO BE USED FOR EXTERIOR/INTERIOR BONDED ELEMENTS

```
MAT REF [ Ao    Umax  Sm    Su ] [ CPF  Cmin   No.  HOOK ]
TYP TYP mm^2    MPa   mm    mm    0-1   mm     LYR  0/1
1   3   1517    2.85  0.005 0.50  0     0      1    0
2   3   2612.7  2.85  0.005 0.50  0     0      1    0
3   3   3034    2.85  0.005 0.50  0     0      1    0
4   3   5225.4  2.85  0.005 0.50  0     0      1    0
/
```

ELEMENT INCIDENCES

****

(A) RECTANGULAR ELEMENTS

```
<<<<< FORMAT >>>>>
ELMT INC1 INC2 INC3 INC4  [ #ELMT d(ELMT) d(INC) ] [ #ELMT d(ELMT) d(INC) ] /
 1   1  14  15  2   4  1  13   12  43  1/
 5  53  66  68  54/
48  54  68  70  55/
91  55  70  72  56/
134 56  72  74  57/
177 57  74  76  58/
220 58  76  78  59/
263 59  78  80  60/
```

```
306 60 80 82 61/
349 61 82 84 62/
392 62 84 86 63/
435 63 86 88 64/
478 64 88 90 65/
 6 66 92 94 68 34 1 26  12 43 2/
 40 950 976 977 952/
 83 952 977 978 954/
126 954 978 979 956/
169 956 979 980 958/
212 958 980 981 960/
255 960 981 982 962/
298 962 982 983 964/
341 964 983 984 966/
384 966 984 985 968/
427 968 985 986 970/
470 970 986 987 972/
513 972 987 988 974/
41  976 989 990 977 3 1 13  12 43 1/
517 1001 1014 1029 1028/
518 1014 1027 1030 1029/
/
```

(B) TRIANGULAR ELEMENTS

```
<<<<< FORMAT >>>>>
ELMT INC1 INC2 INC3  [ #ELMT d(ELMT) d(INC)] [ #ELMT d(ELMT) d(INC) ] /
/
```

(C) TRUSS ELEMENTS

```
<<<<< FORMAT >>>>>
ELMT INC1 INC2 [ #ELMT d(ELMT) d(INC)] [ #ELMT d(ELMT) d(INC) ]  /
 519  3 16  4 1 13 2 43 2/
 523  55 70/
 566  57 74/
 524  70 96 34  1 26 2 43 4/
 558 954 978/
 601 958 980/
 559 978 991  3 1 13 2 43 2/

 605  67 69 12 1 2 6 60 156/
 617  93 95 12 1 2 6 60 156/
 629 119 121 12 1 2 6 60 156/
 641 145 147 12 1 2 6 60 156/
 653 171 173 12 1 2 6 60 156/

 965 197 199 12 1 2 5 12 156/
/
```

(D) LINKAGE ELEMENTS

```
<<<<< FORMAT >>>>
ELMT INC1 INC2 [ #ELMT d(ELMT) d(INC) ] [ #ELMT d(ELMT) d(INC) ]
/
```

(E) CONTACT ELEMENTS

```
<<<<< FORMAT >>>>
ELMT INC1 INC2 INC3 INC4 [ #ELMT d(ELMT) d(INC) ] [ #ELMT d(ELMT) d(INC) ]
1025  66 67 68 69 12 1 2 6 60 156/
```

```
1037  92  93  94  95  12  1  2  6  60  156/
1049 118 119 120 121  12  1  2  6  60  156/
1061 144 145 146 147  12  1  2  6  60  156/
1073 170 171 172 173  12  1  2  6  60  156/
1385 196 197 198 199  12  1  2  5  12  156/
/
```

MATERIAL TYPE ASSIGNMENT

****

```
<<<<< FORMAT >>>>>
ELMT  MAT  ACT  [ #ELMT d(ELMT)] [ #ELMT d(ELMT) ] /
  2   1   1    42  1  5  43/
  1   2   1     5 43/
216   1   1    43  1  5  43/
431   1   1    39  1  2  43/
468   2   1     6  1 /
511   2   1     2  1 /
513   3   1     4  1 /
517   4   1     2  1/

519   1   1    43  1/
562   2   1    43  1/

605   3   1    12  1  6  60/
653   3   1    12  1  6  60/
617   4   1    12  1  6  60/
629   4   1    12  1  6  60/
641   4   1    12  1  6  60/

965   5   1    12  1  5  12/

1025  1   1     4  1  6  60/
1073  1   1     4  1  6  60/
1029  2   1     8  1  6  60/
1077  2   1     8  1  6  60/
1037  3   1     4  1  6  60/
1049  3   1     4  1  6  60/
1061  3   1     4  1  6  60/
1041  4   1     8  1  6  60/
1053  4   1     8  1  6  60/
1065  4   1     8  1  6  60/
1385  4   1    12  1  5  12/
/
```

COORDINATES

****

```
<NOTE:> UNITS: in OR mm
<<<<< FORMAT >>>>>
NODE X Y  [ #NODES d(NODES)  d(X) d(Y) ] [ #NODES d(NODES)  d(X) d(Y) ] /
  1   0   0   5 13 47    0 4  1  0  31.5/
  5   0 126   5 13 47    0 9  1  0  54.25/
 66 235   0  35  26  48.16 0  4  2  0  31.5/
 67 235   0  35  26  48.16 0  4  2  0  31.5/
 74 235 126  35  26  48.16 0  9  2  0  54.25/
 75 235 126  35  26  48.16 0  9  2  0  54.25/
976 1920.6  0  4  13  48.16  0  4  1  0  31.5/
980 1920.6 126  4  13  48.16  0  9  1  0  54.25/
1028 1968.76 585 3  1  48.16  0/
/
```

```
                SUPPORT RESTRAINTS
                ******************
<NOTE:> CODE:  '0' FOR NOT RESTRAINED NODES AND '1' FOR RESTRAINED ONES
<<<<< FORMAT >>>>>
NODE  X-RST  Y-RST [ #NODE d(NODE) ] /
 66 0 1/
1015 1 0  13  1/
1030 1 0/
/


                **************
                * LOAD CASE *
                *   DATA     *
                **************

                LOAD CASE PARAMETERS
                ********************

Structure Title     (30 char. max.)          : RWOA1
Load Case Title     (30 char. max.)          : 1 MM
Load Case File Name  (8 char. max.)          : RWOA1
No. of Loaded Joints                         : 0
No. of Prescribed Support Displacements      : 1
No. of Elements with Temperature Loads       : 0
No. of Elements with Concrete Prestrain      : 0
No. of Elements with Ingress Pressure        : 0

                  JOINT LOADS
                  ***********
<NOTE:> UNITS:  KIPS OR KN
<<<<< FORMAT >>>>>
NODE   Fx   Fy   [ #NODE d(NODE) d(Fx) d(Fy) ] /
/
                SUPPORT DISPLACEMENTS
                *********************
<NOTE:> UNITS: MM OR IN
<<<<< FORMAT >>>>>
JNT  DOF  DISPL   [ #JNT d(JNT) ] /
1014  2   -1.0 /
/
                TEMPERATURE LOADS
                *****************
<NOTE:> UNITS:  F OR C
<<<<< FORMAT >>>>>
ELMT   TEMP   [ #ELMT d(ELMT) d(TEMP) ] [ #ELMT d(ELMT) d(TEMP) ] /
/
                CONCRETE PRESTRAINS
                *******************
<NOTE:> UNITS:  me
<<<<< FORMAT >>>>>
ELMT  STRAIN   [ #ELMT d(ELMT) d(STRAIN) ] [ #ELMT d(ELMT) d(STRAIN) ]  /
/
                INGRESS PRESSURES
                *****************
<NOTE:> UNITS:  MPa
<<<<< FORMAT >>>>>
```

ELMT PRESSURE [#ELMT d(ELMT) d(PRS)] [#ELMT d(ELMT) d(PRS)] /
/

Beam RWOA-2:

```
************
* VECTOR *
* JOB DATA *
************
```

Job Title (30 char. max.) : RWOA2
Job File Name (8 char. max.) : RWOA2
Date (30 char. max.) : Apr 25, 2001

STRUCTURE DATA

Structure Type : 2
File Name (8 char. max.) : RWOA2

LOADING DATA

No. of Load Stages : 226
Starting Load Stage No. : 1
Load Series ID (5 char. max.) : COA2

Load Case	File Name (8 char. max.)	Factors Initial	Final	LS-Inc	Type	Reps	C-Inc
1	RWOA2	0.000	45.000	0.200	1	1	1.000
2	NULL	0.000	0.000	1.000	2	1	0.000
3	NULL	0.000	40.000	0.500	1	1	0.000

ANALYSIS PARAMETERS

Seed File Name (8 char. max.) : NULL
Convergence Limit (factor > 1.0) : 1.000010
Averaging Factor (0.0 to 1.0) : 0.20
Maximum No. of Iterations : 150
Convergence Criteria : 1
Results Files : 2
Output Format : 1

MATERIAL BEHAVIOUR MODELS

Concrete Compression Base Curve (0-3) : 1
Concrete Compression Post-Peak (0-3) : 1
Concrete Compression Softening (0-8) : 1
Concrete Tension Stiffening (0-3) : 1
Concrete Tension Softening (0-3) : 1
Concrete Tension Splitting (0-1) : 1
Concrete Confined Strength (0-2) : 1
Concrete Dilatation (0-1) : 1
Concrete Cracking Criterion (0-4) : 1
Concrete Crack Slip Check (0-2) : 1

Concrete Crack Width Check	(0-2) : 1
Concrete Bond or Adhesion	(0-4) : 1
Concrete Hysteresis	(0-2) : 1
Reinforcement Hysteresis	(0-3) : 1
Reinforcement Dowel Action	(0-1) : 1
Reinforcement Buckling	(0-1) : 1
Element Strain Histories	(0-1) : 1
Element Slip Distortions	(0-4) : 1
Geometric Nonlinearity	(0-1) : 1

****
* STRUCTURE *
* DATA *
****

STRUCTURAL PARAMETERS
****

Structure Title (30 char. max.)	: RWOA2 beam
Structure File Name (8 char. max.)	: RWOA2
No. of R.C. Material Types	: 4
No. of Steel Material Types	: 6
No. of Bond Material Types	: 4
No. of Rectangular Elements	: 638
No. of Triangular Elements	: 0
No. of Truss Elements	: 723
No. of Linkage Elements	: 0
No. of Contact Elements	: 564
No. of Joints	: 1316
No. of Restraints	: 15

MATERIAL SPECIFICATIONS
****

(A) REINFORCED CONCRETE

<NOTE:> TO BE USED IN RECTANGULAR AND TRIANGULAR ELEMENTS ONLY

CONCRETE

MAT TYP	Ns #	T mm	fc MPa	[ft MPa	Ec MPa	e0 me	Mu	Cc /C	Agg][Sx mm	Sy] mm	mm
1	0	305	25.9	1.68	28000	2.00	0.15	0	10	0.0	0.0
2	1	305	25.9	1.68	28000	2.00	0.15	0	10	0.0	0.0
3	1	305	25.9	1.68	28000	2.00	0.15	0	10	0.0	0.0
4	1	305	1.0	1.0	500	4.00	0.15	0	10	0.0	0.0

/

REINFORCEMENT COMPONENTS

MAT TYP	SRF TYP	DIR deg	As %	Db mm	Fy MPa	Fu MPa	Es MPa	Esh MPa	esh me	Cs /C	Dep me
2	1	400.	2.5	6.0	400	600	200000	2000	5	0	0
3	1	400.	5.0	6.0	400	600	200000	2000	5	0	0
4	1	400.	10.0	6.0	400	600	200000	2000	5	0	0

/

(B) STEEL

<NOTE:> TO BE USED FOR TRUSS ELEMENTS ONLY

MAT TYP	REF TYP	AREA mm2	Db mm	Fy MPa	Fu MPa	Es MPa	Esh MPa	esh	Cs /C	Dep me
1	1	1400	29.9	436	700	200000	5000	8.0	0	0
2	1	700	29.9	436	700	200000	5000	8.0	0	0
3	1	1000	25.2	445	615	200000	5000	12.5	0	0
4	3	47.6	0.1	1090	1090	99520	99520	11.0	0	0
5	3	95.2	0.1	1090	1090	99520	99520	11.0	0	0
6	1	0.01	1	10	10	200000	2000	5	0	0

/

(C) BOND

<NOTE:> TO BE USED FOR EXTERIOR/INTERIOR BONDED ELEMENTS

MAT TYP	REF TYP	[Ao mm^2	Umax MPa	Sm mm	Su] mm	[CPF 0-1	Cmin mm	No. LYR	HOOK] 0/1
1	3	1500	3.05	0.005	0.50	0	0	1	0
2	3	2582.3	3.05	0.005	0.50	0	0	1	0
3	3	3000	3.05	0.005	0.50	0	0	1	0
4	3	5164.6	3.05	0.005	0.50	0	0	1	0

/

ELEMENT INCIDENCES

****

(A) RECTANGULAR ELEMENTS

<<<<< FORMAT >>>>>

ELMT INC1 INC2 INC3 INC4 [#ELMT d(ELMT) d(INC)] [#ELMT d(ELMT) d(INC)] /

```
  1  1 14 15  2  2 1 13  12  53  1/
  3 27 40 42 28/
 56 28 42 44 29/
109 29 44 46 30/
162 30 46 48 31/
215 31 48 50 32/
268 32 50 52 33/
321 33 52 54 34/
374 34 54 56 35/
427 35 56 58 36/
480 36 58 60 37/
533 37 60 62 38/
586 38 62 64 39/
  4 40 66 68 42 46 1 26  12  53  2/
 50 1236 1262 1263 1238/
103 1238 1263 1264 1240/
156 1240 1264 1265 1242/
209 1242 1265 1266 1244/
262 1244 1266 1267 1246/
315 1246 1267 1268 1248/
368 1248 1268 1269 1250/
421 1250 1269 1270 1252/
474 1252 1270 1271 1254/
527 1254 1271 1272 1256/
580 1256 1272 1273 1258/
633 1258 1273 1274 1260/
51  1262 1275 1276 1263 3 1 13  12  53  1/
637 1287 1300 1315 1314/
638 1300 1313 1316 1315/
```

```
/
                (B) TRIANGULAR ELEMENTS
                ---------------------
<<<<< FORMAT >>>>>
ELMT INC1 INC2 INC3  [ #ELMT d(ELMT) d(INC)] [ #ELMT d(ELMT) d(INC) ] /
/
                (C) TRUSS ELEMENTS
                ------------------
<<<<< FORMAT >>>>>
ELMT INC1 INC2 [ #ELMT d(ELMT) d(INC)] [ #ELMT d(ELMT) d(INC) ] /
 639  3 16  2 1 13  3  53  1/
 641 29 45/
 694 30 47/
 747 31 49/
 642 45 71 46 1 26  3  53  2/
 688 1241 1264/
 741 1243 1265/
 794 1245 1266/
 689 1264 1277 3  1 13  3  53  1/

 798 41 43 12 1 2 8 60 156/
 810 67 69 12 1 2 8 60 156/
 822 93 95 12 1 2 8 60 156/
 834 119 121 12 1 2 8 60 156/
 846 145 147 12 1 2 8 60 156/

1278 171 173 12 1 2 7 12 156/
/
                (D) LINKAGE ELEMENTS
                --------------------
<<<<< FORMAT >>>>
ELMT INC1 INC2 [ #ELMT d(ELMT) d(INC) ] [ #ELMT d(ELMT) d(INC) ]
/
                (E) CONTACT ELEMENTS
                -------------------
<<<<< FORMAT >>>>
ELMT INC1 INC2 INC3 INC4 [ #ELMT d(ELMT) d(INC) ] [ #ELMT d(ELMT) d(INC) ]
1362 40 41 42 43 12 1 2 8 60 156/
1374 66 67 68 69 12 1 2 8 60 156/
1386 92 93 94 95 12 1 2 8 60 156/
1398 118 119 120 121 12 1 2 8 60 156/
1410 144 145 146 147 12 1 2 8 60 156/
1842 170 171 172 173 12 1 2 7 12 156/
/
                MATERIAL TYPE ASSIGNMENT
                ************************
<<<<< FORMAT >>>>>
ELMT MAT ACT [ #ELMT d(ELMT)] [ #ELMT d(ELMT) ] /
  1  2  1   5 53/
  2  1  1  52 1 5 53/
266  1  1  53 1 5 53/
531  1  1  47 1 2 53/
578  2  1   6 1/
631  2  1   2 1/
633  3  1   4 1/
637  4  1   2 1/
```

```
 639  1  1   53  1/
 692  2  1   53  1/
 745  3  1   53  1/

 798  4  1   12  1  8  60/
 846  4  1   12  1  8  60/
 810  5  1   12  1  8  60/
 822  5  1   12  1  8  60/
 834  5  1   12  1  8  60/

1278  6  1   12  1  7  12/

1362  1  1    4  1  8  60/
1410  1  1    4  1  8  60/
1366  2  1    8  1  8  60/
1414  2  1    8  1  8  60/
1374  3  1    4  1  8  60/
1386  3  1    4  1  8  60/
1398  3  1    4  1  8  60/
1378  4  1    8  1  8  60/
1390  4  1    8  1  8  60/
1402  4  1    8  1  8  60/

1842  4  1   12  1  7  12/
/
                  COORDINATES
                  ***********
<NOTE:> UNITS: in OR mm
<<<<< FORMAT >>>>>
NODE X Y  [ #NODES d(NODES)  d(X) d(Y) ] [ #NODES d(NODES)  d(X) d(Y) ] /
  1   0  0  3  13  56    0 4  1 0 31.5/
  5   0 126  3  13  56    0 9  1 0 54.25/
 40  168  0  2  26  56    0 4  2 0 31.5/
 41  168  0  2  26  56    0 4  2 0 31.5/
 48  168 126  2  26  56    0 9  2 0 54.25/
 49  168 126  2  26  56    0 9  2 0 54.25/
 92  280  0 45  26  47.6  0 4  2 0 31.5/
 93  280  0 45  26  47.6  0 4  2 0 31.5/
100  280 126 45  26  47.6  0 9  2 0 54.25/
101  280 126 45  26  47.6  0 9  2 0 54.25/
1262 2422  0  4  13  47.6  0 4  1 0 31.5/
1266 2422 126  4  13  47.6  0 9  1 0 54.25/
1314 2469.6 585 3  1  47.6  0/
/
                SUPPORT RESTRAINTS
                ******************
<NOTE:> CODE:  '0' FOR NOT RESTRAINED NODES AND '1' FOR RESTRAINED ONES
<<<<< FORMAT >>>>>
NODE  X-RST  Y-RST [ #NODE d(NODE) ]  /
 92 0 1/
1301 1 0  13  1/
1316 1 0/
/
```

```
**************
* LOAD CASE  *
*   DATA     *
**************

 LOAD CASE PARAMETERS
 ********************

Structure Title    (30 char. max.)          : RWOA2
Load Case Title    (30 char. max.)          : 1 MM
Load Case File Name  (8 char. max.)         : RWOA2
No. of Loaded Joints                        : 0
No. of Prescribed Support Displacements     : 1
No. of Elements with Temperature Loads      : 0
No. of Elements with Concrete Prestrain     : 0
No. of Elements with Ingress Pressure       : 0

                JOINT LOADS
                ***********
<NOTE:> UNITS:  KIPS OR KN
<<<<< FORMAT >>>>>
NODE   Fx   Fy   [ #NODE d(NODE) d(Fx) d(Fy) ] /
/
              SUPPORT DISPLACEMENTS
              *********************
<NOTE:> UNITS: MM OR IN
<<<<< FORMAT >>>>>
JNT  DOF  DISPL   [ #JNT d(JNT) ] /
1300  2   -1.0  /
/
               TEMPERATURE LOADS
               *****************
<NOTE:> UNITS:  F OR C
<<<<< FORMAT >>>>>
ELMT   TEMP   [ #ELMT d(ELMT) d(TEMP) ] [ #ELMT d(ELMT) d(TEMP) ] /
/
               CONCRETE PRESTRAINS
               *******************
<NOTE:> UNITS:  me
<<<<< FORMAT >>>>>
ELMT  STRAIN   [ #ELMT d(ELMT) d(STRAIN) ] [ #ELMT d(ELMT) d(STRAIN) ]  /
/
               INGRESS PRESSURES
               *****************
<NOTE:> UNITS:  MPa
<<<<< FORMAT >>>>>
ELMT PRESSURE  [ #ELMT d(ELMT) d(PRS) ] [ #ELMT d(ELMT) d(PRS) ]  /
/
```

Beam RWOA-3:

```
**********
* VECTOR *
* JOB DATA *
**********
```

Job Title (30 char. max.) : RWOA3
Job File Name (8 char. max.) : RWOA3
Date (30 char. max.) : Apr 25, 2001

STRUCTURE DATA

Structure Type : 2
File Name (8 char. max.) : RWOA3

LOADING DATA

No. of Load Stages : 171
Starting Load Stage No. : 1
Load Series ID (5 char. max.) : COA3

Load Case	File Name (8 char. max.)	Factors Initial	Final	LS-Inc	Type	Reps	C-Inc
1	RWOA3	0.000	85.000	0.500	1	1	1.000
2	NULL	0.000	0.000	1.000	2	1	0.000
3	NULL	0.000	40.000	0.500	1	1	0.000

ANALYSIS PARAMETERS

Seed File Name (8 char. max.) : NULL
Convergence Limit (factor > 1.0) : 1.000010
Averaging Factor (0.0 to 1.0) : 0.20
Maximum No. of Iterations : 150
Convergence Criteria : 1
Results Files : 2
Output Format : 1

MATERIAL BEHAVIOUR MODELS

Concrete Compression Base Curve (0-3) : 1
Concrete Compression Post-Peak (0-3) : 1
Concrete Compression Softening (0-8) : 1
Concrete Tension Stiffening (0-3) : 1
Concrete Tension Softening (0-3) : 1
Concrete Tension Splitting (0-1) : 1
Concrete Confined Strength (0-2) : 1
Concrete Dilatation (0-1) : 1
Concrete Cracking Criterion (0-4) : 1
Concrete Crack Slip Check (0-2) : 1
Concrete Crack Width Check (0-2) : 1
Concrete Bond or Adhesion (0-4) : 1
Concrete Hysteresis (0-2) : 1
Reinforcement Hysteresis (0-3) : 1
Reinforcement Dowel Action (0-1) : 1

Reinforcement Buckling	(0-1) : 1
Element Strain Histories	(0-1) : 1
Element Slip Distortions	(0-4) : 1
Geometric Nonlinearity	(0-1) : 1

STRUCTURE DATA

STRUCTURAL PARAMETERS

Structure Title (30 char. max.)	: RWOA3 beam
Structure File Name (8 char. max.)	: RWOA3
No. of R.C. Material Types	: 4
No. of Steel Material Types	: 5
No. of Bond Material Types	: 4
No. of Rectangular Elements	: 683
No. of Triangular Elements	: 0
No. of Truss Elements	: 747
No. of Linkage Elements	: 0
No. of Contact Elements	: 540
No. of Joints	: 1357
No. of Restraints	: 12

MATERIAL SPECIFICATIONS

(A) REINFORCED CONCRETE

<NOTE:> TO BE USED IN RECTANGULAR AND TRIANGULAR ELEMENTS ONLY

CONCRETE

MAT TYP	Ns #	T mm	f'c MPa	[f't MPa	Ec MPa	e0 me	Mu	Cc	Agg /C	][Sx mm	Sy] mm
1	0	305	43.5	2.18	36000	2.00	0.15	0	10	0.0	0.0
2	1	305	43.5	2.18	36000	2.00	0.15	0	10	0.0	0.0
3	1	305	43.5	2.18	36000	2.00	0.15	0	10	0.0	0.0
4	1	305	1.0	1.0	500	4.00	0.15	0	10	0.0	0.0

/

REINFORCEMENT COMPONENTS

MAT TYP	SRF TYP	DIR deg	As %	Db mm	Fy MPa	Fu MPa	Es MPa	Esh MPa	esh me	Cs /C	Dep me
2	1	400	2.5	6	400	600	200000	2000	5	0	0
3	1	400	5.0	6	400	600	200000	2000	5	0	0
4	1	400	10.	6	400	600	200000	2000	5	0	0

/

(B) STEEL

<NOTE:> TO BE USED FOR TRUSS ELEMENTS ONLY

MAT TYP	REF TYP	AREA mm2	Db mm	Fy MPa	Fu MPa	Es MPa	Esh MPa	esh me	Cs /C	Dep me

```
1  1   2100  29.9  436  700  200000  5000  8.0 0 0
2  1   1000  25.2  440  680  200000  7500  7.0 0 0
3  1    700  29.9  436  700  200000  5000  8.0 0 0
4  3     50   0.1 1090 1090   99520 99520 11.0 0 0
5  3    100   0.1 1090 1090   99520 99520 11.0 0 0
/
```

(C) BOND

```
<NOTE:> TO BE USED FOR EXTERIOR/INTERIOR BONDED ELEMENTS
MAT  REF  [ Ao   Umax  Sm   Su ] [ CPF  Cmin   No.  HOOK ]
TYP  TYP  mm^2  MPa   mm   mm    0-1   mm    LYR   0/1
1    3    3250  3.5 0.006 0.50  0     0     1     0
2    3    2715  3.5 0.006 0.50  0     0     1     0
3    3    6500  3.5 0.006 0.50  0     0     1     0
4    3    5430  3.5 0.006 0.50  0     0     1     0
/
```

ELEMENT INCIDENCES

(A) RECTANGULAR ELEMENTS

```
<<<<< FORMAT >>>>>
ELMT INC1 INC2 INC3 INC4  [ #ELMT d(ELMT) d(INC) ] [ #ELMT d(ELMT) d(INC) ] /
  1   1   5   6   2  3  1  1/
  4   5  16  17   6  3  1 11  10 68  1/
  7  38  60  61  39  4  1 22  10 68  1/
 11 126 137 138 127 10 68  1/
 12 137 159 160 138  5  1 22  10 68  1/
 17 247 258 259 248 10 68  1/
 18 258 280 281 259  5  1 22  10 68  1/
 23 368 379 380 369 10 68  1/
 24 379 401 402 380  5  1 22  10 68  1/
 29 489 500 501 490 10 68  1/
 30 500 522 523 501  5  1 22  10 68  1/
 35 610 621 622 611 10 68  1/
 36 621 643 644 622  5  1 22  10 68  1/
 41 731 742 743 732 10 68  1/
 42 742 764 765 743  5  1 22  10 68  1/
 47 852 863 864 853 10 68  1/
 48 863 885 886 864  5  1 22  10 68  1/
 53 973 984 985 974 10 68  1/
 54 984 1006 1007 985  5  1 22  10 68  1/
 59 1094 1105 1106 1095  10 68  1/
 60 1105 1127 1128 1106  5  1 22  10 68  1/
 65 1215 1226 1227 1216  10 68  1/
 66 1226 1248 1249 1227  5  1 22  10 68  1/
 71 1336 1347 1348 1337  10 68  1/
/
```

(B) TRIANGULAR ELEMENTS

```
<<<<< FORMAT >>>>>
ELMT INC1 INC2 INC3  [ #ELMT d(ELMT) d(INC)] [ #ELMT d(ELMT) d(INC) ] /
/
```

(C) TRUSS ELEMENTS

```
<<<<< FORMAT >>>>>
ELMT INC1 INC2 [ #ELMT d(ELMT) d(INC)] [ #ELMT d(ELMT) d(INC) ] /
```

```
 684   2  6 2 69  1/
 822   3  7/
 685   6 17 3   1 11  2 69  1/
 823   7 18 3   1 11/
 688  39 61 4   1 22  2 69  1/
 826  40 62 4   1 22/
 692 127 138 2  69  1/
 830 128 139/
 693 138 160 5   1 22  2 69  1/
 831 139 161 5   1 22/
 698 248 259 2  69  1/
 836 249 260/
 699 259 281 5   1 22  2 69  1/
 837 260 282 5   1 22/
 704 369 380 2  69  1/
 842 370 381/
 705 380 402 5   1 22  2 69  1/
 843 381 403 5   1 22/
 710 490 501 2  69  1/
 848 491 502/
 711 501 523 5   1 22  2 69  1/
 849 502 524 5   1 22/
 716 611 622 2  69  1/
 854 612 623/
 717 622 644 5   1 22  2 69  1/
 855 623 645 5   1 22/
 722 732 743 2  69  1/
 860 733 744/
 723 743 765 5   1 22  2 69  1/
 861 744 766 5   1 22/
 728 853 864 2  69  1/
 866 854 865/
 729 864 886 5   1 22  2 69  1/
 867 865 887 5   1 22/
 734 974 985 2  69  1/
 872 975 986/
 735 985 1007 5  1 22  2 69  1/
 873 986 1008 5  1 22/
 740 1095 1106 2 69  1/
 878 1096 1107/
 741 1106 1128 5  1 22  2 69  1/
 879 1107 1129 5  1 22/
 746 1216 1227 2 69  1/
 884 1217 1228/
 747 1227 1249 5  1 22  2 69  1/
 885 1228 1250 5  1 22/
 752 1337 1348 2 69  1/
 890 1338 1349/

 891  49  50  10  1  1  4  10  22/
 931 148  149  10  1  1 10  50 121/
 941 170  171  10  1  1 10  50 121/
 951 192  193  10  1  1 10  50 121/
 961 214  215  10  1  1 10  50 121/
 971 236  237  10  1  1 10  50 121/
/
```

(D) LINKAGE ELEMENTS

```
<<<<< FORMAT >>>>
ELMT INC1 INC2 [ #ELMT d(ELMT) d(INC) ] [ #ELMT d(ELMT) d(INC) ]
/
```

(E) CONTACT ELEMENTS

```
<<<<< FORMAT >>>>
ELMT INC1 INC2 INC3 INC4 [ #ELMT d(ELMT) d(INC) ] [ #ELMT d(ELMT) d(INC) ]
1431  38  49  39  50  10  1  1  4  10   22/
1471 137 148 138 149  10  1  1 10  50  121/
1481 159 170 160 171  10  1  1 10  50  121/
1491 181 192 182 193  10  1  1 10  50  121/
1501 203 214 204 215  10  1  1 10  50  121/
1511 225 236 226 237  10  1  1 10  50  121/
/
```

MATERIAL TYPE ASSIGNMENT

```
<<<<< FORMAT >>>>>
ELMT  MAT  ACT  [ #ELMT d(ELMT)] [ #ELMT d(ELMT) ] /
  1   2   1    3  1/
  4   1   1   68  1  8  68/
548   1   1   62  1  2  68/
610   2   1    6  1/
678   2   1    2  1/
680   3   1    4  1/
684   4   1    2  1/

684   1   1   69  1/
753   2   1   69  1/
822   3   1   69  1/

891   4   1   10  1  2  30/
931   4   1   10  1 10  50/
971   4   1   10  1 10  50/
901   5   1   10  1  2  10/
941   5   1   10  1 10  50/
951   5   1   10  1 10  50/
961   5   1   10  1 10  50/

1431  1   1    2  1  2  30/
1433  2   1    8  1  2  30/
1441  3   1    2  1  2  10/
1443  4   1    8  1  2  10/
1471  1   1    2  1 10  50/
1473  2   1    8  1 10  50/
1481  3   1    2  1 10  50/
1483  4   1    8  1 10  50/
1491  3   1    2  1 10  50/
1493  4   1    8  1 10  50/
1501  3   1    2  1 10  50/
1503  4   1    8  1 10  50/
1511  1   1    2  1 10  50/
1513  2   1    8  1 10  50/
/
```

COORDINATES

```
<NOTE:> UNITS: in OR mm
```

```
<<<<< FORMAT >>>>>
NODE X Y [ #NODES d(NODES)  d(X) d(Y) ] [ #NODES d(NODES)  d(X) d(Y) ] /
  1   0     0  3   1   0  63/
  4   0   180.3/
  5  25     0  4  11  57.25  0  3   1   0  63/
  8  25   180.3 4  11  57.25  0  8   1   0  54.3/
 49 196.75  0  3   1   0  63/
 52 196.75 180.3 8   1   0  54.3/
 60 254     0  4  22  50     0  3   1   0  63/
 63 254   180.3 4  22  50     0  8   1   0  54.3/
 71 254     0  3  22  50     0  3   1   0  63/
 74 254   180.3 3  22  50     0  8   1   0  54.3/
137 454     0  6  22  50     0  3   1   0  63/
140 454   180.3 6  22  50     0  8   1   0  54.3/
148 454     0  5  22  50     0  3   1   0  63/
151 454   180.3 5  22  50     0  8   1   0  54.3/
258 754     0  6  22  50     0  3   1   0  63/
261 754   180.3 6  22  50     0  8   1   0  54.3/
269 754     0  5  22  50     0  3   1   0  63/
272 754   180.3 5  22  50     0  8   1   0  54.3/
379 1054    0  6  22  50     0  3   1   0  63/
382 1054  180.3 6  22  50     0  8   1   0  54.3/
390 1054    0  5  22  50     0  3   1   0  63/
393 1054  180.3 5  22  50     0  8   1   0  54.3/
500 1354    0  6  22  50     0  3   1   0  63/
503 1354  180.3 6  22  50     0  8   1   0  54.3/
511 1354    0  5  22  50     0  3   1   0  63/
514 1354  180.3 5  22  50     0  8   1   0  54.3/
621 1654    0  6  22  50     0  3   1   0  63/
624 1654  180.3 6  22  50     0  8   1   0  54.3/
632 1654    0  5  22  50     0  3   1   0  63/
635 1654  180.3 5  22  50     0  8   1   0  54.3/
742 1954    0  6  22  50     0  3   1   0  63/
745 1954  180.3 6  22  50     0  8   1   0  54.3/
753 1954    0  5  22  50     0  3   1   0  63/
756 1954  180.3 5  22  50     0  8   1   0  54.3/
863 2254    0  6  22  50     0  3   1   0  63/
866 2254  180.3 6  22  50     0  8   1   0  54.3/
874 2254    0  5  22  50     0  3   1   0  63/
877 2254  180.3 5  22  50     0  8   1   0  54.3/
984 2554    0  6  22  50     0  3   1   0  63/
987 2554  180.3 6  22  50     0  8   1   0  54.3/
995 2554    0  5  22  50     0  3   1   0  63/
998 2554  180.3 5  22  50     0  8   1   0  54.3/
1105 2854   0  6  22  50     0  3   1   0  63/
1108 2854 180.3 6  22  50     0  8   1   0  54.3/
1116 2854   0  5  22  50     0  3   1   0  63/
1119 2854 180.3 5  22  50     0  8   1   0  54.3/
1226 3154   0  6  22  50     0  3   1   0  63/
1229 3154 180.3 6  22  50     0  8   1   0  54.3/
1237 3154   0  5  22  50     0  3   1   0  63/
1240 3154 180.3 5  22  50     0  8   1   0  54.3/
1347 3454   0  3   1   0  63/
1350 3454 180.3 8   1   0  54.3/
/
```

SUPPORT RESTRAINTS

****

<NOTE:> CODE: '0' FOR NOT RESTRAINED NODES AND '1' FOR RESTRAINED ONES
<<<<< FORMAT >>>>>
NODE X-RST Y-RST [#NODE d(NODE)] /
60 0 1/
1347 1 0 11 1/
/

****
* LOAD CASE *
* DATA *
****

LOAD CASE PARAMETERS
****

Structure Title (30 char. max.) : RWOA3
Load Case Title (30 char. max.) : 1 MM
Load Case File Name (8 char. max.) : RWOA3
No. of Loaded Joints : 0
No. of Prescribed Support Displacements : 1
No. of Elements with Temperature Loads : 0
No. of Elements with Concrete Prestrain : 0
No. of Elements with Ingress Pressure : 0

JOINT LOADS
****
<NOTE:> UNITS: KIPS OR KN
<<<<< FORMAT >>>>>
NODE Fx Fy [#NODE d(NODE) d(Fx) d(Fy)] /
/

SUPPORT DISPLACEMENTS
****
<NOTE:> UNITS: MM OR IN
<<<<< FORMAT >>>>>
JNT DOF DISPL [#JNT d(JNT)] /
1346 2 -1.0 /
/

TEMPERATURE LOADS
****
<NOTE:> UNITS: F OR C
<<<<< FORMAT >>>>>
ELMT TEMP [#ELMT d(ELMT) d(TEMP)] [#ELMT d(ELMT) d(TEMP)] /
/

CONCRETE PRESTRAINS
****
<NOTE:> UNITS: me
<<<<< FORMAT >>>>>
ELMT STRAIN [#ELMT d(ELMT) d(STRAIN)] [#ELMT d(ELMT) d(STRAIN)] /
/

INGRESS PRESSURES
****
<NOTE:> UNITS: MPa
<<<<< FORMAT >>>>>
ELMT PRESSURE [#ELMT d(ELMT) d(PRS)] [#ELMT d(ELMT) d(PRS)] /

APPENDIX E

DEFLECTED SHAPES AND CRACK PATTERNS FOR SPECIMENS ANALYZED WITH PROGRAM VECTOR2

All plots presented are taken at the stage of peak load, for half of the member except for the De Rose beam.

ŽARNIĆ SLAB STRIP:

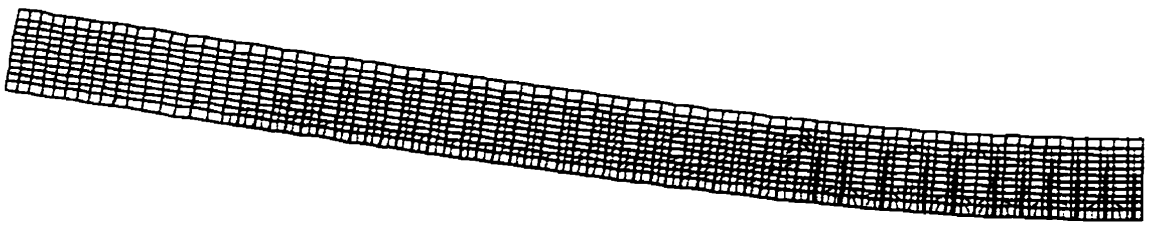

Magnification: 3×

Crack widths: thin < 1 mm, thick > 2 mm

ŽARNIĆ BEAM:

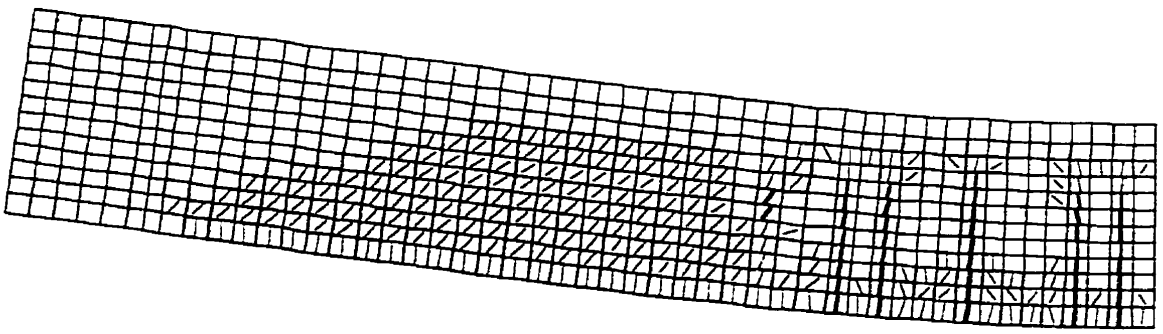

Magnification: 6×

Crack widths: thin < 1 mm, thick > 2 mm

EL-REFAIE SPECIMENS (CB3):

Magnification: 5×

Crack widths: thin < 1 mm, thick > 2 mm

DE ROSE SLAB:

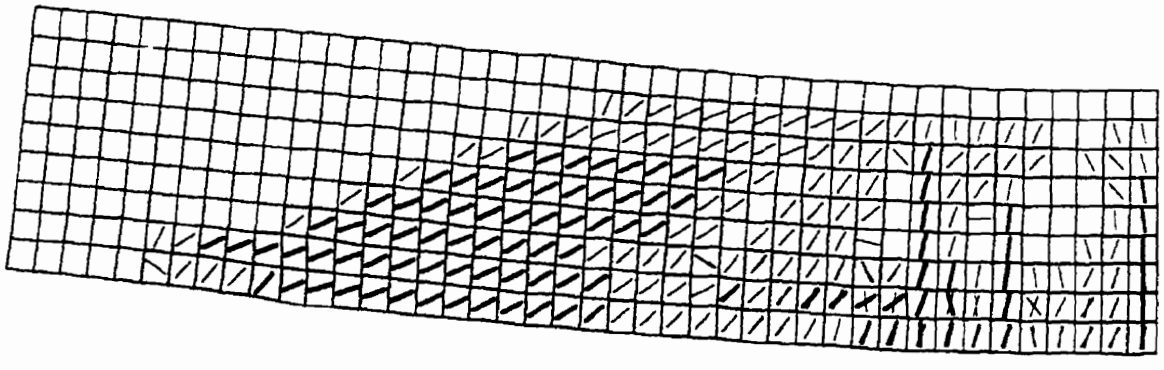

Magnification: 6×

Crack widths: thin < 1 mm, thick > 2 mm

DE ROSE BEAM:

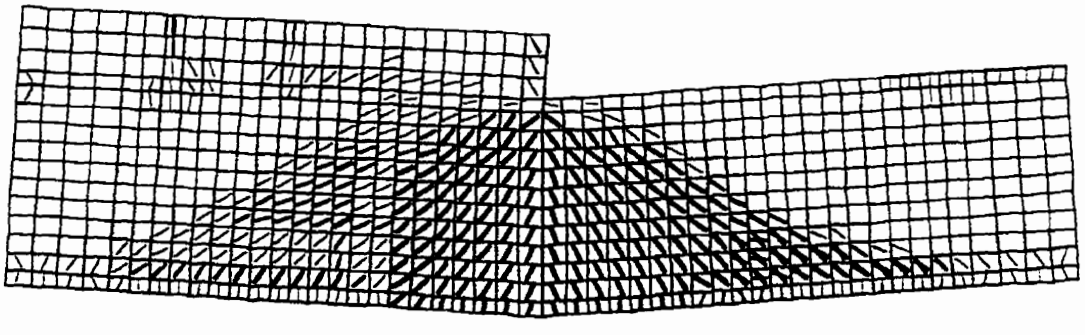

Magnification: 2×

Crack widths: thin < 1 mm, thick > 2 mm

RWOA-1:

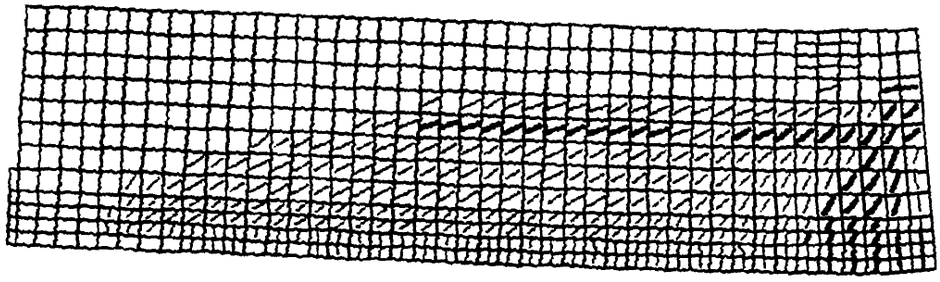

Crack widths: thin < 1 mm, thick > 2 mm

Magnification: 6×

RWOA-2:

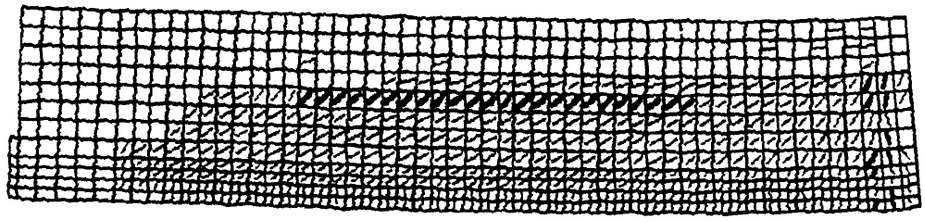

Crack widths: thin < 1 mm, thick > 2 mm

Magnification: 6×

RWOA-3:

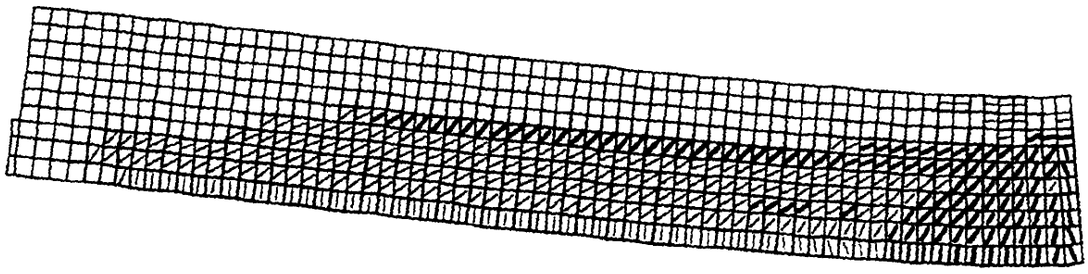

Crack widths: thin < 1 mm, thick > 2 mm

Magnification: 6×